Synthesis and Coordination Chemistry of Entangled Ligands Derived from a Pybox-Based Macrocycle

Gemma Louise Parker

A thesis submitted in partial fulfilment of the requirements for the degree of Doctor of Philosophy in Chemistry

University of Warwick

Department of Chemistry

November 2020

WARWICK

This thesis is dedicated to Sophie Boothe,

who always believed in me.

Table of Contents

Acknowledgments

First and foremost I would like to thank my supervisor Dr Adrian Chaplin for providing me with this opportunity to conduct my research in the Chaplin group. Thank you for all of your patience, guidance and support over the last 4 years. In particular, thank you for being understanding and especially supportive in my final year. As an aside, many thanks for accommodating my creative license – the Christmas tree poster is my personal favourite.

I would like to extend my gratitude towards Dr Ivan Prokes and Rob Perry for their assistance with NMR spectroscopy, especially with my usage over the last year, I really appreciate your time and help. Thank you to the mass spectrometry staff Dr Lijiang Song, Lynette Walsh and Jim Morrey, also thank you for taking the time to send all the raw data.

Thanks must go to the past Chaplin group members. To Rich, thank you for your guidance and supervision during my first year at Warwick and teaching me how to do columns, even if I dropped the pipette in one too many times, I really appreciate all your time and patience. Thanks must go to Matt, thank you for your help and support during my PhD, for running my VT NMR samples and teaching me how to quench reactions properly. To Baptiste, thank you for your help with computational analysis and taking the time to help me understand what it means. I must also thank you for all your delicious baked goods, they are truly amazing!

Sam, thank you for your support and guidance in the lab and helping me keep organised. I am also really grateful for you taking the time to check over my thesis. Thank you for helping me to build up my confidence as a chemist and for being there for me in Helsinki too. To Amy, thank you for brightening up the lab with your love of eggs, dinosaurs and sweets, spreading the joy of Kelsey's (and the eliminator), and for being a supportive and caring friend.

Jack and Caroline, thank you both for making me feel so welcome when I first started in the group and introducing me to pool – even if I am terrible. To Jack, thank you for all your guidance and chemistry wisdom over the years. Thank you for helping me deal with my clumsy lab incidents and being the best fume hood neighbour, even if I did take up the whole desk. Caroline, thank you so much for all your help, especially for your help with this thesis. Thank you for always being there for me, being a shoulder to cry on and consoling me after *that* rotaxane incident.

To the current Chaplin group members, I wish you all the best in your PhDs. Thank you for the Exploding Kittens drama at the coffee mornings and for accommodating me with the

lab shifts. To Matt, thank you for your help with the last minute NMRs, I really appreciate it! Also, thanks for the spice mixes and biltong, they were really good! Jennifer, thank you for the amazing periodic table face mask and sharing my excitement for the free common room food. Alex, thank you for all the amazing cakes, I pray that the crystal gods treat you well during your PhD!

To the Shipmen, thank you for providing a safe haven when I needed a break from the lab. Conor, thank you for the spontaneous trips to the hills, piazza drinks and dealing much better than me with the gincident. To George, thank you for being a really great friend and helping me with all my chemistry problems, checking over bits of this thesis and for being an excellent decipherer, I really appreciate it!

To my amazing friends, thank you for humouring my love of scribbl, helping me proofread and being really supportive with this PhD and everything else. Georgia, I'm sad it took us so many ale festivals to become friends, but I can't wait until we can properly go out and celebrate! Fran, thank you for being the best running partner, for all the fun evenings (and wine) at yours and Alun's, and for being such a great friend. I'm so glad that you moved to the Midlands, I couldn't imagine my time here without you.

Aisha, thank you for supporting me during my PhD and also when we were at Durham. I am really grateful that you are always there for me and that we can talk to each other about anything; you always know how to cheer me up. Thank you for being such an amazing friend, even when I waste all the vials and drag you to World's Strongest Man with me, here's to many more adventures!

To Tom, I don't even know how to say how grateful I am for everything you have done for me over the last four years. Thank you for keeping me sane over lockdown and being there for me when things got tough, both with the chemistry stresses and other life dramas. You know I wouldn't have made it here without you, thank you for all your help, your friendship and making my time at Warwick so memorable.

To my family, thank you for supporting me during my time at Warwick and Durham. Thank you for always being there to talk to, even if it's my fifth call of the day about food, and reminding me of what's important.

Finally, I'd like to thank my friend Sophie, who motivated me to pursue this PhD and supported me in every aspect of my life. I really wish you had got the chance to read this, I know you'd be really proud of me. Thank you for being the best friend anyone could ever ask for and making me the woman I am today.

Declaration of Collaborative and Published Work

This thesis is submitted to the University of Warwick in support of my application for the degree of Doctor of Philosophy. It has been composed by myself and has not been submitted in any previous application for any degree.

The work presented (including data generated and data analysis) was carried out by the author except in the cases outlined below:

- Crystallographic analysis of all compounds, for which solid-state structures are described, was conducted by Dr Adrian B. Chaplin, Reader, University of Warwick.
- The computational investigation of the dynamics of rhodium(I) carbonyl complexes (**20a** and **20b**, Chapter 3) was conducted by Dr Baptiste Leforestier, PhD graduate, University of Warwick.
- The computational investigation of the formation of σ-alkane complexes and geometry optimisation (Chapter 4) was performed by Dr Adrian B. Chaplin, Reader, University of Warwick.
- The low temperature NMR data (Chapter 3, Section 3) was collected by Dr Ivan Prokes, Senior NMR Technician, University of Warwick.
- The variable temperature NMR data (Chapter 4) was collected by Dr Ivan Prokes, Senior NMR Technician, University of Warwick; and Dr Matthew R. Gyton, Postdoctoral Researcher, University of Warwick.

Parts of this thesis have been published by the author:

1. G. L. Parker, S. Lau, B. Leforestier and A. B. Chaplin, *Eur. J. Inorg. Chem.*, 2019, **2019**, 3791–3798.

Abbreviations

Ar	Aryl
aq	Aqueous
biph	Biphenyl
calcd	Calculated
COD	1,5-Cyclooctadiene
COE	Cyclooctene
COSY	Correlation spectroscopy
Cy	Cyclohexyl
d	Day
DCM	Dichloromethane
DiFB	1,2-Difluorobenzene
DFT	Density functional theory
DME	Dimethoxyethane
DMF	Dimethylformamide
DMSO	Dimethylsulfoxide
dr	Diastereomeric ratio
EDTA	Ethylenediaminetetraacetic acid
ee	Enantiomeric excess
eq	Equivalents
ESI	Electrospray ionisation
FB	Fluorobenzene
FPT	Freeze-pump-thaw
GC	Gas chromatography
HMBC	Heteronuclear multiple bond correlation
HMDSO	Hexamethyldisiloxane

HMPA	Hexamethylphosphoramide
HR	High resolution
HSQC	Heteronuclear single bond quantum coherence
IR	Infrared
LR	Low resolution
Me	Methyl
MS	Mass spectrometry
MTBE	Methyl *tert*-butyl ether
m/z	Mass to charge ratio
NMP	*N*-Methyl-2-pyrrolidone
NMR	Nuclear magnetic resonance
ox	Oxazoline
Ph	Phenyl
PhMe	Toluene
py	Pyridine
Pybox	Pyridine-2,6-bis(oxazoline)
RCM	Ring-closing metathesis
rt	Room temperature
*t*Bu	Tertiary butyl
Terpy	2,2′:6′,2′′-Terpyridine
THF	Tetrahydrofuran
TLC	Thin layer chromatography
TMS	Tetramethylsilane
VE	Valence electron
VT	Variable temperature
XRD	X-ray diffraction

Abstract

Rigid tridentate pincer ligands are frequently used in organometallic chemistry and catalysis, conferring thermal stability and supporting a wide range of metal-based reactivity. Studying the coordination chemistry of alkanes is a formidable challenge in synthetic inorganic chemistry, but systems supported by pincer ligands have shown considerable promise. For instance, use of a rhodium(I) PONOP complex has enabled the synthesis and characterisation of a σ-methane derivative at low temperature. Seeking to circumvent difficulties associated with dissociation of the hydrocarbon substrate, macrocyclic rhodium systems featuring a mechanically interlocked alkyl chain are proposed to facilitate investigation of intermolecular M···H–C bonding interactions.

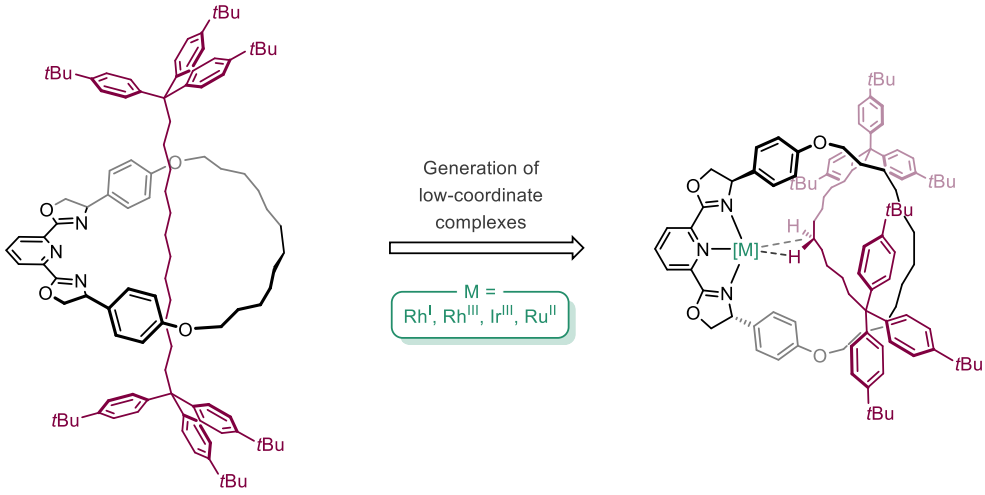

The synthesis and coordination chemistry of the pybox-based [2]rotaxane **^{R}pybox** is herein described. This novel ligand was prepared following optimisation of a reported active metal template procedure, where the interlocked architecture is captured using a nickel-catalysed C(sp^3)–C(sp^3) homocoupling reaction. Rhodium(I/III), iridium(III) and ruthenium(II) complexes of **^{R}pybox** have been investigated, supplemented by explorative work using the macrocyclic component (**^{M}pybox**) and an acyclic variant (**^{Ph}pybox**). Low coordinate cationic rhodium complexes of **^{R}pybox** could be generated using halide abstraction reactions and the presence of M···H–C interactions was probed using spectroscopic techniques.

Chapter 1: Introduction

1.1. Pincer ligands

Rigid tridentate pincer ligands are frequently used in organometallic chemistry and catalysis, they are able to confer thermal stability and can support a wide range of metal-based reactivity.[1,2] Pincer ligands are tridentate chelators that favourably bind in meridional coordination geometry, however, a more flexible backbone can accommodate a facial coordination mode.[3,4] Pincer ligands can be readily adapted, enabling the steric and electronic properties of metal derivatives to be tuned (Figure 1.1).[5] Modification typically involves straightforward changes to either the donor groups, donor substituents or the scaffold itself.[6]

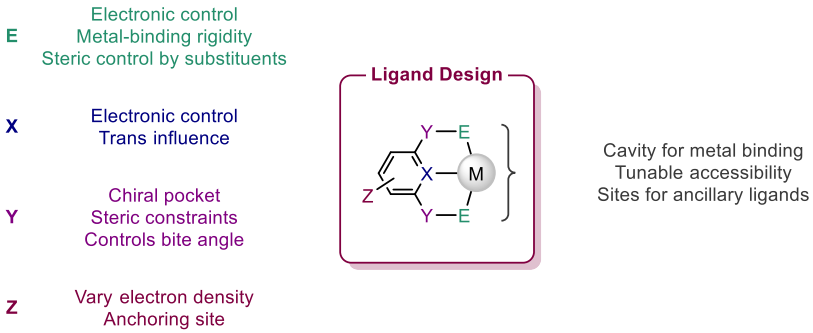

Figure 1.1. Pincer ligand design, highlighting how to tune metal-based reactivity.[7]

The earliest organometallic pincer complexes were reported in the mid 1970s by Shaw, these featured a central anionic carbon with two flanking groups (ECE).[8,9] However, it wasn't until 1989 that the 'pincer' terminology was formally introduced, generating a new ligand class.[10] The donor composition of these systems has since been expanded from the original 'ECE' to include a vast number of alternative groups, including CNC, PNP and NNN variants; many of these ligands can share the same properties as the traditional PCP or NCN-type systems.[2,5] To differentiate between types of pincers, it has recently been suggested that the terms 'palindromic' and 'non-palindromic' be used to describe symmetric and non-symmetric ligands (Figure 1.2).[1]

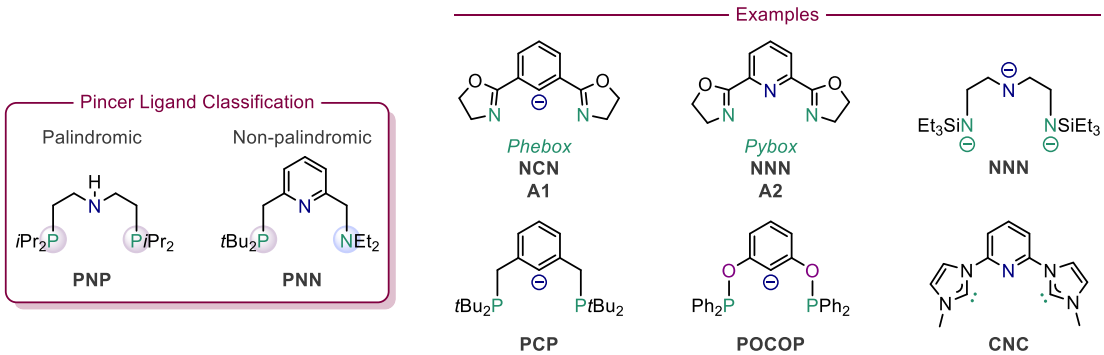

Figure 1.2. Palindromic and non-palindromic pincer ligands.

Pincer complexes have demonstrated their suitability as catalysts for a wide range of transformations, owing to their tunable nature and ability to form stable transition metal complexes.[11,12] The ability to control steric and electronic properties allows pincer ligands to be fine-tuned for specific purposes, thus enabling design of highly selective catalysts.[13,14] For example, a recent computational study on concerted metalation–deprotonation by iridium(III) complexes showed that exchanging a phebox (**A1**) for pybox (**A2**) ancillary ligand lowered the barrier for C–H activation, as a result of the increased electrophilicity of the metal centre.[15]

Dehydrogenation reactions have utilised pincer ligands to catalyse the valuable transformation from naturally abundant alkanes into important and versatile alkenes.[16] Iridium PCP pincer complexes were found to be efficient alkane dehydrogenation catalysts, first reported in 1996 (Scheme 1.1).[17,18]

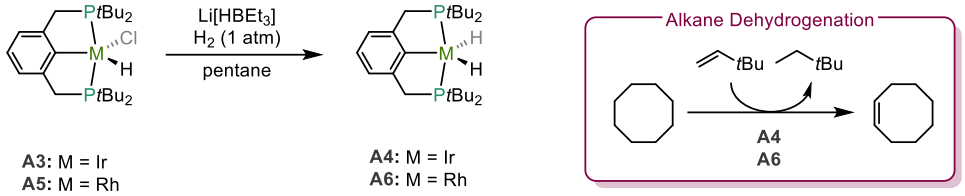

Scheme 1.1. Alkane dehydrogenation catalysed by PCP pincer complexes.

The iridium complex **A4** was synthesised from **A3** in very good yield (85%) and could effectively catalyse the transfer dehydrogenation of cyclooctane, in the presence of the sacrificial hydrogen acceptor *tert*-butylethylene (TBE).[19,20] The analogous rhodium complex **A6** was characterised by a far lower activity at 150 °C (**A6**; 0.8 turnovers/h, **A4**; 82 turnovers/h), which was attributed to the less energetically favourable oxidative addition of H_2 and C–H bonds to the rhodium centre.[21] Both the rhodium and iridium complexes demonstrated exceptional thermal stability at 150 °C with no decomposition observed over one week. The reaction scope has since been extended to other cycloalkanes including cyclohexane, methylcyclohexane as well as *n*-akanes.[22] Notably, the first example of an efficient acceptorless dehydrogenation reaction employed PCP iridium complex **A4**, under reflux conditions.[23]

Pincer complexes have been employed in the activation of small molecules; iridium complex **A9** has been used to generate a stable monomeric amido hydride complex **A10** through oxidative addition of ammonia (Scheme 1.2).[24]

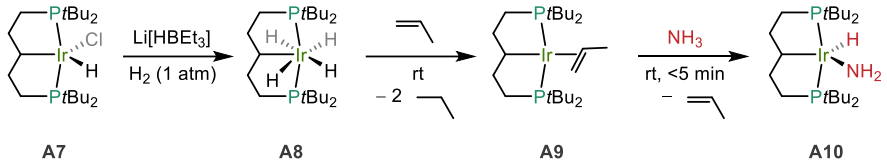

Scheme 1.2. Formation of a stable amido hydride complex *via* oxidative addition of ammonia.

The tetrahydride complex **A8** was synthesised from the hydridochloro complex **A7**, after which it was transformed to the propene complex **A9**. Treatment with ammonia yielded the amido hydride complex **A10** within 5 minutes and in excellent yield (90%), characterised by ^{1}H NMR spectroscopy, combustion analysis and X-ray diffraction. Contrary to the usual binding of ammonia, *via* the lone pair, the aliphatic PCP pincer ligand was able to create an electron rich iridium(I) centre to enable cleavage of a N–H bond and form **A10**. Interestingly, the analogous aryl PCP pincer did not form a stable amido hydride complex; above −10 °C reductive elimination of ammonia generates an iridium(I) ammonia complex.[25] This further illustrates how modifications to the pincer backbone can drastically influence reactivity.[26]

Other notable catalytic transformations include alkane metathesis and ester hydrogenation (Figure 1.3). Goldman, Brookhart and co-workers developed a tandem dehydrogenation–olefin metathesis method for alkane metathesis, which utilises iridium pincer complexes for the alkane dehydrogenation and alkene hydrogenation steps (**A11**-**A13**, Figure 1.3a).[27] As a consequence of alkene isomerisation a broad distribution of hydrocarbon chain lengths were achieved. In addition, the process was highly selective and generated linear *n*-alkanes only. A second Schrock-type catalyst was used for the olefin metathesis step, however, under the reaction conditions (125 °C) this co-catalyst decomposes over time which limited turnover. Milstein's catalyst **A14** represents an archetypal pincer complex that can catalyse the hydrogenation of esters to alcohols (Figure 1.3b).[28] The catalytic activity of the bifunctional PNN complex stems from the reversible aromatisation/dearomatisation of the pincer backbone.[29] Catalyst **A14** has also been applied to the splitting of water into dioxygen and dihydrogen, and the synthesis of amides from alcohols and amines.[30,31]

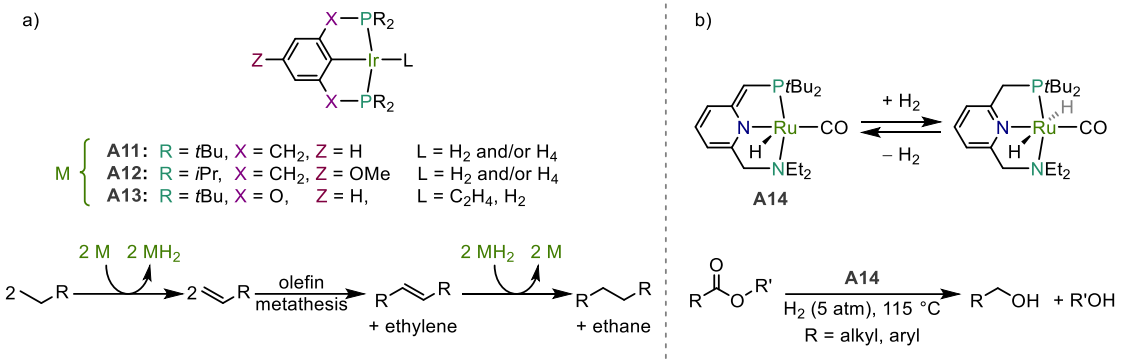

Figure 1.3. Pincer complexes used as catalysts in a) alkane metathesis, and b) ester hydrogenation.

The use of pincers as bifunctional ligands has notably enabled the application of abundant first row transition metals in dehydrogenation/hydrogenation reactions.[32] Importantly, pincer complexes have shown an exceptional thermal stability making them suitable in a huge range of catalytic applications.[33–35] Modification of the ligand framework to incorporate a chiral component can allow these systems to be further utilised in asymmetric catalysis.[36,37] To summarise, pincer ligands represent a huge area of organometallic chemistry with many successful applications in catalysis, the stabilisation of reactive metal species, activation of small molecules, and the facilitation of unusual bonding modes and reactivity.[38–41]

1.2. NNN-type pincer ligands

1.2.1. Overview

Tridentate NNN pincer ligands represent an impressive and highly successful ligand class; the structural diversity is illustrated in Figure 1.4.[42] Applications of NNN-based metal complexes include asymmetric homogenous catalysis, nickel-catalysed C(sp^3)–C(sp^3) cross-coupling reactions, and for the stabilisation of low-valent and low-coordinate complexes.[43–45] Trianionic NNN^{3-} ligands (**A15**), pioneered by Schrock and co-workers, have been successfully utilised in the molybdenum catalysed reduction of nitrogen to ammonia.[46–49] Monoanionic NNN pincers which contain a central nitrogen σ-donor, for example **A16**, **A17** and **A18**, are prolific ligands in asymmetric catalysis.[43] Pyridine-2,6-dicarboxamide (**A19**) based scaffolds have been shown to stabilise reactive species, such as high-oxidation state metal-hydroxo species, as a consequence of incorporating strongly σ-donating amide groups and protective bulky substituents.[50]

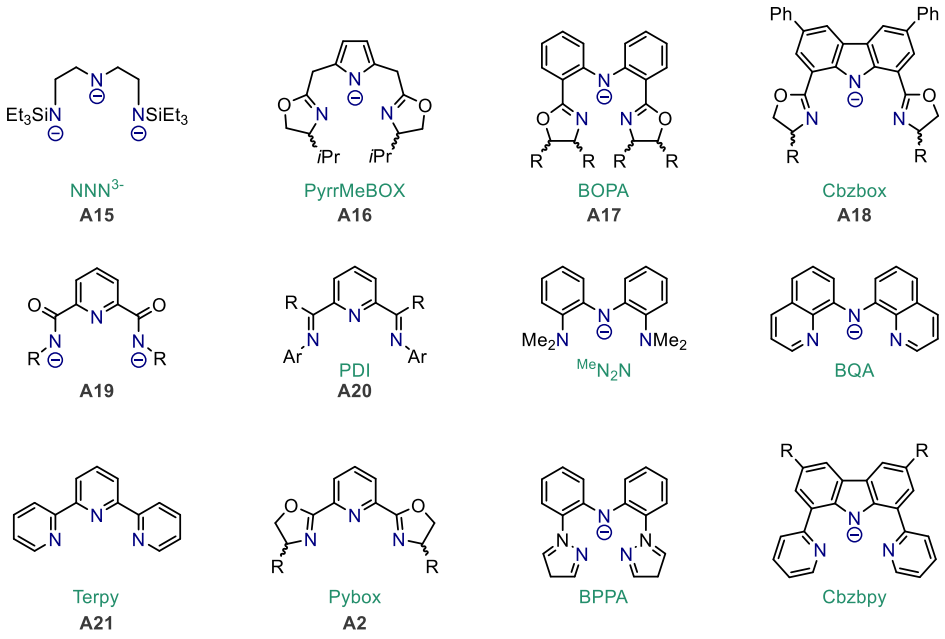

Figure 1.4. NNN pincer ligands.

Brookhart has shown that bulky bidentate α-diimine containing palladium(II)- and nickel(II)-complexes possess a high catalytic activity for the conversion of ethylene and α-olefins into high molar mass polymers.[51,52] Inspired by these results, iron(II) and cobalt(II) dihalide complexes of pyridine(diimine) pincer ligands (**A20**), containing bulky substituted arylimine moieties, have displayed excellent catalytic activity for the polymerisation of ethylene into oligomers.[53,54] With the aim to study the active catalyst for olefin polymerisation, the ruthenium(II) methyl ethylene complex **A22** was investigated as a model for the iron(II) systems (Figure 1.5).[55] The cationic complex **A22** was found to be

remarkably stable and it was unable to act as a polymerisation catalyst; the migratory insertion of ethylene into the metal alkyl is unfavourable. An isoelectronic dicationic rhodium(III) complex was also prepared, however, it did not exhibit any catalytic activity either.

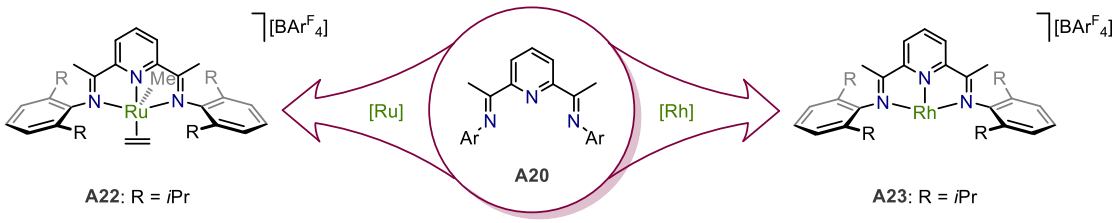

Figure 1.5. Brookhart's stable cationic ruthenium(II) complex (**A22**) and rhodium(I) complex (**A23**).

The synthesis of a stable cationic rhodium(I) complex **A23** was reported by Brookhart and co-workers through halide abstraction from the corresponding rhodium(I) chloride complex using Na[BAr$^F_4$] in dichloromethane (Figure 1.5).[45,56] The 14-electron, 3-coordinate rhodium complex could be isolated and stored indefinitely under an inert atmosphere. **A23** showed remarkable stability against the oxidative addition of dichloromethane, even when heated at 40°C, which is unusual for rhodium(I) complexes of this type.[56–58] The unusual stability was attributed to the steric environment created by the ligand which creates a protective binding pocket. When less sterically demanding *ortho* substituents were used the oxidative addition of dichloromethane was observed (R = H or Me).

However, it is important to consider that **A23** could exhibit dichloromethane binding as opposed to existing purely as the low-coordinate analogue; this is suggested by liberation of dichloromethane upon dissolving **A23** in THF-d_8 and the broadness of the ^{1}H NMR spectrum in CD_2Cl_2.[59] Stable adducts were generated upon treatment of **A23** with acetophenone or *p*-tolualdehyde and the molecular structure of the latter was characterised by X-ray crystallography, indicating η^1 coordination of the aldehyde tightly positioned in the cavity created by the bulky aryl groups. Catalytic studies demonstrated the ability of **A23** to act as a potent Lewis-acid catalyst for Mukaiyama-aldol, hydrosilylation and cyclopropanation reactions.

The π-acidic pyridine(diimine) pincer ligands have been utilised to support low-valent ruthenium(0) and iron(0) complexes, the latter could act as an effective catalyst for hydrogenation and hydrosilylation reactions.[60–64] For the purpose of ligands relevant to this thesis, only the NNN pincer ligands terpyridine (terpy) (**A21**) and pyridine bis(oxazoline) (pybox) (**A2**) will be discussed in further detail, with a focus on ruthenium, rhodium and iridium coordination chemistry.

1.2.2. Terpyridine ligands

2,2':6',2''-Terpyridine (terpy, **A21**) pincer ligands have been widely studied since the first reported synthesis by Morgan in 1932.[65] Terpy has the potential to act as a 'non-innocent' ligand, as a consequence of the co-planar pyridines which allows for good conjugation between the metal cation and the aromatic rings.[66] Applications include the stabilisation of low-valent metals such as iron, cobalt, nickel and manganese, high catalytic activity including for C–C bond forming transformations and asymmetric reactions, as well as frequent incorporation into supramolecular architectures.[67,68]

1.2.2.1. Synthesis of terpyridine ligands

The main synthetic routes to terpyridine ligands involve either condensation reactions between ammonia and a 1,5-dione (**A24**) or palladium-catalysed cross-coupling reactions, typically Stille; however, Negishi or Suzuki coupling can also be utilised (Scheme 1.3).[69–73] Introduction of an aryl moiety at the 4'-position of the central pyridyl donor has been shown to affect the photophysical properties of the bis(terpy) metal complexes; a number of high yielding routes have been developed to incorporate this functionality.[74,75] In addition, synthesis of halogen-containing terpy scaffolds like **A25** can be further utilised in palladium-catalysed cross-coupling reactions to introduce additional functionality.[76]

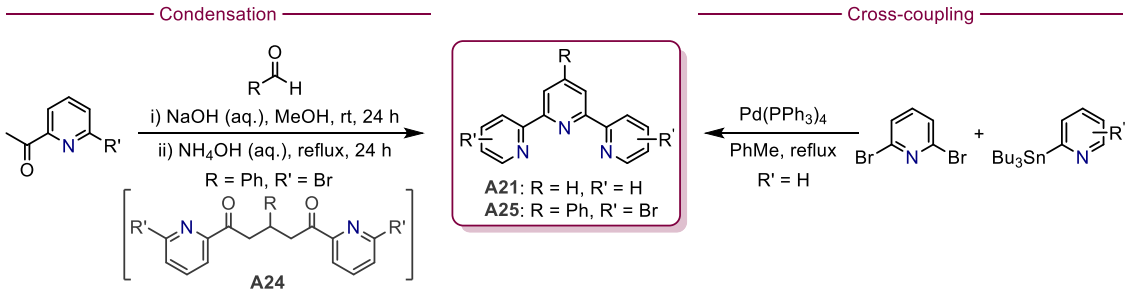

Scheme 1.3. Preparation of terpyridine ligands.[77,78]

1.2.2.2. Complexes of terpyridine ligands

Terpyridine ligands feature prominently in catalytic transformations owing to their desirable electronics (strong σ-donor and π-acceptor) which can stabilise both low and high-valent metal complexes (Figure 1.6).[79–81]

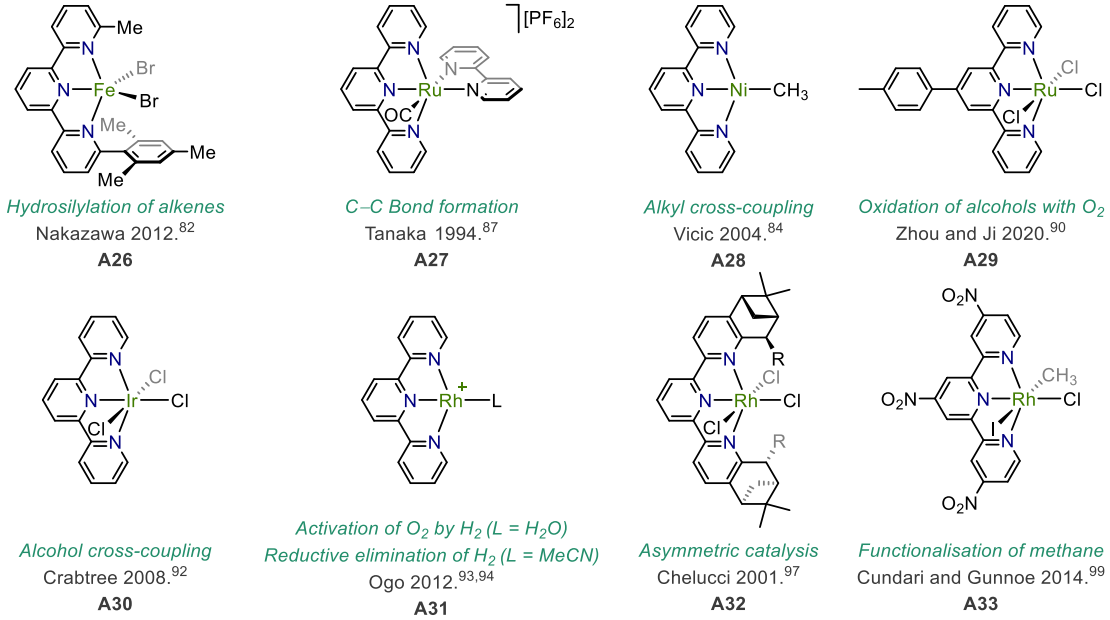

Figure 1.6. Selected terpyridine-based complexes, the relevant application(s) are indicated.

Iron terpy-based complexes appear prominently in catalytic transformations. Complex **A26** contains an asymmetric terpy-derivative, which exhibited high catalytic activity for the hydrosilylation of alkenes with hydrosilanes.[71,82] Carbon–carbon bond forming reactions have shown to be effectively catalysed by complexes **A27** and **A28**, through the electrochemical reduction of carbon dioxide, and nickel-catalysed cross-coupling of alkyl halides with alkyl nucleophiles, respectively (Figure 1.7).[83–88] Methyl transfer from **A28** to cyclohexyl iodide was observed, generating methylcyclohexane in good yield, with an absence of olefinic products which would result from *β*-hydride elimination reactions. Terpy complexes have also been shown to catalyse a number of oxidation reactions, including the oxidation of alcohols to carbonyl compounds by ruthenium(III) complex **A29** with molecular oxygen.[89–91] Crabtree has demonstrated alcohol cross-coupling reactions, between primary alcohols and secondary benzylic alcohols, which can be catalysed by terpy complexes such as the iridium(III) complex **A30**, in an air-stable system.[92]

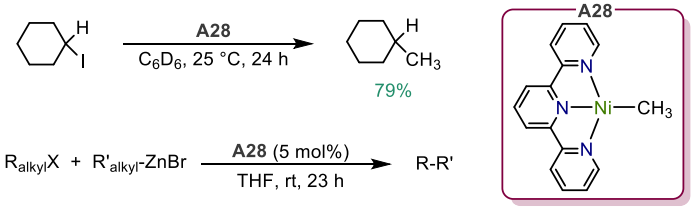

Figure 1.7. Nickel-catalysed alkyl cross-coupling reactions.

Ogo and co-workers have utilised low-valent rhodium(I) complex **A31** (L = H_2O) for the activation of O_2 by H_2 in water, a process which involves a rhodium(III) peroxo intermediate, and for the reductive elimination of H_2 from a rhodium(III) monohydride species generated *in situ* by treatment of acetonitrile complex **A31** (L = MeCN) with triflic acid.[93,94] Rhodium complexes have been further employed in catalytic transformations including the asymmetric cyclopropanation of styrene with diazoacetates and hydrosilylation reactions through use of complex **A32**.[95–98] Gunnoe and co-workers have shown how electronics of the terpy scaffold influences the reactivity of rhodium(III)–CH_3 complex **A33**, by introduction of electron-withdrawing nitro substituents, which facilitate reductive elimination of alkyl halides.[99,100] These examples set a precedent for stabilisation of the $Rh^{I/III}$ couple through use of terpy NNN ligands.

1.2.3. Pyridine-bis(oxazoline) ligands

1.2.3.1. Synthesis of pyridine-bis(oxazoline) ligands

First synthesised in 1989 by Nishiyama, pyridine-2,6-bis(oxazoline) (pybox, **A2**) ligands are C_2-symmetric 'NNN' pincer ligands.[101] Pybox ligands are typically synthesised by reactions of chiral 1,2-aminols, or amino acids, with either pyridine-2,6-dicarbonyl dichloride (Method A) or 2,6-dicyanopyridine (Method B, Scheme 1.4).[102] Pybox metal complexes can be tuned to achieve a high asymmetric induction through modification of the substituent at the *para*-position of the pyridine moiety, to control the electronics, and sterically through variation of the oxazoline donors to create a chiral reaction site.[103–106]

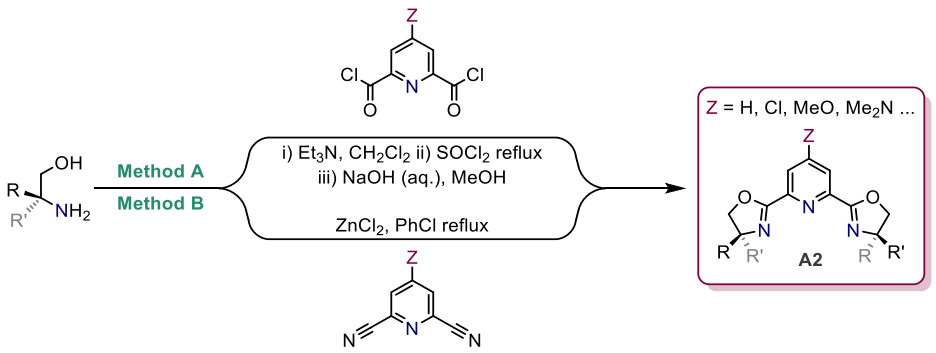

Scheme 1.4. Synthesis of pybox ligands.

1.2.3.2. Complexes of pyridine-bis(oxazoline) ligands

Transition metal complexes containing enantiopure pybox ligands have been shown to catalyse a number of asymmetric reactions including Mukaiyama-aldol reactions, iron-catalysed hydrosilylation of ketones, and ruthenium-catalysed cyclopropanation of olefins with diazoacetates.[102,107–109] Although many of the reported asymmetric syntheses involve generation of the active catalysts *in situ*, through reaction of the pybox ligand with a metal

precursor, a number of examples in which the complex is preformed and utilised as an active catalyst have been demonstrated (Figure 1.8).[110–113]

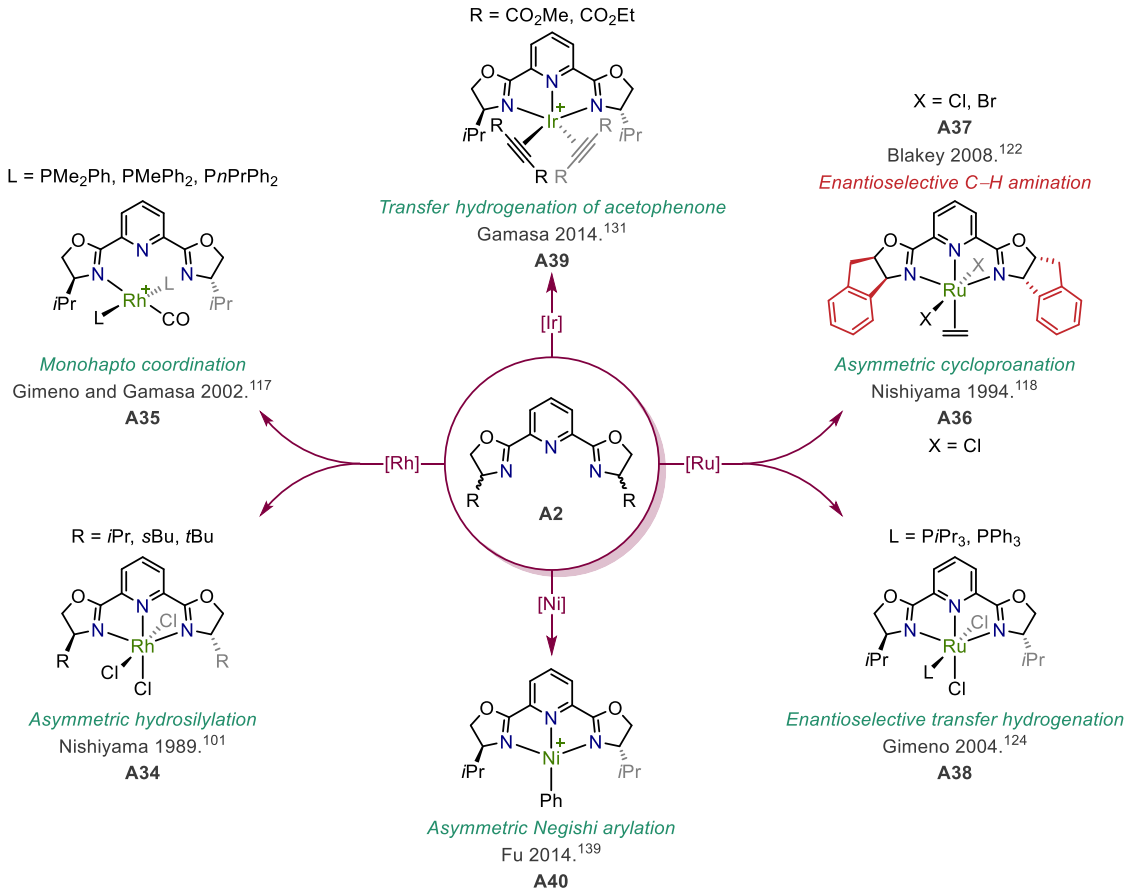

Figure 1.8. Selected pybox metal complexes, notable applications are shown. Counter anions omitted for clarity.

Seminal work by Nishiyama introduced the pybox ligand as a new chiral tridentate ligand.[101] Rhodium(III) pybox complexes (**A34**), synthesised through treatment of pybox with $[RhCl_3(H_2O)_3]$, were found to be highly enantioselective catalysts for the asymmetric hydrosilylation of ketones, as well as for the enantioselective hydrosilylation of methyl ketone derivatives.[114] Several other rhodium(III) pybox systems have been reported by the groups of Nishiyama and Gimeno.[58,115,116] These were obtained through oxidative addition reactions, either through addition of alkyl chlorides to yield stable (alkyl)rhodium adducts or through addition of allyl or acyl chlorides to yield organorhodium(III) complexes suitable for asymmetric hydrosilylation of acetophenone. Gimeno and co-workers established pathways to the first rhodium(I) pybox complexes; formation of **A35** was achieved *via* addition of monodentate phosphines to the rhodium(I) pybox carbonyl complex.[117] **A35** exhibited unusual monodentate coordination of pybox in the solid-state, as confirmed by X-ray crystallography.

The *i*Pr-pybox ruthenium(II) ethylene complex **A36** was shown to be an efficient asymmetric catalyst for the cyclopropanation of olefins with diazoacetates and as a catalyst for olefin polymerisation in the presence of a cocatalyst (Figure 1.9).[118–120] Enantioselective C–H amination using similar dihalide ruthenium(II) pybox catalysts (**A37**) was reported by Blakey; the use of a sterically bulky indenyl-pybox was found to confer the highest activity.[121,122] Transformation of ethylene complex **A36** into ruthenium(II) phosphine complexes (**A38**) was reported by Gimeno.[123,124] The dichloride complexes were found to be highly enantioselective catalysts for the transfer hydrogenation of ketones; the *cis* complexes possessed the highest activities capable of near quantitative conversions and up to 95% *ee*.

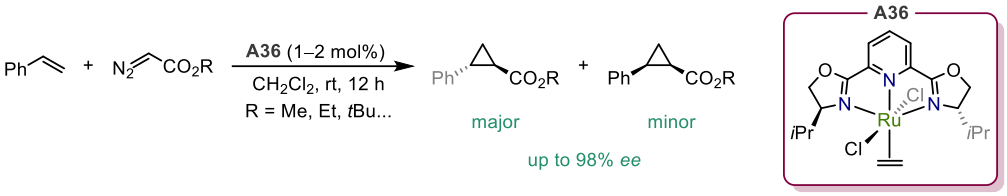

Figure 1.9. Asymmetric cyclopropanation of olefins.

Iridium complexes bearing enantiopure pybox ligands are prominent in asymmetric catalysis.[125,126] Early work by Gamasa and co-workers focused on the reactivity of bis(ethylene) complexes of iridium(I), specifically substitution and oxidative addition reactions.[127–130] Replacement of the ethylene ligands with acetylenedicarboxylate derivatives yielded **A39**, which were utilised as catalysts for the asymmetric transfer hydrogenation of acetophenone in up to 70% *ee*.[131]

Nickel-catalysed C–C cross-coupling reactions are generally less understood than the related palladium processes.[132] The groups of Fu, Vicic and many others have considerably expanded this field through establishment of nickel-catalysed methodology for Negishi cross-couplings.[86,133–136] These cross-coupling reactions typically utilise nickel pybox catalysts, however, the active species are generally generated *in situ*.[137,138] Pybox ligands have been shown to form effective catalysts for the Negishi coupling of unactivated alkyl halides, whereas phosphines and carbene ligands have failed to produce any coupled product.[135,138] Further to this, the pybox scaffold has been shown to prevent *β*-hydride elimination during the coupling procedure. A recent mechanistic investigation by Fu showed that the nickel(II)–pybox complex **A40** played a key role in Negishi arylations of propargylic bromides and was likely the predominant nickel complex under the catalytic conditions.[139]

1.2.4. Outlook

Pincer ligands have remained at the forefront of coordination chemistry with numerous successful applications in homogenous catalysis.[1] Macrocyclic variants have also been developed and found notable application in the synthesis of mechanically interlocked compounds, as well as in catalysis and as chemical sensors.[140–144] The following section will focus on the synthesis of interlocked architectures, particularly metal-templated methods which exploit macrocyclic ligands.

1.3. Interlocked molecules

1.3.1. Overview

Synthetic routes for the generation of mechanically interlocked molecules have considerably advanced since the first documented statistical threading method of a [2]catenane by Wasserman in 1960 (<1% yield).[145] Through coordination-based preorganisation of components, passive metal template approaches have enabled the preparation of catenanes in near quantitative yield.[146,147] Notable recent developments also exploit metal-based reactivity to capture the interlocked topology. These so called 'active metal template' methods have primarily been applied to the synthesis of rotaxanes. Square brackets are used to describe the number of components involved in the interlocked structure; a [2]catenane consists of two interlocked rings, and a [2]rotaxane consists of one macrocycle with one axle component (Figure 1.10).[148]

[2]catenane [3]catenane [2]rotaxane [3]rotaxane

Figure 1.10. Interlocked molecule nomenclature.

1.3.2. Rotaxanes

1.3.2.1. The first rotaxanes

Rotaxanes are mechanically interlocked molecules which feature a macrocycle component threaded with an axle terminated by bulky stopping groups which prevent separation of the two components. Originally coined 'hooplane', the first recorded synthesis of a rotaxane was in 1967 by Harrison *et al.* (Scheme 1.5).[149] The synthesis utilised a column of a resin-bound acyloin-based macrocycle **A41**, which underwent repeated treatment with a solution of decane-1,10-diol and triphenylmethyl chloride to form the interlocked species through S_N1 bistritylation reactions (6% yield with 70 treatments of the column). Hydrolysis of rotaxane **A42a** from the resin was achieved by reflux with sodium bicarbonate in methanol to give **A42b**. The product **A42b** was purified by column chromatography and found to be stable up to 200 °C. Confirmation of the threading was achieved through analysis of the degradation products.

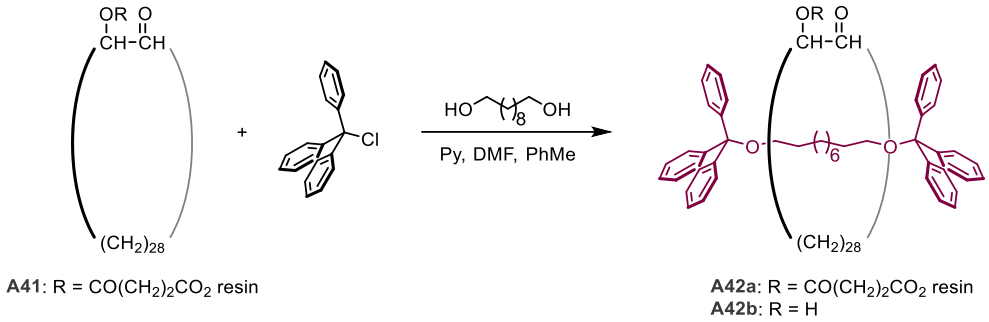

Scheme 1.5. Harrison's rotaxane synthesis.

The term 'rotaxane' was introduced the same year by Schill *et al.* whose synthetic pathway focused on an entirely different concept to Harrison: the macrocycle and axle were threaded to afford **A43** through a series of intramolecular reactions, as opposed to Harrison's intermolecular threading (Scheme 1.6).[150–152] This was followed by S_N2 reactions to attach bulky stopper groups to both ends of the thread to generate **A44a/b**, after which several further reactions were necessary to cleave the axle and macrocycle to yield interlocked rotaxanes **A45a/b** (41/46% overall yield). However, both Schill and Harrison's preparations left much to be desired in terms of synthetic simplicity and practical overall yields.[153]

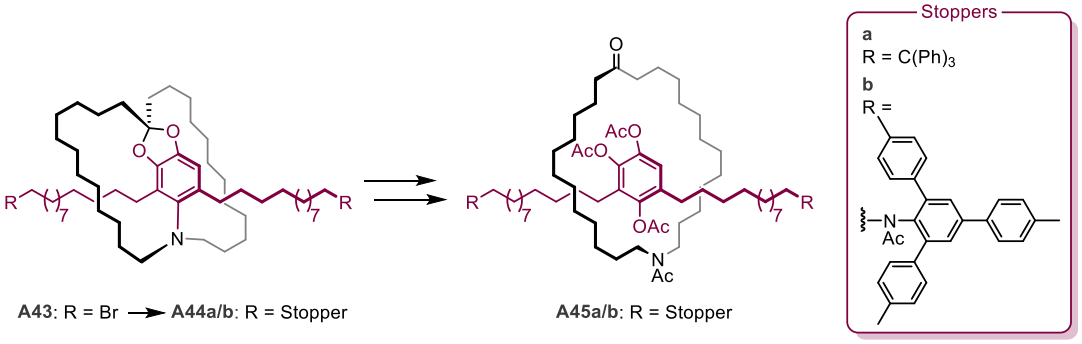

Scheme 1.6. Schill's rotaxane synthesis.

1.3.2.2. Active metal template methods

Synthetic routes for the generation of mechanically interlocked molecules have considerably advanced since the first documented statistical threading method of a [2]rotaxane by Harrison *et al.* in 1967.[149] Active metal template synthesis methods are at the forefront and exploit metal-based reactivity to couple two threads through the annulus of a coordinated macrocyclic ligand. A requirement of this procedure is the presence of coordinating heteroatoms in the macrocyclic component, typically nitrogen donors. Methods of this type frequently result in the incorporation of a new functional group into the axle, for example triazole functionality from CuAAC cycloaddition reactions; or the generation of unsaturated cumulene (**A46**) or polyyne (**A47**) axles from Glaser coupling (Figure 1.11).[154,155,156]

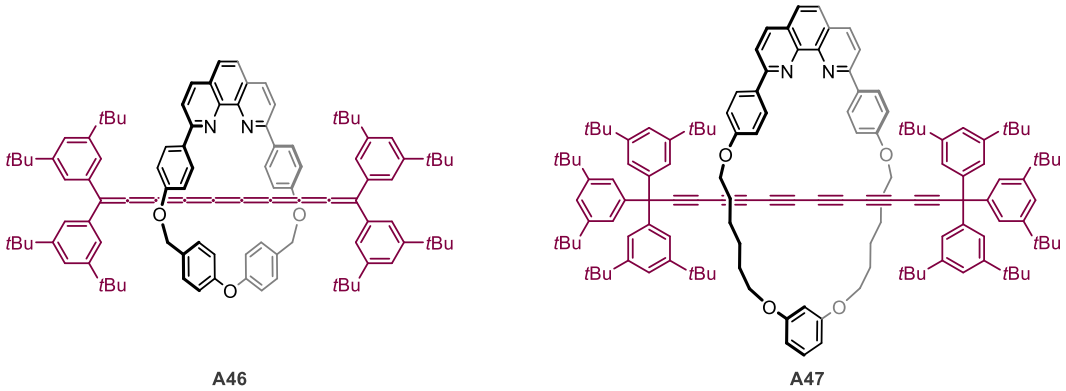

Figure 1.11. Phenanthroline-based rotaxanes with hydrocarbon axles: **A46** with a [9]cumulene axle,[154] and **A47** with polyyne axle.[155]

Active metal templates are capable of generating interlocked molecules in very high yields. For example, a method by Leigh based on nickel–copper-mediated alkyne homocoupling through a bidentate macrocyclic ligand, produced bis-acetylene threaded rotaxanes in yields of up to 95%.[157] Similarly, Goldup *et al.* have attained excellent yields of oligo[*n*]rotaxanes through use of an iterative synthesis (67% yield for [6]rotaxane **A48**, Scheme 1.7).[158] By utilising click chemistry, a number of high yielding active templated copper-mediated alkyne–azide cycloadditions (AT-CuAAC) are used to form a series of mechanical bonds (>90% yield per mechanical bond). Controlled by the use of an acetylene protecting group, the synthesis of a specific precision-engineered oligomeric rotaxane is achievable.

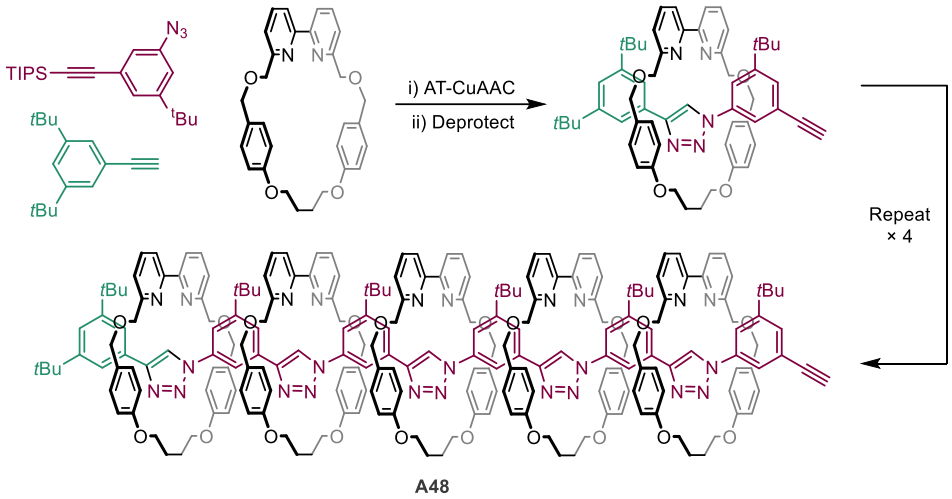

Scheme 1.7. Iterative [6]rotaxane synthesis by Goldup.

The recent emergence of 'impossible' rotaxanes, those that bear an axle with no feasible retrosynthetic disconnection, *via* the typical active template coupling methods have fuelled research into structurally-minimalistic interlocked systems.[159–161]

1.3.2.3. Nickel-catalysed pathways to rotaxanes

Leigh *et al*. found nickel to be an effective catalyst for the active template synthesis of [2]-, [3]- and [4]rotaxanes through C(sp^3)–C(sp^3) homocoupling of unactivated alkyl bromides through use of pybox or terpy-based macrocycles.[160,162,163] Use of bulky triaryl stoppered bromides (*viz.* **A49**) generated an alkyl-based axle upon reductive elimination. These are some of the earliest successful demonstrations of catalytic active metal template rotaxane synthesis, enabling threading of multiple axles through a single macrocycle.[162] It was found that macrocycle size and axle length play an important role on the system. De-threading can occur if the macrocyclic cavity is too large, however, conditions can be optimised to favour the chosen interlocked products.[163]

The development of methodology by Leigh began with the establishment of an active metal templated synthesis of a pybox-based [2]rotaxane (Scheme 1.8). Nickel-catalysed C(sp^3)–C(sp^3) homocoupling was utilised to couple unactivated alkyl bromides through the macrocyclic cavity.

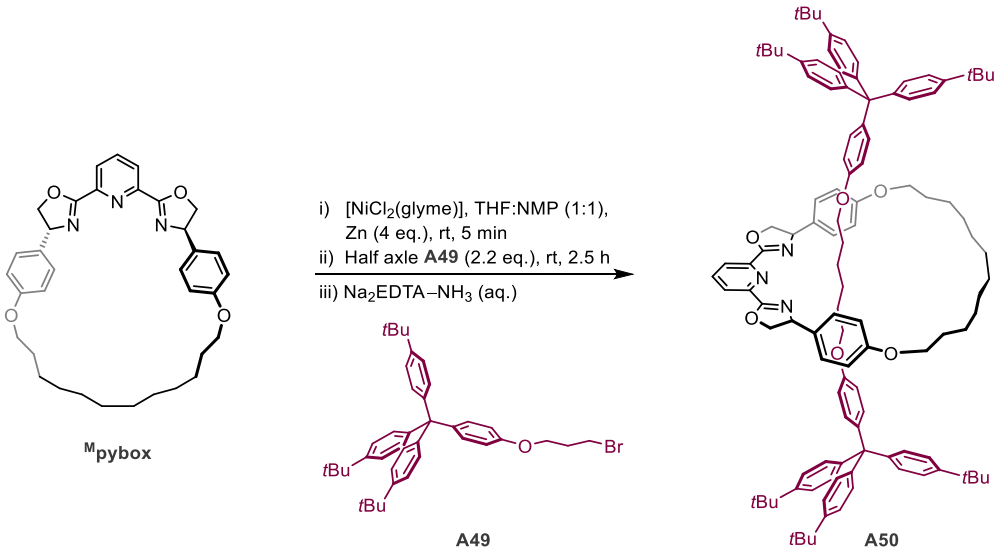

Scheme 1.8. Pybox-based [2]rotaxane **A50**; synthesised by nickel-catalysed C(sp^3)–C(sp^3) homocoupling.

Attempting to exploit Negishi coupling Leigh was able to produce [2]rotaxane **A50** in modest yield (24%).[164] Optimisation of the reaction conditions allowed an almost doubling in yield (46%). Using 1-bromo-3-phenoxypropane as a model, it was found that the acyclic pincer ligands (*R*,*R*)-Ph-pybox and terpy afforded the highest conversions to the homocoupled product (93% and 86% respectively; THF:NMP at room temperature with 5 mol% catalyst loading). Monodentate pyridine and bidentate 2,2'-bipyridine ligands yielded almost no homocoupled product under these conditions (<5%), which further reinforced the need for incorporation of a rigid tridentate pincer scaffold into the macrocycle component.[86]

The proposed homocoupling mechanism is depicted in Figure 1.12. The nickel(II) precatalyst was generated *in situ* by reaction of [$NiCl_2$(glyme)] with the pybox ligand, and then reduced with activated zinc. Sonication was used to increase the solubility of the complex and generate the active [Ni^0] catalyst, as indicated by a colour change from green to dark purple. Oxidative addition of the alkyl bromide (R–Br) generated [Ni^{II}](R)(X), which was subsequently reduced to a species of the form [Ni^{I}](R) that is able to activate a second equivalent of alkyl bromide and form [Ni^{III}](R)(R)(X). Isomerisation to a *cis* geometry and reductive elimination produces the homocoupled alkyl product (R–R) and [Ni^{I}](X), which can be reduced back to [Ni^0] by zinc and the catalytic cycle can restart.[83] This mechanism is similar to a number of other accepted nickel-catalysed couplings, including Kochi's coupling of aryl halides to form biaryls and Weix's reductive cross-coupling of aryl halides with alkyl halides.[165–167]

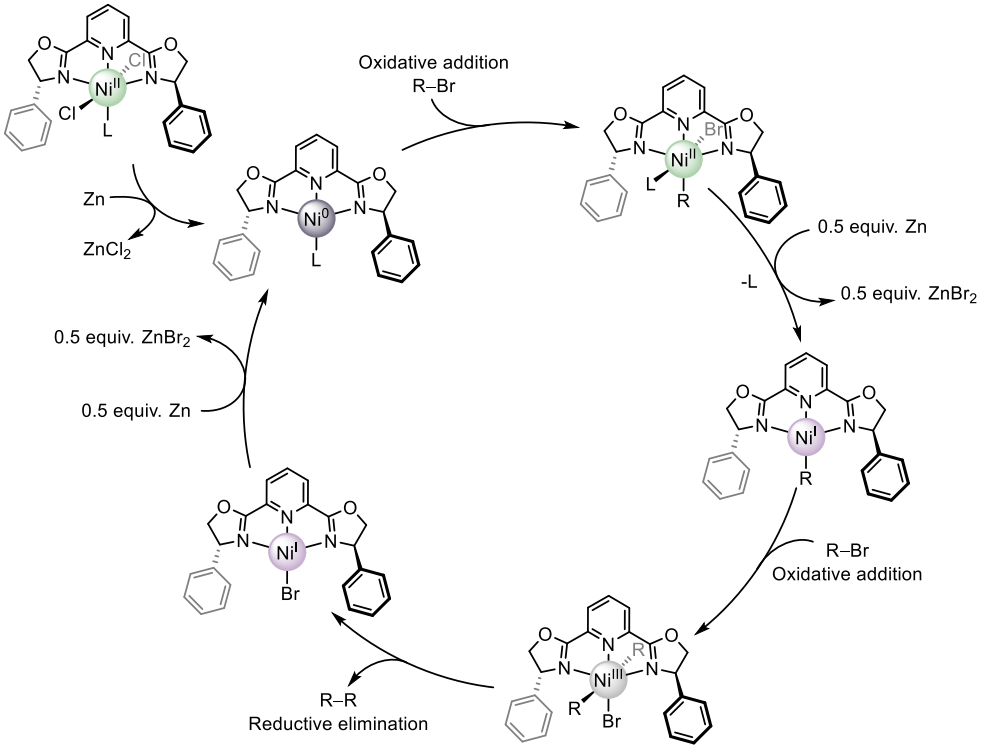

Figure 1.12. Leigh's proposed mechanistic homocoupling pathway, L = solvent donor, R = alkyl. The acyclic pybox ligand is shown for clarity, [2]rotaxane **A50** formation will employ pybox-based macrocycle **^{M}pybox** and half axle **A49** (for rotaxane synthesis R = $(CH_2)_3OC_6H_4C(t\text{Bu})C_6H_4)_3$).

The same methodology has been used to synthesise [2]- and [3]rotaxanes containing the 2,2′:6′,2″-terpyridylmacrocycle **A51** in a one-pot procedure (Scheme 1.9).[162] Crystal structures of both rotaxanes were obtained; it was the first time a one-ring-two-thread [3]rotaxane structure had been characterised in the solid-state.

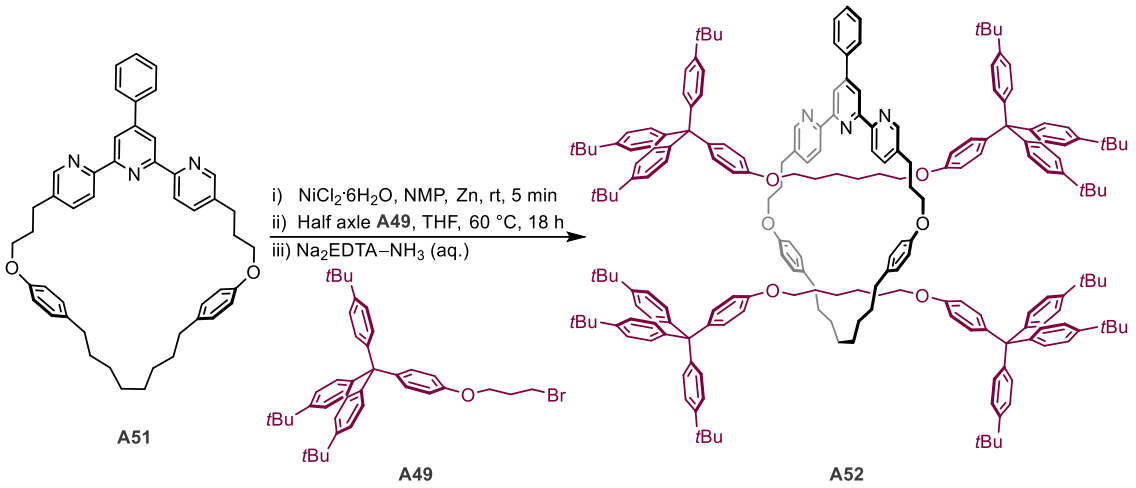

Scheme 1.9. Synthesis of [3]rotaxane **A52**, the [2]rotaxane was also generated through this route.

Terpy macrocycle **A51** was used over the pybox-based variant **^{M}pybox**, due to the instability of the pybox moiety which is prone to decomposition.[160] The 35-membered macrocyclic ring contained an endotopic binding site which was able to sequentially thread 2 axles to make **A52** in good yields, up to 51% when 20 equivalents of **A49** were used in the homocoupling reaction. Interestingly, when only 5 equivalents of **A49** were employed, a 48% yield of the analogous [2]rotaxane was formed with only trace **A52** (9%).

More recently, the syntheses of several triply-threaded [4]rotaxanes (**A54**) has been achieved using the one-pot nickel-catalysed C(sp^3)–C(sp^3) homocoupling procedure (Scheme 1.10).[163] The effect of the half axle length and macrocycle size were both investigated.

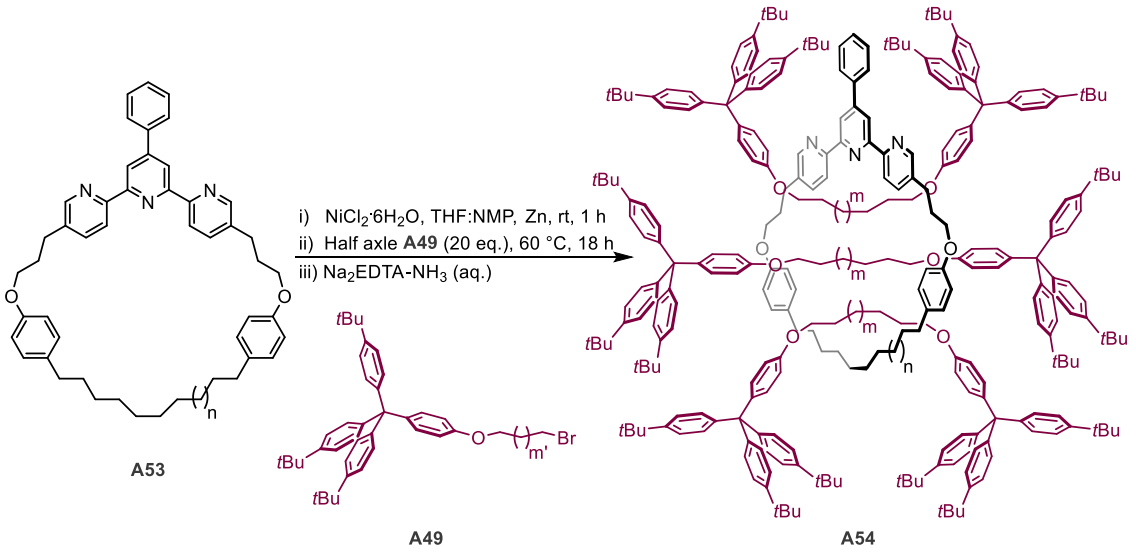

Scheme 1.10. Synthesis of [4]rotaxane **A54** through nickel-catalysed homocoupling (n = 1, 2, 3; m' = 1, 4, 10; m = 1, 7, 19). [3]Rotaxane products also obtained through this procedure.

Surprisingly, no singly threaded [2]rotaxane was isolated. This was attributed to the larger macrocyclic size (*cf*. **A51**, 35-membered ring), which allowed the axle to slip through the cavity of **A53**. However, the nickel [2]rotaxanate must be an intermediate in the generation of [3]- and [4]rotaxanes, with coordination of the nickel and interpenetration of the thread reducing the cavity size. After purification by size-exclusion chromatography [3]- and [4]rotaxanes were isolated in yields of approximately 20% and <10% respectively, as well as a significant amount of macrocycle **A53**, credited to the dethreading of intermediate nickel [2]rotaxanate upon removal of the metal template during the workup. It was found that increasing the half axle alkyl chain length had little effect on the yield and distribution of [3]- and [4]rotaxanes, showing that the steric congestion from the thread had no effect on the homocoupling reaction. Rotaxanes obtained from 37- and 38-membered macrocyclic rings showed similar yields. The 39-membered ring, however, showed no conversion to any interlocked products, which suggests that the ring is too large to keep the first homocoupled axle from slipping out of the cavity, even when coordinated to the nickel metal centre.

Leigh's homocoupling methodology has a wide range of potential uses, both in the synthesis of mechanically interlocked molecules and more generally for organic syntheses. For example, similar methodology has recently been applied for the synthesis of natural products chimonanthine and folicanthine.[168] In addition, a similar nickel-catalysed active template $C(sp^3)$–$C(sp^3)$ coupling procedures for the synthesis of bipyridine-based rotaxanes has recently been developed by Leigh.[161] It employs alkylzinc reagents and redox-active esters to create unsymmetrical axle containing [2]rotaxanes in yields up to 56%.

1.3.3. Catenanes

Catenanes are mechanically interlinked cyclic molecules which attract considerable contemporary interest, especially in the context of synthetic molecular machines.[169] Like rotaxanes, square brackets are used to describe the number of interlocked components involved, for example a [2]catenane consists of two interlocked rings. Catenanes are typically prepared using passive or active metal template methods, but π–π stacking and donor-acceptor interactions have also been exploited.[170,171]

1.3.3.1. The first catenanes

It was not until 1960 that the first catenane was successfully synthesised by Wasserman, albeit in extremely low yield (<1%, Figure 1.13).[145,172] The [2]catenane **A55** was generated by statistical threading of a diester through a macrocycle, during an acyloin condensation.

To overcome the limitations associated with statistical methods a covalent-bond-directed synthesis by Schill and Lüttringhaus was subsequently applied to the synthesis of both [2] and [3]catenanes.[173–175] Catenane **A56** was the first catenane composed exclusively of unbranched rings and was characterised by NMR spectroscopy, mass spectrometry and combustion analysis.[153,176,177] In addition, polymethlyene catenane **A57** containing 28- and 46-membered rings was synthesised by Schill and remains the only example of an unbranched and saturated all-hydrocarbon catenane.[178]

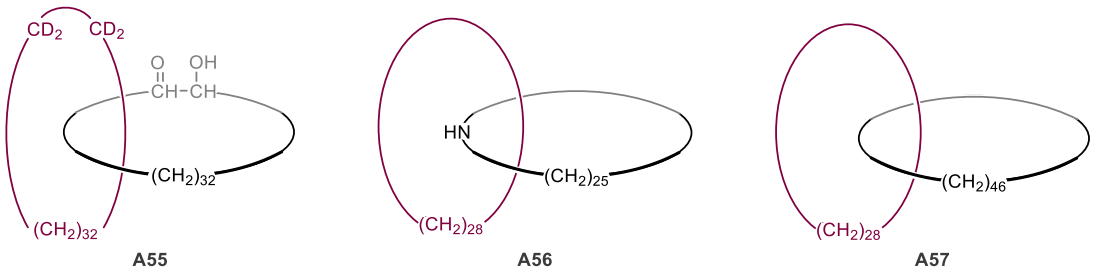

Figure 1.13. Wasserman's [2]catenane **A55**, Schill's [2]catenanes **A56** and **A57**.

1.3.3.2. Passive metal template synthesis of catenanes

The pioneering work of Sauvage introduced the use of a metal template to prepare interlocked structures, which allowed for increased yields and shorter synthetic procedures (Scheme 1.11).[146,147] The macrocyclic and acyclic catenane components were assembled in to the required geometries by coordination to a copper(I) centre, affording the catenate product **A58** following 'clipping' *via* Williamson ether macrocyclisation reactions (threading and clipping 42%; double clipping 27%). Reaction with tetramethylammonium cyanide in an acetonitrile–water (1:4) mixture successfully liberated free [2]catenane. However, both potassium and sodium cyanide salts showed a poor affinity to demetalate the catenate due to the coordination of the alkali metal cation. This synthetic route can be extended to generate doubly interlocked [2]catenanes.[179]

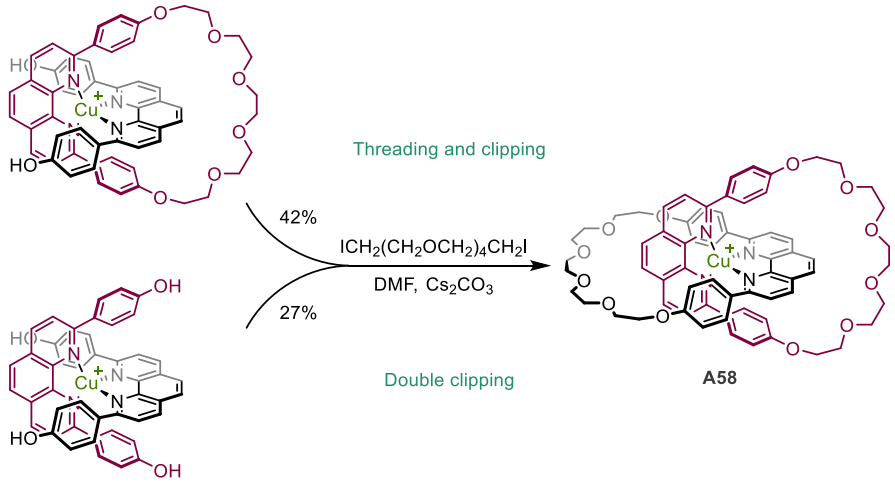

Scheme 1.11. Synthesis of catenate **A58**, counter ions omitted for clarity.

Remetalation of **A58** with transition metals resulted in the stabilisation of low oxidation states as a result of the macrocyclic environement.[180] Compared with the acyclic open-chain analogues (2,9-diphenyl-1,10-phenanthroline, dpp), the catenates demonstrated increased stability due to restricted dissociation of the ligands. Complexes of Zn(II), Cd(II), Li(I), and Ni(II) were found to be stable in the solid-state, however, the corresponding acyclic species could not be isolated. Although the reduction potentials of acyclic and interlocked complexes were found to be similar, the kinetic stability of the reduced catenate to dissociation or reoxidation was found to be greater than the corresponding acyclic variant.

Improved catenane yields could be achieved by use of Grubbs-catalysed ring closing metathesis (RCM) to capture the interlocked topology in near quantitative yield (*viz.* **A59**, Scheme 1.12).[181,182] Catenates generated through RCM contain mostly *trans* configured double bonds, the most energetically favourable isomer.

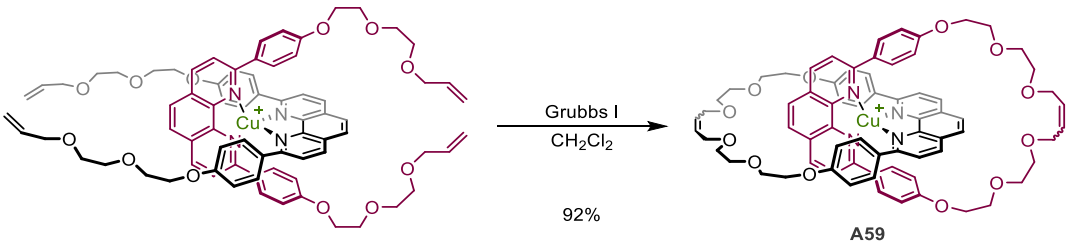

Scheme 1.12. Catenate generated through ring closing metathesis. Counter ions omitted for clarity.

1,10-Phenanthroline-based catenanes can also be prepared through oxidative coupling of terminal acetylenes, using Glaser coupling.[183] This synthetic route can also be exploited for the synthesis of multi-ring catenates, up to a [7]catenate.[184] Diyne-based catenanes can be subjected to remetalation with Ag(I), Zn(II), Co(II) or Ni(II) to generate symmetrical bimetallic [3]catenates.[185]

1.3.3.3. Octahedral complex templated catenane synthesis

Although uncommon, octahedral metal templates have been used to prepare interlocked architectures, including catenanes in good yields.[186] Removal of the metal template can be problematic and require special conditions, such as changing the oxidation state of the metal or transformation of the ligand binding motif.[187–192] Examples of octahedral templated catenates are depicted in Figure 1.14. However, removal of the metal template from these terpyridine-based catenates **A60** and **A61** was not reported.[187,193,194]

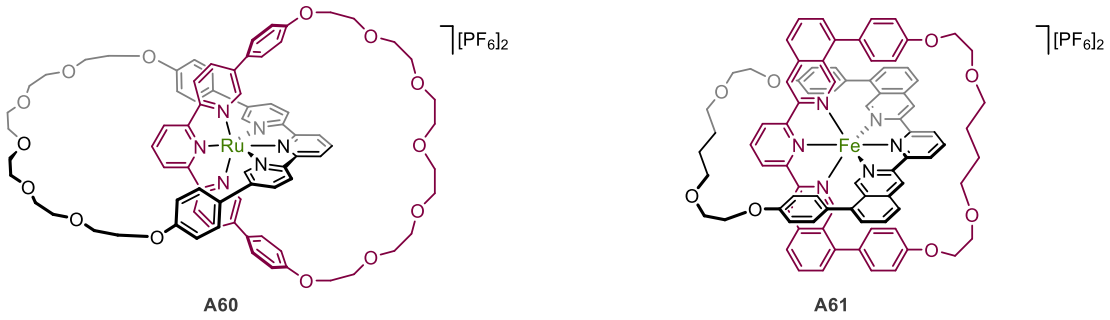

Figure 1.14. Sauvage's octahedral templated catenates.

Catenane **A62**, a notable example relevant to this thesis, was prepared by Leigh (Scheme 1.13).[190] The system is based on neutral pyridine-2,6-diimino pincer ligands that favour orthogonal *mer* coordination to M(II) centres (M = Mn/Fe/Co/Ni/Cu/Zn/Cd/Hg). Alkene metathesis was employed to capture the interlocked structure. The metal template could not be removed by reaction with excess disodium EDTA, but reduction of the imine groups with sodium borohydride followed by washing with aqueous disodium EDTA liberated the free amine catenane **A62**. A related pyridine-2,6-diimino-based [2]rotaxane has been synthesised through similar methodology.[195]

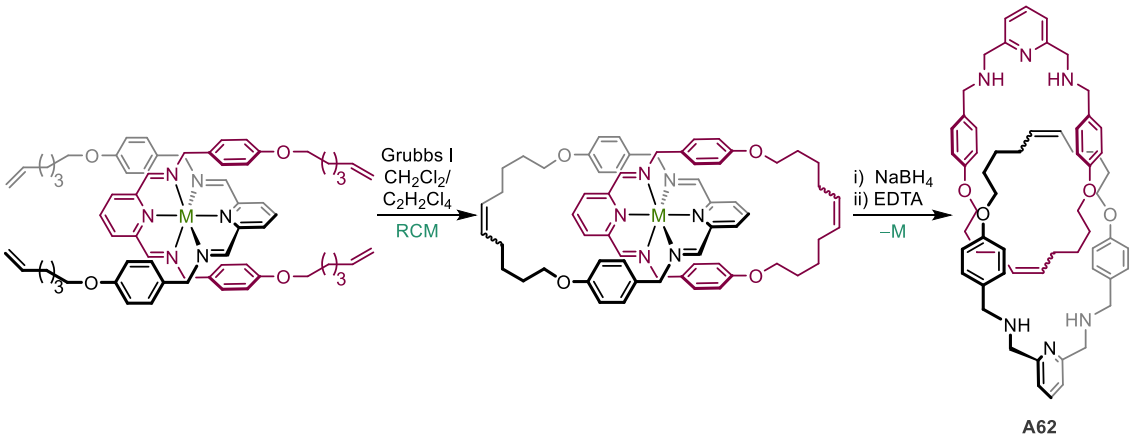

Scheme 1.13. Synthesis of benzylic imine catenane **A62**,
M(II) = Mn/Fe/Co/Ni/Cu/Zn/Cd/Hg, counter ions omitted for clarity.

1.3.3.4. Active metal template synthesis of catenanes

In the last decade several active metal template methods have been extended to the synthesis of catenanes (*viz*. **A63**).[196] Reaction manifolds include copper-based azide-alkyne cycloaddition (CuAAC) reactions, known for their mild conditions and high yielding nature, palladium- and copper-catalysed alkyne couplings (Scheme 1.14), and palladium-catalysed Heck couplings.[197–199]

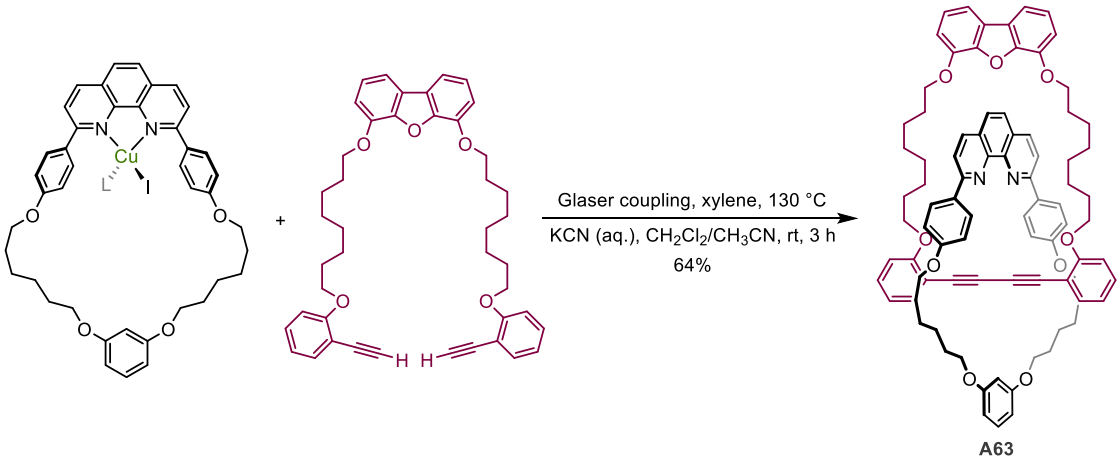

Scheme 1.14. Synthesis of [2]catenane **A63** through Glaser coupling.

1.3.4. Interlocked molecules as ligands

Metals are frequently used in the synthesis of interlocked systems, either as templates or through incorporation of a metal complex into the component parts to form hybrid metallo-supramolecular systems (*i.e.* using a metal complex as a stopper group).[200–203] Furthermore, molecular switches and machines have exploited the coordination ability of interlocked molecules, often containing several metal binding sites, to achieve mechanical motion through a number of different stimuli.[204–210] However, the coordination chemistry of metal-free rotaxanes and catenanes has been relatively unexplored.

The Sauvage catenane **A64** was used as a 'homoleptic' bis-phenanthroline ligand to investigate how the interlocked-topology affected kinetics and the stability of metal complexes (Figure 1.15).

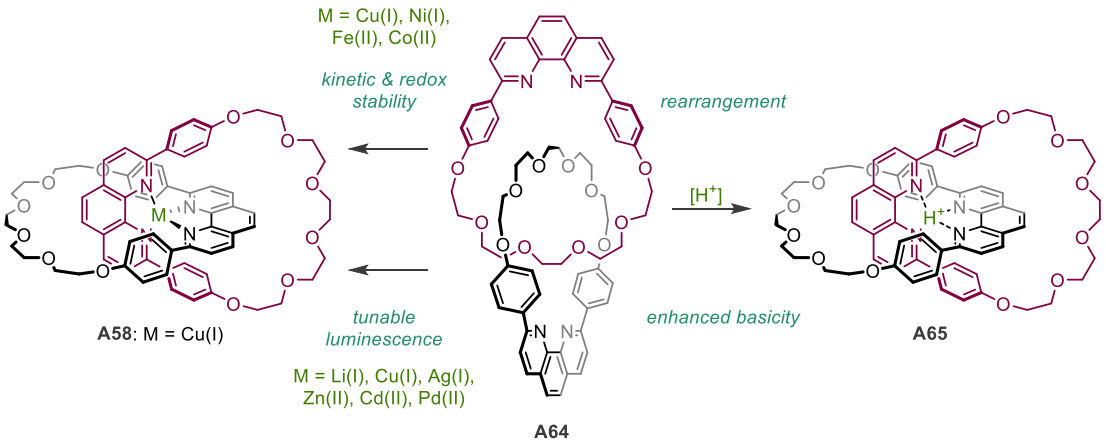

Figure 1.15. Sauvage catenane systems, which demonstrate the catenand effect.

The demetalation of copper(I) catenate **A58** by cyanide anions proceeds considerably slower than the analogous acyclic and monocyclic complexes and is attributed to a kinetic catenand effect, whereby **A58** is stabilised due to the interlocked topography.[211] Metalation of free catenane **A64** with nickel nitrate proceeded slowly to yield the

nickel(II) catenate complex in good yield (48 hours, room temperature; 70% yield).[212] This could then be electrochemically reduced to form a nickel(I) complex which displayed exceptional redox stability, compared with an acyclic analogue, again attributed to the interlocked ligand. Further studies with catenane **A64** showed that it could kinetically stabilise low oxidation states of several other transition-metals.[180] Remarkably, in the case of iron(II) and cobalt(II) the corresponding M(III) species could not be attained. Furthermore, the absorption and emission properties of **A64** are substantially influenced by coordination of metal ions or protonation.[213] Interestingly, monoprotonated catenate **A65**, generated through treatment with perchloric acid, retained a similar molecular topography to the copper(I) catenante.[214] The remarkably high basicity of **A64** is further demonstration of the catenand effect.

Since these original findings by Sauvage *et al.* there has been limited work in this area.[215,216] However, recent investigations by Goldup, Roessler and co-workers have showcased how the mechanical bond can be used to alter structural and electronic properties (Figure 1.16).[217]

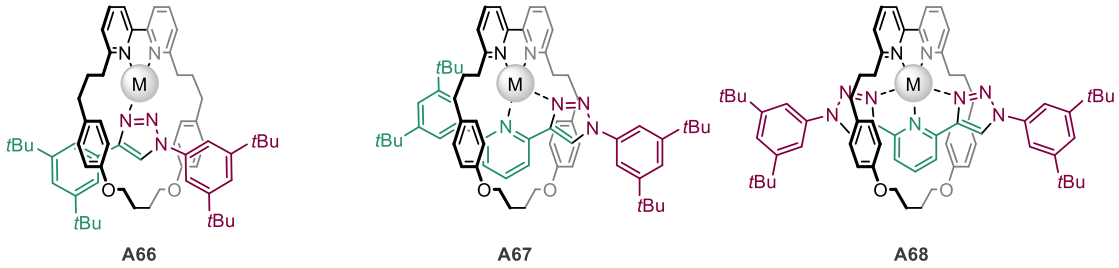

Figure 1.16. Rotaxane complexes, M = Co(II), Ni(II), Cu(II), Zn(II). Axles are coloured to represent the components created through AT-CuAAC. Anions omitted for clarity.

A series of tri- (**A66**), tetra- (**A67**) and pentadentate (**A67**) interlocked ligands were synthesised through active template Cu-mediated alkyne–azide cycloaddition reactions (AT-CuAAC).[218] Binding studies with transition metals Co(II), Ni(II), Cu(II) and Zn(II) yielded heteroleptic rotaxane complexes, these were compared with the analogous non-interlocked ligands. Solid-state structures for the majority of rotaxane complexes were obtained by X-ray diffraction and revealed unusual arrangements and coordination geometries imposed by the mechanical bond. The solid-state structures of interlocked Cu(II) complexes were consistent with electron paramagnetic resonance (EPR) data and the EPR spectrum of electrochemically reduced [Ni(**A67**)]$^{2+}$ confirmed formation of a stable Ni(I) species. Cyclic voltammetry assessed the electrochemical stabilities of the interlocked Cu(II) complexes. The pentacoordinate complex displayed enhanced electrochemical and chemical reversibility for the $Cu^{I/II}$ redox couple, compared to the non-interlocked variant. Therefore, similar to Sauvage's catenate complexes, the

mechanical bond can stabilise low oxidation states by preventing ligand reorganisation that could normally lead to the degradation of non-interlocked analogues.

Recent developments in this field include the synthesis of an interlocked platinum(II) rotaxane complex.[219] It was found that the mechanical bond stabilised the cyclometallated Pt(II) luminophore to oxidation and displacement of the Pt(II)–triazole bond, further demonstrating the catenand effect. Rotaxanes also have the potential to be effective catalysts through their unusual metal coordination geometries and steric environments enforced by mechanical bonds.[220,221] For example, a mechanically planar chiral rotaxane gold(I) complex was found to be an effective enantioselective catalyst for the cyclopropanation of benzoate esters, and was even comparable to a similar previously reported covalent catalyst (42%-77% *ee vs* 68% *ee*).[222]

Recent work in the Chaplin group has illustrated the catenand effect through the unusual reactivity of rhodium(I) complex **A69** (Scheme 1.15).[223] Oxidative addition of the interlocked 1,3-diyne under forcing conditions was promoted by the mechanical bond, resulting in formation of bis(alkynyl) complex **A70** which could be trapped out by reaction with carbon monoxide (**A71**). Divergent reactivity of the related acyclic congener was observed; facile substitution of the alkyne substrate was demonstrated alongside formation of the corresponding carbonyl complex. Incorporation of the mechanical bond enabled the normally hidden reactivity to be accessed, by disfavouring substitution of the entrapped substrate, and permitting the oxidative addition of the C(sp)–C(sp) bond. Other work in the group has similarly demonstrated divergent reactivity and selectivity of macrocyclic complexes compared to their acyclic analogues.[224–226]

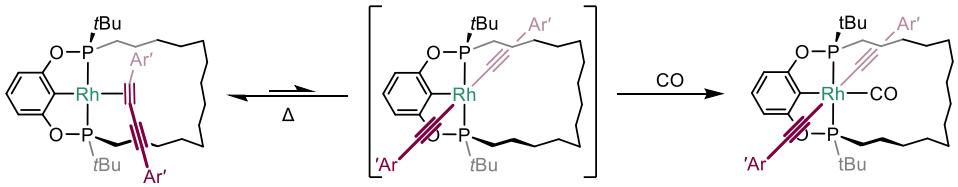

Scheme 1.15. Oxidative addition of mechanically entrapped C(sp)–C(sp) bond. Ar' = 3,5-*t*Bu$_2$C$_6$H$_3$.

1.3.5. Outlook

Routes to interlocked molecules have rapidly expanded since the first low-yielding syntheses of catenanes and rotaxanes; passive and active metal templated strategies have paved the way for more efficient preparations.[159] Active template reactions predominantly feature nitrogen donors embedded in the macrocyclic component, with AT-CuAAC reactions at the forefront.[159] Desirable preparations utilise high yielding syntheses of precursor components and efficient conversions to interlocked molecules.[218] However, a

consequence of active template methodologies is incorporation of functional groups into the interlocked architecture; the so-called 'impossible' rotaxanes are therefore more uncommon and typically prepared through covalent syntheses.[227,228] Another important consideration is the removal of the metal template after the interlocked structure has been captured, although this is typically achieved with standard demetallation reagents (*i.e.* EDTA, KCN) modification of the coordination motif may be necessary.[190,191]

Applications of mechanically interlocked molecules have focused mainly as components of molecular machines,[229] other possible applications include catalysis,[222,230] and as systems for drug delivery.[231] The coordination chemistry of catenanes and rotaxanes has remained relatively unexplored; the unique spatial environment of the ligand and kinetic stabilisation of the metal centre (catenand effect) offers vast potential for exploitation.

1.4. Coordination chemistry of alkanes

1.4.1. C–H bond activation

Considerable research has been undertaken investigating the conversion of inexpensive alkanes, attained from petroleum and natural gas, into more valuable and desirable products.[232–238] This objective, however, is hindered by the inertness of the strong constituent C–H bonds (the bond dissociation energy of C–H in methane is 439 kJ mol^{-1}).[235] Unlike the cracking of alkanes, C–H bond activation can be achieved under mild conditions using homogenous metal complexes, typically those of the second- and third-row transition metals. Key historical examples are provided in Figure 1.17.[239–244]

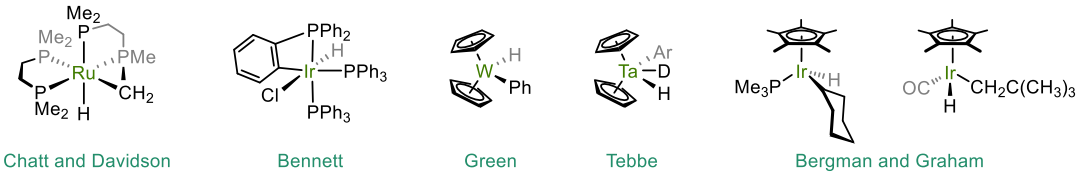

Figure 1.17. Notable C–H bond activation products.

The cleavage of C–H bonds by oxidative addition to a transition metal complex is a widely exploited method and is generally considered to proceed *via* formation of transient intermediates featuring coordinated C–H bonds, termed agostic and σ-complexes (Figure 1.18).[245,246] These interactions will be discussed in detail in the forthcoming sections.

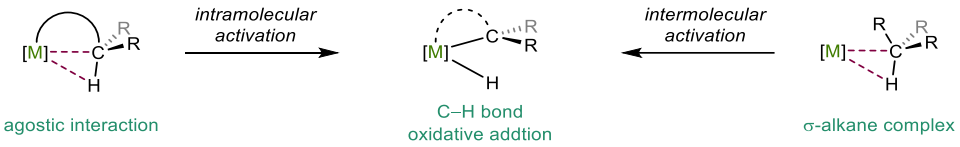

Figure 1.18. Metal mediated intra- and intermolecular C–H bond oxidative addition.

1.4.2. Complexes featuring agostic interactions

An agostic interaction is an intramolecular three-centre two-electron M···H–C interaction, originally introduced by Brookhart and Green (Figure 1.19).[247] Agostic interactions play critical roles in reaction mechanisms and stabilisation of reactive transition metal complexes, and as such represent an important area of organometallic chemsitry.[248] The first structurally characterised example was Green's titanium-ethyl complex **A72**, which features a β-agostic interaction; the analogous α-agostic methyl complex was also characterised.[249] Other notable examples include the neutral three-coordinate alkylrhodium(I) complex **A73** which is stabilised with a γ-C–H agostic interaction, and Binor complex **A74** which features a C–C sigma interaction from a cyclopropane group alongside a γ-agostic C–H interaction from an alkyl phosphine ligand.[250,251] More recently, weak agostic interactions have been observed in pincer-based macrocyclic complexes

(**A75**).[252] The solid-state structure revealed ε-agostic interactions between the iridium or rhodium centre with the macrocyclic tether, remarkably these interactions persisted upon dissolution and therefore could be characterised by NMR and IR spectroscopy.

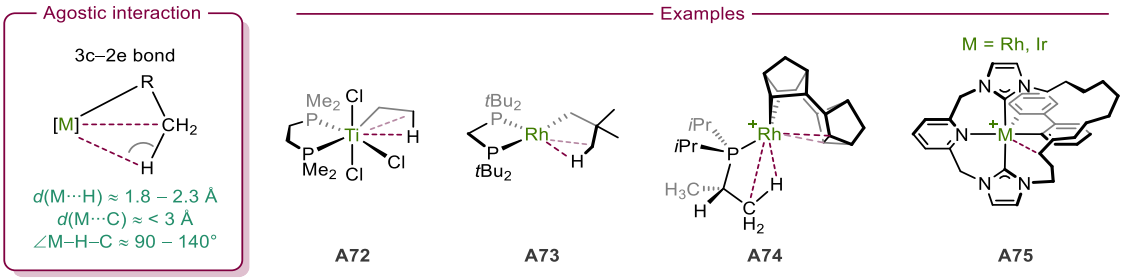

Figure 1.19. Complexes featuring agostic interactions.

1.4.3. σ-Alkane complexes

1.4.3.1. Overview

Intermolecular three-centre two-electron M···H–C bonding is invoked in the intact coordination of alkanes to transition metals.[253] These so called σ-alkane complexes are conceptually similar to species featuring agostic interactions, but considerably less stable without the stabilisation provided by chelation to the metal centre. As a consequence they are typically transient and short-lived species, with very few well defined examples. Intermolecular alkane coordination was first highlighted by Hodges in the early 1970s after a homogenous platinum(II) system, similar to those used by Shilov, catalysed the hydrogen-deuterium exchange of saturated alkanes.[254] However, no direct evidence of the *in situ* alkane complex formed was obtained.

1.4.3.2. The first σ-alkane complexes

The first experimental evidence for the formation of σ-alkane complexes was provided by Turner *et al* who observed transient σ-alkane species whilst exploring the photochemistry of $M(CO)_6$ species (**A76**, Scheme 1.16).[255,256] Photoejection of a carbonyl ligand in methane-doped argon matrices at cryogenic temperature afforded methane complex **A77**, evidenced through ultraviolet (UV) and visible spectroscopy. Around this time it was also shown that transient alkane complex **A78** could be generated through flash photolysis of $[Cr(CO)_6]$ in cyclohexane solution, similarly observed through UV/visible spectroscopy.[257,258] However, this route was found to be extremely sensitive to solvent impurities. Development of time-resolved IR spectroscopy (TRIR) allowed further characterisation of these transient species.[259,260] The enthalpy of the metal–alkane interactions have since been quantified using photoacoustic calorimetric measurements (*e.g.* **A78** = 53 kJ mol^{-1}).[261] Further to this, gas-phase TRIR has also been used to

investigate binding-strengths, for example longer chain alkanes bind more strongly to $[W(CO)_5]$.[262]

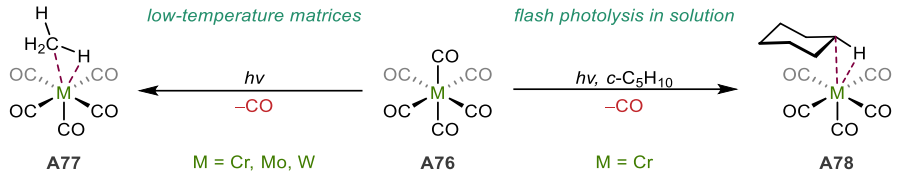

Scheme 1.16. Transient σ-alkane complexes generated *via* photolysis of hexacarbonyl complexes.

Half-sandwich σ-alkane complexes have observed through photolysis reactions.[263–265] Moore and Bergman studied the photolysis of **A79** in liquid krypton using TRIR spectroscopy (Scheme 1.17).[266] Ejection of the carbonyl ligand generated an intermediate species that was capable of interaction with deuterated neopentane (**A80**), however, this was only fleetingly observed before oxidative addition yielded the neopentyl deuteride complex. Although evidence of σ-alkanes could be attained by these techniques, structural detail of the bonding interaction was significantly limited. The first σ-alkane directly observed using low temperature NMR spectroscopy wasn't reported until 1998.[267] Generated by the photolysis of **A81**, high-field signals in both the ^{1}H and ^{13}C NMR spectra could be unambiguously assigned to the M···H–C interaction in **A82**. Further *in situ* photogenerated σ-alkane complexes have since been detected using NMR spectroscopy in this manner.[268] The use of low temperature NMR, IR and UV/visible spectroscopies continue to be useful tools for the observation and characterisation of these transient species.[269,270]

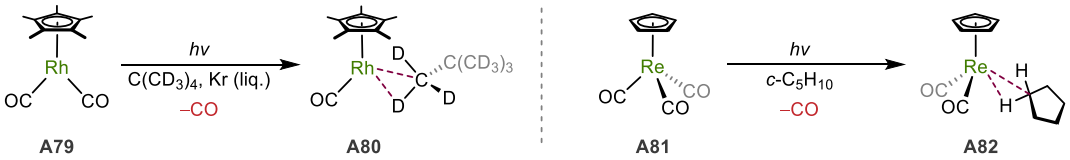

Scheme 1.17. Photolytic routes to half-sandwich σ-alkane complexes, characterised *in situ*.

1.4.3.3. Preparation from metal alkyls

σ-Alkane complexes can also be prepared through protonation of alkyl complexes, directly generating a coordinated alkane at the metal centre. This technique, however, necessitates very low temperatures to slow alkane elimination in conjunction with use of a weakly coordinating solvent. Seminal work by Brookhart in 2009 demonstrated the *in situ* preparation of rhodium σ-methane complex **A84a**, achieved through protonation of the rhodium-methyl precursor **A83a** in $CDCl_2F$ at –110 °C (Scheme 1.18).[271] Full solution characterisation of **A84a** was achieved by NMR spectroscopy. The ^{1}H NMR spectrum of exhibited a broad doublet at –0.86 ppm ($^{1}J_{RhH}$ = 8.3 *Hz*), the proton coupled ^{13}C NMR spectrum of the ^{13}C labelled isotopologue displayed a quintet at –41.7 ppm ($^{1}J_{HC}$ = 124 *Hz*);

assigned to the bound methane, these signals indicate all four protons were in rapid exchange by 'tumbling' of methane within the coordination sphere. Above −87 °C methane loss was evidenced by NMR spectroscopy, the product of which was suggested to be a solvent adduct (the dichloromethane adduct has since been characterised).[59] The instability of σ-alkane complex **A84a** is in stark contrast to the analogous rhodium(I) η²-dihydrogen adduct which was stable at ambient temperature in dichloromethane.[272]

The σ-ethane complex **A84b** could also be prepared in an analogous manner through protonolysis of the ethyl complex **A83b** at −150 °C (Scheme 1.18).[273] The barrier for ethane loss from **A84b** was deduced by spectroscopic studies to be 5 kcal mol^{-1} lower than for methane elimination, and ethane was quickly lost above −132 °C (*cf.* **A84a**, −87 °C). This difference in stability was attributed to increased steric repulsion between the bulkier alkane and the pincer *tert*-butyl groups. Despite the decreased stability, **A84b** was fully characterised by NMR spectroscopy at −143 °C. Variable temperature $^{13}C\{^1H\}$ NMR spectroscopy revealed that upon warming **A84b** to −132 °C the ethane signals broadened significantly, which corresponded to exchange between the α- and β-carbon sites *via* alkane 'chain walking'.

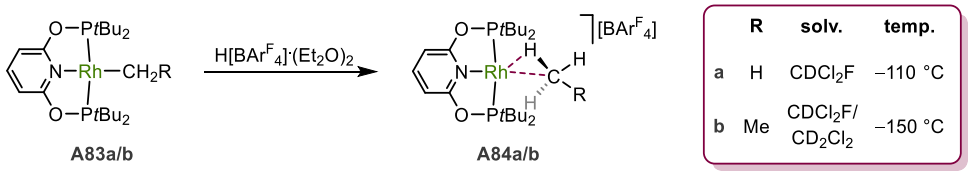

Scheme 1.18. Synthesis of σ-alkane complexes, by Brookhart *et al*.

The analogous iridium system has also been investigated; protonolysis of the iridium(I) methyl complex **A85** yielded the 16-valence electron iridium(III) methyl hydride complex **A86** which was surprisingly resistant towards methane elimination (Scheme 1.19).[274] Rapid proton exchange in complex **A86**, observed by ^{1}NMR spectroscopy, between the Ir–H and Ir–CH_3 proton sites implicated the presence of a transient iridium(I) σ-methane complex **A87**. Further effort to extend the methodology to other systems is limited to PONOP-based pincer complexes of group 9 or 10 metals.[275]

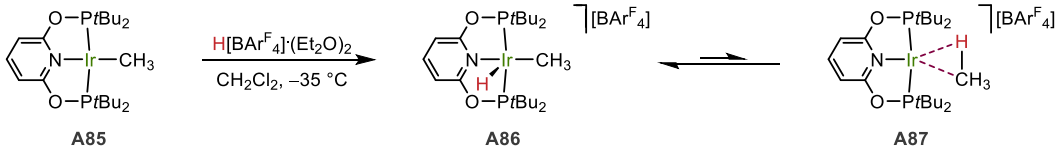

Scheme 1.19. Observation of σ-methane intermediates in iridium PONOP systems.

1.4.3.4. Solid-state characterisations

The first crystallographically characterised alkane–metal interaction was reported in 1997 using the iron(II) double A-frame porphyrin **A88** (Figure 1.20).[276] Crystallisation by diffusion of heptane into a fluorobenzene solution of **A88** resulted in heptane inclusion, although disorder in the crystallographic data prohibited a detailed analysis of the heptane–iron interaction. However, η²-alkane coordination was suggested by M···C distances of 2.5 – 3.0 Å and analysis by DFT supported this conclusion. In a similar manner, recrystallisation of a highly reactive tris-aryl oxide uranium(III) complex from *n*-pentane with excess cycloalkanes/linear alkanes afforded alkane complex **A89**.[277] Again, crystallographic disorder limited interpretation but alkane coordination is proposed, albeit with long M···C bond lengths (3.7 – 3.9 Å). Metal–alkane interactions have also been detected in the solid-state within metal-organic frameworks and in alkali metal complexes, supported by noncovalent forces.[278,279] These examples showcase the ability of host-guest interactions to facilitate the characterisation of σ-alkane complexes.

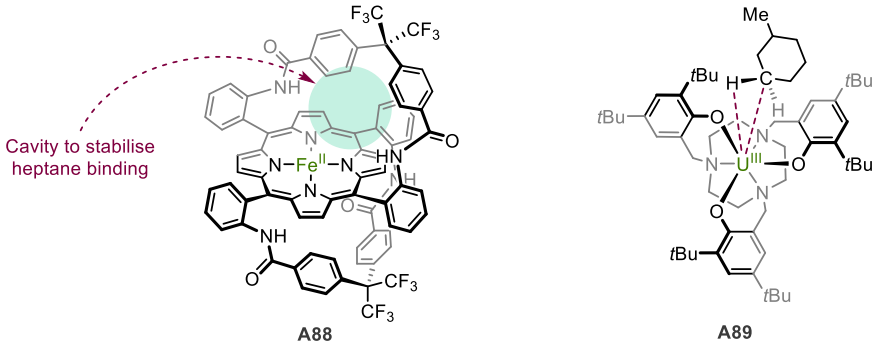

Figure 1.20. Solid-state characterisations of σ-alkane complexes.

In the last decade Weller has pioneered solid-state methodologies to obtain more catalytically relevant examples of σ-alkane complexes through single–crystal to single–crystal solid/gas reactions (Scheme 1.20).[280] The use of solid-state transformations removes the need for solvents, which hinders isolation and characterisation of σ-alkane complexes.

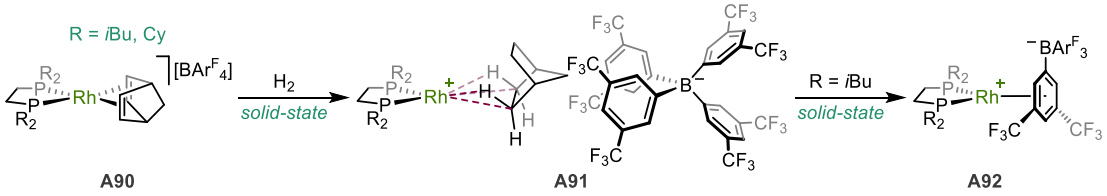

Scheme 1.20. Weller's solid-gas synthesis of σ-alkane complexes *via* hydrogenation of norbornadiene.

The addition of hydrogen (2 bar, 298 K) to norbornadiene precursors **A90** led to the quantitative production of σ-alkane complexes **A91**, the structures of which were determined by single-crystal X-ray crystallography. The norbornane ligand was bound

through two σ-C–H bonds resulting in a d^8-rhodium(I) pseudosquare planar complex. The *i*Bu-substituted complex was found to be considerably less stable than the Cy-substituted analogue; above 253 K norbornane was lost to form the $[BAr^F{}_4]^-$ coordinated zwitterion **A92**, in contrast the Cy-complex was stable for several months at room temperature under argon.[281] The bulkier Cy substituents are believed to confer a higher barrier for alkane substitution.[282] The close Rh···C bond distances obtained from the solid-state structures (≈ 2.5, 2.4 Å), in conjunction with short Rh···H contacts (≈ 1.9 Å), acute Rh–C–H angles, and elongation of the C–H bonds supported the η^2,η^2 alkane binding to the metal centre. The transformation from diene to alkane is enabled by encapsulation of the cationic metal fragment within octahedrally arranged $[BAr^F{}_4]^-$ anions, which provided a well-defined lattice. Solid-state NMR spectroscopy and DFT analysis further substantiated the presence of Rh···H–C bonding interactions, unfortunately upon dissolution (in $CDFCl_2$ or fluorobenzene) the alkane ligand is not retained even at low temperatures (133 K).[283]

This methodology has since been extend to the synthesis of a σ-pentane complex, a cobalt(I) σ-alkane complex, and rhodium(III) η^1-σ-alkane complex.[284–286] The rhodium σ-alkane complex **A91** catalyses the transfer dehydrogenation reaction of butane and can be used as a starting point to prepare alkene complexes (*e.g.* **A93**), which are catalysts for alkene isomerisation reactions and propane complexes (*e.g.* **A94**), which undergo spontaneous acceptorless dehydrogenation at room temperature (Scheme 1.21).

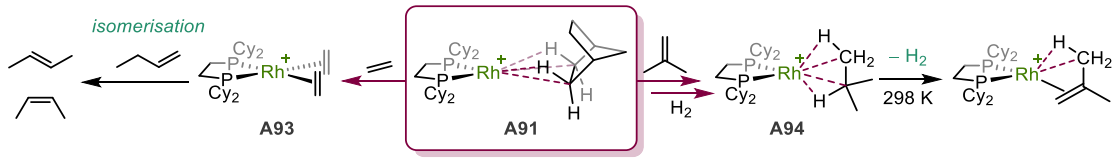

Scheme 1.21. Solid-gas reactivity of rhodium σ-complexes, counter anions omitted for clarity.

1.4.4. Outlook

σ-Alkane complexes represent a fundamentally important area of chemistry which has the potential for further exploration, into both structural characterisation and onward reactivity. Despite the state-of-the-art accomplishments by Brookhart and Weller, the associated synthetic routes are limited to characterisation in either solution *or* the solid state, respectively. The bound alkane dissociates from Brookhart's σ-complexes at higher temperatures, preventing characterisation in the solid state, whilst coordination of the anion in Weller's σ-alkane complexes displaces the alkane. Ultimately, the full characterisation of a σ-alkane complex in both the solution *and* solid state has remained elusive; a greater understanding of these complexes could aid the development of more efficient and selective catalysts for C–H bond activation processes and the functionalisation of alkanes.[281,287]

1.5. Aims and objectives

The overarching aim of this project is to investigate the coordination chemistry of C–H bonds in solution through the use of transition metal systems comprising a macrocyclic pybox-based pincer ligand combined with an interlocked hydrocarbon substrate. The synthesis and characterisation of intermolecular σ-complexes of this nature is generally challenging due to the weakly interacting nature of C–H bonds and competing solvent and/or anion coordination. As a consequence of their instability, the full characterisation of a σ-alkane complex has yet to be achieved. With the target supramolecular inspired systems, it is hypothesised that mechanical entrapment of the hydrocarbon substrate in close proximity to a suitable reactive metal will stabilise the ensuing M···H–C interaction, facilitate its characterisation in the solution state, and potentially enable isolation of these nominally unstable σ-complexes in the solid state.

Through adaption of methodology developed by Leigh, the first objective of the project is to synthesise a pybox-based [2]rotaxane ligand featuring a pure hydrocarbon axle: to ensure heteroatom coordination is avoided.[160] A closely related and ditopic [2]catenane ligand has also been identified as a potential target and its synthesis will be explored. The second phase will focus on the coordination chemistry of the interlocked ligands with late transition metals and will be supported by work using the more readily accessed acyclic analogue (*R*,*R*)-Ph-pybox. Ultimately, the synthesis of low-coordinate metal derivatives is targeted, as these are required to bring about the M···H–C interaction in the target interlocked systems.

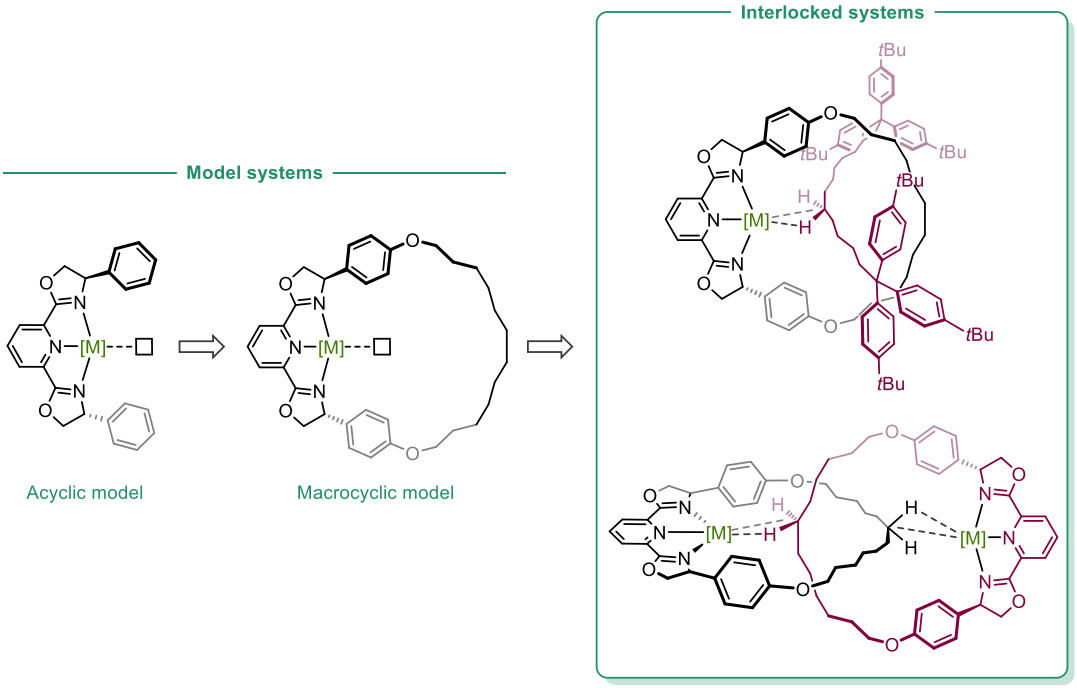

Chapter 2: Ligand Synthesis

This chapter describes work focused on the preparation of entangled ligands derived from trinitrogen-based macrocycles. Nickel was used as both an active and passive template for the synthesis of novel rotaxane (Part I) and catenane (Part II) derivatives.

Part I: Rotaxane

The first part of this chapter focuses on the application of nickel-catalysed C(sp^3)–C(sp^3) homocoupling[160] to the synthesis of new rotaxanes based on pybox and terpyridine-based macrocycles ^{M}**pybox** and ^{M}**terpy** (Scheme 2.1). This methodology was first evaluated with acyclic ligands (^{Ph}**pybox** and ^{Ph}**terpy**) using 1-bromohexane as the substrate. Whilst this procedure proved ineffective for terpyridine-based ligands, an optimised variant was developed to enable isolation of a novel pybox-based [2]rotaxane containing an interlocked hydrocarbon thread (^{R}**pybox**).

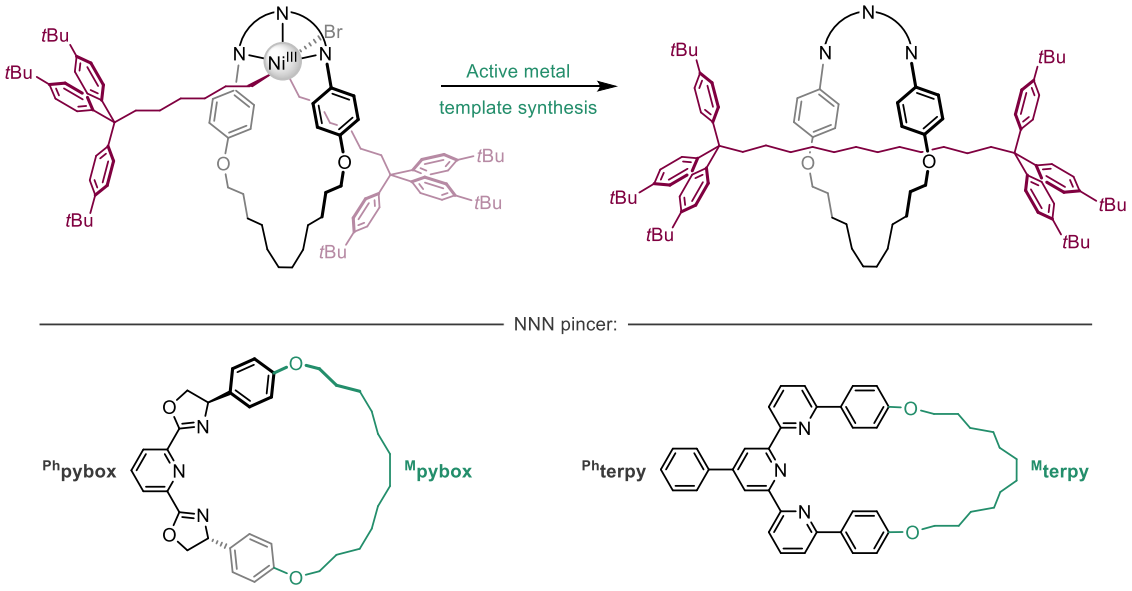

Scheme 2.1. Nickel-catalysed synthesis of [2]rotaxanes; ^{R}**pybox** when 'NNN' macrocycle = ^{M}**pybox**.

2.1. Synthesis of macrocyclic ligands

2.1.1. Synthesis of macrocyclic pybox

The pybox-based macrocycle **^{M}pybox** is a key component of the target rotaxane ligand, which has been previously exploited in Leigh's active metal-based synthesis of a related [2]rotaxane (**A50**).[160] The synthesis of **^{M}pybox** is a challenging multistep procedure (5% overall yield, Scheme 2.2). The poor overall yield can be attributed to several low-yielding steps including the amide bond formation, subsequent reduction and the high dilution macrocyclisation. Minor changes to the original literature procedure were needed to maximise the overall yield.

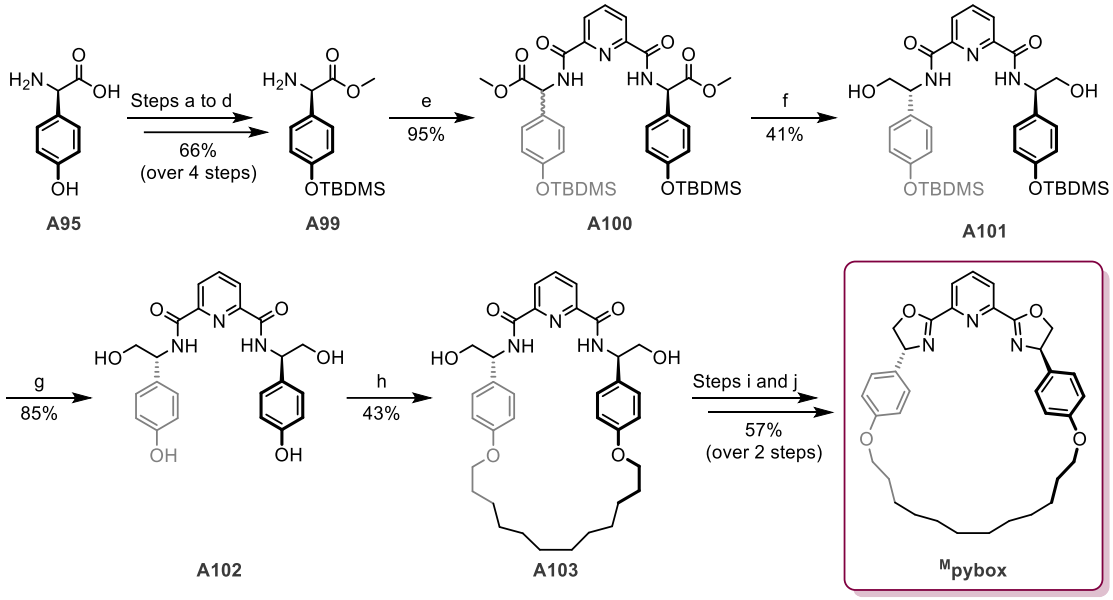

Scheme 2.2. Ten-step synthetic route to pybox macrocycle **^{M}pybox**. Reagents and conditions: a) $SOCl_2$, MeOH, 0 °C to rt, 18 h; b) Boc_2O, Et_3N, THF, reflux, 18 h; c) TBDMSCl, imidazole, DMF, 0 °C to rt, 18 h; d) TFA, CH_2Cl_2, rt, 18 h; e) 2,6-pyridinedicarbonyl dichloride, Et_3N, $CHCl_3$, 0 °C to rt, 18 h; f) $NaBH_4$, THF, MeOH, rt, 2 h; g) AcCl, MeOH, rt, 48 h; h) 1,12-dibromododecane, K_2CO_3, DMF, 100 °C, 72 h; i) $SOCl_2$, $CHCl_3$, reflux, 8 h; j) TBAF, THF, rt, 18 h.

Amide bond formation between the protected phenylglycine-derived amine **A99** and 2,6-pyridinedicarbonyl dichloride proceeded with a significant degree of racemisation, producing a mixture of (*R*,*R*)- and *meso*-**A100** diastereomers in 95% yield (step 'e', Scheme 2.2). Isolation of the desired (*R*,*R*)-**A100** diastereomer, assigned retroactively, was achieved by column chromatography in 53% yield. Subsequent reduction of ester **A100** also induced racemisation (step 'f', Scheme 2.2). In an attempt to increase the overall recovery of the desired diastereomer (*R*,*R*)-**A101**, the reduction was carried out using a diastereomeric mixture of **A100**. The crude mixture could be purified and (*R*,*R*)-**A101** was separated from the unwanted diastereomer by column chromatography with a yield of 39% (over two steps). Whilst the yield is similar to that achieved by isolation of diastereopure (*R*,*R*)-**A100** and subsequent reduction (38%, 2 steps), this variation is

operationally simpler, requiring only the comparatively facile separation of the alcohol *vs* the methyl ester diastereomers. As a consequence of racemisation in these steps, the intermediates obtained were not enantiopure, and as such, the resulting **^{M}pybox** was racemic. In schemes going forward, **^{M}pybox** will be depicted as the (*R*,*R*)-enantiomer.

The macrocyclisation step is reported with a yield of 22% but longer reaction times increased the yield of **A103** (72 hours *vs* 48 hours, step 'h', Scheme 2.2). In addition, formation of the oxazoline ring in step 'j' required an additional equivalent of TBAF for complete conversion. This avoided the need for purification by column chromatography which is problematic due to the hydrolysis of the oxazoline rings on silica. The melting point of **^{M}pybox** corresponded well with literature data.[160] The ^{1}H NMR spectrum in $CDCl_3$ displayed a triplet at δ 4.01 corresponding to the alkyl protons adjacent to the oxygen of the tether, furthermore, diagnostic oxazolinyl resonances at δ 5.38, 4.76 and 4.51 evidenced the formation of the pybox moiety. The HR ESI-MS displayed a strong molecular ion peak at 568.3173 (calcd 568.3170) *m*/*z*, corroborating the formation of **^{M}pybox**.

Surprisingly, it was discovered that **^{M}pybox** was prone to decomposition on extended storage, even under an inert atmosphere. We speculate that this could be due to the sensitivity of the oxazoline groups to acidic conditions if not fully neutralised after work-up.[288] Decomposition resulted in the appearance of signals in the ^{1}H NMR spectrum consistent with the presence of **A103**, alongside other unidentified hydrolysis products. Therefore, it was beneficial to store the direct precursor **A104** and form the oxazoline groups when required.

2.1.2. Synthesis of macrocyclic terpyridine

In combination with nickel, the acyclic trinitrogen pincer ligand 2,2':6',2"-terpyridine (**A21**, terpy) was shown to homocouple alkyl bromides almost as efficiently as the acyclic (*R*,*R*)-Ph-pybox ligand.[160] Indeed, the nickel complex of **A51** is an efficient C(sp^3)–C(sp^3) homocoupling catalyst, which has been utilised in the formation of [2]- and [3]rotaxanes.[162] Therefore, a terpy-based macrocycle **^{M}terpy** was envisaged, which contains a terpyridine motif with the same phenol-linked saturated alkyl chain found in **^{M}pybox** (Figure 2.1). Through 6,6''-substitution of terpyridine (*cf*. 5,5''-substituted **A51**) it was hoped that the number of axle components able to be threaded through the ring would be limited, to enable the preferential preparation of a [2]rotaxane.

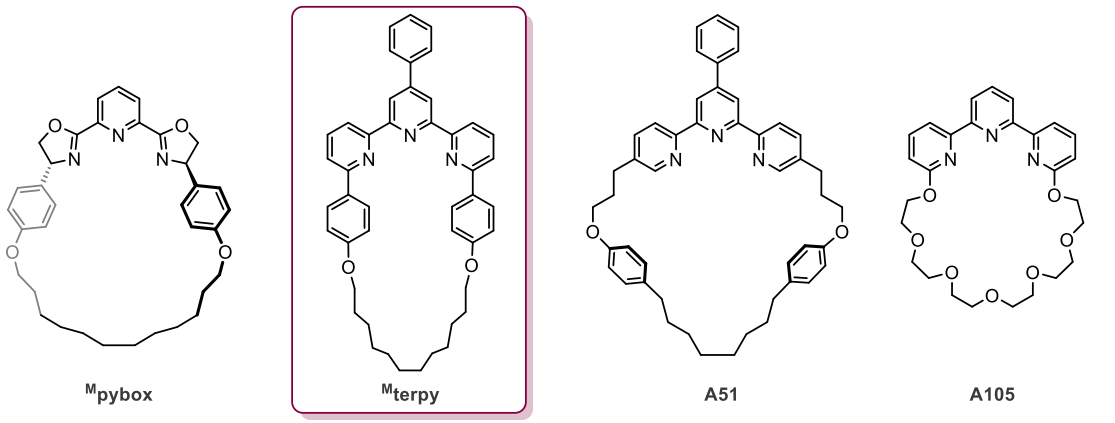

Figure 2.1. Terpy-based macrocyclic ligands, alongside **Mpybox**.

The proposed synthesis of **Mterpy** required the preparation of acyclic phenol-substituted terpyridine pincer **1**, from which the tether could be subsequently incorporated. Synthesis of **1** was achieved in high yield (84%) using a modified literature procedure, involving a Suzuki cross-coupling, and was fully characterised by NMR spectroscopy and ESI-MS (Scheme 2.3).[71] The hydroxyl protons notably give rise to a downfield singlet at δ 9.8 in the ^{1}H NMR spectrum in DMSO-d_6. In addition, the ESI-MS spectra contained a major peak at 494.1862 (calcd 494.1863) m/z corresponding to the $[M+H]^+$ ion.

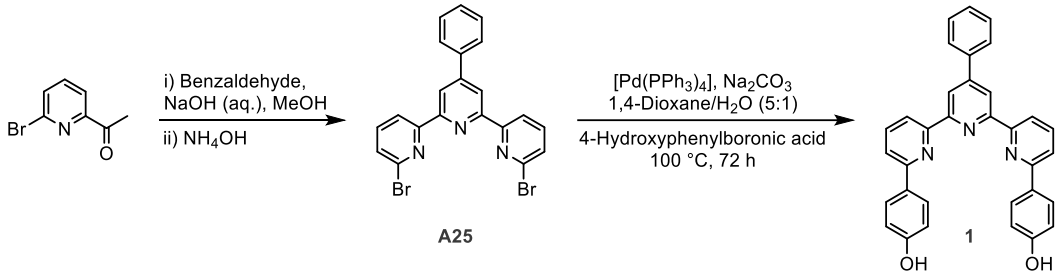

Scheme 2.3. Synthesis of phenol-terpyridine **1** *via* a Suzuki cross-coupling.

Installation of the macrocyclic tether was attempted by a S_N2 reaction of phenol-terpy **1** with 1,12-dibromododecane (Scheme 2.4). High dilution conditions (3 mM) and lengthy reaction times (120 h) were utilised to maximise yield of macrocycle product (**Mterpy**). After aqueous work up, the crude mixture was extracted into hot dichloromethane, to remove insoluble impurities, yielding a pale yellow solid. The resulting ^{1}H NMR spectrum indicated one main C_{2v} symmetric species but only in 90% purity. Similar difficulties were encountered in the synthesis of the related 6,6''-substituted terpyridine macrocycle **A105** (Figure 2.1).[289] Direct substitution on the acyclic 6,6''-dibromo-2,2′:6′,2''-terpyridine resulted in poor yields of macrocyclic products, however, this was remedied by a different, multistep procedure which incorporated the tether before formation of the central pyridine moiety.

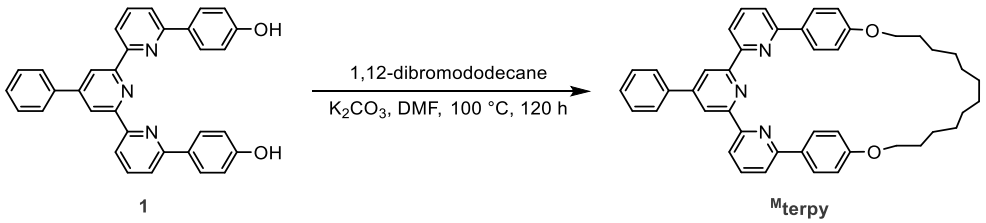

Scheme 2.4. Attempted preparation of **^{M}terpy**.

Purification by column chromatography proved challenging due to poor solubility of the target compound. Further purification attempts by precipitation were also not fruitful. Although **^{M}terpy** could not be isolated cleanly, its structure was unambiguously established through analysis by NMR spectroscopy and ESI-MS. The ^{1}H NMR spectrum in $CDCl_3$ showed significant resonances in the alkyl region due to the introduction of the dodecyl tether. Furthermore, a triplet at δ 4.04 was observed, corresponding to the alkyl protons adjacent to the phenolic oxygen atoms, and closely matches the analogous protons from **^{M}pybox** (δ 4.01). The ESI-MS displayed a signal at 660.3586 (calcd 660.3585) m/z which was attributed to the $[M+H]^+$ ion of the target compound **^{M}terpy**.

2.2. Optimisation of homocoupling conditions

2.2.1. Pybox

Optimisation of the C(sp^3)–C(sp^3) homocoupling procedure, whereby two half axle components are fused together within the macrocyclic ring forming the interlocked rotaxane architecture, was primarily investigated using the less synthetically demanding acyclic analogue 2,6-bis[4'-(*R*)-phenyloxazolin-2'-yl]pyridine ((*R*,*R*)-Ph-pybox, ^{Ph}**pybox**). ^{Ph}**Pybox** was synthesised in good overall yield from 2,6-pyridinecarboxylic acid and (*R*)-phenylglycinol following a modified literature procedure (38% overall yield) and was characterised (Scheme 2.5).[101,114] Spectroscopic data agrees well with the literature.[290]

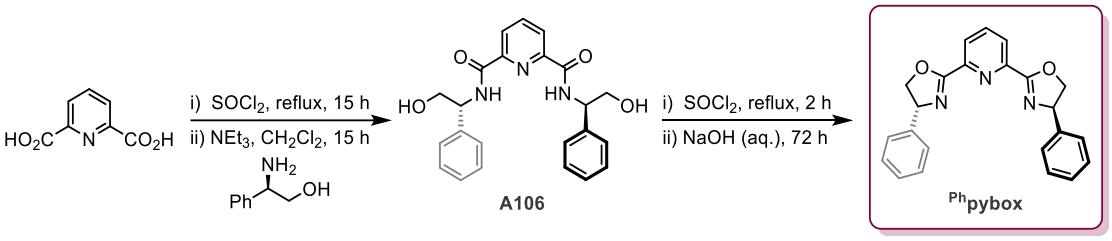

Scheme 2.5. Synthesis of ^{Ph}**pybox**.

Optimisation studies were carried out for the homocoupling of 1-bromohexane to dodecane, which can be conveniently monitored by GC analysis, initially with ^{Ph}**pybox** and then ^{M}**pybox** (Table 2.1). This differs from the literature use of 1-bromo-3-phenoxypropane as a model for the optimisation of the rotaxanation, but in this case 1-bromohexane was considered to be more appropriate for the target half-axle component (**2**, *vide infra*).[160] Promising conversion from 1-bromohexane to dodecane (59%) were generated using ^{Ph}**pybox** under the previously reported rotaxanation conditions of 41 mol% catalyst loading, 2.5 h reaction time in solvents *N*-methyl-2-pyrrolidone (NMP) and THF.[160] Extending the reaction time from 2.5 to 4.5 hours was found to significantly increase the conversion to near quantitative (96%). In order to fully assess the effect of different solvents on conversion, a lower catalyst loading of 5 mol% was employed. Solvent combinations using THF, DMF and NMP were all probed, as these have been shown to be effective media for nickel-catalysed coupling reactions.[88] Both acyclic and macrocyclic pybox ligands (^{Ph}**pybox** and ^{M}**pybox**) were utilised to assess whether the dodecyl tether influenced the homocoupling procedure; we found notable differences in the conversions to homocoupled product depending on the ligand employed.

Table 2.1. Ni-catalysed homocoupling of 1-bromohexane using pybox ligands.

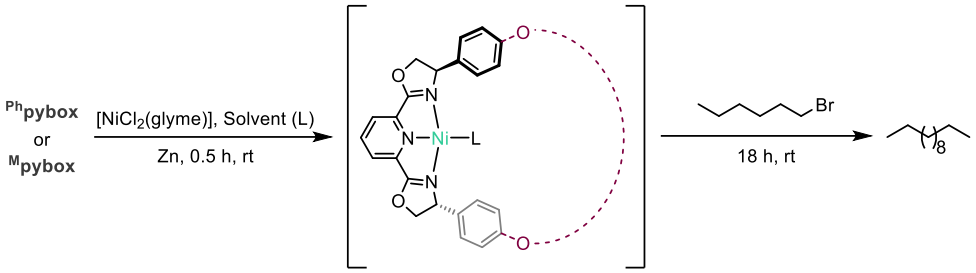

Entry	Solvent	Ligand	Substrate conc. / mM	Conversion / %
1	THF:DMF	**Phpybox**	55	57
2	THF:NMP	**Phpybox**	55	87
3	NMP:DMF	**Phpybox**	55	2
4	NMP	**Phpybox**	55	19
5	DMF	**Phpybox**	55	61
6	THF	**Phpybox**	55	2
7	THF:NMP	**Phpybox**	28	50
8	THF:NMP	**Phpybox**	110	>99
9	THF:DMF	**Mpybox**	55	75
10	THF:NMP	**Mpybox**	55	88
11	NMP:DMF	**Mpybox**	55	68
12	NMP	**Mpybox**	55	52
13	DMF	**Mpybox**	55	33
14	THF	**Mpybox**	55	3

5 mol% [$NiCl_2$(glyme)], 5 mol% ligand. 1:1 mixtures of solvent where relevant. Conversions determined by GC analysis.

The optimised protocol entailed sonication of a solution of [$NiCl_2$(glyme)] and pybox ligand (**Phpybox** or **Mpybox**) over excess activated zinc powder for 30 minutes, before addition of 1-bromohexane. The resulting suspension was then stirred at ambient temperature for 18 hours, after which conversion was deduced by gas chromatography (GC) analysis. The optimal solvent system for the homocoupling of 1-bromohexane using both **Phpybox** and **Mpybox** was found to be a 1:1 mixture of THF:NMP (entries 2 and 10). This is consistent with the optimised system for the literature homocoupling of 1-bromo-3-phenoxypropane and for the synthesis of [2]rotaxane **A50** which used THF:NMP (1:1).[160] Generally higher conversions were found when using **Mpybox**. The effect of concentration on the homocoupling was probed with the acyclic **Phpybox** system in THF:NMP (1:1) following the same general procedure (5 mol% catalyst loading). It was found that a higher concentration of substrate favoured a higher conversion to homocoupled product (entries 7 and 8), therefore, the concentration dependence must be considered for rotaxane synthesis.

2.2.2. Terpyridine

The acyclic ligand 2,2':6',2''-terpyridine (**A21**) has been shown to homocouple several unactivated alkyl bromides, including 1-bromo-3-phenoxypropane, which was utilised as part of the literature model system.[160] In order to model the homocoupling ability of macrocyclic **^{M}terpy**, the known acyclic 6,6''-substitued terpyridine (**^{Ph}terpy**) was synthesised. Synthesis of **^{Ph}terpy** was achieved by a Suzuki cross-coupling to attach the phenyl moieties to the pincer scaffold in good yield (72%; Scheme 2.6).[71,77]

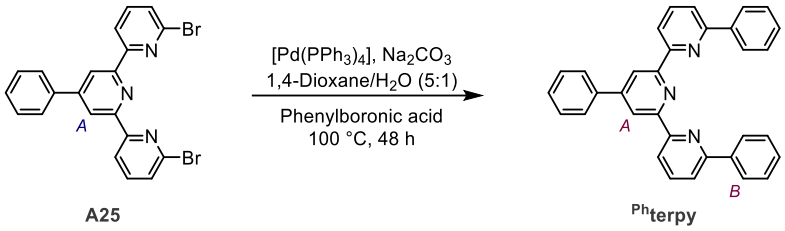

A25 ^{Ph}terpy

Scheme 2.6. Synthesis of **^{Ph}terpy**.

The melting point of **^{Ph}terpy** corresponded well with literature data.[72] However, due to the absence of NMR data, **^{Ph}terpy** was further characterised by NMR spectroscopy. Most notably, the *meta*-pyridine protons H_A in the ^{1}H NMR spectrum ($CDCl_3$) shifted downfield relative to the dibromide **A25** (δ 8.92; $\Delta\delta$ 0.23, Figure 2.2). Furthermore, the addition of the phenyl moiety was substantiated by increased aromatic resonances including the doublet at δ 8.20 assigned to H_B.

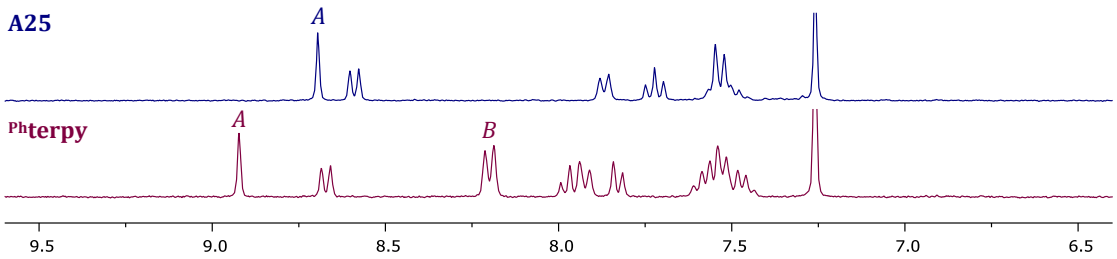

Figure 2.2. ^{1}H NMR spectra of **A25** (*top*) and **^{Ph}terpy** (*bottom*) (300 MHz, $CDCl_3$, 298 K).

The homocoupling of 1-bromohexane was further explored using ^{Ph}**terpy** (Table 2.2).

Table 2.2. Ni-catalysed homocoupling of 1-bromohexane using terpyridine.

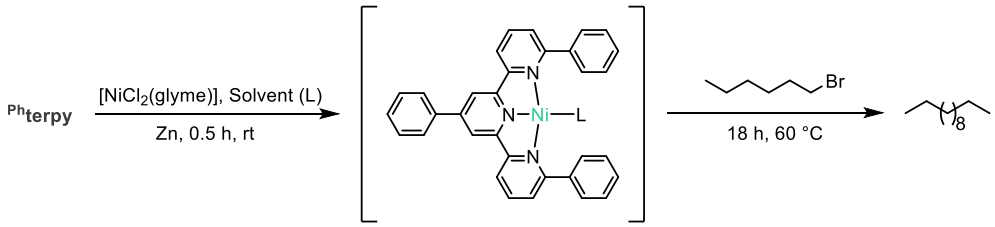

Entry	Solvent	Ligand	Substrate conc. / mM	Conversion / %
1[a]	THF:NMP	^{Ph}**terpy**	55	2
2	THF:DMF	^{Ph}**terpy**	55	<1
3	THF:NMP	^{Ph}**terpy**	55	4
4	NMP:DMF	^{Ph}**terpy**	55	<1
5	NMP	^{Ph}**terpy**	55	<1
6	DMF	^{Ph}**terpy**	55	3
7	THF	^{Ph}**terpy**	55	2

[a] Reaction at rt. 5 mol% [$NiCl_2$(glyme)], 5 mol% ligand. 1:1 mixtures of solvent where relevant. Conversions determined by GC analysis.

Under the optimised conditions established from the homocoupling of 1-bromohexane with ^{Ph}**pybox**, only low conversion to dodecane was evidenced by GC analysis when ^{Ph}**terpy** was employed (entry 1). Heating the reaction to 60 °C did not lead to any significant improvement. Furthermore, increased catalyst loadings (20 mol%) also produced poor conversions, with the highest attained only 15% (NMP:THF). The homocoupling was also attempted with impure ^{M}**terpy**, however, no detectable quantity of dodecane was observed. The ineffectiveness of ^{Ph}**terpy** as a ligand for the homocoupling is presumably attributed to substitution at the 6,6''-terpyridine positions, which results in a considerably more sterically encumbered ancillary than **A51**, for which homocoupling reactions within the ring are possible. Based on these results and alongside difficulties associated with its isolation, rotaxane synthesis using ^{M}**terpy** was not investigated further.

2.3. Synthesis of axle components

For the synthesis of a rotaxane, the nickel-catalysed homocoupling procedure requires a sterically bulky alkyl bromide to prevent dethreading. It is also necessary to avoid heteroatoms in the thread when using the resulting [2]rotaxane (**^{R}pybox**) as a ligand for the formation of low-coordinate metal complexes. Based on Leigh's system, a dodecamethylene chain terminated with bulky triaryl groups was chosen (Figure 2.3).[160]

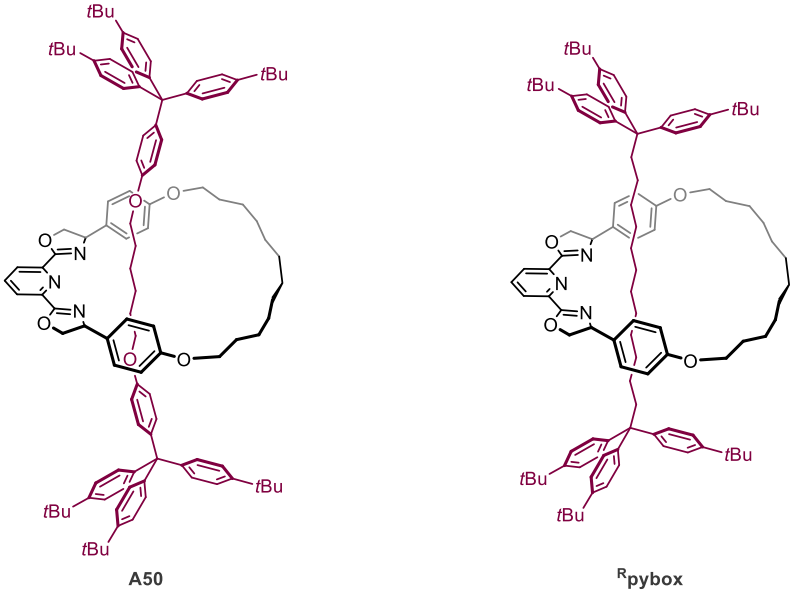

Figure 2.3. Leigh's [2]rotaxane with phenol-based axle **A50** and rotaxane target **^{R}pybox**.

The necessary half axle **2** was prepared using a protocol adapted from structurally related compounds, by reaction between *in situ* generated lithiated tris(4-*tert*-butylphenyl)methane ($CH(C_6H_4tBu)_3$, **A107**) and a vast excess of 1,6-dibromohexane (Scheme 2.7).[291] The use of hexamethylphosphoramide (HMPA) was found to greatly increase the yield of stoppered products due to the improved nucleophilicity of the lithiated stopper anion, which reacts more readily through an S_N2 reaction pathway.[292–294]

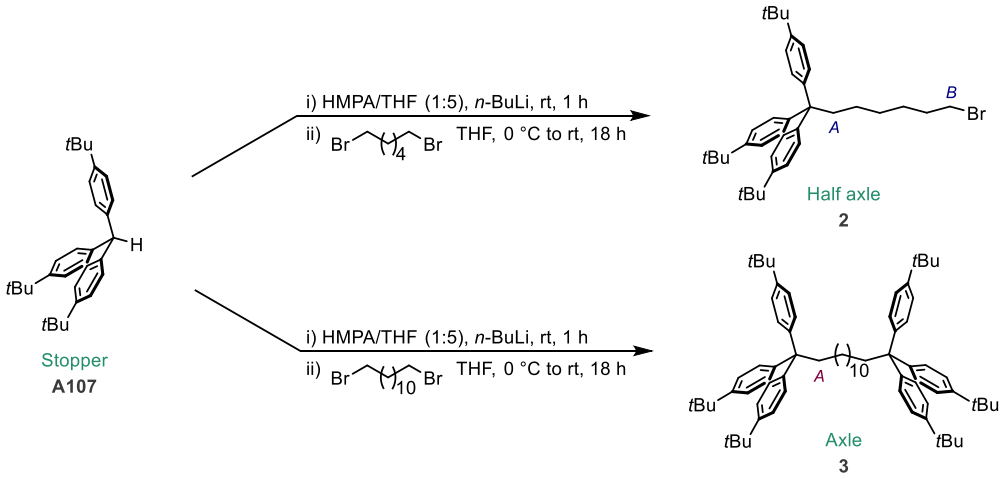

Scheme 2.7. Synthesis of half axle **2** and axle **3**.

Reaction of the lithiated stopper with 20 equivalents of 1,6-dibromohexane produced poor yields of **2** (<10%) due to the formation of the bis-substituted product. In an attempt to increase yields of the half axle, the lithiated stopper group was added dropwise over an hour to neat 1,6-dibromohexane at 0 °C. Removal of 1,6-dibromohexane afforded a crude mixture containing **2** with only traces of the bis-substituted side product as observed in the crude ^{1}H NMR spectrum (ca. 1%). Purification using column chromatography yielded analytically pure **2** in high yield (80%) and was fully characterised. The most indicative signal in the ^{1}H NMR spectrum ($CDCl_3$) was a triplet at δ 3.34, which corresponds to the methylene protons alpha to the bromide (H_B, Figure 2.4, Scheme 2.7).

Similarly, the novel hydrocarbon axle **3** was prepared for comparison. The axle was isolated in good yield (73%) and was fully characterised. The methylene protons adjacent to the stopper group (H_A) give rise to a distinctive multiplet in the ^{1}H NMR spectrum ($CDCl_3$) at δ 2.49, which is nearly identical to that of the half axle (H_A δ 2.50, Figure 2.4). Removal of the unreacted stopper group (**A107** δ 5.44) was achieved by column chromatography.

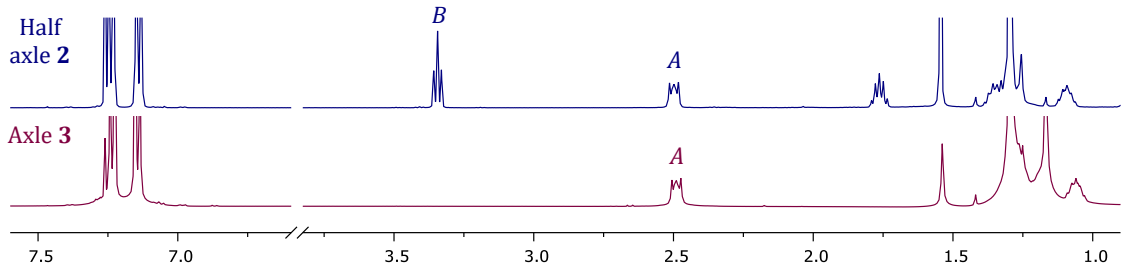

Figure 2.4. ^{1}H NMR spectra of **2** (*top*) and **3** (*bottom*) (500 MHz, $CDCl_3$, 298 K).

2.4. Rotaxane synthesis and characterisation

2.4.1. Optimisation

The nickel catalysed homocoupling of **2** employing ^{Ph}**pybox** as the ligand under the optimised conditions (THF:NMP) resulted in a meagre 22% conversion compared to that of 1-bromohexane (87%). While this degree of conversion is in principle sufficient to enable rotaxanation, subsequent evaluation flagged the need for further optimisation, in both concentration of ^{M}**pybox** and half axle **2**, as well as the reaction time (Table 2.3).

Table 2.3. Synthesis of rotaxanes ^{R}**pybox** and ^{R*}**pybox**.

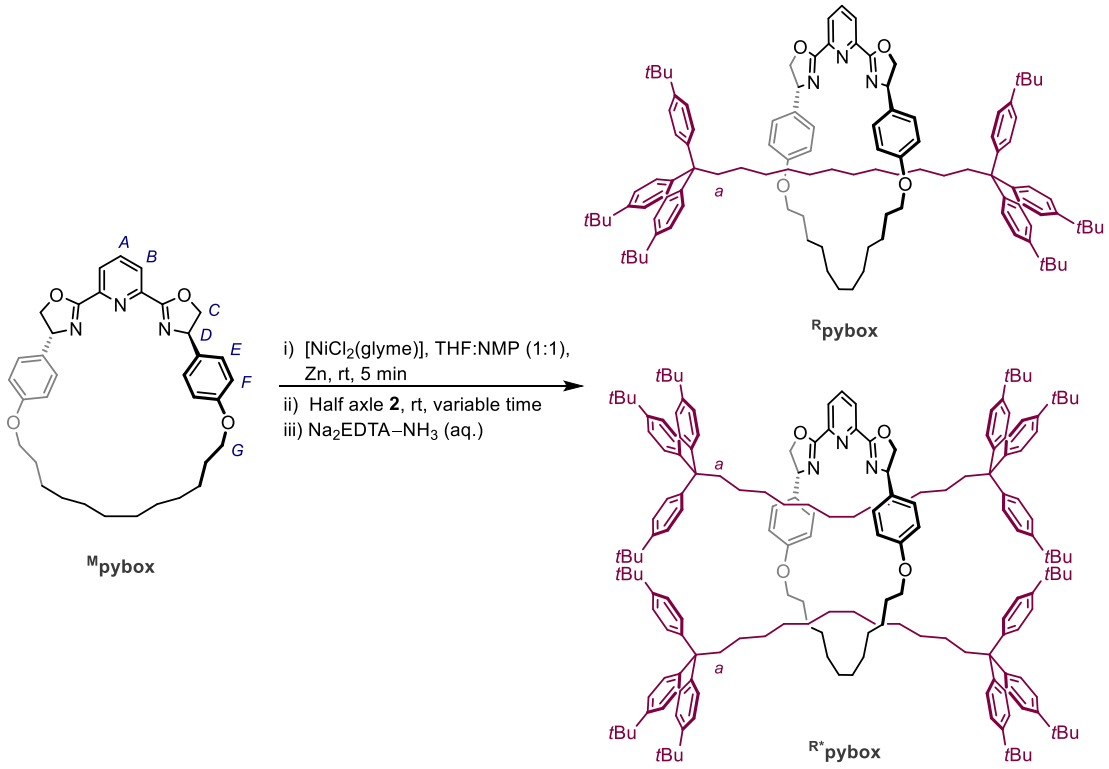

Entry	Conc. ^{M}**pybox** / mM	Conc. **2** / mM	Equiv. **2**	Reaction time / h	Percentage of pybox-containing species in crude / %		
					^{M}**pybox**	^{R}**pybox**	^{R*}**pybox**
1	25	59	2.4	2.5	61	39	0
2	25	59	2.4	5	48	52	0
3	28	110	4	5	8	72	20
4	25	60	2.4	18	40	60	0
5	25	105	4.2	18	10	70	20
6	28	83	3	15	33	67	0
7	44	132	3	15	9	80	11
8	44	220	5	15	0	59	41
9	25	123	5	24	15	66	19
10	44	176	4	5	7	55	37
11	44	132	3	5	9	74	17

[$NiCl_2$(glyme)] (1 eq. per ^{M}**pybox**), Zn (10 eq.), THF:NMP (1:1), rt. Conversions calculated by ^{1}H NMR.

Conversions to interlocked products were calculated from the ^{1}H NMR spectra using the pyridine resonances H_B of the pybox moiety at δ 8.11/7.99/7.86, for **^{M}pybox**, **^{R}pybox** and **^{R*}pybox** respectively. Using Leigh's conditions, low conversion to the [2]rotaxane **^{R}pybox** was found (entry 1).[160] Therefore the reaction time was extended to 5 hours which showed a small improvement (39% to 52%, entries 1 and 2). By increasing the concentration and number of equivalents of **2**, we were able to drive the reaction to higher conversions of **^{R}pybox** (52% to 72%, entries 2 and 3). However, under these conditions a second pybox-based product was detected on analysis of the mixture by ^{1}H NMR spectroscopy, which was postulated to be the doubly-threaded [3]rotaxane **^{R*}pybox**. Comparison of the reaction at 5 hours or 18 hours (entries 3 and 5) displayed near identical results, which suggested the consumption of **2** is complete within 5 hours. However, using higher concentrations of the macrocycle encouraged **^{R}pybox** formation in 80% conversion (28 mM *vs* 44 mM, entries 6 and 7). Formation of the doubly-interlocked **^{R*}pybox** is favoured with higher concentration of **^{M}pybox** and **2** (entry 8), although significant amounts of **^{R}pybox** are also formed alongside this product.

The homocoupling reaction using the conditions outlined in entry 9 (Table 2.3) was examined in more detail by analysis of aliquots taken over 24 hours by ^{1}H NMR spectroscopy (Figure 2.5). This data confirms that **^{R*}pybox** is only formed after **^{R}pybox**. After 6 hours the half axle **2** was completely consumed, suggesting that production of **3**, *i.e.* homocoupling outside the ring, is significant.

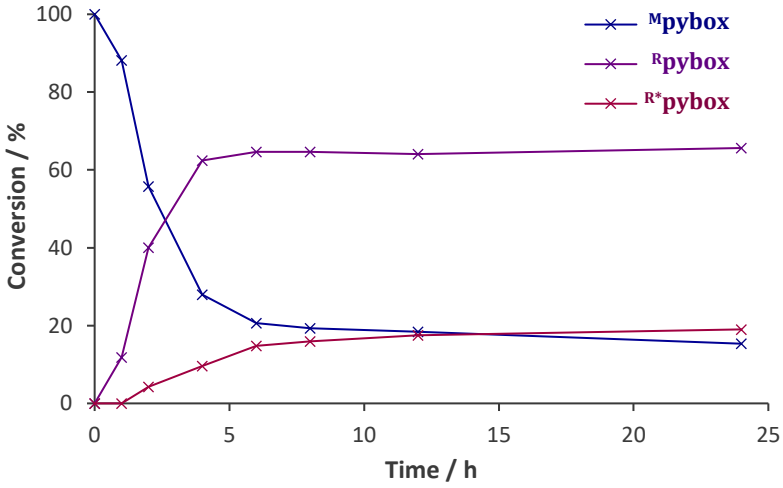

Figure 2.5. Time course plot showing ratios of pybox containing species over time. Conditions: 25 mM, 4 mL total volume (THF:NMP (1:1)), 5 equiv. **2**, 0.2 mL aliquots. Conversions calculated from ^{1}H NMR spectroscopy ($CDCl_3$) from ratios between macrocycle (**^{M}pybox**), [2]rotaxane (**^{R}pybox**) and [3]rotaxane (**^{R*}pybox**) (py signals).

2.4.2. Synthesis and characterisation

The highest apparent conversion to **^{R}pybox** and **^{R*}pybox** was observed after reacting for 15 hours (entries 7 and 8, Table 2.3), though this was not reflected in the isolated yield (<11%). In fact, reaction times in excess of 5 hours were found to be detrimental to the isolated yield of both rotaxane products. This was attributed to the instability of the oxazoline moiety under the reaction conditions. Indeed, this observation has previously been suggested.[160]

The [2]rotaxane **^{R}pybox** was ultimately prepared through employing 3 equivalents of **2**, 10 equivalents of activated zinc and allowing for a 5 hour reaction time (entry 11, Table 2.3). Following removal of nickel with ammoniacal disodium EDTA, the crude product was found to contain non-interlocked **^{M}pybox** and axle **3** alongside the desired rotaxane products. Extraction of unreacted **^{M}pybox** from the crude mixture with acetonitrile allows it to be recycled for future rotaxane syntheses, minimising the wastage of this valuable and synthetically challenging material. Purification of **^{R}pybox** was attempted by C_{18} reverse phase column chromatography. A major difficulty associated with purification of **^{R}pybox** is the separation of the free axle **3**, which has a near identical retention factor. In this way **^{R}pybox** was obtained in 18% yield, but contaminated with *ca*. 10% of axle **3**, as confirmed by ^{1}H NMR spectroscopy. Analytically pure samples could be obtained following successive column purification, but in very low yield.

Likewise, the [3]rotaxane **^{R*}pybox** was prepared through employing 5 equivalents of **2**, 10 equivalents of activated zinc and a 15 hour reaction time (entry 8, Table 2.3). The resulting crude product contained no unreacted **^{M}pybox** due to the increased concentration of half axle **2** in the homocoupling reaction. Purification of **^{R*}pybox** was achieved through C_{18} reverse phase column chromatography which was easily separable from **3**. Analytically pure **^{R*}pybox** was isolated in 9% yield, confirmed by ^{1}H NMR spectroscopy. The appreciably lower yield was attributed to the longer reaction time which was needed for conversion, but detrimental to the isolated yield (*vide supra*).

Comparison of the ^{1}H NMR spectra ($CDCl_3$) of **^{R}pybox** and **^{R*}pybox** with **^{M}pybox** and **3** helps verify the interlocked nature of the rotaxanes (Figure 2.6). The upfield shifts of many of the macrocycle and axle signals are characteristic for interlocked molecules, and attributed to increased shielding from the aromatic phenyl rings.[160,295,296] Diagnostic changes include: the pyridine resonances H_A (δ 7.92/7.57/7.45) and H_B (δ 8.11/7.99/7.86) which are shifted upfield, as well as those of the macrocyclic phenyl group H_F (δ 6.85/6.70/6.59) (see Table 2.3 for labelling). The changes in chemical shift are most pronounced for the resonances assigned to **^{R*}pybox**, consistent with the more confined

environment. Another diagnostic tool was the resonance assigned to the axle protons H_a adjacent to the stopper groups. This signal was significantly broadened in the case of the [3]rotaxane as a consequence of the additional steric crowding in the macrocyclic cavity.[163] The oxazoline resonances remained relatively unchanged in this series, with the oxazolinyl methine protons at δ 5.38/5.34/5.46 (H_D) and the diastereotopic methylene protons at δ 4.76/4.66/4.66 (H_C) and δ 4.51/4.42/4.52 ($H_{C'}$), for **^{M}pybox**, **^{R}pybox** and **^{R*}pybox** respectively.

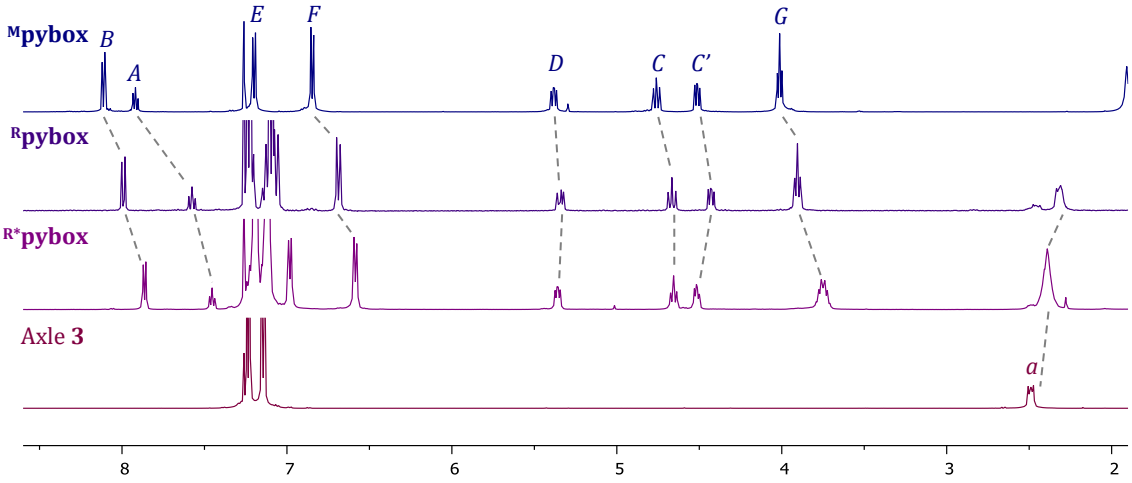

Figure 2.6. ^{1}H NMR spectra of **^{M}pybox**, **^{R}pybox**, **^{R*}pybox** and **3** (*top to bottom*) (500 MHz, $CDCl_3$, 298 K).

The high-resolution ESI-MS of **^{R}pybox** further corroborated its interlocked nature, with the spectrum exhibiting a molecular ion peak at 1581.0994 *m/z* (calcd 1581.0971; [**^{R}pybox**+Na]$^+$) that fragments into 590.2992 *m/*z (calcd 590.2989; [**^{M}pybox**+Na]$^+$) under tandem MS conditions (100 eV).[297,298] The structure of **^{R*}pybox** was likewise confirmed by high-resolution ESI-MS, which showed a peak at 2549.9143 *m/z* [**^{R*}pybox**+H]$^+$ corresponding to the doubly-threaded rotaxane.

Part II: Catenane

A classical method, based on the use of nickel as a sacrificial 'passive' template, was investigated for the synthesis of a pybox-based [2]catenane (Scheme 2.8). The synthetic approach was informed by the coordination chemistry of the acyclic pybox ligand ^{Ph}**pybox**. The heptenyl-pybox precursor ligand was readily obtained following adaption of the procedures involved in the synthesis of ^{M}**pybox**. Capture of a nickel catenate was achieved following Grubbs' ring closing metathesis (RCM) and subsequent hydrogenation, but demetalation proved problematic.

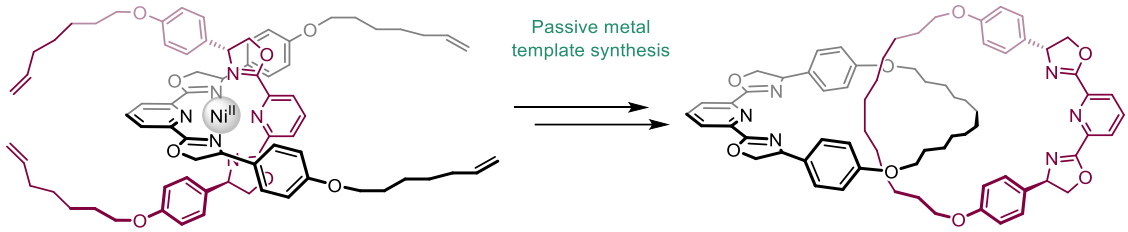

Scheme 2.8. Nickel-templated [2]catenane synthesis.

2.5. Proposed passive metal template synthesis and model nickel complex

As part of work investigating coordination chemistry of **^{Ph}pybox** (*cf.* Chapter 3), the preparation of nickel chloride complex [NiCl(**^{Ph}pybox**)][BAr^F_4] was attempted through reaction of **^{Ph}pybox** with [$NiCl_2$(glyme)] and Na[BAr^F_4] in dichloromethane. However, this was unsuccessful and instead formed bis complex [Ni(**^{Ph}pybox**)$_2$][BAr^F_4]$_2$, as evidenced by X-ray crystallography. In addition, broad signals in the ^{1}H NMR spectroscopy were indicative of the paramagnetic nickel(II) metal centre.

Subsequently [Ni(**^{Ph}pybox**)$_2$][BF_4]$_2$ (**4**) was prepared by stirring two equivalents of **^{Ph}pybox** with [$NiCl_2$(glyme)] in dichloromethane for 18 hours, followed by chloride anion metathesis using 0.1 M $NH_4[BF_4]$ (Scheme 2.9).

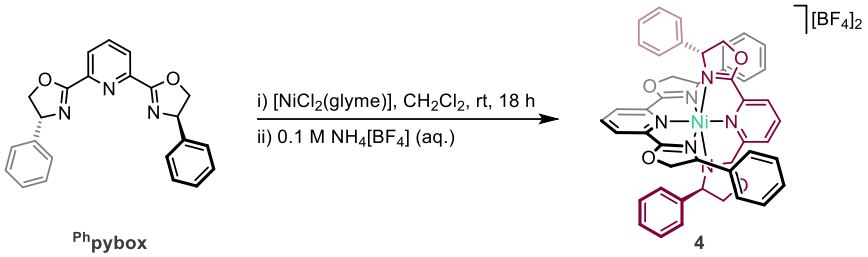

Scheme 2.9. Synthesis of nickel(II) complex **4**.

Characterisation of nickel complex **4** by NMR spectroscopy was limited as a result of the paramagnetic nickel(II) centre. Therefore, electron paramagnetic resonance (EPR) spectroscopy was attempted on a Q-band (34 GHz) spectrometer, however, at this frequency no signal was observed. This suggested a high zero field splitting energy, which would require a high-field EPR measurement to be detected. HR ESI-MS confirmed formation of **4**, with a signal at 883.2343 *m*/*z* (calcd 883.2337) assigned to $[M+BF_4]^+$. Determination of the solution state paramagnetic susceptibility of the sample was achieved using the Evans method.[299–301] The resulting value of 2.71 μ_B is in good agreement with the expected μ(spin-only) value of 2.83 μ_B. Crystals suitable for X-ray crystallography were obtained by layering a dichloromethane solution of **4** with *n*-hexane at room temperature (Figure 2.7).

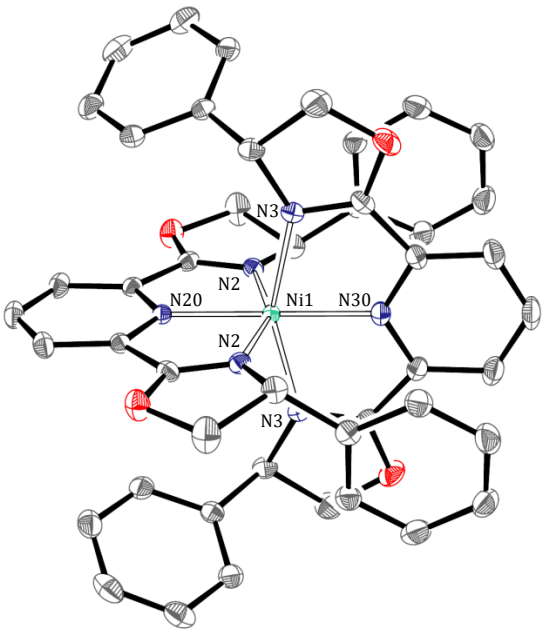

Figure 2.7. Solid-state structure of **4**. Thermal ellipsoids at 50% probability, hydrogen atoms and counter anions omitted for clarity. Selected bond lengths (Å) and angles (°): Ni1-N2, 2.124(2); Ni1-N3, 2.090(2); Ni1-N20, 1.999(3); Ni1-N30, 2.009(3); N2-Ni1-N20, 77.86(6); N3-Ni1-N30, 77.51(6); N2-Ni1-N2*, 155.72(13); N3-Ni1-N3, 155.03 (13); N20-Ni1-N30, 180.0.

The solid-state structure of **4** shows a distorted octahedral geometry with intraligand N(*ox*)-Ni-N(*py*) angles of 77.86(6)° and 77.51(6)° as a consequence of smaller chelate bite angles. The bond metrics obtained correspond well to other nickel(II) pybox derivatives.[302] Formation of homoleptic pybox complexes has been observed in literature with a number featuring late transition metals. The bond metrics of **4** were compared to these structures and found to lie in the expected realm.[303–305]

Discovery of this homoleptic bis(pybox) complex of nickel inspired us to develop a passive metal template catenane synthesis, whereby two precursor ligands are orientated by the nickel centre followed by fusion to form two mechanically bonded rings. Therefore preparation of [2]catenate **Ni-12** was envisioned *via* formation of nickel(II) bis(pybox) complex **11** followed by ring-closing metathesis and subsequent hydrogenation to form **Ni-12** (Scheme 2.10).

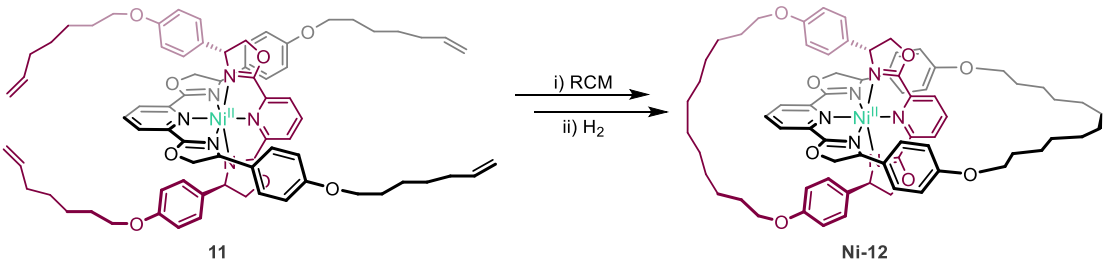

Scheme 2.10. Proposed synthetic preparation of catenate **Ni-12**. $[BF_4]^-$ counter anions omitted for clarity.

2.6. Synthesis of terminal alkene precursor ligand

Synthetic routes to the terminal alkene precursor (*R*,*R*)-(6-heptenyl)-phenol pybox **10** were explored. Initial pathways utilised the *meso*-**A101** diastereomer as the starting material, which was produced during the synthesis of **^{M}pybox** (Scheme 2.11). The undesired *meso*-diastereomer was used for optimisation to avoid wasting (*R*,*R*)-**A101**.

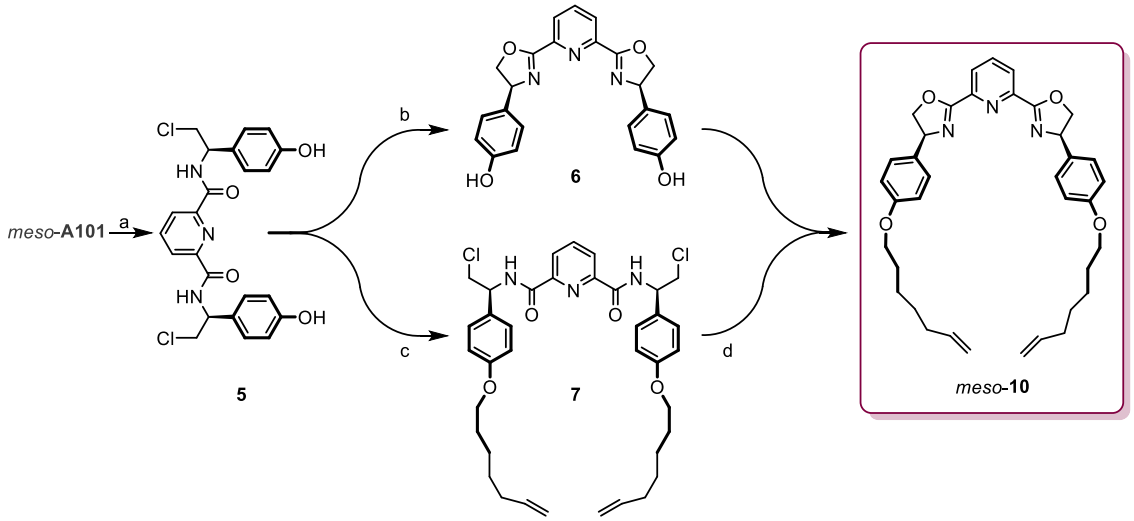

Scheme 2.11. Proposed synthesis of **10**. Reagents and conditions: a) $SOCl_2$, $CHCl_3$, reflux, 48 h, 88%; b) TBAF, THF; c) 7-bromo-1-heptene, K_2CO_3, DMF, 40 °C, 72 h, 26%; d) TBAF, THF, rt, 18 h.

The first synthetic route trialled involved the generation of phenol pybox **6**, followed by substitution of the phenols with 7-bromo-1-heptene to install the terminal alkene chains. Treatment of *meso*-**A101** with thionyl chloride gave **5** in 88% yield. Mild basic conditions induced cyclisation to form oxazoline compound **6** in *ca*. 50% purity. ESI-MS confirmed formation of **6**, with a signal at 402.1431 *m*/*z* (calcd 402.1448) assigned to $[M+H]^+$. Unfortunately, a number of impurities were produced *via* this route and purification on silica was encumbered by the instability of oxazoline to hydrolysis. Addition of the heptenyl chains before formation of the oxazoline moiety was next investigated. It was found that the chloride analogue **5** did not selectively undergo substitution at phenol and ultimately **7** was not produced in high purity.

As the first two proposed methods proved unsuccessful, a synthetic pathway starting from **A102** was developed, initially using *meso*-**A102** and then applied to the preparation of **10** (Scheme 2.12).

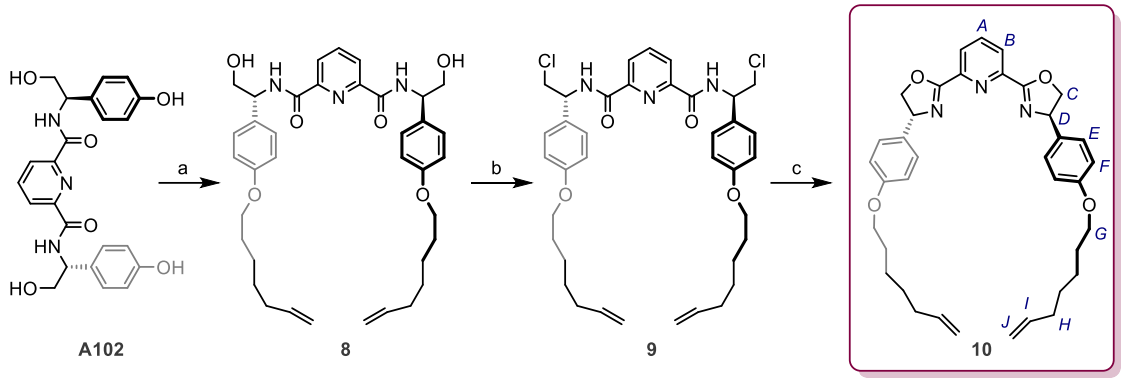

Scheme 2.12. Synthesis of **10**. Reagents and conditions: a) 7-bromo-1-heptene, K_2CO_3, DMF, 50 °C, 72 h, 54%; b) $SOCl_2$, $CHCl_3$, reflux, 48 h, 85%; c) TBAF, THF, rt, 72 h, 80%.

The substitution reaction of 7-bromo-1-heptene with **A102** resulted in a respectable yield of **8** (54%), without any substitution observed on the primary alcohol. Analysis of **8** by ^{1}H NMR spectroscopy ($CDCl_3$) confirmed the successful installation of the heptenyl chains, with the presence of terminal alkene signals at δ 5.81, 5.02 – 4.99 and 4.96 – 4.94, as well as a triplet at δ 3.95 corresponding to the alkyl group adjacent to the phenol oxygen atom. The ESI-MS of **8** also displayed a signal at 652.3364 (calcd 652.3363) *m*/*z* assigned to $[M+Na]^+$. Refluxing **8** in $SOCl_2$ generated chloride product **9** in a good yield (85%) following purification by column chromatography, and was fully characterised. The most diagnostic evidence in the ^{1}H NMR spectrum ($CDCl_3$) was a downfield shifted C<u>H</u>NH resonance, resulting from introduction of the electron withdrawing chlorine atom (**8**: δ 5.20, **9**: δ 5.49).

Ring closure to form the oxazoline groups gave pybox **10** in a high yield (80%). Analysis of **10** by ^{1}H NMR spectroscopy confirmed formation of the oxazoline moieties, with characteristic resonances at δ 5.40 (H_D), 4.89 (H_C) and 4.40 ($H_{C'}$), assigned to the oxazolinyl methine and two diastereotopic methylene signals respectively. In addition, an intense molecular ion peak was observed by ESI-MS at 616.3150 (calcd 616.3146) *m*/*z* that can be assigned to $[M+Na]^+$.

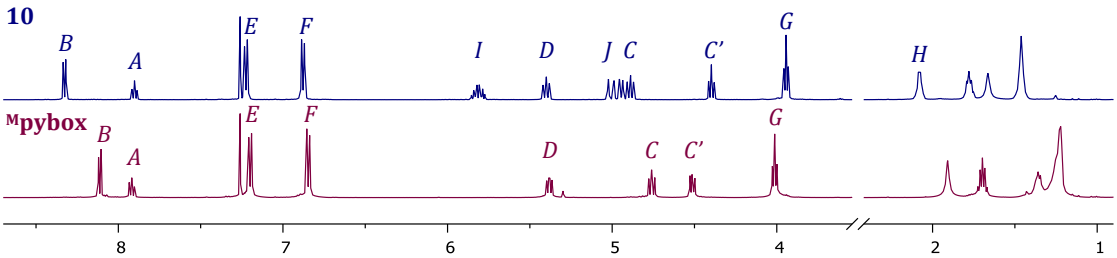

Figure 2.8. ^{1}H NMR spectra of **10** (*top*) and **Mpybox** (*bottom*) (500 MHz, $CDCl_3$, 298 K).

2.7. Attempted nickel-templated catenane synthesis

In an analogous manner to **4** (Scheme 2.9), bis(pybox) nickel(II) complex **11** was prepared by reaction of two equivalents of **10** with [$NiCl_2$(glyme)] in dichloromethane, followed by washing with ammonium tetrafluoroborate, in excellent yield (92%; Scheme 2.13).

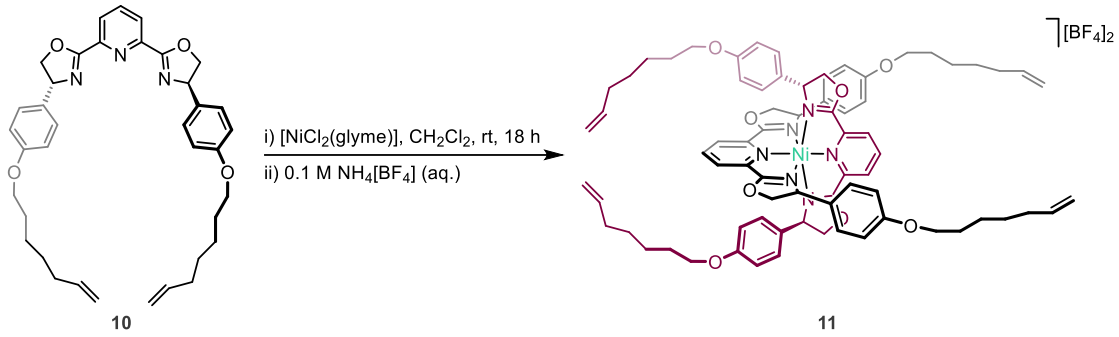

Scheme 2.13. Synthesis of catenane precursor **11**.

High-resolution ESI-MS of **11** showed a peak at 1331.5905 (calcd 1331.5896) m/z, which was attributed to $[M–BF_4]^+$. An effective magnetic moment μ_{eff} = 2.93 μ_B was determined for **11** using the Evans method in CD_3CN, consistent with an octahedral nickel(II) complex ($\mu_{spin\text{-}only}$ = 2.83 μ_B) and **4** (2.71 μ_B). The ^{1}H NMR spectrum of **11** in $CDCl_3$ displayed predominantly broad signals, as expected for paramagnetic broadening from a nickel(II) centre. However, the alkene signals, which are remote from the metal centre, could be identified at δ 5.22 – 4.86, similar to unbound **10** (δ 5.04 – 4.92).[306] Crystals suitable for X-ray crystallography were also obtained from diffusion of *n*-hexane into a dichloromethane solution of **11** (Figure 2.9).

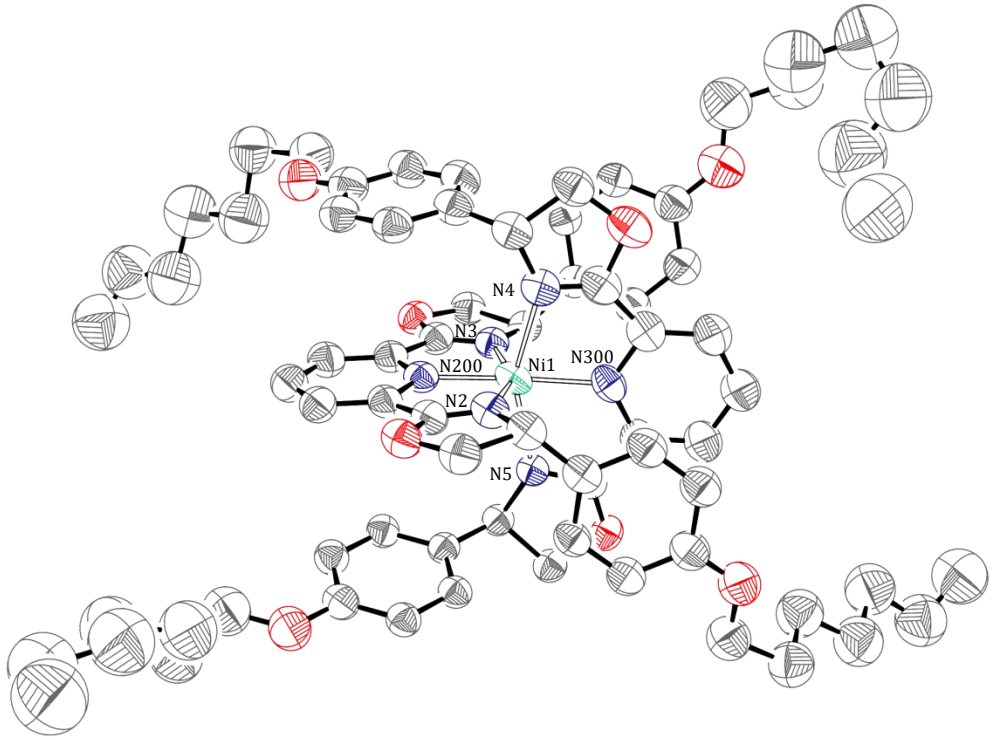

Figure 2.9. Solid-state structure of **11**. Thermal ellipsoids at 30% probability. $[BF_4]^-$ counter anions and hydrogen atoms omitted for clarity.

As a consequence of poor quality crystals, the solid-state structure of **11** can be used for connectivity purposes only. Like nickel complex **4**, the structure displayed the expected distorted octahedral geometry with similarly small chelate bite angles of approximately 78° (N(*ox*)-Ni-N(*py*)). The heptenyl chains are highly disordered, but in this conformation ring closing metathesis of the terminal alkene groups seems feasible.

Complex **11** was subjected to Grubbs I catalysed ring closing metathesis to capture the interlocked architecture, followed by subsequent hydrogenation (Pd/C, 4 bar H_2, 100 °C, 72 hours), both of which were monitored by mass spectrometry. High-resolution ESI-MS of pre-hydrogenated **Ni-12** displayed a peak at 1275.5293 (calcd 1275.5269) *m*/*z*, which can be attributed to $[M-BF_4]^+$. Under hydrogenation conditions over 72 hours this signal was replaced by one possessing a higher molecular mass by 4 Da, that is correspondingly assigned to the hydrogenation product **Ni-12** ($[M-BF_4]^+$ 1279.5565 (calcd 1279.5577) *m*/*z*). Analysis of **Ni-12** by ^1H NMR spectroscopy confirmed hydrogenation of the alkene groups, by disappearance of the corresponding signals seen in **11** (δ 5.22 – 4.86, $CDCl_3$) and retention of the coordinated nickel(II) template by the broadness of the spectrum (Figure 2.10). Analysis of crude samples of **Ni-12** using DOSY NMR spectroscopy suggested several compounds of similar diffusion coefficients were present, leaving questions over the bulk purity of the material. Preliminary attempts to purify **Ni-12** by C_{18} reverse phase chromatography resulted in orange-brown streaking consistent with

demetalation on the column. Therefore crude **Ni-12** was subsequently treated with demetalation reagents.

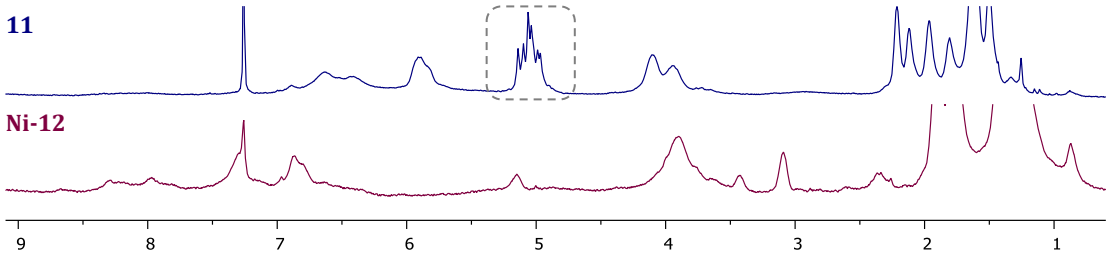

Figure 2.10. ^{1}H NMR spectra showing **11** (*top*); nickel catenate **Ni-12** (*bottom*). Alkene signals highlighted with dashed square, (300 MHz, $CDCl_3$, 298 K).

In attempt to remove nickel, **Ni-12** was treated with the chelating reagent ethylenediaminetetraacetic acid (EDTA), as well as potassium cyanide (KCN), both of which are frequently employed as reagents to remove metal templates from interlocked molecules (Scheme 2.14).[307]

Unfortunately, washing with ammoniacal EDTA disodium solution was ineffective as evidenced by a unchanged ^{1}H NMR spectrum which displayed the characteristic broadness associated with paramagnetic nickel(II) centre. Purification of this material by column chromatography (C_{18} silica) was attempted. A large amount of dark material deposited on the silica alongside significant streaking, consistent with demetalation on the column, however, no fractions could be assigned to **12**. Refluxing with di- and tetra-sodium EDTA was attempted, but this also failed to demetalate **Ni-12**. The room temperature reaction of **Ni-12** with KCN was unsuccessful at removing nickel, whilst use of more forcing conditions (refluxing MeCN) generated an intractable mixture of compounds unable to be purified by reverse phase column chromatography (C_{18} silica).

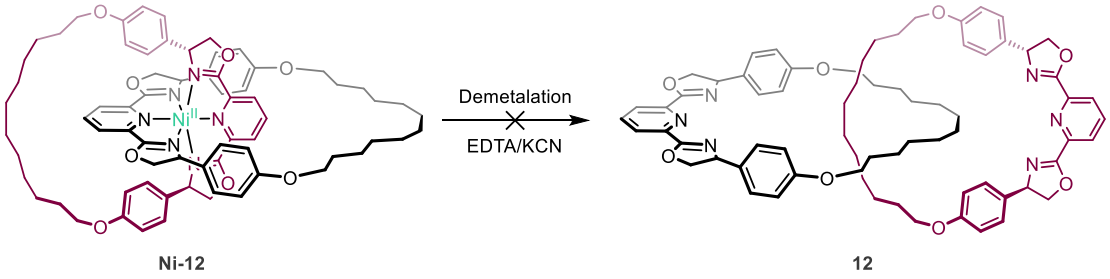

Scheme 2.14. Attempted demetalation of **Ni-12**.

The robust binding of nickel is consistent with other examples of octahedral templated catenanes. For instance, catenane **A62** contains neutral pyridine-2,6-diimino pincer ligands, the removal of the metal template was only achieved following reduction of the imine and subsequent washing with aqueous Na_2EDTA.[195] Similarly, a cobalt(III)-catenate containing pyridine-2,6-dicarboxamide based macrocycles was able to be demetalated by reduction of the metal to cobalt(II) under acidic conditions.[191] Restricted conformational

mobility has been shown to inhibit demetalation; for instance, a more flexible interlocked macrocycle enables more facile metal removal.[308] Therefore, the sterically encapsulated nickel(II) centre in **Ni-12** was unlikely to be demetalated without transformation of the oxazoline moiety to weaken catenane binding.

Whilst bulk demetalation of **Ni-12** proved elusive, analysis of the aforementioned attempts by ESI-MS suggested at least in the gas phase this is conceptually possible. In one instance a signal at 1193.6301 (calcd 1193.6298) *m*/*z* was assigned to **12** flying as the ion [**12**+2H_2O+Na]$^+$. Analysis of this ion by tandem mass spectrometry, frequently employed to confirm the formation of interlocked molecules,[297,298,309] showed fragmentation into a singular macrocycle, with a signal at 590.2978 [^{M}**pybox**+Na]$^+$ (calcd 590.2989) *m*/*z*, supporting the interlocked nature proposed for **12**.

2.8. Summary

The synthesis of interlocked molecules derived from a pybox-based macrocycle has been explored. The first part of this chapter focused on the known nickel-catalysed C(sp^3)–C(sp^3) homocoupling procedure for the generation of rotaxanes. The conditions were initially studied using the acyclic and macrocyclic models, ^{Ph}**pybox** and ^{M}**pybox** respectively.[160] Related terpyridine-based ligands were also explored, however, the homocoupling procedure proved ineffective. Optimisation of the rotaxanation conditions enabled preparation of the desired [2]rotaxane product (^{R}**pybox**), following separation from an unexpected doubly-threaded [3]rotaxane (^{R*}**pybox**) and non-interlocked axle (**3**).

Inspired by the serendipitous isolation of a homoleptic nickel(II) ^{Ph}**pybox** complex (**4**), preparation of catenane **12** was targeted. A synthetic route to the heptenyl-pybox precursor ligand was established and the corresponding octahedral nickel(II) complex prepared. Fusion of the rings could be achieved by ring-closing metathesis followed by hydrogenation to form catenate **Ni-12**, however, conditions for removing the nickel template could not be identified.

As a consequence of the challenging syntheses of both the macrocyclic and interlocked ligands, with ^{R}**pybox** produced in an overall yield of <1%, it was necessary to initially probe the coordination chemistry with the acyclic variant, ^{Ph}**pybox**. The results of this investigation are described in the following chapter.

Chapter 3: Coordination Chemistry of Acyclic Ligands

This chapter focuses on the chemistry of rhodium, iridium and ruthenium complexes of the acyclic ligand ^{Ph}**pybox**, with a view to optimising the synthetic procedures and establishing metal based reactivity for the more demanding targets containing macrocyclic (^{M}**pybox**) and interlocked (^{R}**pybox**) pybox ligands (Figure 3.1).

Rhodium(I) and rhodium(III) chloride complexes were prepared and halide abstraction was shown to be a viable route to low-coordinate ^{Ph}**pybox** derivatives. The donor properties of the pybox ligand were examined through use of rhodium carbonyl fragments, and were compared to related pincer ligands.[310] Five coordinate 2,2'-biphenyl complexes of rhodium(III) and iridium(III) were investigated, exploiting [Rh(2,2'-biphenyl)(dtbpm)Cl] and [Ir(2,2'-biphenyl)(COD)Cl]$_2$ as convenient and well defined sources of rhodium(III) and iridium(III). Finally, as neutral isoelectronic analogues of these M(III) derivatives, ruthenium(II) chloride complexes were prepared.

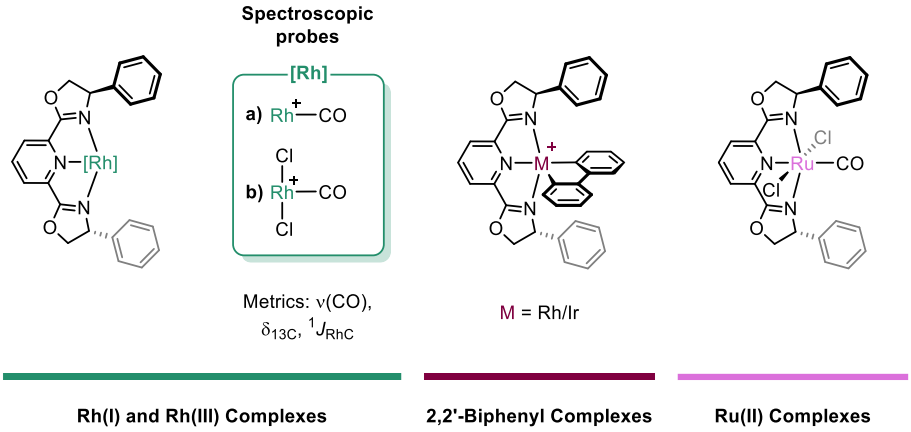

Figure 3.1. Model acyclic ^{Ph}**pybox** complexes.

Publications resulting from the work described in this chapter:

- G. L. Parker, S. Lau, B. Leforestier and A. B. Chaplin, *Eur. J. Inorg. Chem.*, 2019, **2019**, 3791–3798.

3.1. Introduction

3.1.1. Rhodium complexes

Pincer ligands can be utilised for the stabilisation of reactive rhodium fragments. For instance, use of a bis(imino)pyridine ligand enables synthesis of the low-coordinate cationic complex **A23**, *via* chloride abstraction from the corresponding rhodium(I) chloride complex in dichloromethane (Figure 3.2).[45] Significantly, **A23** was found to be stable to the oxidative addition of dichloromethane, which is often observed for rhodium(I) complexes of this type.[56] As noted earlier, employment of a PONOP pincer ligand permits the characterisation of a rhodium σ-methane complex (**A84a**) by NMR spectroscopy in $CDCl_2F$ at −110 °C.[271] Research by Nishiyama provides precedent for the formation of stable rhodium(III) pybox complexes (*e.g.* **A34**), which were shown to be effective enantioselective precatalysts.[58,101] Motivated by these examples, pybox-based rhodium complexes will be targeted for the generation of low-coordinate species.

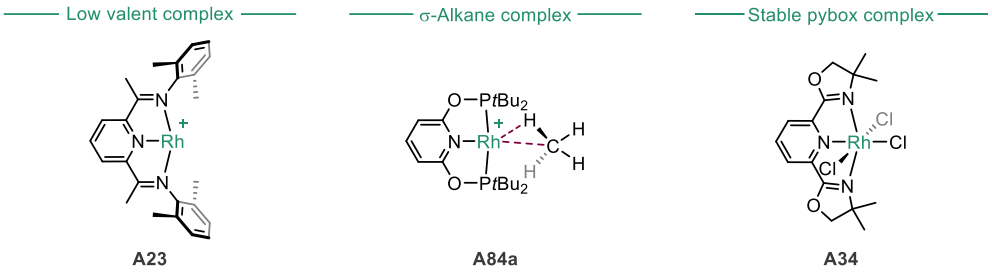

Figure 3.2. Pincer-based rhodium complexes, counter anions omitted for clarity.

3.1.2. Rhodium and iridium 2,2'-biphenyl complexes

Research in the Chaplin group has utilised the well-defined species **A108** and **A109** as precursors for iridium(III) and rhodium(III) complexes containing the high trans-influence 2,2'-biphenyl ancillary ligand (Figure 3.3).[311,312] The low-coordinate derivatives **A110** adopt agostic interactions in the solid-state and solution, as evidenced by NMR spectroscopy.[313] The five-coordinate pincer complexes **A111** were found to be structurally dynamic; pseudorotation of the biphenyl moiety was observed in solution (Scheme 3.1).[314]

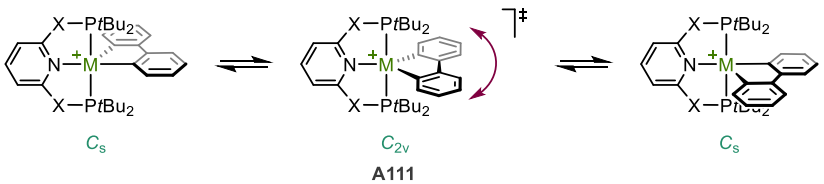

Scheme 3.1. Pseudorotation of the 2,2'-biphenyl ligand. M = Rh, Ir; X = O, CH_2.

In addition, low-coordinate macrocyclic complexes **A75** displayed agostic M···H–C interactions in the solid-state, which were remarkably maintained in solution at room temperature.[252] Similarly, metalation of macrocyclic PNP and PONOP pincer ligands with

A109 generated low-coordinate complexes **A112**.[315] The CNC pincer complex **A113** is notable for η²-coordination of benzene and fluoroarenes, with preference for coordination *via* the HC=CH site neighbouring a fluorine substituent.[316] Combined these examples demonstrate the ability of the 2,2'-biphenyl ligand to support generation of low-coordinate species and permit study of weakly binding substrates such as agostic interactions and η²-arene complexes.

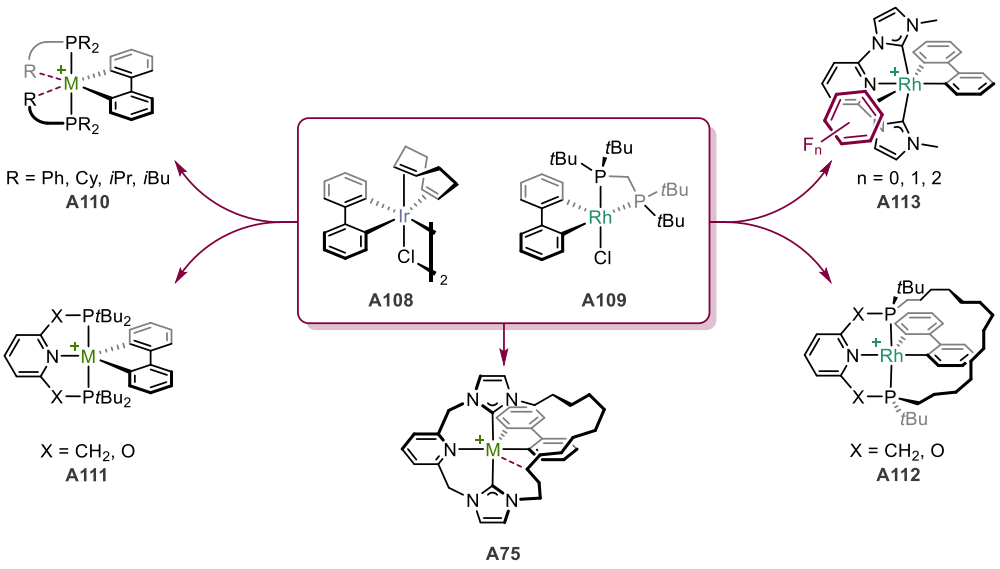

Figure 3.3. Rhodium and iridium complexes bearing the 2,2'-biphenyl ancillary ligand. M = Rh, Ir. $[BAr^F_4]^-$ counter anions omitted for clarity.

3.1.3. Ruthenium complexes

Ruthenium(II) complexes of nitrogen-based pincer ligands have been shown to be effective catalysts (Figure 3.4).[124] For instance, the ruthenium-pybox complex **A114** is capable of catalysing the enantioselective hydrogenation and transfer hydrogenation of imines.[317] Treatment of the bis(imino)pyridine ruthenium ethylene complex **A115** with hydrosilanes generated low-valent complexes in arene solvents.[64] Furthermore, ruthenium(II) complexes have been shown to support the formation of agostic bonds. The strong η²-C–H agostic bonds formed in pincer complex **A116** were observed by NMR, IR and solid-state characterisation techniques.[318] Cationic ruthenium(II) complexes have also demonstrated agostic interactions (**A117** and **A118**).[319,320]

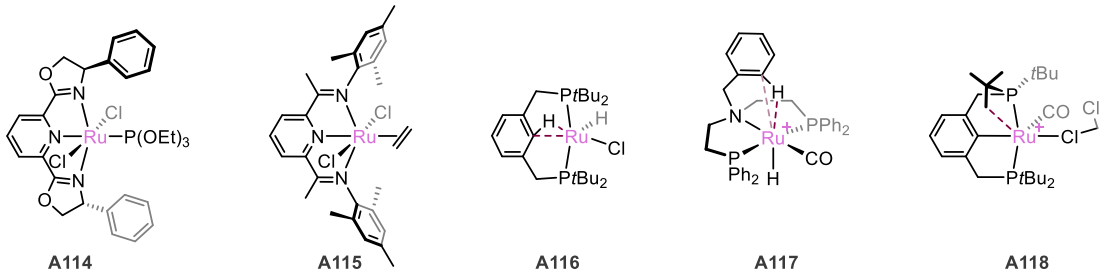

Figure 3.4. Ruthenium(II) complexes, $[BAr^F_4]^-$ counter anions omitted for clarity.

3.2. Rhodium complexes

3.2.1. Synthesis and characterisation of rhodium chloride complexes

Rhodium(I) chloride complex **13a** was synthesised from the reaction of metal precursor $[Rh(COE)_2Cl]_2$ with ^{Ph}**pybox** in THF at room temperature (Scheme 3.2), precipitating out of solution as a blue-black solid in good yield (86%).

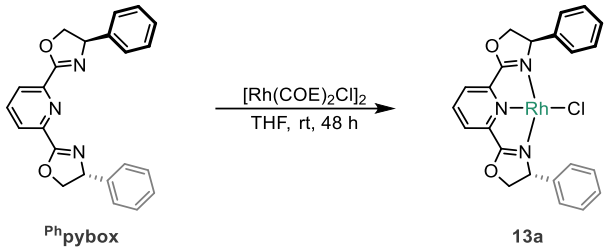

Scheme 3.2. Synthesis of rhodium(I) chloride complex **13a**.

Complex **13a** is surprisingly insoluble in organic solvents. In addition to THF, insoluble products were obtained when this reaction was repeated in methanol, benzene, 1,2-difluorobenzene and fluorobenzene. Similar observations have been noted by Vrieze, who prepared a range of bis(imino)pyridine pincer-based rhodium(I) chloride complexes in refluxing benzene; the products crystallised upon cooling and proved too insoluble to be characterised by ^{1}H NMR spectroscopy.[56] Crystals of **13a** suitable for X-ray diffraction were obtained by slow diffusion of heptane into a 1,2-diflurobenzene solution of the complex (Figure 3.5).

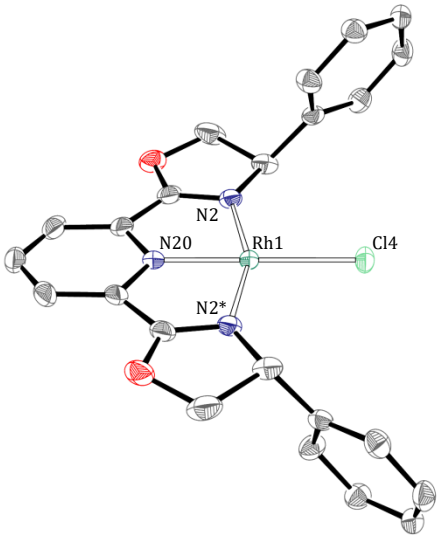

Figure 3.5. Solid-state structure of **13a**. Thermal ellipsoids drawn at 40% probability; * atoms generated by the symmetry operation 1−x, −y, +z. Hydrogen atoms are omitted for clarity. Selected bond lengths (Å) and angles (°): Rh1-N2, 2.052(3); Rh1-Cl4, 2.3097(9); Rh1-N20, 1.913(3); N2-Rh1-N2*, 158.45(17); N20-Rh1-Cl4, 180.0.

In the solid-state **13a** exhibits a pseudo-square planar geometry with N2-Rh-N2* angle of 158.45(17)°, imine Rh–N2 bond lengths of 2.052(3) Å, and pyridine Rh–N20 bond length

of 1.913(3) Å. Complex **13a** is sparingly soluble in C_6D_6 but sufficient to permit characterisation by ^{1}H NMR spectroscopy; a weak spectrum was obtained but required 128 scans. Characteristic changes compared to free ^{Ph}**pybox** were observed, as expected upon complexation, with the resonance for the oxazolinyl methine proton, which was shifted downfield by $\Delta\delta$ 0.37, and the *meta*-pyridine protons, which were shifted $\Delta\delta$ 1.34 upfield, most notable. The ^{1}H NMR spectrum of **13a** was consistent with adoption of C_2 symmetry in solution as evidenced by three oxazoline resonances at δ 5.46, 4.22 and 4.10. Acquisition of ^{13}C{^{1}H} NMR data was, however, not possible in C_6D_6 or any solvent trialled (*e.g.* toluene, THF and CD_3OD). Formation of **13a** was further evidenced by HR ESI-MS, which showed the molecular ion peak at 508.0293 (calcd 508.0294) m/z attributed to the $[M+H]^+$ ion. In addition, elemental microanalysis confirmed the bulk purity of **13a**.

Dissolving **13a** in CH_2Cl_2 resulted in oxidative addition of the solvent and formation of rhodium(III) complex **14**, as indicated by a colour change from black to a bright yellow, which was isolated in 84% yield (Scheme 3.3). The ^{1}H NMR spectrum (CD_2Cl_2) of **14** displays signals assigned to the bound chloromethyl moiety at δ 4.34 and 3.89, further supported by doublet of doublet multiplicity ($^2J_{HH}$ = 5.3/5.2 Hz; $^2J_{RhH}$ = 3.2/3.1 Hz). In addition, the bound chloromethyl carbon could be identified using ^{13}C{^{1}H} NMR spectroscopy (δ 39.3; $^1J_{RhC}$ = 26 Hz). The related bis(4,4-dimethyloxazolin-2-yl)pyridine (dm-pybox) (chloromethyl)rhodium(III) complex is characterised by a similar resonance in the ^{13}C{^{1}H} NMR spectrum (δ 38.9; $^1J_{RhC}$ = 25, $CDCl_3$).[58] This reactivity has been observed in related rhodium(I) chloride pincer complexes, including NNN pincer systems; steric effects enforced by the 2,6-diisopropylphenyl substituents notably prevent oxidative addition in complex **A23** (*vide supra*).[45,56]

In a similar manner, the known rhodium(III) trichloride complex **13b** was prepared through oxidation of **13a** with iodobenzene dichloride ($PhICl_2$, Scheme 3.3).

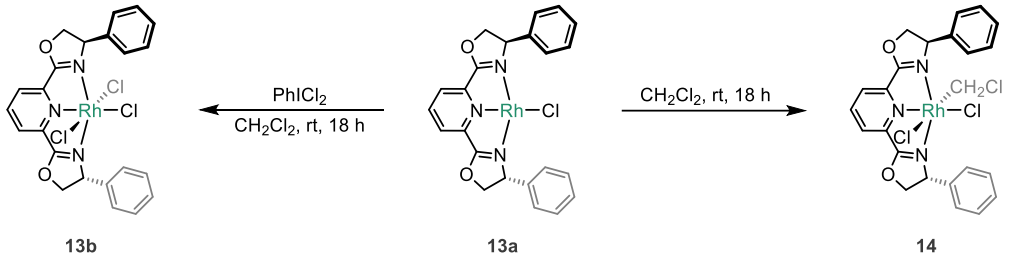

Scheme 3.3. Oxidation addition reactions of **13a**.

Initial attempts to oxidise **13a** in THF at room temperature resulted in poor yields of **13b** due to limited solubility of **13a**, whilst use of elevated temperatures lead to intractable decomposition products. Dichloromethane was found to be the most effective solvent. The trichloride **13b** was formed selectively over the dichloromethane activation product **14**,

due to the instantaneous nature of the oxidation with $PhICl_2$, and isolated in good yield (79%). The ^1H NMR spectroscopic data was in good agreement with the literature.[114] Crystals of **13b** suitable for X-ray diffraction were obtained from diffusion of methanol into a dichloromethane solution of the complex (Figure 3.6).

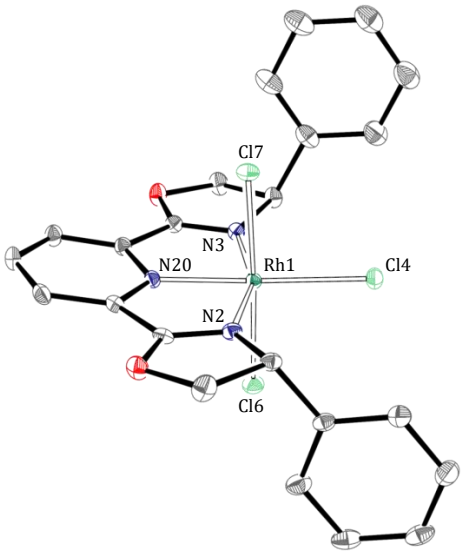

Figure 3.6. Solid-state structure of **13b**. Thermal ellipsoids drawn at 40% probability. Hydrogen atoms are omitted for clarity. Selected bond lengths (Å) and angles (°): Rh1-N2, 2.045(3); Rh1-N3, 2.063(3); Rh1-Cl4, 2.3412(7); Rh1-Cl6, 2.3227(8); Rh1-Cl7, 2.3541(8); Rh1-N20, 1.964(2); N2-Rh1-N3, 158.83(10); N20-Rh1-Cl4, 178.04(8); Cl6-Rh1-Cl7, 176.97(3).

Compared to the rhodium(I) complex **13a**, the imine Rh–N bonds of **13b** are the same within error (2.045(3), 2.063(3) *cf*. 2.052(3) Å), but the pyridine Rh–N is appreciably elongated (1.964(2) *cf*. 1.1913(3) Å). The imine N-Rh-N angles in **13a/b** showed little difference, however, the pyridyl donor in **13b** is slightly bent out of the plane, with a N20-Rh-C4 angle of 178.04(8)° compared to the 180° in **13a**.

3.2.2. Synthesis and characterisation of cationic rhodium(I) complexes

Chloride abstraction of **13a** using $Na[BAr^F_4]$ in weakly coordinating solvent fluorobenzene was proposed to form the cationic 14 VE rhodium derivative **15a** (Scheme 3.4, Figure 3.7).[321] Dissolution of the starting material and accompanying formation of a burgundy solution is consistent with this suggestion, and further supported by analysis *in situ* by ^1H NMR spectroscopy. Subsequent reaction of **15a** with the solvent was observed within 2 hours by ^1H NMR spectroscopy, resulting from C–H activation of fluorobenzene.

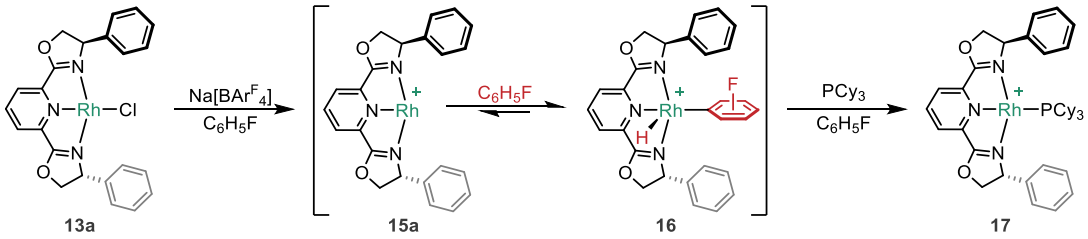

Scheme 3.4. Formation and reactions of **15a**. $[BAr^F_4]^-$ counter anions omitted for clarity.

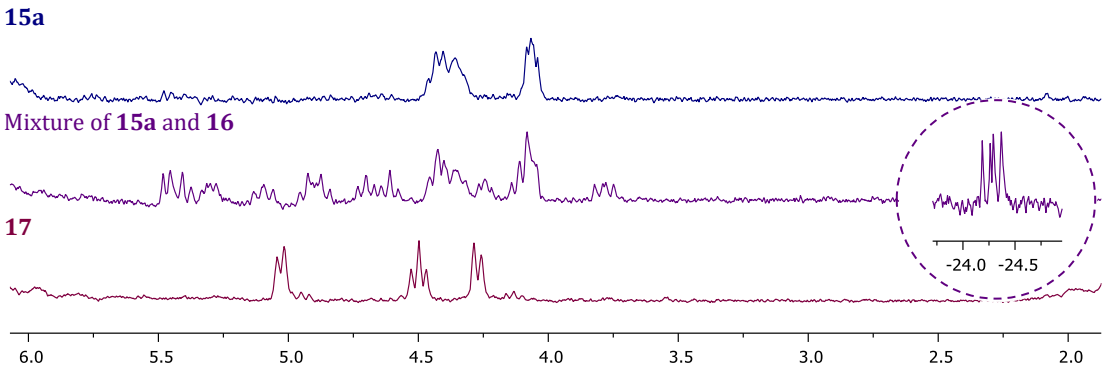

Figure 3.7. ^{1}H NMR spectra of **15a** (*top*), mixture of **15a** and **16** with hydride signals displayed in the circle (*middle*), PCy_3 complex **17** (*bottom*). Selected region displaying oxazoline signals shown for clarity (C_6H_5F, 300 MHz, 298 K).

Two sets of doublets in a 1:1 ratio were observed in the upfield region of the ^{1}H NMR spectrum of **16** at δ −24.22 ($^{1}J_{RhH}$ = 22.4 Hz) and δ −24.33 ($^{1}J_{RhH}$ = 23.3 Hz), indicative of two Rh–H environments. Based on literature precedent for the selective *ortho* activation of fluorobenzene, the formation of 2 rotamers is proposed (Figure 3.8).[322,323]

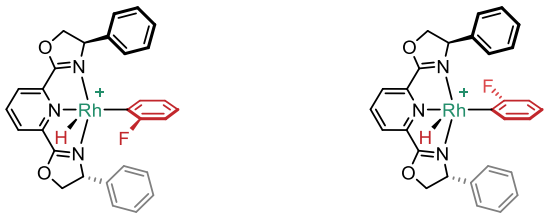

Figure 3.8. Possible rotamers of **16**. $[BAr^{F}_4]^-$ counter anions omitted for clarity.

The addition of PCy_3 as a 'trapping' reagent to the mixture of **15a** and **16** resulted in quantitative conversion to the phosphine complex **17** instantaneously, as evidenced by ^{1}H NMR spectroscopy. This process was accompanied by a colour change from dark red to pink. Complex **17** was subsequently isolated by reaction of **13a** with $Na[BAr^{F}_4]$ and PCy_3 in fluorobenzene at room temperature in good yield (79%). In solution, **17** shows time-averaged C_2 symmetry with three oxazolinyl resonances in the ^{1}H NMR spectrum (CD_2Cl_2) at δ 5.18, 4.95 and 4.70. Furthermore, the $^{31}P\{^{1}H\}$ NMR spectrum of **17** in CD_2Cl_2 showed a doublet at δ 36.14 with a $^{1}J_{RhP}$ value of 167 Hz, consistent with related PCy_3 PNP complexes (154–163 Hz).[324] Formation of **17** was further evidenced by HR ESI-MS, which showed a major peak at 752.2847 (calcd 752.2847) m/z attributed to the $[M]^+$ ion.

The structure of **17** is supported by independent synthesis from the reaction of **^{Ph}pybox** with $[Rh(Binor\text{-}S)(PCy_3)][BAr^{F}_4]$ (**A119**) in 1,2-difluorobenzene at room temperature (Scheme 3.5). The rhodium(III) complex **A119** is an established latent source of the rhodium(I) fragment $\{Rh(PR_3)\}^+$, through reductive elimination of Binor-S (Binor-S = 1,2,4,5,6,8-dimetheno-s-indacene).[251,325,326] In this way complex **17** is generated in

quantitative spectroscopic yield. The $^{31}P\{^{1}H\}$ signal of **17** (δ 36.14; $^{1}J_{RhP}$ = 167 Hz) is distinct from the starting material [Rh(Binor-S)(PCy_3)][BAr^F_4] (δ 35.84; $^{1}J_{RhP}$ = 211 Hz).[325]

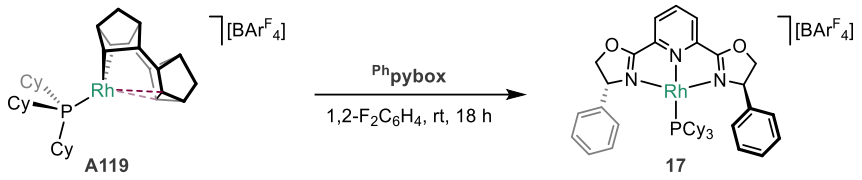

Scheme 3.5. Synthesis of the phosphine complex **17**.

The metal precursor [Rh(acetone)$_2$(COE)$_2$][PF_6] was also explored as alternative source of cationic rhodium(I). The reaction of ^{Ph}**pybox** with [Rh(acetone)$_2$(COE)$_2$][PF_6] in CD_3CN at room temperature proceeded quantitatively within 1 hour to generate **18** (Scheme 3.6).

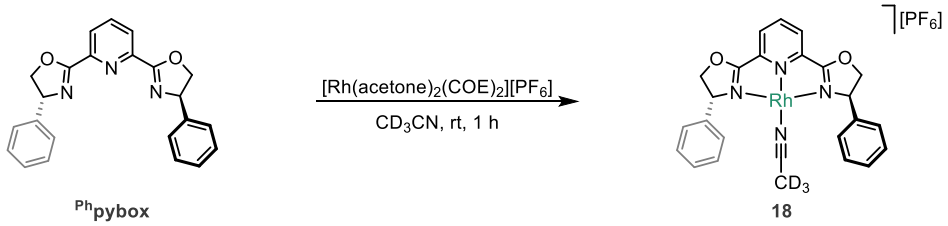

Scheme 3.6. Synthesis of cationic rhodium(I) acetonitrile complex **18**.

Formation of **18** was evidenced by the liberation of acetone (δ 2.09) and cyclooctene (δ 5.63, 2.13 and 1.50) into solution by ^{1}H NMR spectroscopy (CD_3CN). Complex **18** adopts C_2 symmetry in solution as evidenced by diagnostic pyridine resonances at δ 8.20 and 7.70. Layering the deep orange acetonitrile solution with diethyl ether produced a dark brown solid and small orange crystals suitable for X-ray crystallography, which surprisingly proved to be rhodium(II) complex [Rh(^{Ph}**pybox**)$_2$][PF_6]$_2$ (**19**; Scheme 3.7). The formation of a paramagnetic nickel(II) bis(pybox) complex was previously discussed in Chapter 2 and formation of rhodium(II) complex **19** is hypothesised to occur by disproportionation of rhodium(I) **18**, with concomitant generation of Rh^0 (brown solid). However, further work would be required to confirm this, for example cyclic voltammetry studies.[327]

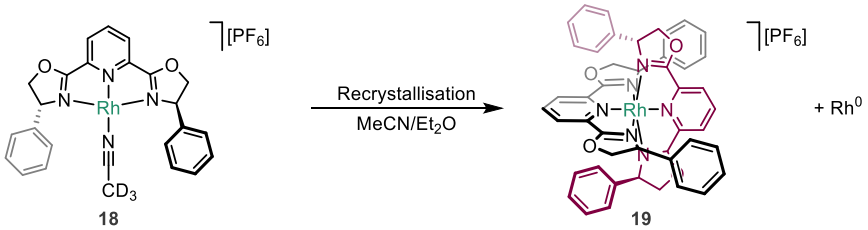

Scheme 3.7. Generation of bis(pybox) complex **19**.

3.2.3. Synthesis and characterisation of rhodium carbonyl complexes

Building on the findings described in the preceding section, carbon monoxide was employed as an alternative trapping reagent. The reaction of **13a** with Na[Bar^F_4] in fluorobenzene at room temperature generated the low-coordinate complex **15a** *in situ*,

which was immediately treated with CO (1 atm) forming carbonyl derivative **20a**, evidenced by a colour change to dark green and was isolated in very good yield (85%) (Scheme 3.8).

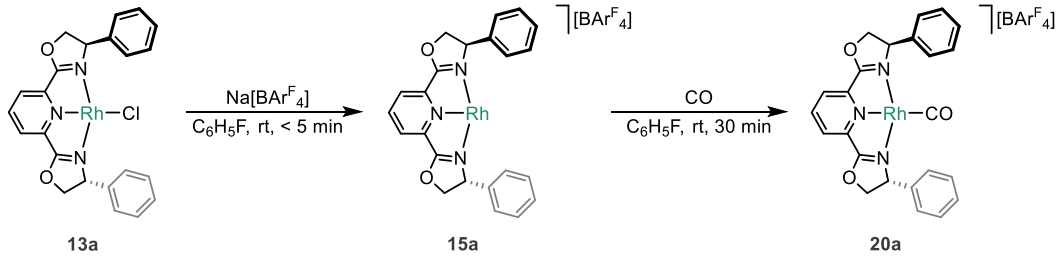

Scheme 3.8. Synthesis of rhodium(I) carbonyl complex **20a**.

Formation of the carbonyl complex was corroborated by HR ESI-MS, with a peak at 500.0518 (calcd 500.0521) *m*/*z* attributed to the parent cation $[M]^+$. Coordination of carbon monoxide was further confirmed by examination of the $^{13}C\{^1H\}$ NMR spectrum, which showed a doublet at δ 188.1 with $^1J_{RhC}$ = 77 Hz, assigned to Rh(CO). Furthermore, a carbonyl stretching frequency of 2019 cm^{-1} was determined by FT-IR spectroscopy in dichloromethane. The ν(CO) value of the related complex [Rh{(*R*,*R*)-*i*Pr-pybox}(CO)]$^+$ is 1981 cm^{-1} (KBr), suggesting a stronger C–O bond in **20a**.[117] In addition, analogous terpyridine-based complexes possessed carbonyl stretching frequencies in the same realm as **20a**, in the range of 1990 to 2020 cm^{-1}.[328,329]

Abstraction of the chloride from **13b** using Na[Bar$^F_4$] in fluorobenzene or CD_2Cl_2 at room temperature resulted in formation of the low-coordinate derivative [Rh(**^{Ph}pybox**)Cl_2][BAr$^F_4$] (**15b**) in quantitative spectroscopic yield, which was characterised *in situ* by ^1H NMR spectroscopy (Scheme 3.9). Unlike the rhodium(I) congener **15a**, activation of the halogenated solvents was not observed, notably permitting structural verification by ^1H NMR spectroscopy in CD_2Cl_2.

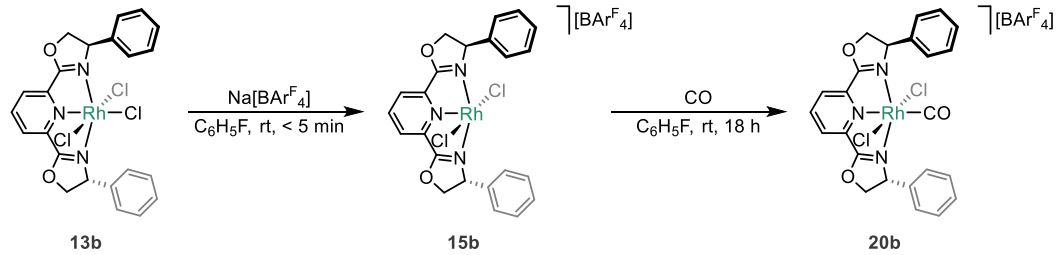

Scheme 3.9. Synthesis of rhodium(III) carbonyl complex **20b**.

Addition of carbon monoxide to 16 VE complex **15b**, was remarkably slow requiring 18 hours and vigorous stirring to proceed to completion, contrasting to the fast addition of CO to **15a** (30 min). The resulting carbonyl adduct **20b** is characterised by a carbonyl stretching frequency of 2151 cm^{-1} in dichloromethane. Although higher than that of free CO (2143 cm^{-1}), **20b** is stable under an argon atmosphere and did not lose CO upon drying

in vacuo.[330] This 'non-classical' behaviour is typically rationalised by minimal π-backbonding and significant electrostatic interactions between CO and the cationic metal fragment, which strengthens the C–O bond. This phenomenon is rare for rhodium complexes and more typically associated with complexes of coinage metals.[331] Coordination of the carbonyl was further evidenced by $^{13}C\{^{1}H\}$ NMR spectroscopy (CD_2Cl_2), with a resonance at δ 171.8 ($^{1}J_{RhC}$ = 55 Hz) assigned to CO moiety.

Crystals of **20b** suitable for X-ray diffraction were obtained by slow diffusion of pentane into a dichloromethane solution of the complex at room temperature (Figure 3.9).

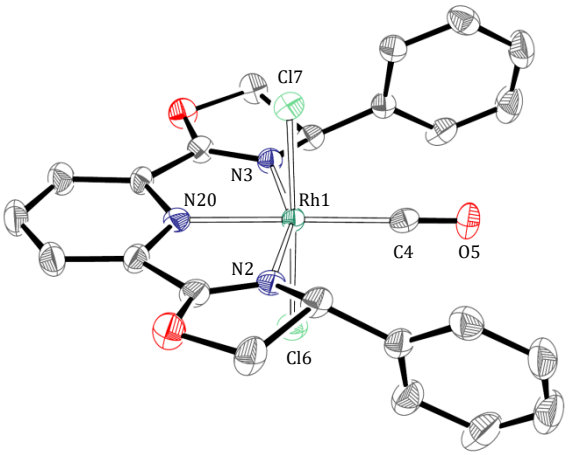

Figure 3.9. Solid-state structure of **20b**. Thermal ellipsoids drawn at 40% probability. Anion and hydrogen atoms and are omitted for clarity. Selected bond lengths (Å) and angles (°): Rh1-N2, 2.043(8); Rh1-N3, 2.016(8); Rh1-C4, 1.931(10); Rh1-Cl6, 2.326(3); Rh1-Cl7, 2.324(3); Rh1-N20, 1.990(8); C4-O5, 1.117(13); N2-Rh1-N3, 157.7(3); N20-Rh1-C4, 179.0(5); Cl6-Rh1-Cl7, 177.85(11).

The solid-state structure of **20b** confirmed the atypically shortened C=O bond length of 1.117(13) Å when compared with free CO (1.128 Å).[332] Comparison of **20b** with the solid-state structure of Rh(III) chloride derivative **13b** showed no significant changes in the other bond lengths and angles.

3.2.3.1. Redox shuttling between Rh(I) and Rh(III) carbonyls

Interconversion between rhodium(I) carbonyl complex **20a** and rhodium(III) derivative **20b** was possible in THF at ambient temperature (Scheme 3.10).

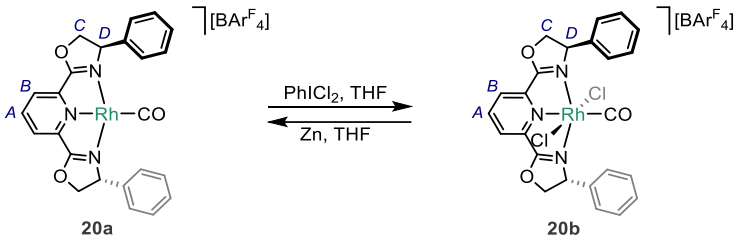

Scheme 3.10. Transformation between rhodium(I) and rhodium(III) carbonyl complexes.

Oxidation was achieved using iodobenzene dichloride and the corresponding reduction employed activated zinc. Both redox processes were complete within 1 hour and

proceeded in quantitative spectroscopic yield, as determined by ^{1}H NMR spectroscopy (Figure 3.10). Diagnostic pyridine signals in the ^{1}H NMR spectra permitted differentiation between the two complexes in proteo-THF (**20a**/**20b** δ 8.71/9.17 (H_A); 8.47/9.01 (H_B)).

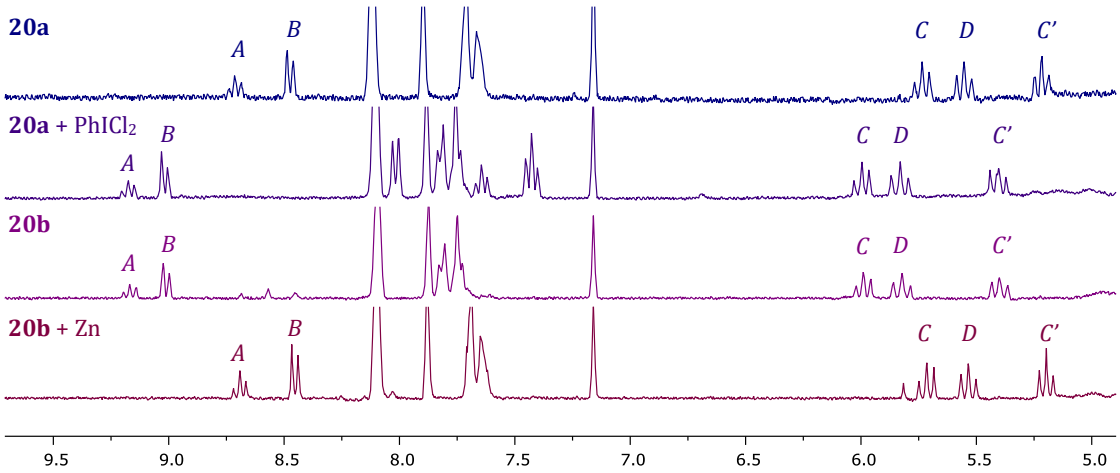

Figure 3.10. ^{1}H NMR spectra of (*top to bottom*) authentic sample of **20a**, **20a** + $PhICl_2$, authentic sample of **20b**, **20b** + Zn (298 K, THF, 300 MHz).

3.2.4. Perspectives

The preparative routes to **13a** and **13b** are reliable methods that can be extended to the more complicated macrocyclic and interlocked systems (see Chapter 4). The aforementioned halide abstraction reactions demonstrate that complexes of this nature are viable synthons for the generation of reactive low-coordinate rhodium(I) and rhodium(III) derivatives, respectively (Scheme 3.11). Trapping reactions with CO support this suggestion and provide insight into the electronic structure of these fragments.

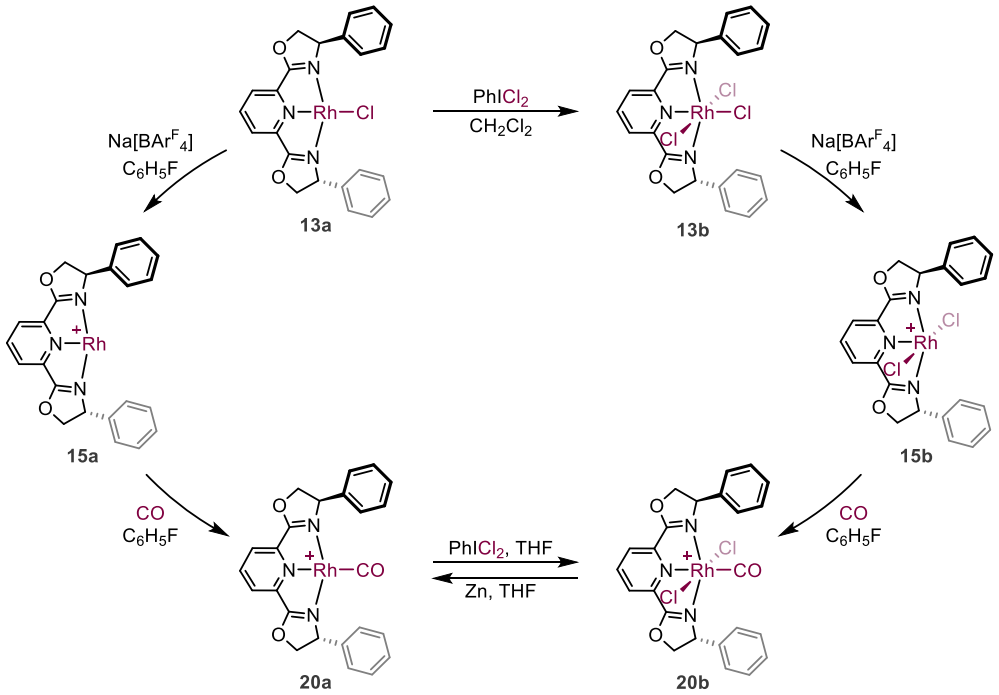

Scheme 3.11. Generation of low-coordinate **15a** and **15b** and subsequent trapping with CO.

3.2.5. Probing the donor properties of pincer ligands

The donor properties of monodentate ligands can be probed using spectroscopic reporter groups, with metal carbonyl derivatives most frequently employed. Tolman's electronic parameter, for example, is based on the carbonyl stretching frequencies of $[Ni(CO)_3L]$ that are readily determined using infrared spectroscopy.[333,334] More recent analogues include the use of less toxic complexes such as *cis*-$[RhCl(CO)_2L]$ or *cis*-$[IrCl(CO)_2]$.[335–339] ^{13}C NMR spectroscopy has also been utilised in the interrogation of palladium–carbene and platinum–carbide bonds through examination of the associated δ_{13C} and $^1J_{MC}$, however, this approach is not really extended pincer ligands.[340–343]

To this end, a series of rhodium(I) and rhodium(III) carbonyl complexes were critically analysed to assess whether the CO group can be used to probe the relative donor properties of pincer ligands.[310] In addition to ^{Ph}**pybox**, three other pyridyl-based pincer ligands were explored: *N*-heterocyclic carbene-based **A120** and **A121**, and phosphine-based **A122**.[344] Selected spectroscopic and structural data attained from these complexes is shown in Table 3.1.

Table 3.1. Pincer ligands investigated with rhodium(I) and rhodium(III) carbonyl probes, with selected spectroscopic data and structural parameters. $[BAr^F_4]^-$counter anions omitted for clarity.

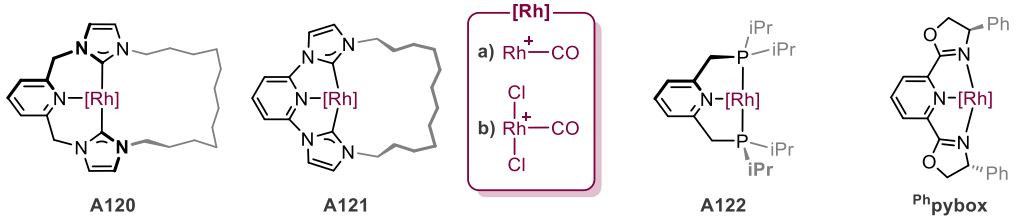

A120 — **CNC pincer** (C^N^C-12) | **A121** — **CNC pincer** (C-N-C-12) | **Probe** | **A122** — **PNP pincer** (*i*Pr-PNP) | ^{Ph}**pybox** — **NNN pincer**

Probe	Ligand		ν(CO) / cm^{-1}	δ_{13C} (CO) / ppm	$^1J_{RhC}$(CO) / Hz	r(*Rh*CO) / Å	
						Expt.	DFT[a]
a) Rh—CO	C^N^C-12	(**A120a**)	1979	194.0	80	1.804(3)	1.827
	C-N-C-12	(**A121a**)	1986	196.8	78	1.836(4)	1.852
	*i*Pr-PNP	(**A122a**)	1998	193.0	69	1.828(3)	1.841
	^{Ph}**pybox**	(**20a**)	2019	188.1	77	-	1.878
b) Cl, Rh—CO, Cl	C^N^C-12	(**A120b**)	2110	180.7	57	-	1.869
	CNC-12	(**A121b**)	2111	181.6	57	1.945(3)	1.900
	*i*Pr-PNP	(**A122b**)	2110	179.7	54	1.884(3)	1.895
	^{Ph}**pybox**	(**20b**)	2151	171.8	55	1.931(10)	1.940

[a] Calculated parameters for **A120** and **A121** use truncated pincer ligand models. IR data acquired in CH_2Cl_2 solution, NMR data acquired in CD_2Cl_2.

The spectroscopic data for the series of rhodium(I) and rhodium(III) carbonyl complexes were obtained under the same conditions in equivalent solvents, to ensure meaningful analysis. The infrared spectroscopic data was notably all acquired in dichloromethane, a solvent chosen for its chemical compatibility and frequent use in analysis of late transition metal complexes by IR spectroscopy.[333] The location of vibrational bands in particular can vary significantly between different solvents.[334,345,346]

Solid-state structures of the carbonyl pincer complexes allowed comparison of the C–O and *Rh–C*O bond lengths. Longer C–O bond lengths (and shorter *Rh–C*O) should in principle arise from stronger π-backdonation from the filled rhodium dπ orbitals to the carbonyl π* molecular orbitals, which is gauged by lower energy ν(CO) values as a consequence of the weakened CO bond. However, no correlation was found between the *Rh–C*O bond lengths and the ν(CO) values measured for the rhodium(I) or rhodium(III) carbonyl complexes. The d(C–O) bond length has not been be used to compare the donor properties of these pincer ligands; in related studies this distance has been found to be an inaccurate indicator for donor abilities of ligands, especially when comparing different ligand classes using this metric.[345]

Comparison of ν(CO) values of the Rh(I)/Rh(III) pairs showed, as expected, that the rhodium(III) complexes are characterised by considerably higher frequencies ($\Delta\nu$(CO) = 110 – 130 cm^{-1}). Moreover, the rhodium(III) complexes display values over a very narrow range preventing a trend to be elucidated, with **20b** notable for its unusually high ν(CO) (*vide supra*). Fortunately the stretching frequencies of the rhodium(I) carbonyl complexes showed considerable variation and allowed a trend to be substantiated: the *net* donor strength of the pincer ligand increasing in the order: ^{Ph}**pybox** (2019 cm^{-1}) < *i*Pr-PNP (1998 cm^{-1}) < C-N-C-12 (1986 cm^{-1}) < C^N^C-12 (1979 cm^{-1}).

Examination of the data acquired by ^{13}C{^{1}H} NMR spectroscopy showed a modest negative correlation with the ν(CO) values (δ_{13}(CO), R^2 = 0.95; $^{1}J_{RhC}$, R^2 = 0.89). However, this trend is primarily a consequence of the large differences between the Rh(I) and Rh(III) complexes and does not fully reflect the subtle differences between the individual pincer ligands, particularly in the case of the $^{1}J_{RhC}$ values. Consideration of the separate Rh(I) and Rh(III) data sets showed no clear correlation of the NMR parameters (R^2 < 0.25), however, the δ_{13}(CO) chemical shifts loosely follow the trend: NNN < PNP < CNC. Ultimately, the spectroscopic parameters explored were not as insightful as initially anticipated and attention turned to a DFT-based computational analysis.

3.2.5.1. Computational analysis

Computational analysis was performed to gain deeper insight into the relationship between the donor properties and the values of ν(CO).[†] For computational simplicity, the macrocyclic CNC pincers were truncated to their respective methyl-substituted analogues. As vindication of the computational methodology, a strong positive correlation between the computed and experimental carbonyl stretching frequencies was noted (R^2 = 0.99). The ETS-NOCV method was used to delineate the molecular orbital contributions between the {Rh(pincer)}$^+$/CO, {Rh(pincer)Cl_2}$^+$/CO (Table 3.2) and {Rh(CO)}$^+$/pincer fragments (Table 3.3).

Decomposition of the metal–carbonyl bond showed that σ-donation contributions from the CO were greater and the π* back donation contributions were smaller for the rhodium(III) carbonyl complexes, compared to their respective rhodium(I) analogues, consistent with the higher oxidation state (Table 3.2).

In the case of the rhodium(I) carbonyl complexes, contributions from σ-donation and π-backbonding were approximately equal in magnitude and the sum of these values accounted for over 90% of the interfragment orbital stabilisation energy (Table 3.2). The strongest energy interactions were found with **A120a** and the weakest in **20a** (ΔE_{orb} = −114.6 *vs*. −93.3 kcal mol^{-1}); this data corresponds well with the experimental IR stretching frequencies as **A120a** had the lowest ν(CO) and conversely **20a** the highest (1979 *vs*. 2019 cm^{-1}).

The smallest π-backbonding contribution was calculated for **20b** in agreement with the measured ν(CO) which displayed the highest wavenumber in the series (2151 cm^{-1}). Natural population analysis (NPA) of the charge on rhodium in the rhodium(III) carbonyl complexes shows that **20b** had the most positive rhodium centre (NPA: **A120b**, 0.46; **A121b**, 0.45; **A122b**, 0.24; **20b**, 0.68). Both characteristics are consistent with the non-classical nature of carbonyl bonding in this case.[330]

[†] Computational calculations performed by Dr Baptiste Leforestier, employing Grimme's dispersion corrected ωB97X-D3 functional and the extended transition state method for energy decomposition analysis combined with the natural orbitals for chemical valence theory (ETS-NOCV), as implemented in ORCA 4.1.0.[310]

Table 3.2. Calculated orbital stabilisation energies for the {Rh(pincer)}$^+$/CO and {Rh(pincer)Cl$_2$}$^+$/CO fragments (kcal mol^{-1}).[a]

	σ({RhL}$^+$←CO)	π({RhL}$^+$→CO)$^\perp$	π({RhL}$^+$→CO)$^\parallel$	Σπ({RhL}$^+$→CO)	Total (ΔE_{orb})
A120a	−52.3	−27.3	−24.6	−52.2	−114.6
A121a	−47.2	−23.6	−24.8	−48.5	−103.6
A122a	−52.1	−25.5	−23.5	−49.0	−108.8
20a	−46.0	−20.3	−19.9	−40.2	−93.3
A120b	−72.0	−16.7	−14.4	−31.1	−109.7
A121b	−61.6	−16.1	−12.9	−28.9	−96.3
A122b	−63.4	−15.8	−13.1	−28.9	−98.3
20b	−58.4	−11.7	−10.3	−22.0	−85.5

[a] The character of the interactions are classified from visual inspection of the NOCV orbitals; into carbonyl donation of local σ-symmetry and out-of-plane (⊥) and in-plane (∥) π-back bonding.

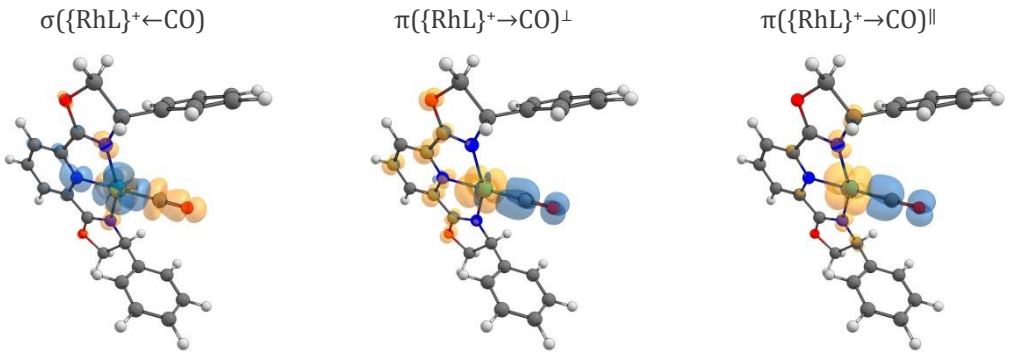

Figure 3.11. Selected NOCV deformation densities associated with **20a**. Charge flow from orange to blue.

Decomposition of the metal-pincer interaction for the rhodium(I) complexes showed that σ-donation accounted for over 60% of the interfragment stabilisation energy (Table 3.3). The conformation of the pincer backbone, specifically the twisting of the central pyridyl donor out of the coordination plane, was also seen to appreciably affect the stabilisation energies. The σ-donating capacity was found to increase in the order NNN < PNP < CNC, with the twisted C^N^C NHC ligand (**A120**) donating marginally less than the planar C-N-C (**A121**) (−176.0 *vs.* −176.9 kcal mol^{-1}). Lutidine-based pincer complexes **A120a** and **A122a** showed a significantly lower degree of π-backdonation with the pyridyl donor. This can be attributed to the flexibility of the central donor to twist out of the coordination plane, which reduces the π-acidity of the pincer ligand, and is postulated to be the main cause of the divergence between the CNC-based ligands (**A120** and **A121**) observed spectroscopically.

Table 3.3. Calculated orbital stabilisation energies for the {Rh(CO)}$^{+}$/pincer fragment (kcal mol^{-1})[a].

	σ(L→{Rh(CO)}$^{+}$)	π(L←{Rh(CO)}$^{+}$)^{D}	π(L←{Rh(CO)}$^{+}$)^{py}	Σπ(L←{Rh(CO)}$^{+}$)	Total (ΔE_{orb})
A120a	−176.0	−28.8	−4.4	−33.2	−240.1
A121a	−176.9	−29.9	−11.4	−41.3	−245.5
A122a	−157.6	−43.6	−7.0	−50.6	−234.5
20a	−124.7	−31.3	−11.3	−42.6	−198.5

[a] The character of the interactions are classified from visual inspection of the NOCV orbitals; into pincer ligand donation of local σ-symmetry and π-back bonding into the terminal (D) and central pyridyl (py) donor groups.

Finally, a good correlation (R^2 = 0.91) was found between the difference in carbonyl stretching frequencies ($\Delta\nu$(CO)) and the calculated thermodynamics of the Rh(I)/Rh(III) redox pairs. These were found to be more exergonic in order: PNP (−40.1 kcal mol^{-1}) < C-N-C (−45.6 kcal mol^{-1}) < NNN (−47.9 kcal mol^{-1}) < C^N^C (−50.1 kcal mol^{-1}). This metric has the potential to be a useful mechanistic tool.

3.3. Rhodium and iridium 2,2'-biphenyl complexes

Synthetic routes to the complexes of the form [M(**^{Ph}pybox**)(biph)][BAr^F_4] (M = Rh, **22**; Ir, **24**; biph = 2,2'-biphenyl) were investigated (Scheme 3.12). As previously noted, low-coordinate complexes of this nature are good platforms for studying the coordination chemistry of C–H bonds. The precursors [Rh(biph)(dtbpm)Cl] (**A109**, dtbpm = bis(di-*tert*-butylphosphino)methane) and $[Ir(biph)(COD)Cl]_2$ (**A108**) first described by Jones and Crabtree respectively, were utilised as convenient sources of {M(III)(biph)Cl}.[311,312]

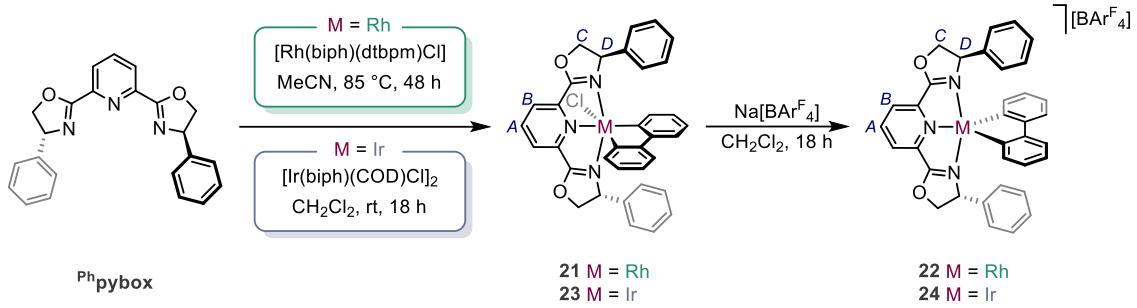

Scheme 3.12. Synthesis of biphenyl complexes from the chloride analogues, M = Rh/Ir.

Substitution of the chelating phosphine dtbpm with **^{Ph}pybox** in [Rh(biph)(dtbpm)Cl] afforded **21**. It was found that a strongly donating solvent was essential and early attempts using dichloromethane were unsuccessful, even at elevated temperatures. This observation indicated that substitution of the diphosphine ligand was kinetically unfavourable with the pybox ligand alone, and required an external donor solvent to aid displacement. Although rare, monohapto pybox coordination has been observed with rhodium(I) complexes featuring bulky phosphine ligands, but in the presence of excess phosphine the pybox was completely displaced from the metal.[117] Based on this precedent, it seems in this case that complete displacement of dtbpm by the solvent precedes pybox coordination.

Use of acetonitrile as the solvent enabled good conversion to **21**, when heated at 85 °C for 48 hours. The resulting crude product was purified by column chromatography and was isolated as a dark red solid in good yield (74%). Complex **21** adopts C_1 symmetry in CD_2Cl_2 as evidenced by six oxazolinyl proton resonances ($H_{C/D}$) in the ^{1}H NMR spectrum (δ 5.11, 4.94, 4.82, 4.55, 4.51 and 4.28). The formation of **21** is supported by ESI-MS analysis, which shows a strong peak at 624.1156 (calcd 624.1153) m/z attributed to the cationic fragment $[M–Cl]^+$.

Halide abstraction of **21** with Na[BAr^F_4] in dichloromethane generated the coordinatevely unsaturated 16 VE rhodium(III) species **22** in good yield (79%). The ^{1}H NMR spectrum (CD_2Cl_2) of **22** contained a number of broad signals at room temperature, indicating a

structurally dynamic, time-averaged C_2 symmetric species in solution. For instance, the oxazolinyl methine resonance (H_D) at δ 4.53 was appreciably line broadened, as well as the phenyl signals (δ 7.12, 6.91 and 6.42). By analogy to **A111** (*vide supra*), the dynamics are attributed to pseudorotation of the biphenyl ligand on the NMR spectroscopy timescale. Consistent with this interpretation, cooling **22** to 225 K resulted in decoalescence of signals and adoption of C_1 symmetry (Figure 3.12). Diagnostic inequivalent oxazoline resonances were observed at δ 5.18, 5.02, 4.96, 4.78, 4.73 and 4.27 ($H_{C/D}$).

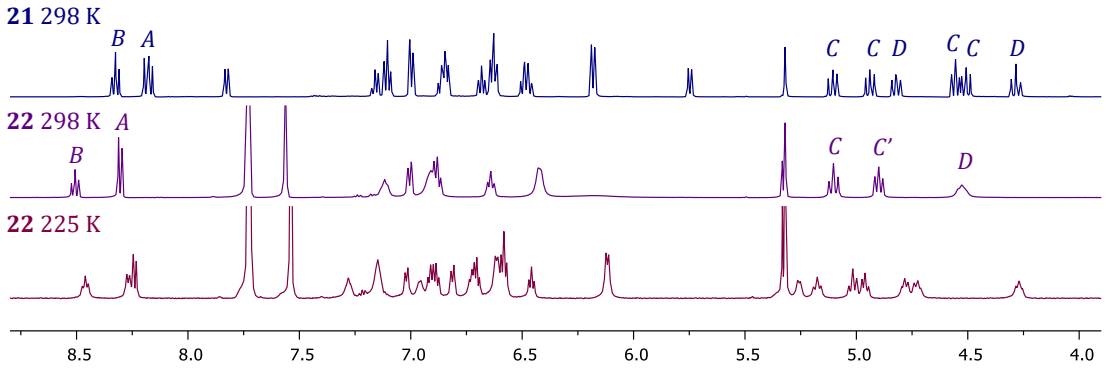

Figure 3.12. ^{1}H NMR spectra of **21** (*top*), **22** at room temperature (*middle*) and **22** at 225 K (*bottom*). Selected region shown for clarity (CD_2Cl_2, 500 MHz).

Crystals suitable for X-ray diffraction were obtained from diffusion of pentane into a saturated solution of **22** in toluene at room temperature (Figure 3.13). Interestingly, the solid-state structure features an η^2-coordinated toluene (**tol-22**). Unfortunately, the crystallographic data are poor, so can only be used for connectivity purposes. With this in mind, η^2-toluene coordination was measured to be Rh–(C=C) 2.739(16) Å, appreciably longer than related rhodium(III) η^2-arene complexes.[347] **A113**, bearing a CNC pincer ligand, displayed Rh–(C=C) bond lengths of 2.622(2) – 2.643(2) Å.[316] Analysis of the crystals in CD_2Cl_2 by ^{1}H NMR spectroscopy indicated adoption of time-averaged C_2 symmetry and liberation of toluene. Combined, this data suggests that toluene is only weakly bound in **tol-22**.

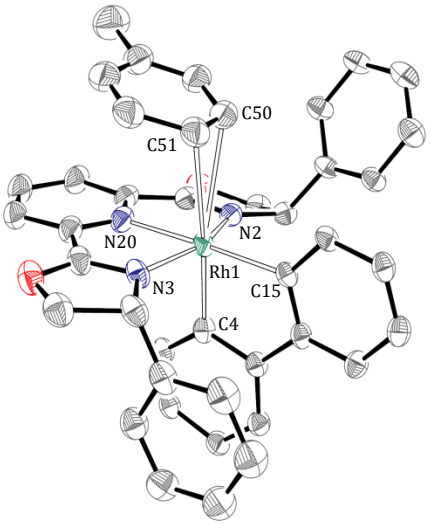

Figure 3.13. Solid-state structure of **tol-22**. Thermal ellipsoids drawn at 30% probability. $[BAr^F{}_4]^-$ counter anion and hydrogen atoms are omitted for clarity. The structure shown is one of two independent molecules ($Z' = 2$).

The iridium(III) 2,2'-biphenyl derivative **23** was synthesised from the reaction of $[Ir(biph)(COD)Cl]_2$ and ^{Ph}**pybox** in dichloromethane and isolated in good yield (85%). The reaction proceeded readily at room temperature and required no further purification, unlike that of rhodium analogue **21**. The more facile substitution of the iridium(III) compared to rhodium(III) precursor is reconciled by the relative binding strengths of COD and dtbpm. Like the rhodium counterpart **21**, complex **23** exhibited C_1 symmetry in solution, evidenced by inequivalent oxazoline resonances ($H_{C/D}$) at δ 5.22, 5.02, 4.87, 4.68, 4.66 and 4.27.

Halide abstraction of **23** using $Na[BAr^F{}_4]$ in dichloromethane at room temperature was facile and generated the coordinatively unsaturated complex **24**, which was isolated in good yield (71%). Unlike the time-averaged C_2 symmetry observed for **22** at room temperature, the ^{1}H NMR spectrum of **24** suggests adoption of C_1 symmetry in solution, with diagnostic inequivalent oxazolinyl protons ($H_{C/D}$ δ 5.33, 5.11 (2H), 4.91, 4.84 and 4.27; Figure 3.14). The line broadening observed in the ^{1}H NMR spectrum of **24** could be attributed to reversible dichloromethane binding at the iridium centre, or higher energy pseudorotation of the biphenyl moiety, in line with expectation for the heavier group 9 congener and literature precedents.[314]

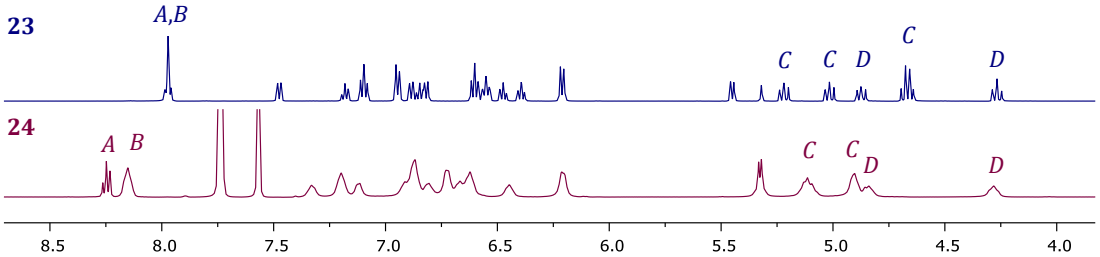

Figure 3.14. ^{1}H NMR spectra of **23** (*top*) and **24** (*bottom*) (CD_2Cl_2, 500 MHz, 298 K).

3.3.1. Attempted synthesis of terpyridine complexes

Building on the procedures established for ^{Ph}**pybox**, metalation reactions of ^{Ph}**terpy** were investigated (Figure 3.15).

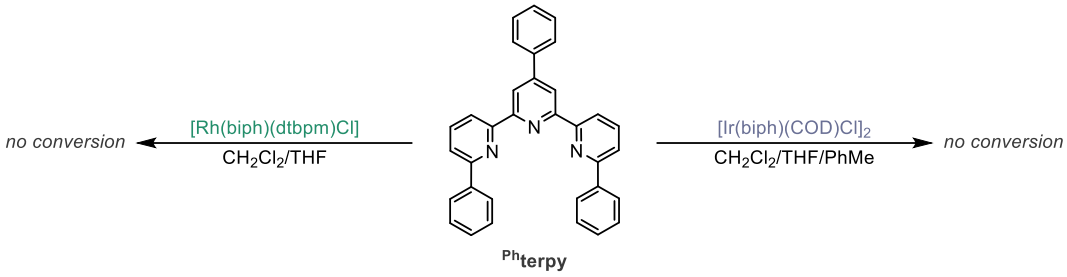

Figure 3.15. Attempted metalation of ^{Ph}**terpy** with rhodium and iridium precursors.

Reaction of [Rh(biph)(dtbpm)Cl] with ^{Ph}**terpy** was initially attempted in dichloromethane at room temperature, however, this failed to produce the desired complex and more coordinating solvents were trialled. Unfortunately, even prolonged heating in THF resulted in no conversion to product with only intractable decomposition observed by ^{1}H NMR spectroscopy. Similar solvent systems and conditions were applied to the attempted metalation with $[Ir(biph)(COD)Cl]_2$ including reflux in dichloromethane, THF and toluene, but they also failed to produce the desired iridium product. Instead, iridium(0) was evidenced by formation of black precipitate.

These findings contrast the numerous reported examples of metal complexes bearing 2,2':6',2''-terpyridine ligands as well as their frequent employment in catalytic processes.[66,328,348] Interestingly, the first pincer complex prepared from Crabtree's $[Ir(biph)(COD)Cl]_2$ precursor was a terpyridine complex.[312] The stark difference in reactivity can be rationalised by considering the steric constraints imposed by the introduction of phenyl substituents at the 6,6''-terpyridine positions in ^{Ph}**terpy**. This likely created a large amount of steric congestion which inhibited coordination.[349,350]

3.4. Ruthenium complexes

Ruthenium(II) is isoelectronic with rhodium(III), and motivated the preparation of ruthenium(II) analogues of rhodium(III) chloride complexes **15b** and **20b** (Scheme 3.13).

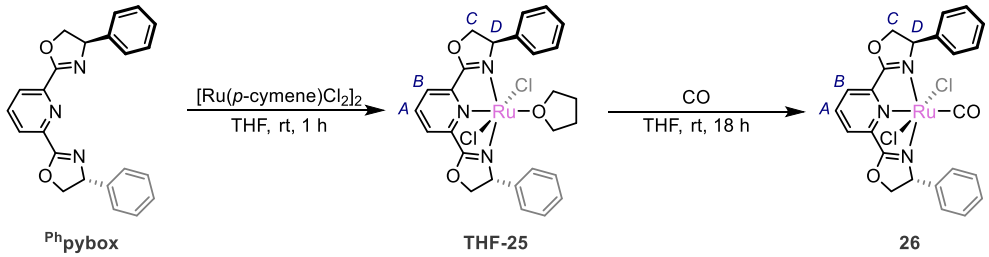

Scheme 3.13. Synthesis of ruthenium(II) complexes.

Synthesis of [Ru(**^{Ph}pybox**)(THF)Cl_2] (**THF-25**) was achieved through stirring [Ru(*p*-cymene)Cl_2]$_2$ with acyclic **^{Ph}pybox** in THF for 1 hour at room temperature, and subsequently isolated in excellent yield (93%). Complex **THF-25** adopts C_2 symmetry in solution as evidenced by ^{1}H NMR spectroscopy (THF), with diagnostic pyridine resonances at δ 8.01 (H_B) and 7.74 (H_A). Dark purple crystals suitable for X-ray diffraction were obtained by diffusion of hexane into a THF solution of **THF-25** (Figure 3.16).

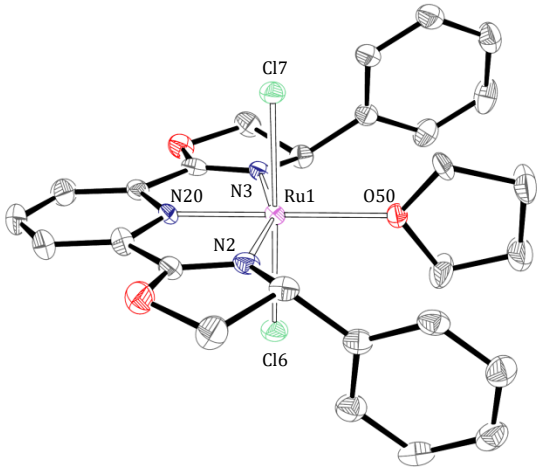

Figure 3.16. Solid-state structure of **THF-25**. Thermal ellipsoids drawn at 40% probability. Hydrogen atoms are omitted for clarity. The structure shown is one of four independent molecules (Z' = 4). Selected bond lengths (Å) and angles (°): Ru1-N2, 2.045(6); Ru1-N3, 2.068(6); Ru1-N20, 1.914(6); Ru1-O50, 2.187(6); Ru1-Cl6, 2.3882(18); Ru1-Cl7, 2.3798(18); N2-Ru1-N3, 158.5(3); N20-Ru1-O50, 178.6(3); Cl6-Ru1-Cl7, 178.86(7).

In the solid state **THF-25** adopts an octahedral metal geometry, with the N2-Ru-N3 bond angle of 158.5(3)°, similar to those found in **13a**, **13b** and **20b** (*ca*. 158°); the M–N bond lengths are also comparable. A Ru–O distance of 2.187(6) Å was measured, which closely matches the bond length of a related ruthenium(II) bis(imino)pyridine THF complex (Ru–O: 2.192(2) Å).[351]

Crystals of **THF-25** were dissolved in CD_2Cl_2 for further characterisation. Despite the absence of THF in the lattice, both bound and uncoordinated THF were observed in the ^{1}H NMR spectrum suggesting that THF is labile enough to be substituted by dichloromethane to form [Ru(**^{Ph}pybox**)(DCM)Cl_2] (**DCM-25**). Two C_2 symmetric organometallic species were observed in the ^{1}H NMR spectrum in a *ca*. 2:3 ratio. The minor species was identified as the THF complex **THF-25** through integration, with diagnostic resonances at δ 3.62, 3.50, 1.124 – 1.15 and 1.10 – 1.02 assigned to bound THF. Dissolving the mixture of **THF-25** and **DCM-25** resulted in complete conversion back to **THF-25**, as evidenced by ^{1}H NMR spectroscopy.

Synthesis of the analogous ether complex [Ru(**^{Ph}pybox**)(MTBE)Cl_2] (**MTBE-25**) was attempted by reaction of **^{Ph}pybox** with [Ru(*p*-cymene)Cl_2]$_2$ in methyl *tert*-butyl ether (MTBE), to probe the strength of the Ru–ether linkage: this adduct would be C_1 symmetric. Although **^{Ph}pybox** was poorly soluble in MTBE, an intense pink coloured poorly soluble species was formed within 1 hour. This species is tentatively characterised as **MTBE-25** through *in situ* ^{1}H NMR spectroscopy, although the apparent C_2 symmetry in solution suggests ether coordination is highly dynamic.

The synthesis of ruthenium(II) carbonyl complex **26** could be achieved by substitution of THF by carbon monoxide (1 atm) at room temperature, either from isolated or *in situ* generated **THF-25** in THF within 18 hours, as gauged by analysis *in situ* using ^{1}H NMR spectroscopy (Figure 3.17). When performed in CH_2Cl_2 substitution is, however, significantly faster (<1 h).

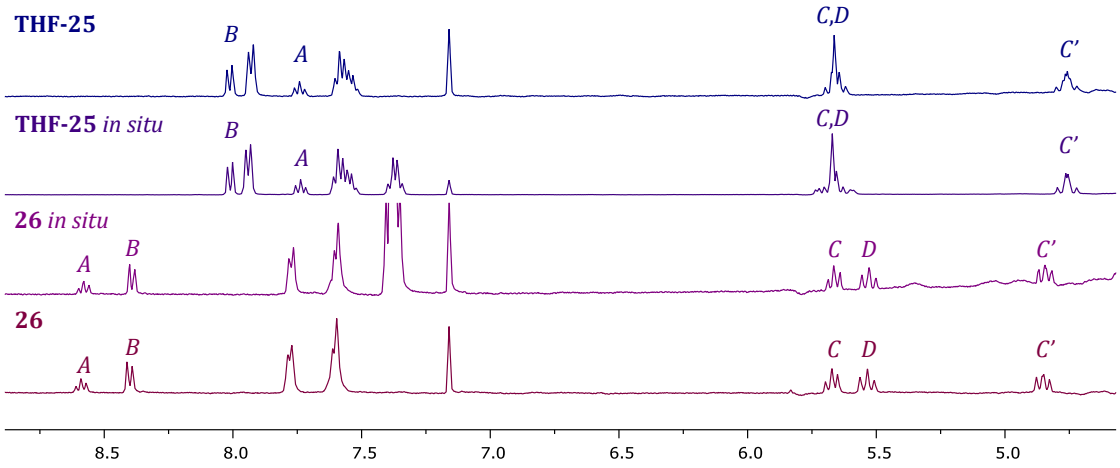

Figure 3.17. ^{1}H NMR spectra of (*top to bottom*): authentic sample of **THF-25**, *in situ* **THF-25**, *in situ* **26** and authentic sample of **26**. Selected region shown for clarity (THF, 400 MHz).

The carbonyl complex **26** was subsequently isolated in 89% yield. The successful formation of **26** was evidenced by the presence of characteristically high frequency carbonyl resonance in the ^{13}C{H} NMR spectrum (δ 204.4). Furthermore, ESI-MS showed a

signal at 591.9740 (calcd 591.9740) m/z attributed to the cationic species $[M+Na]^+$. Dark brown-red crystals of **26** suitable for X-ray diffraction were obtained by diffusion of hexane into a solution of the complex in dichloromethane, at room temperature (Figure 3.18). Whilst the imine Ru–N2 bond distances are similar to **THF-25**, the pyridine Ru–N20 distance is appreciably elongated upon CO coordination from 1.914(6) Å to 2.039(4) Å in line with the relative *trans*-influence of CO compared to THF.

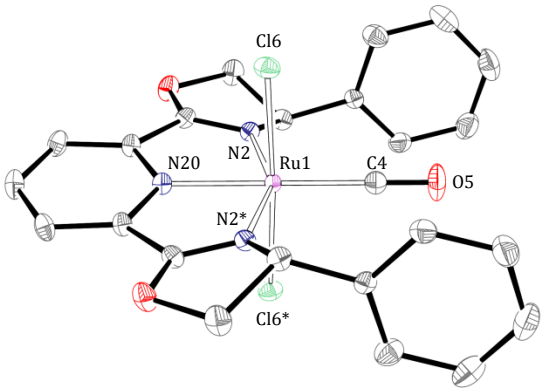

Figure 3.18. Solid-state structure of **26**. Thermal ellipsoids drawn at 40% probability, * atoms generated by the symmetry operation 1−x, +y, 1−z. Hydrogen atoms are omitted for clarity. The structure shown is one of two independent molecules (Z' = 2×0.5). Selected bond lengths (Å) and angles (°): Ru1-N2, 2.055(2); Ru1-N20, 2.039(4); Ru1-C4, 1.882(6); Ru1-Cl6, 2.33864(7); C4-O5, 1.135(7); N2-Ru1-N2, 154.20(13); N20-Ru1-C4, 180.0; Cl6-Ru1-Cl6, 176.16(5).

A carbonyl stretching frequency of 1977 cm^{-1} (CH_2Cl_2 solution) was determined using IR spectroscopy. The analogous *i*Pr-pybox complex *trans*-[Ru(*i*Pr-pybox)Cl_2(CO)] exhibits a ν(CO) = 1965 cm^{-1} (KBr disc), consistent with the presence of more electron donating *i*Pr substituents, whilst terpyridine complex *trans*-[Ru(terpy)Cl_2(CO)] shows a ν(CO) = 1966 cm^{-1} (CH_2Cl_2 solution).[119,352,353] The cationic rhodium carbonyl complexes **20a** and **20b** are both characterised by higher frequency ν(CO) values (*cf.* **20a** = 2019 cm^{-1}; **20b** = 2151 cm^{-1}), indicating much stronger M–CO bonding in **26**, reflected in its excellent air and silica stability compared to the rhodium analogues.

3.5. Summary

In this chapter rhodium, iridium and ruthenium complexes of ^{Ph}**pybox** were investigated. Rhodium(I) chloride complex **13a** was prepared, and subsequent chloride abstraction enabled synthesis of PCy_3 and CO derivatives **17** and **20a**, respectively (Scheme 3.14). Oxidation of **13a** with iodobenzene dichloride gave the rhodium(III) trichloride complex **13b**, which likewise provided a means to access rhodium(III) carbonyl complex **20b**. Interconversion between carbonyl complexes **20a** and **20b** could also be mediated by oxidation with $PhICl_2$ and reduction over zinc.

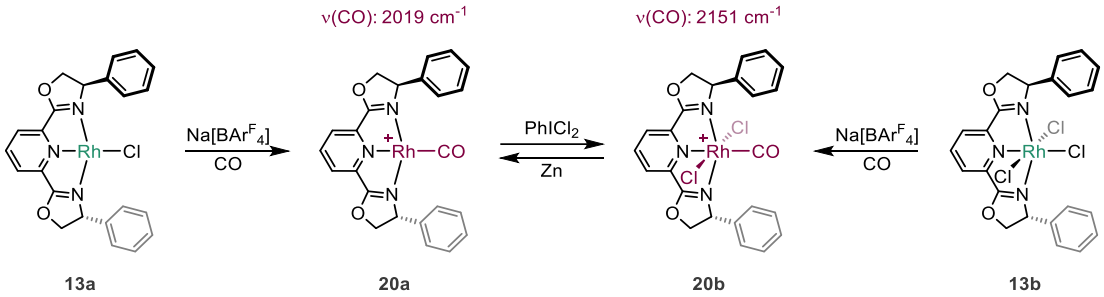

Scheme 3.14. Synthesis of rhodium carbonyl complexes **20a** and **20b**, counter anions omitted for clarity.

The rhodium carbonyl fragments were exploited to probe the net donor properties of the pybox ligand relative to other common pincer ligands. The carbonyl stretching frequencies of the rhodium(I) congeners proved to be the most diagnostic spectroscopic tool. Using this spectroscopic metric the net donor strength increased in the order: pybox < phosphine-based PNP ligands < NHC-based CNC ligands.

Other systems examined include rhodium(III) and iridium(III) 2,2'-biphenyl complexes and ruthenium(II) dichloride complexes. Ultimately, these were all prepared successfully and paved the way for the study of macrocyclic and interlocked variants, which will be discussed in the subsequent chapter.

Chapter 4: Coordination Chemistry of Macrocyclic and Interlocked Ligands

This chapter builds on the coordination chemistry established for acyclic **^{Ph}pybox**, described in Chapter 3, to access rhodium(I/III), iridium(III) and ruthenium(II) complexes of the macrocyclic (**^{M}pybox**) and rotaxane (**^{R}pybox**) variants. In doing so, differences in reactivity between the pybox ligands were uncovered. These differences are attributed to the unique steric profiles of the more elaborate scaffolds.

With a view to generating σ-complexes, halide abstraction reactions of rhodium(I) and rhodium(III) chloride complexes of **^{R}pybox** were studied. The structure of the resulting low coordinate derivatives were interrogated using variable temperature NMR spectroscopy, particularly to establish if Rh···H–C interactions were present (Figure 4.1). Subsequent reaction with CO generated the corresponding carbonyl complexes, evidencing formation of low coordinate species and providing a convenient spectroscopic handle to gauge the electronics at the metal centre. Complexes of **^{R}pybox** notably displayed higher ν(CO) bands compared to those of **^{Ph}pybox** and **^{M}pybox**, which is attributed to the unfavourable steric interactions between the axle and carbonyl ligand.

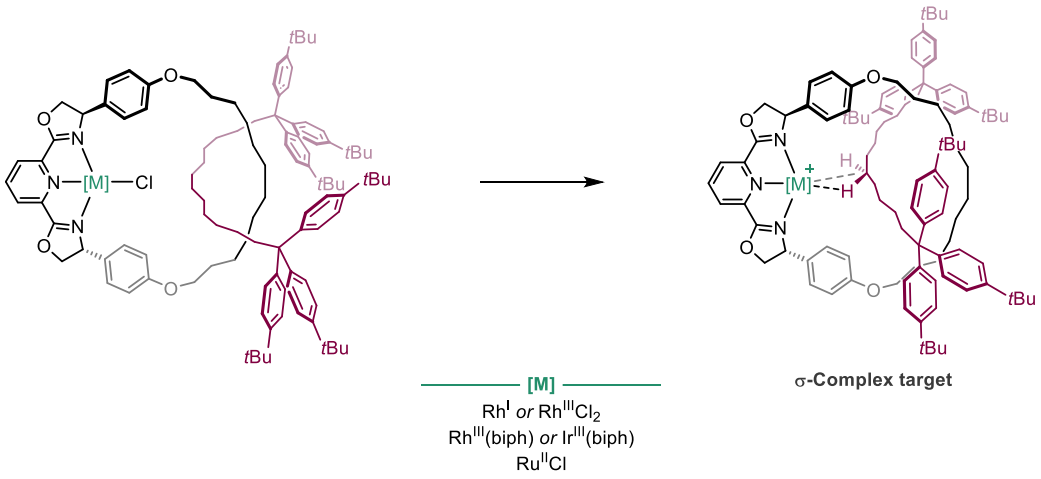

Figure 4.1. Target low coordinate complexes of **^{R}pybox** derivatives.

4.1. Introduction

With the aim to isolate and characterise a σ-complex in solution and the solid-state, the rotaxane **^{R}pybox** has been identified as a suitable ligand. The macrocyclic NNN pincer enforces the saturated hydrocarbon axle into close proximity with bound metal fragments, as a consequence of its mechanical entrapment.

The nomenclature used to describe σ-complexes of C–H bonds represents an interesting discussion for the proposed M···H–C bonding interactions between the components of a metal-based rotaxane (Figure 4.2). Agostic interactions are when the C–H donor is from a group already bound to the metal, and as such these are *intramolecular* interactions.[233] On the other hand, a σ-alkane complex is an *intermolecular* interaction between a C–H σ-bond and a metal. It is also important to note that M···H–C interactions are not exclusively η^2. For example, a recently characterised cobalt σ-alkane complex exhibited η^1-alkane interactions, more in line with hydrogen bonding interactions.[248,285] It becomes difficult to categorise the proposed M···H–C bonding as mechanical bonds represent a 'grey area', since they are by definition not chemical bonds.[354] Therefore, it becomes subjective in the assignment of whether these interactions are *intra*- or *intermolecular*, depending on how one interprets the mechanical bond itself. For the purpose of this thesis, the proposed M···H–C interaction will be classified as an *intermolecular* σ-bond interaction.

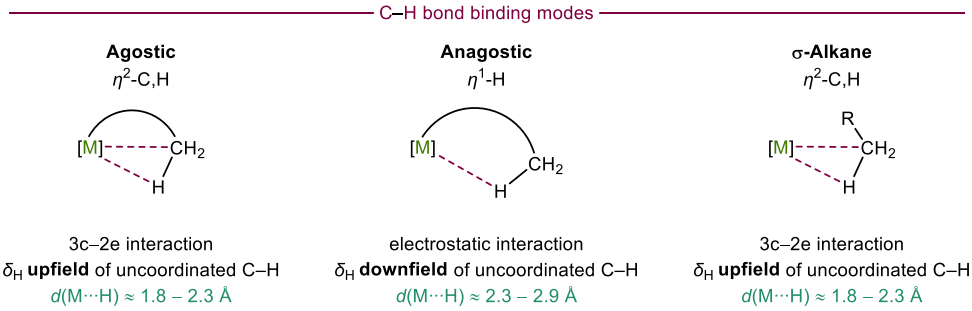

Figure 4.2. Possible C–H bond binding to an unsaturated metal centre.[248,287]

With the ambition of studying intermolecular M···H–C bonding interactions, this chapter focuses on the synthesis and characterisation of low coordinate complexes of **^{R}pybox**.

4.2. Rhodium complexes

With established synthetic routes to rhodium chloride and carbonyl ^{Ph}**pybox** derivatives, the preparation of ^{M}**pybox** and ^{R}**pybox** complexes were targeted. Preliminary studies with rhodium complexes of ^{R}**pybox** gave promising results, when compared to 2,2'-biphenyl and ruthenium based systems (*vide infra*), so are the main focus of this chapter.

4.2.1. Synthesis and characterisation of rhodium chloride complexes

4.2.1.1. Macrocyclic complexes

The rhodium(I) chloride complex of ^{M}**pybox** (**27a**) was prepared, using the conditions developed with the acyclic model as a guide, and isolated in good yield (73%, Scheme 4.1).

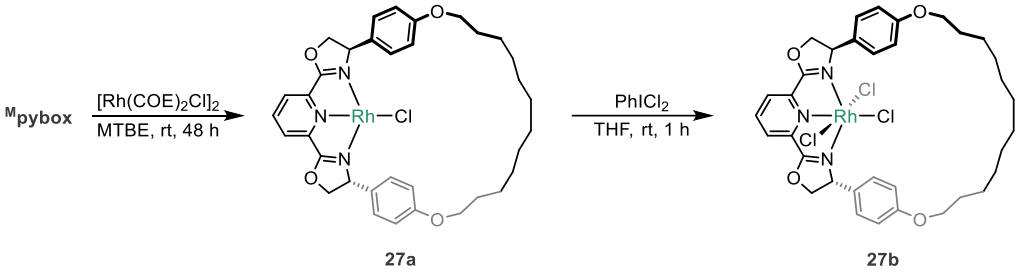

Scheme 4.1. Synthesis of macrocyclic rhodium chloride complexes.

The synthesis of **27a** could be achieved by reaction of ^{M}**pybox** with $[Rh(COE)_2Cl]_2$ in a number of solvents including benzene, MTBE and THF, but MTBE gave the highest yield (73%). Complex **27a** showed low solubility in both C_6D_6 and MTBE, as previously noted for acyclic analogue **13a**, which was surprising given the presence of the solubilising alkyl linker of the macrocycle. However, the solubility of **27a** in THF is good and permitted full characterisation by NMR spectroscopy. In addition, the HR ESI-MS of **27a** displayed a signal at 670.2147 (calcd 670.2147) *m*/*z*, assigned to the cation $[M-Cl]^+$.

Interestingly, at room temperature the ^{1}H NMR spectrum of **27a** in THF-d_8 showed two pybox-containing complexes in a *ca*. 1:9 ratio. Diagnostic oxazolinyl methylene resonances were used to identify the two structurally similar complexes: the major species displayed signals at δ 5.26 and 4.47; whilst the minor species displayed downfield shifted resonances at δ 5.32 and 4.55. In addition, the pyridine resonances of the minor species were shifted downfield ($\Delta\delta$ 0.1) relative to the major complex. Similar outcomes were noted in other solvents. Attempted purification by recrystallisation, extraction or washing were unsuccessful. Therefore, it was postulated that the mixture results from an equilibrium between inner- and outer-sphere chloride complexes. Whilst the insolubility of **13a** prevented direct comparison, this suggestion has precedent in the literature.[355]

The rhodium(III) trichloride complex **27b** was prepared through oxidation of **27a** with iodobenzene dichloride in THF and subsequently isolated in good yield (71%). Purification of the crude complex could be readily achieved by column chromatography. Complex **27b** was characterised using a combination of NMR spectroscopy and mass spectrometry. The ^{1}H NMR spectrum (CD_2Cl_2) of **27b** exhibited C_2 symmetry at room temperature, substantiated by two pyridine resonances at δ 8.34 and 8.15, which correlated well to the acyclic congener **13b** (δ 8.36 and 8.17). The assignment was further supported by the HR ESI-MS of **27b** which displayed a signal at 798.1113 (calcd 798.1110) m/z, assigned to the $[M+Na]^+$ cation.

4.2.1.2. Rotaxane complexes

The rhodium(I) chloride complex **28a** was synthesised by reaction of **^{R}pybox** with $[Rh(COE)_2Cl]_2$ in THF for 48 hours at room temperature and associated with a drastic colour change from yellow to black (Scheme 4.2). Alternative solvents were also investigated. MTBE was found to be suitable, however, MeOD and C_6D_6 were ineffective due to the limited solubility of **^{R}pybox** in these solvents. As discussed in Chapter 2, **^{R}pybox** was unable to be fully separated from free axle **3**, therefore, to access pure **28a** it was necessary to remove this impurity along with the liberated cyclooctene. Complex **28a** is highly soluble in non-polar solvents and was unable to be washed with pentane or hexane, as was the case for the non-interlocked model counterparts. Instead, tetramethylsilane (TMS) was employed with 6 consecutive washes, alongside sonication, found to be necessary to afford pure complex **28a** in good yield (80%).

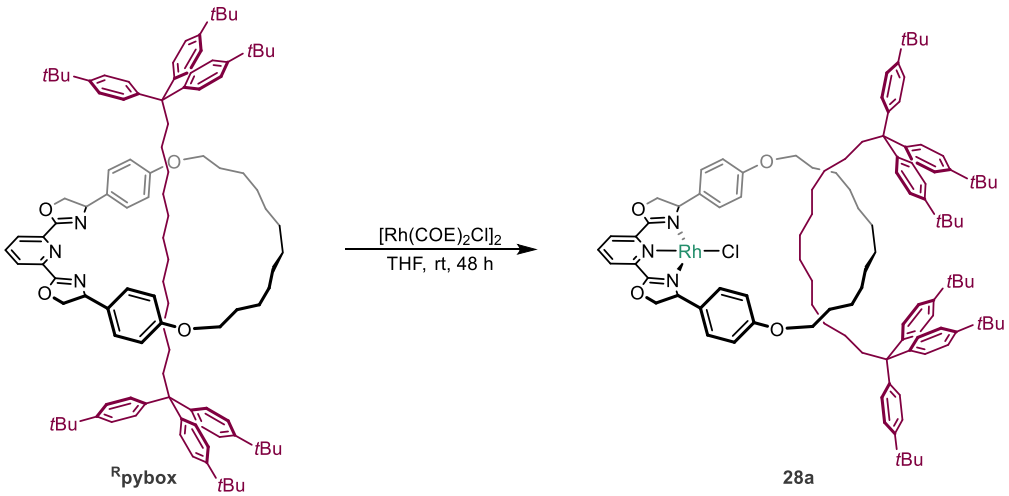

Scheme 4.2. Synthesis of the interlocked rhodium(I) chloride complex **28a**.

Characterisation of **28a** was achieved by a combination of NMR spectroscopy and mass spectrometry; the HR ESI-MS displayed a signal at 1661.0127 (calcd 1661.0128) m/z, assigned to the $[M–Cl]^+$ ion. Complex **28a** was characterised in both THF-d_8 and toluene-d_8

by NMR spectroscopy. As with the macrocyclic complex **27a**, a mixture of the outer- and inner-sphere chloride complexes was observed in both solvents in a ratio of *ca*. 1:9 by ^{1}H NMR spectroscopy. This was evidenced in THF-d_8 by two sets of *para*-pyridine resonances (δ 8.48 and 8.39) as well as distinct oxazoline methylene resonances (δ 4.38 and 4.32), with the minor species exhibiting the most downfield shifted signals.

Characterisation of **28a** was also attempted in CD_2Cl_2 as it was hoped oxidative addition of the solvent would be prevented by the sterically demanding environment around the rhodium centre (*cf*. **14**, see Chapter 3). However, within 30 minutes in CD_2Cl_2 complete conversion of **28a** into an asymmetric species was observed by NMR spectroscopy, alongside an informative colour change from black to bright yellow (Scheme 4.3). This product was assigned to the rhodium(III) oxidative addition product **29**, supported by HR ESI-MS which displayed a signal at 1746.9733 (calcd 1746.9787) *m*/*z*, assigned to the cation [M–Cl]$^{+}$. The C_1 symmetric species is characterised by ^{1}H NMR spectroscopy by six oxazolinyl resonances including 1H methylene protons at δ 4.76 and 4.51, which are shifted upfield relative to the acyclic analogue (*cf*. **14** δ 5.07 and 4.75). In addition, the ^{13}C{^{1}H} NMR spectrum displayed characteristic signals assigned to the cleaved CD_2Cl fragment (δ 40.9; $^{1}J_{RhC}$ = 21 Hz),[56] in close agreement with those of the acyclic variant **14** (δ 39.3; $^{1}J_{RhC}$ = 26 Hz).

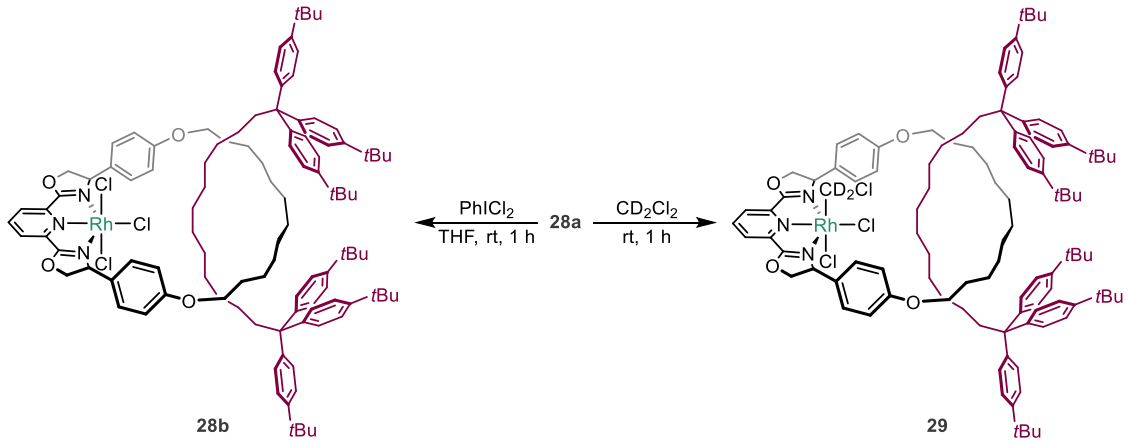

Scheme 4.3. Oxidative addition reactions of **28a**.

The rhodium(III) trichloride complex **28b** was prepared in good yield (70%) by oxidation of **28a** with iodobenzene dichloride in THF at room temperature. The ^{1}H NMR spectrum (CD_2Cl_2) of **28b** closely matches the spectra obtained for the macrocyclic and acyclic congeners, **27b** and **13b** respectively, as illustrated by diagnostic pyridine resonances at δ 8.30/8.34/8.36 and δ 8.13/8.15/8.17. The HR ESI-MS supported formation of **28b** by a signal at 1788.9086 (calcd 1788.9091) *m*/*z*, assigned to the cation [M+Na]$^{+}$. Unlike **28a** which was characterised as a mixture of inner- and outer-sphere chlorides, the ^{1}H NMR

spectrum (CD_2Cl_2) of **28b** displayed one C_2 symmetric species, evidenced by three oxazoline resonances at δ 5.46, 5.27 and 4.65.

4.2.2. Halide abstraction reactions

4.2.2.1. Synthesis of low coordinate macrocyclic complexes

Chloride abstraction from **27a** was achieved using $Tl[BAr^F{}_4]$ in either THF or MTBE, the latter being specifically employed to assess whether **30a** was in fact the target low coordinate species or the corresponding solvent adduct (Scheme 4.4). Formation of a MTBE adduct would be evident from the symmetry of the ^{1}H NMR spectrum.

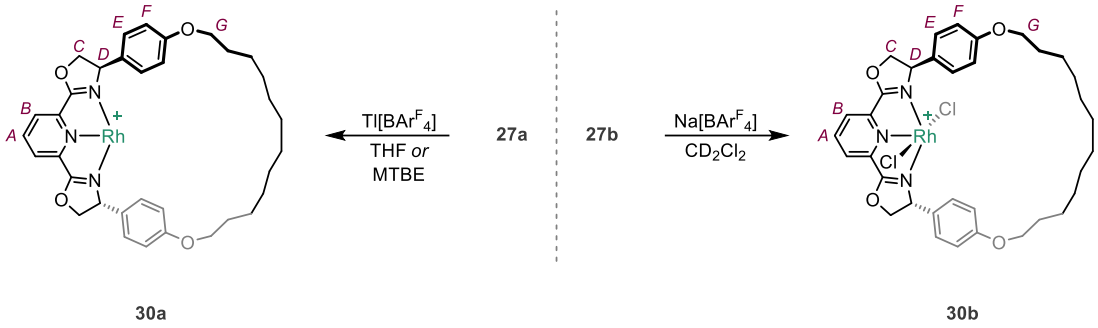

Scheme 4.4. Synthesis of low coordinate macrocyclic complexes **30a** and **30b**. Counter anions omitted for clarity.

Removal of the halide is apparent by a pronounced change of colour from black to an intense dark red. In both solvents, the formation of a single C_2 symmetric product was apparent upon analysis using ^{1}H NMR spectroscopy (Figure 4.3). In THF the most notable spectroscopic changes were the downfield shift of the *meta*-pyridine resonance (H_B) at δ 7.96 ($\Delta\delta$ 0.38) and the oxazolinyl protons ($H_{C/D}$) at δ 5.88 – 5.69 (**27a** δ 6.60 and 5.57). Combined, these outcomes do not exclude formation of solvent adducts, but do indicate solvent binding is at least weak. No change in the spectra was observed after 1 hour at room temperature, suggesting that **30a** is stable in solution over this time period. The formation of a single species also supports the proposed equilibration of **27a**, involving outer- and inner-sphere chloride coordination.

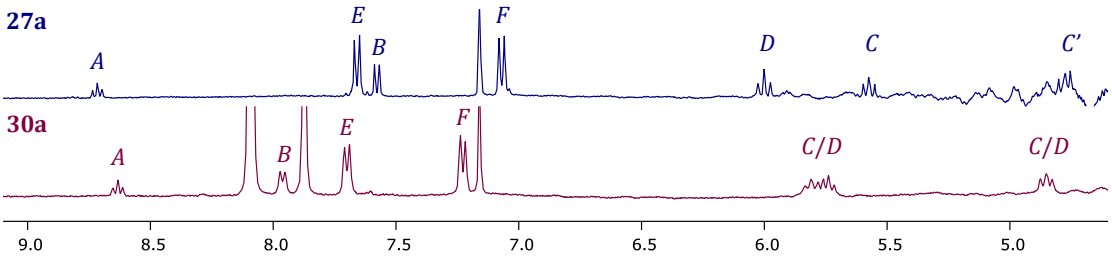

Figure 4.3. ^{1}H NMR spectra of **27a** and **30a** (298 K, THF, 400 MHz).

Abstraction of chloride from **27b** using Na[BAr$^{F}_{4}$] in CD_2Cl_2 was facile at room temperature, generating five-coordinate complex **30b** which was characterised *in situ* by ^{1}H NMR spectroscopy. No noticeable colour change was observed, but successful chloride removal was apparent by analysis *in situ* using ^{1}H NMR spectroscopy (CD_2Cl_2; Figure 4.4). The most notable spectroscopic changes were the oxazoline resonances ($H_{C/D}$), two signals became coincidental at δ 5.50 – 5.40 (**27b** δ 5.48 and 5.38), whilst the other oxazolinyl methylene resonance shifted downfield to δ 4.88 – 4.74 (**27b** δ 4.73).

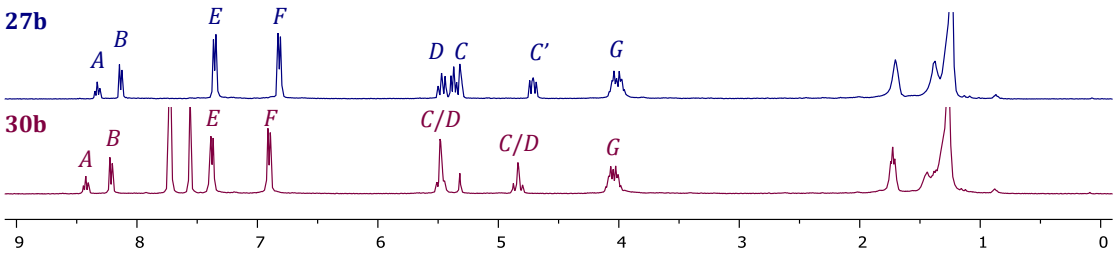

Figure 4.4. ^{1}H NMR spectra of **27b** and **30b** (298 K, CD_2Cl_2, 400 MHz).

4.2.2.2. Synthesis of low coordinate rotaxane complexes

Following success with the acyclic and macrocyclic variants, the key targets **31a** and **31b** were generated *via* chloride abstraction, using either Tl or Na[BAr$^{F}_{4}$] in several solvent systems and investigated with variable temperature NMR spectroscopy and IR spectroscopy (Scheme 4.5).

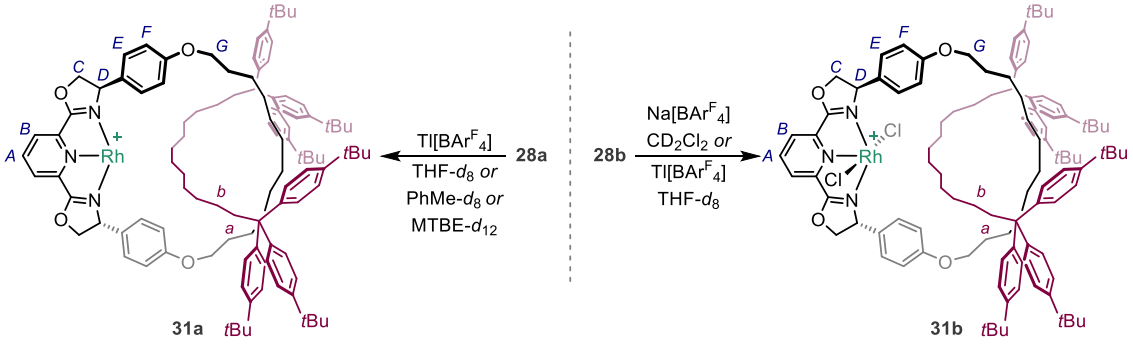

Scheme 4.5. Synthesis of low coordinate interlocked complexes. Counter anions omitted for clarity.

Abstraction of the chloride from **28a** with Tl[BAr$^{F}_{4}$] could be achieved in THF, MTBE and toluene; the reaction proceeded with a distinctive colour change from black to deep red, analogous to that for **27a** to **30a**. Formation of the C_2 symmetric low coordinate complex **31a** was also evident by changes in the ^{1}H NMR spectrum (THF-d_8, 298 K), including the *meta*-pyridine resonance (H_B) which was shifted downfield to δ 7.89 (**28a** obsc δ 7.29 – 7.19), and coincidence of two oxazoline 2H signals ($H_{C/D}$) resulting in a 4H multiplet at δ 5.46 – 5.31 (**28a** δ 5.50 and 5.23; Figure 4.5). In proteo THF, **31a** displayed the *para*-pyridine triplet at δ 8.72 and oxazoline multiplets at δ 5.86 – 5.64 and 4.94 – 4.75 (*vide infra*).

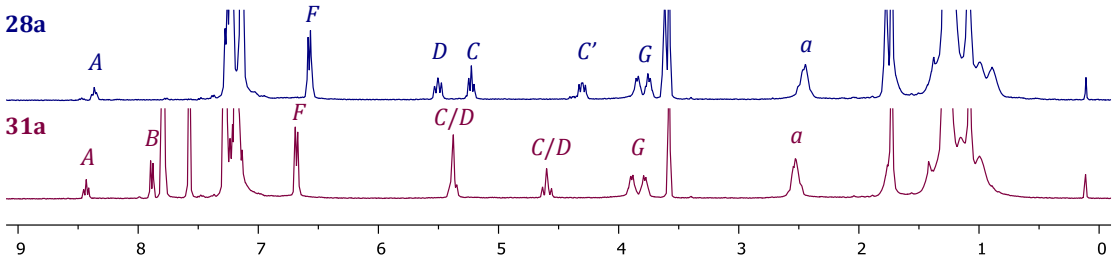

Figure 4.5. ^{1}H NMR spectra of **28a** and **31a** (298 K, THF-d_8, 400 MHz).

Complex **31a** proved sufficiently stable to permit analysis by IR spectroscopy under an inert atmosphere, either in the solid-state upon removal of the solvent, or in solution by subsequent dissolution in CH_2Cl_2 or toluene (Figure 4.6). Unfortunately, the ATR IR spectra collected of **31a** did not display any ν(CH) bands of reduced wavenumber as expected for M···H–C interactions (≈ 2700–2300 cm^{-1}).[252,356]

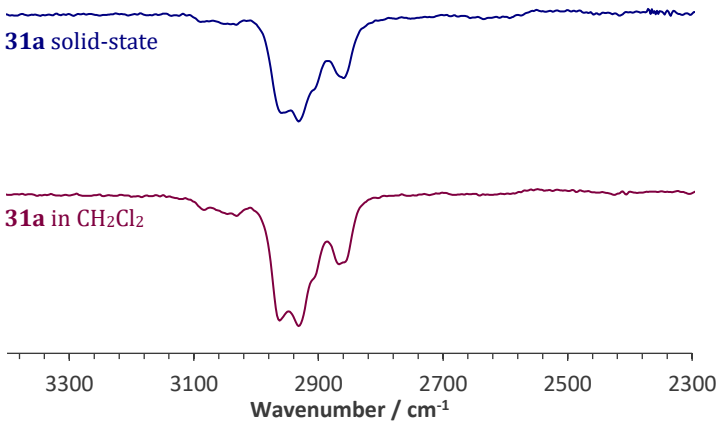

Figure 4.6. IR spectra of **31a** in the solid-state and in CH_2Cl_2. The traces have been scaled and stacked to allow for a clear comparison.

In order to circumvent the need to prepare **28a**, which proved to be challenging to both purify and handle, the direct synthesis of the low coordinate complex **31a** was attempted from the cationic metal precursor [Rh(Binor-S)(PCy_3)][BAr^F_4] (**A119**; Scheme 4.6). This precursor had previously been exploited to prepare ^{Ph}**pybox** containing PCy_3 complex **17**. In the case of **31a**, however, the cavity provided by the rotaxane ligand prevents coordination of the bulky phosphine ligand, and **31a** can be generated by reaction of ^{R}**pybox** with [Rh(Binor-S)(PCy_3)][BAr^F_4] in fluorobenzene at room temperature for 18 hours, as evidenced by a colour change from orange to a characteristically deep red. Quantitative conversion was observed by ^{1}H NMR spectroscopy, evidenced by loss of signals attributed to ^{R}**pybox** alongside the formation of a broad species assigned to **31a**.

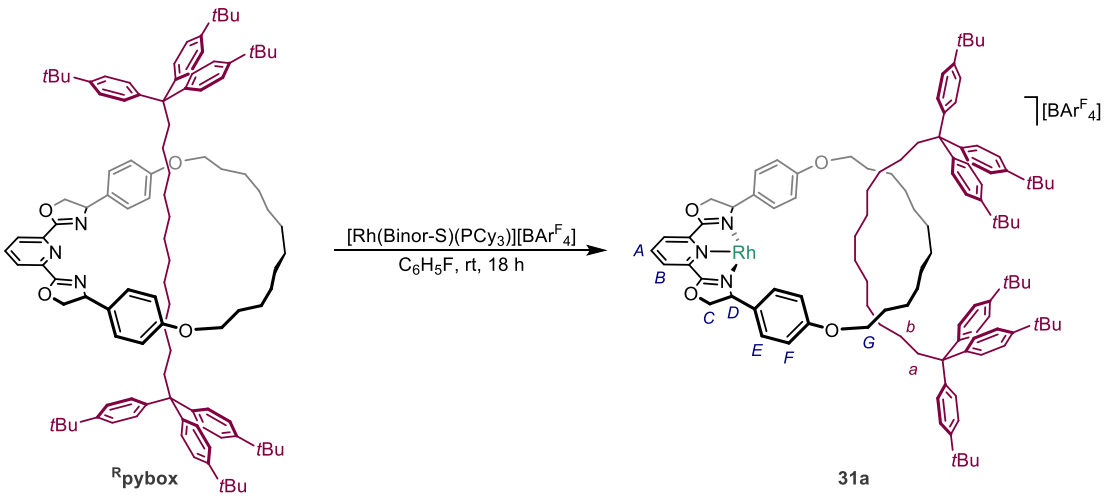

Scheme 4.6. Direct synthesis of **31a**.

To confirm generation of **31a** *via* this method, the solvent was removed *in vacuo* and the ^{1}H NMR was attained in THF and MTBE for comparison. The ^{1}H NMR spectra in both solvents showed identical pybox-containing species to that of **31a** generated by halide abstraction (*vide supra*). Unfortunately, purification of **31a** generated in this way could not be accomplished due to inability to remove liberated Binor-S and PCy_3 through washing, extraction or recrystallisation making this route unviable.

Abstraction of the chloride from **28b** proceeded rapidly in CD_2Cl_2 at room temperature using Na[BAr^F_4]. The room temperature ^{1}H NMR spectrum demonstrated the formation of **31b** through significantly shifted signals compared to **28b** (Figure 4.7). For instance, coincidence of the oxazolinyl resonances ($H_{C/D}$) from δ 5.46 and 5.27 to δ 5.45 – 5.29, similar to **15b** and **30b**, as well as broadening of the methylene protons assigned to the dodecamethylene linkers of the axle and macrocycle (*e.g.* H_a and H_G). This complex and **31a** were further investigated by VT NMR spectroscopy as discussed in the following section.

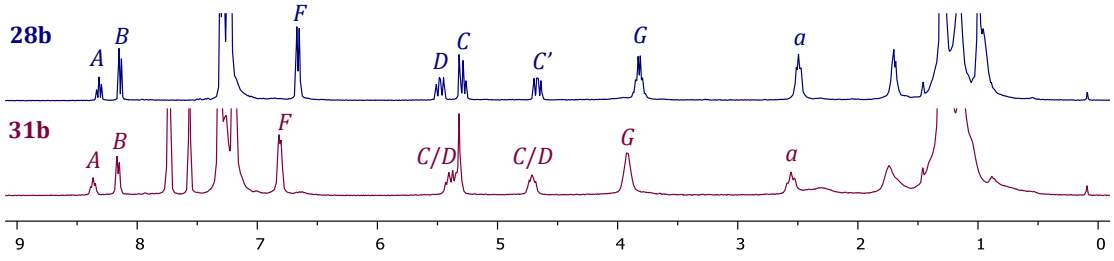

Figure 4.7. ^{1}H NMR spectra of **28b** and **31b** (298 K, CD_2Cl_2, 400 MHz).

4.2.2.3. Variable temperature NMR spectroscopy of rotaxane complexes

Variable temperature ^{1}H NMR experiments (185 – 298 K, 500/600 MHz) were used to investigate the presence of M···H–C bonding interactions in low coordinate complexes **31a** and **31b**. Samples were prepared immediately before measurements and stored at −78 °C

at all times, although these low coordinate complexes are surprisingly stable to decomposition. The VT NMR spectra obtained for **31a** were measured in THF-d_8, toluene-d_8, MTBE-d_{12} and CD_2Cl_2, whilst those of **31b** were measured in THF-d_8 and CD_2Cl_2.

It is important to note that several VT NMR measurements were obtained shortly after the reopening of the department following the recent COVID-19 lockdown. The stricter rules put in place to facilitate the reopening of the department made booking machine time for full VT NMR analysis difficult. As a result, some measurements were only collected at selected temperatures.

Rhodium(I) rotaxane complex

As a logical starting point, THF-d_8 was employed as the solvent to investigate **31a** by VT NMR spectroscopy, between 298 – 185 K (600 MHz; Figure 4.8).

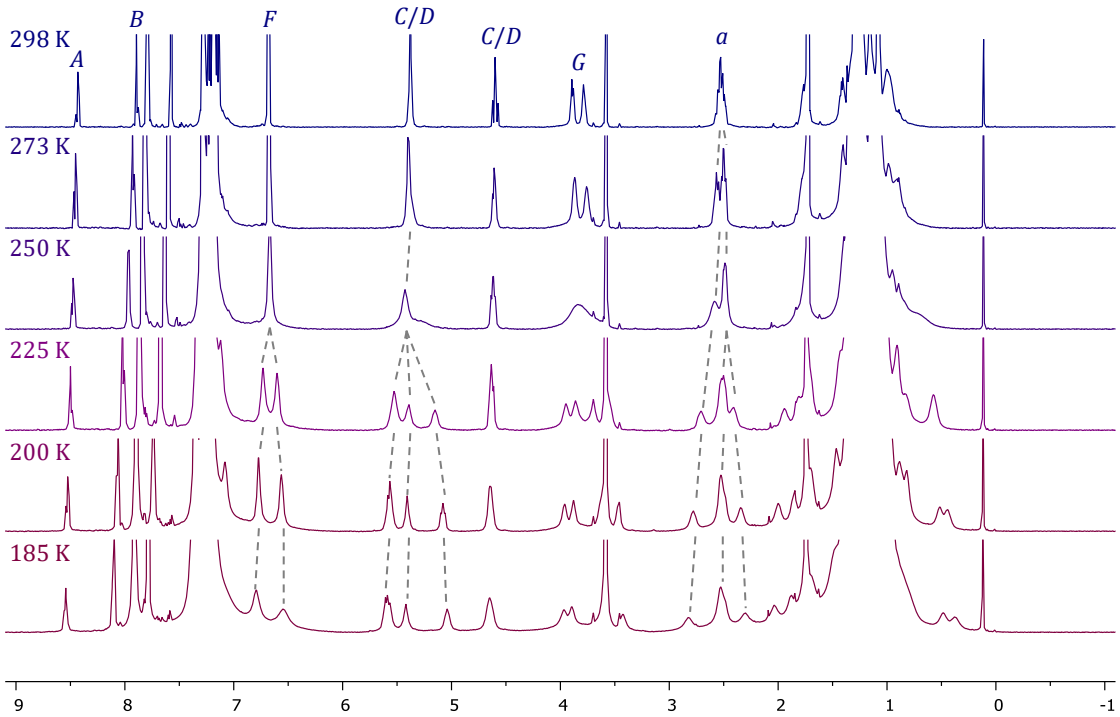

Figure 4.8. ^{1}H NMR spectra of **31a** recorded in THF-d_8 at different temperatures (600 MHz).

At 298 K **31a** adopts C_2 symmetry in solution, evident by 2 pyridine resonances at δ 8.43 and 7.89 (H_A and H_B). The pybox aryl substituents display resonances (H_F) at δ 7.22 and 7.14 and 2 coincidental signals at δ 6.68. Upon cooling to 225 K, hindered rotation is apparent by decoalescence into 4 unique signals, with further broadening observed at 185 K indicating loss of overall C_2 symmetry. This loss of symmetry is more apparent from the oxazoline resonances ($H_{C/D}$ δ 5.46 – 5.31), which separate and decoalesce at 225 K. Adoption of C_1 symmetry is also evident from the axle resonance H_a which decoalesces upon cooling to 225 K. The observation of a broad low frequency signal at δ 0.57 at 225 K is intriguing, especially as this signal decoalesces at 185 K to signals at δ 0.48 and 0.37. It

could indicate the presence of a Rh···H–C interaction, although the chemical shift is significantly higher than expected based on literature precedents ($\delta \approx -1$).[271,273] This could instead be the result of a CH–π interaction.

In order to further probe for Rh···H–C interactions the less coordinating toluene-d_8 was utilised as the solvent.[357] However, the resulting ^{1}H NMR data obtained were broad and uninformative, with the low temperature spectra potentially adversely affected by poor shimming.

To further investigate solvent effects, a sample of **31a** prepared in THF using Tl[BAr$^4{}_4$] was transferred into CD_2Cl_2 and analysed. Two low temperature ^{1}H spectra were obtained, one at 200 K and the other at 185 K (Figure 4.9). Unfortunately, residual THF (200 K: δ 3.59, 1.75) could be identified in the spectra from insufficient drying of **31a**. High-field signals at δ 0.49 and 0.36 were observed at 200 K, however, again it is difficult to assign this to a specific interaction with the data available. Upon standing at room temperature the sample became paler; after 24 hours analysis by ^{1}H NMR spectroscopy indicated formation of a new C_1 symmetric complex (*ca*. 75%) and complete disappearance of **31a**. This is presumably the result of CD_2Cl_2 oxidative addition (*vide supra*).

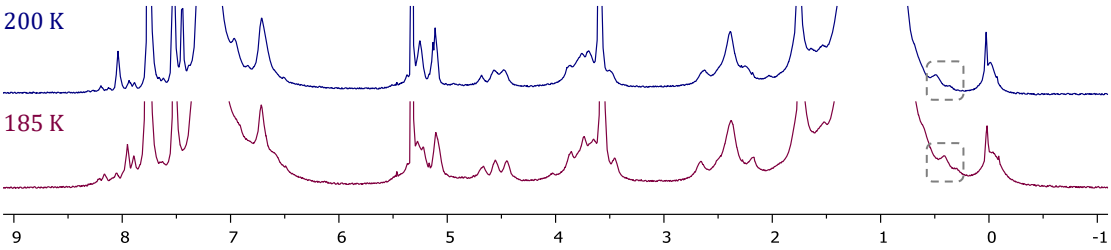

Figure 4.9. ^{1}H NMR spectra of **31a** recorded in CD_2Cl_2 at different temperatures (600 MHz).

The final solvent investigated was MTBE, however, it was necessary to synthesise the deuterated analogue for NMR measurements. Synthesis was achieved through modification of a literature procedure utilising CD_3OD, *t*-butanol-d_8 and D_2SO_4.[358] Although isolated in a lower yield than expected, sufficient MTBE-d_{12} was obtained (2.65 mL, 12%). Unfortunately, only a spectrum at 200 K was able to be measured (Figure 4.10). As with other solvents, a broad high-field signal was observed at 0.53 ppm. This signal is not present in a spectrum of the starting material at room temperature.

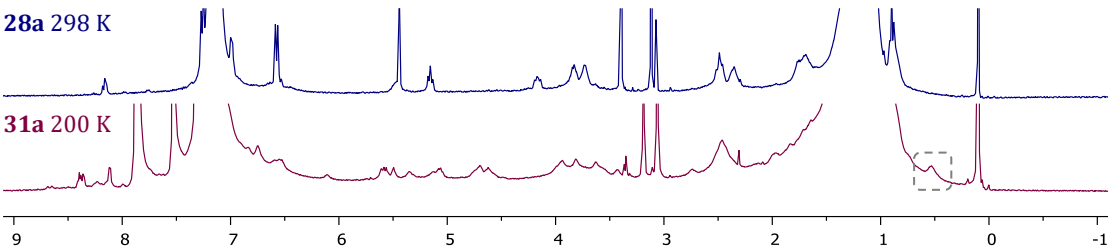

Figure 4.10. ^{1}H NMR spectra of **28a** at 298 K and **31a** at 200 K recorded in MTBE-d_{12} (600 MHz).

In conclusion, analysis of **31a** by VT NMR spectroscopy reveals the loss of symmetry, but definitive evidence for formation of Rh···H–C bonding interactions could not be obtained.

Rhodium(III) rotaxane complex

Complex **31b** was investigated using VT NMR spectroscopy (600 MHz) in both THF-d_8 and CD_2Cl_2. As with **31a**, decoalescence from C_2 to C_1 was observed upon cooling in THF-d_8; particularly apparent from one of the oxazoline signals ($H_{C/D}$) from δ 4.88 at 298 K to δ 5.21 and δ 4.75 at 185 K (Figure 4.11). No signals below 1 ppm were observed in this case. In comparison to **31a**, however, formation of a σ-complex is less likely based on the higher oxidation state of **31b**. Likewise, steric clashing of the axle with the ancillary chloride ligands is likely to prevent approach of the axle linker with the metal.

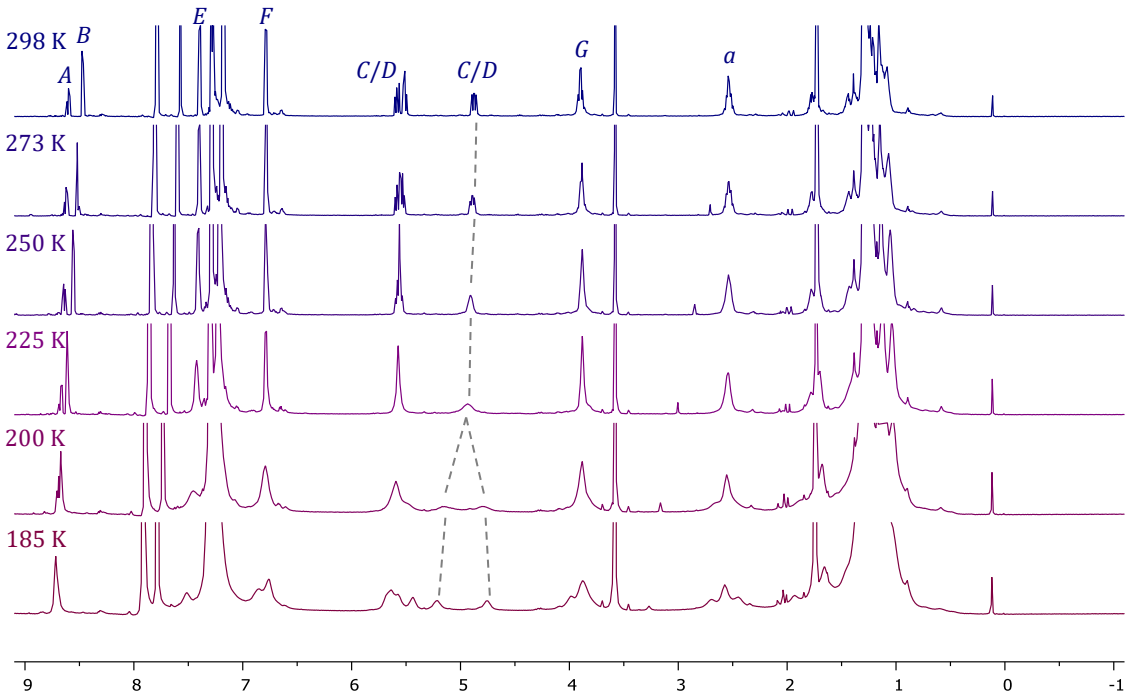

Figure 4.11. ^{1}H NMR spectra of **31b** recorded THF-d_8 at different temperatures (600 MHz).

As a less coordinating solvent, it was hoped that CD_2Cl_2 would provide the greatest chance to observe a Rh···H–C bonding interaction (Figure 4.12). Indeed, at 273 K a broad high-field signal was observed at δ 0.28 which shifted to δ −0.15 at 185 K. A COSY experiment was conducted at 200 K and indicated that the high-field signal (δ −0.15 ppm) coupled to the broad signal at δ 2.65 (marked with '↓' in Figure 4.12). The signal at 2.65 ppm appears to be one of the decoalesced protons alpha to the triaryl stopper unit (H_a), which suggests that the high-field signal corresponds to one of the beta protons (H_b). As H_b are likely to be in close proximity to the pybox aryl substituents, this finding supports the hypothesis that the high-field signal in **31a** and **31b** results from ring current effects, rather than interaction with rhodium.

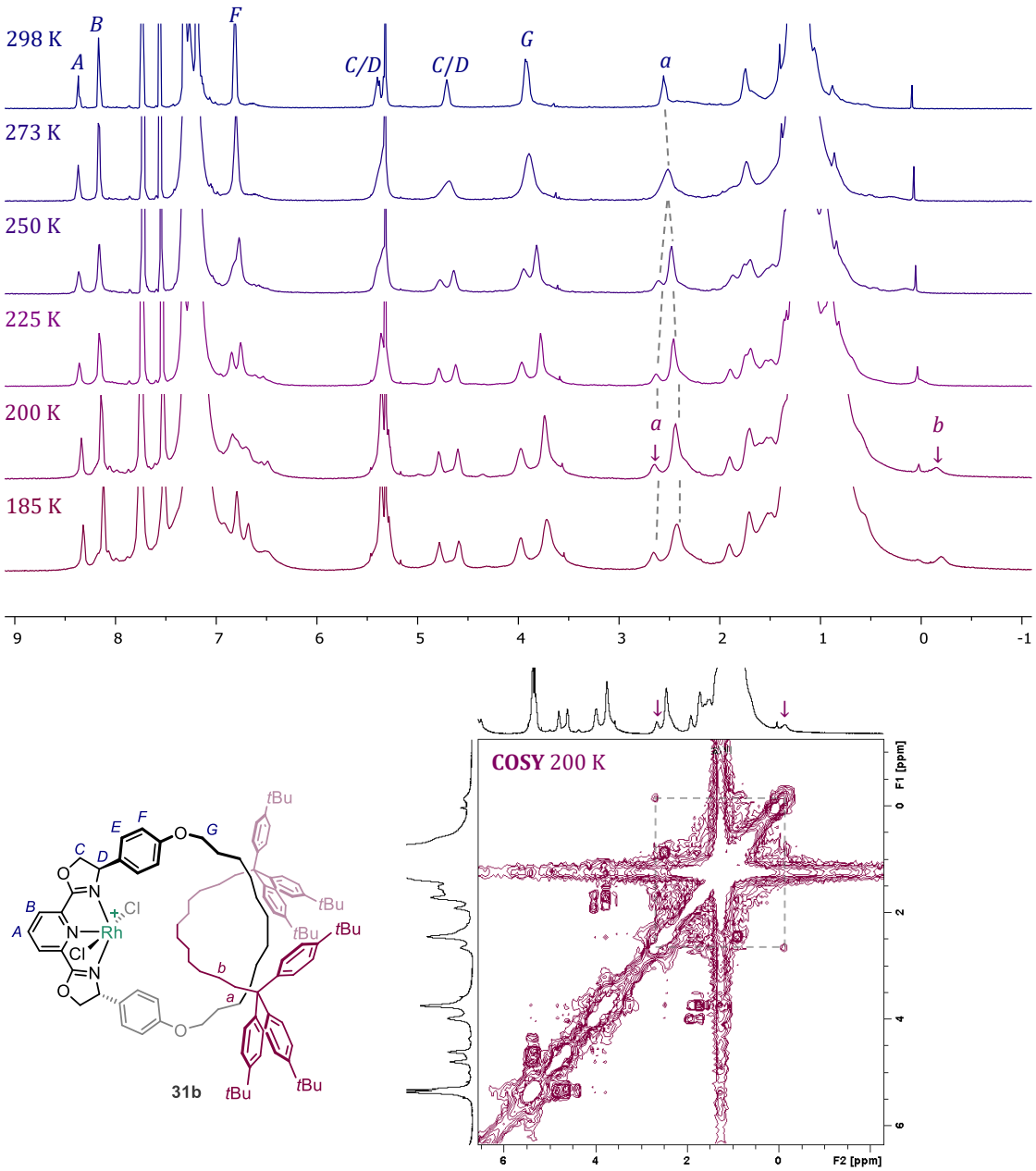

Figure 4.12. *Top*: Variable temperature ^{1}H NMR spectra of **31b** recorded in CD_2Cl_2. *Bottom*: COSY data at 200 K. (CD_2Cl_2, 600 MHz). Signals of interest marked with '↓'.

To further establish the nature of the signals, additional spectroscopic or solid-state evidence would be necessary, such as: low temperature HSQC and NOESY correlation experiments, a low temperature ^{13}C NMR experiment, and IR spectra of **31b** in solution and the solid-state.

4.2.3. Carbonyl derivatives

4.2.3.1. Macrocyclic carbonyl complexes

Carbonyl complex **32a** was formed by placing a solution of **30a** in MTBE at room temperature under an atmosphere of carbon monoxide (1 atm), marked by an immediate colour change from red to dark green, and subsequently isolated in good yield (76%; Scheme 4.7). The carbonyl stretching frequency of **32a** measured in dichloromethane is 2022 cm^{-1}, the same within error as **20a** (2019 cm^{-1}), which is expected for ligands with equivalent donor properties. Indeed, this has been previously noted for NHC-based rhodium(I) carbonyl complexes, in which the ν(CO) is unchanged between the acyclic and macrocyclic analogues.[226,344,359] The formation of **32a** is substantiated by observation of C_2 symmetry by ^{1}H NMR spectroscopy (CD_2Cl_2), with diagnostic oxazoline resonances at δ 5.35, 5.12 and 4.67, and a characteristic high frequency carbonyl resonance at δ 187.5 ($^1J_{RhC}$ = 75.9 Hz).

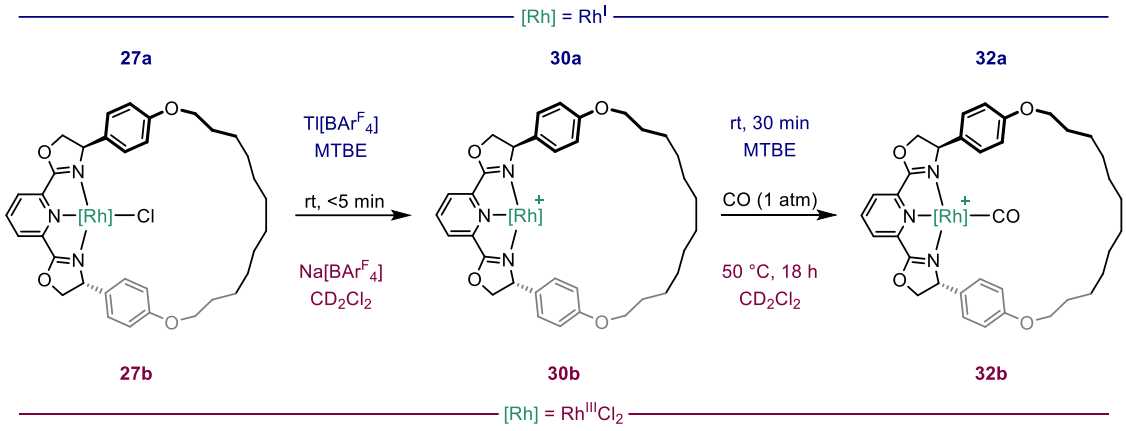

Scheme 4.7. Trapping of macrocyclic low coordinate complexes with CO. Counter anions omitted for clarity.

Trapping of **30a** with PCy_3 in fluorobenzene was also attempted, however, analysis *in situ* by NMR spectroscopy showed no evidence of phosphine coordination. This is in contrast to the related **^{Ph}pybox** system, in which quantitative formation of the PCy_3 complex **17** was observed under the same conditions. This difference in reactivity is attributed to the unique steric constraints of the macrocyclic cavity, which is too small to accommodate coordination of such a sterically demanding ligand.

The related rhodium(III) carbonyl complex **32b** was prepared by placing a solution of **30b** under an atmosphere of CO (1 atm) in CD_2Cl_2, although heating at 50 °C for 18 hours was required to achieve complete conversion; similarly, slow time frames are associated with the formation of acyclic complex **20b** (*vide supra*). Complex **32b** was subsequently isolated in a yield of 59% and characterised by NMR and IR spectroscopy as well as MS spectrometry. The HR ESI-MS of **32b** showed a signal at 822.1548 (calcd 822.1560) m/z,

assigned to [M+NaOMe]$^+$. The carbonyl stretching frequency of **32b** measured in dichloromethane is 2150 cm^{-1}, higher than that of free CO (*cf*. 2143 cm^{-1}), and the same within error as **20b** (2151 cm^{-1}). Furthermore, the $^{13}C\{^1H\}$ NMR spectrum of **32b** evidenced a characteristically high frequency carbonyl resonance at δ 171.3 ($^1J_{RhC}$ = 54 Hz), in excellent agreement with the acyclic congener **20b** (δ 171.8; $^1J_{RhC}$ = 55 Hz).

4.2.3.2. Rotaxane carbonyl complexes

The low coordinate species **31a** and **31b** could be trapped out with carbon monoxide to form the corresponding interlocked carbonyl complexes **33a** and **33b** (Scheme 4.8). The carbonyl derivatives were subsequently investigated and compared to the model systems using spectroscopic techniques.

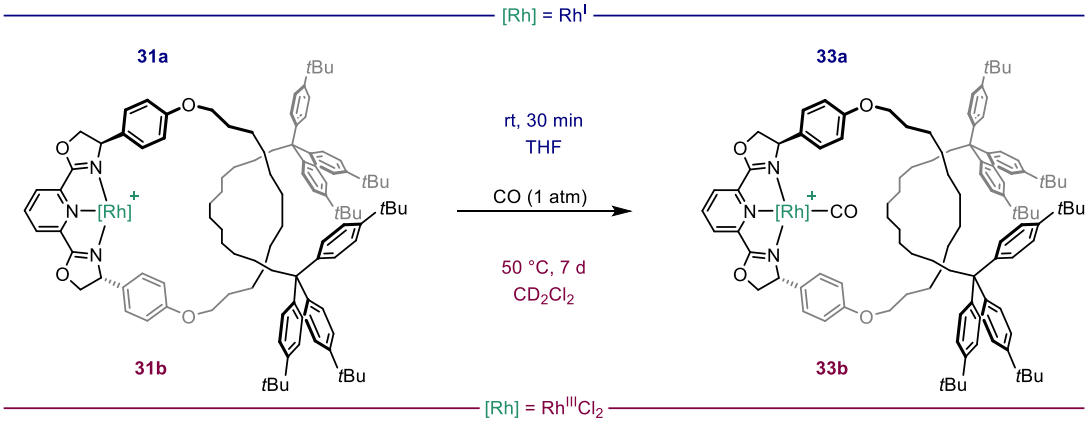

Scheme 4.8. Trapping of low coordinate rotaxane complexes with CO. Counter anion omitted for clarity.

Placing a solution of **31a** (in THF, MTBE or toluene) under an atmosphere of CO (1 atm) rapidly generated a yellow complex which became green upon removal of the solvent. It is proposed that this involves transformation of a bis-carbonyl complex (*bis*-**33a**) to the expected green mono-carbonyl complex (*mono*-**33a**), which was isolated in good yield (74%). This reaction can also be induced by freeze-pump-thaw degassing a solution of *bis*-**33a**. The IR spectrum of *bis*-**33a** in CH_2Cl_2 under CO shows two signals at 2041 and 2101 cm^{-1}, whilst pure *mono*-**33a** (prepared by successive drying/dissolving) has a single CO band at 2030 cm^{-1} (Figure 4.13).

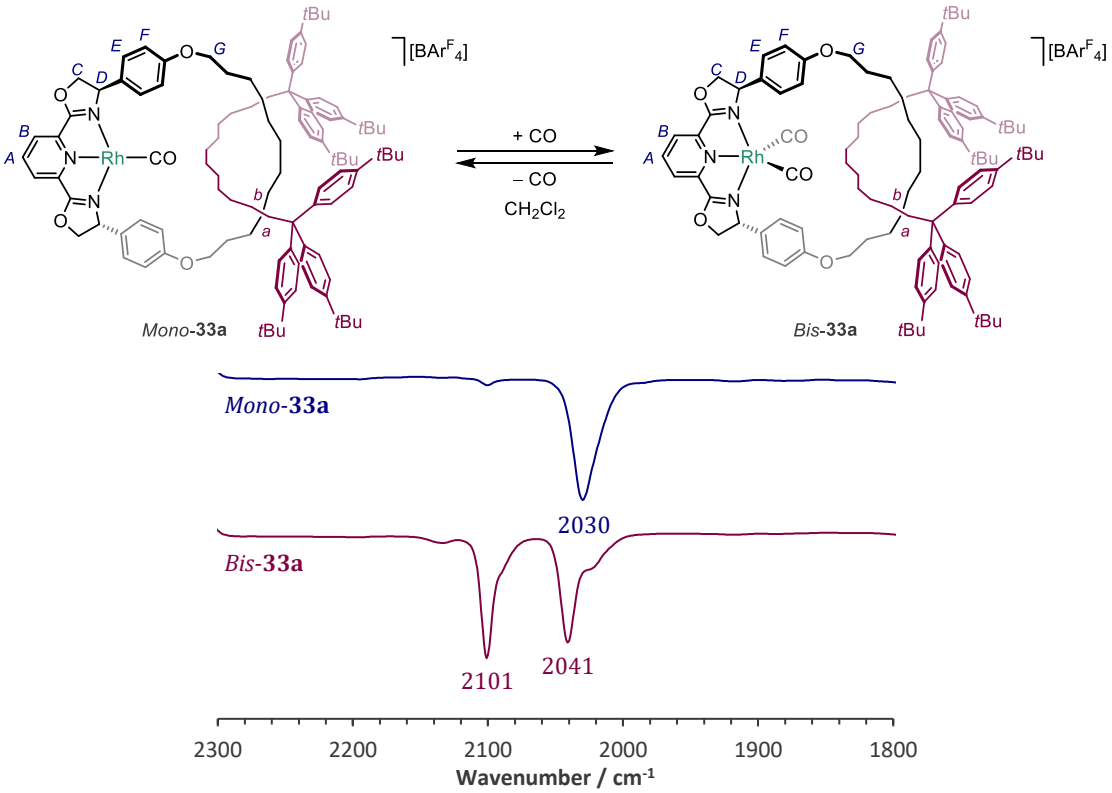

Figure 4.13. IR spectra of *mono*-**33a** and *bis*-**33a**, measured in CH_2Cl_2. The traces have been scaled and stacked to allow for a clear comparison.

The ν(CO) of *mono*-**33a** (2030 cm^{-1}) is distinctly higher than those of ^{Ph}**pybox** and ^{M}**pybox** complexes **20** (2019 cm^{-1}) and **32a** (2022 cm^{-1}), respectively (Figure 4.14). This blue-shift is attributed to steric buttressing of CO with the axle, resulting in deviation from ideal coordination geometry and therefore reduced metal backbonding into the π* (CO) orbital. Destabilisation of the square planar geometry in this way would also explain the capacity of the metal to bind a second equivalent of CO, something that is not observed in **20a** or **32a** at room temperature. Interestingly, cooling solutions of **20a** and **32a** in CD_2Cl_2 under CO (1 atm) to −78 °C resulted in colour changes from green to yellow, indicating that formation of *bis*-carbonyl derivatives occurs at low temperature. Equilibrium between *mono*- and *bis*-carbonyl complexes has previously been reported for a macrocyclic NHC-based rhodium complex.[360]

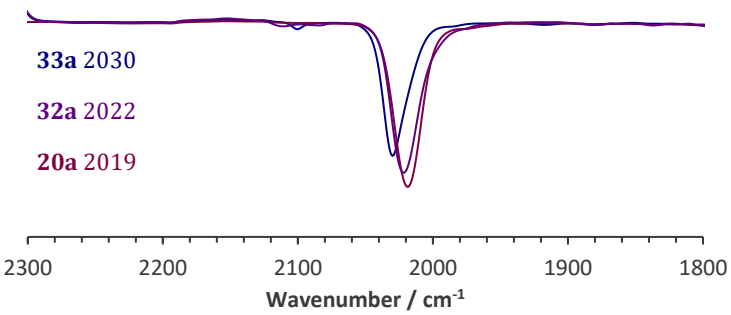

Figure 4.14. IR spectra of rhodium(I) complexes [Rh(x**pybox**)CO][BAr^F_4], where x = Ph (**20a**), M (**32a**), R (*mono*-**33a**). The traces have been scaled and superimposed to allow for a clear comparison.

Analysis of *mono*- and *bis*-**33a** by NMR spectroscopy in both CD_2Cl_2 and THF-d_8 indicated adoption of C_2 symmetry (Figure 4.15). For *mono*-**33a**, a carbonyl resonance with a very similar spectroscopic signature to **32a** was observed in CD_2Cl_2 at δ 187.8 with $^1J_{RhC}$ =75 Hz (*cf.* **32a** 187.5; $^1J_{RhC}$ = 76 Hz). However, no carbonyl resonance could be observed for *bis*-**33a**. Analysis by HR-ESI in both cases only revealed a signal at 1689.0043 (calcd 1689.0077) *m*/*z* for a mono carbonyl fragment; loss of the second CO is presumably facile under the mass spectrometry conditions. Combined with the IR data, we propose a trigonal bipyramidal structure for *bis*-**33a**, similar to that predicted computationally for the related macrocyclic NHC system.[360]

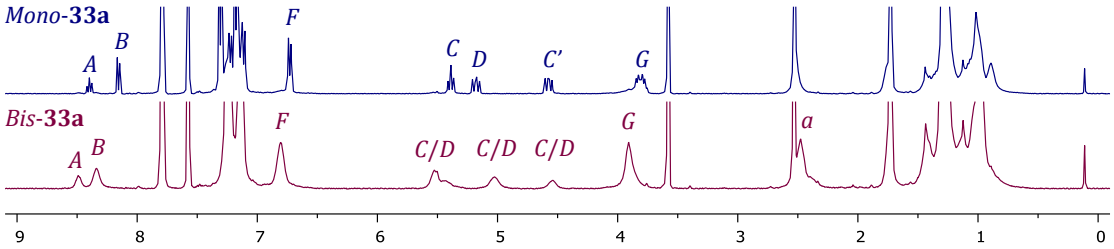

Figure 4.15. ^{1}H NMR spectra of *mono*-**33a** and *bis*-**33a** (298 K, THF-d_8, 400 MHz).

To help interpret the spectroscopic data collected for **31a** at low temperature, VT NMR data was collected for **31a** + CO in THF-d_8 for comparison (Figure 4.16). The ^{1}H NMR spectrum of **31a** + CO at 185 K is notable for C_2 symmetry, contrasting the asymmetric spectrum observed for **31a** at this temperature. Both exhibit high-field signals below 1 ppm, but for coordinatively saturated **31a** + CO, these are shifted downfield to δ 0.74 and 0.68 (*cf.* **31a** δ 0.48 and 0.37). This observation further supports the hypothesis that these signals result from CH–π interactions with the pybox aryl substituent and not M···H–C bonding.

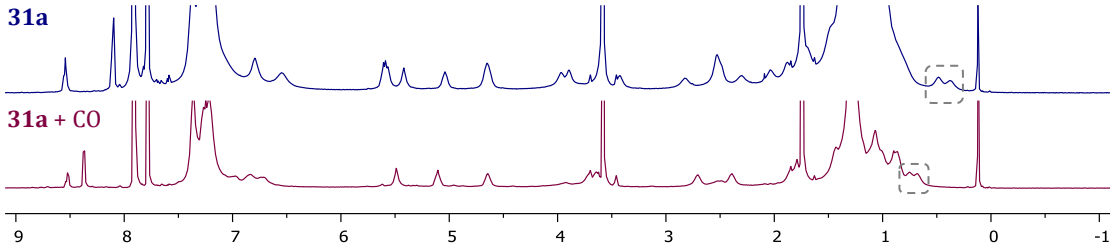

Figure 4.16. Stacked ^{1}H NMR spectra of **31a** and **31a** + CO, recorded at 185 K (THF-d_8, 600 MHz).

Formation of the rhodium(III) carbonyl complex **33b** required forcing conditions of 168 hours in refluxing CD_2Cl_2 under CO (1 atm) for full conversion to **31b**, but was subsequently isolated in excellent yield (89%). Given the relative ease in forming these rhodium(III) carbonyl complexes decreases in the order pincer = ^{Ph}**pybox** > ^{M}**pybox** > ^{R}**pybox**: steric factors clearly play a major role.[361,362] Formation of **33b** was evidenced by analysis using ^{1}H NMR spectroscopy (CD_2Cl_2), which showed a diagnostic downfield *para*-

pyridine resonance at δ 8.64; significantly shifted compared to the corresponding low coordinate analogue (**31b**, δ 8.37). Further evidence was provided by $^{13}C\{^{1}H\}$ NMR spectroscopy, in which a characteristically high frequency carbonyl resonance at δ 172.7 ($^{1}J_{RhC}$ = 55 Hz) was located for **33b**, and by IR spectroscopy, with the carbonyl band in CH_2Cl_2 at 2154 cm^{-1}. This data is in excellent agreement with the acyclic (**20b**) and macrocyclic (**32b**) congeners described above.

As for the rhodium(I) system, **33b** was used to help interpret the spectroscopic data gathered for **31b**. The ^{1}H NMR spectrum of **33b** in CD_2Cl_2 at 185 K was measured and compared to **31b** (Figure 4.17). The coordinatively saturated carbonyl derivative is notable for higher symmetry and the absence of any signals below 1 ppm. This data is consistent with the aforementioned interpretation that the high-field signal results from C–H interactions, although the origin cannot be definitively assigned.

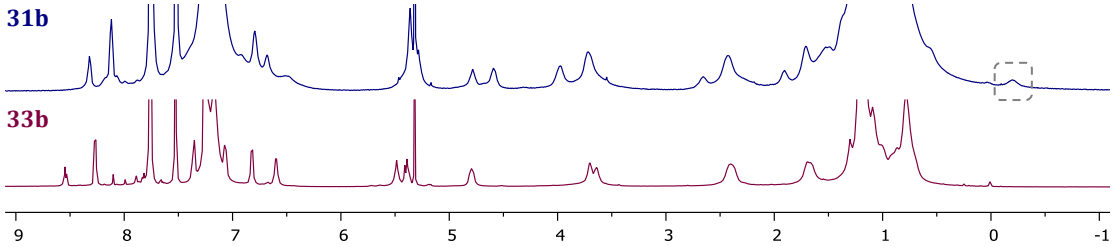

Figure 4.17. ^{1}H NMR spectra of **31b** and **33b** recorded at 185 K (CD_2Cl_2, 600 MHz).

The redox shuttling conditions identified for the acyclic system could also be applied to carbonyl complexes **33a** and **33b**. At room temperature in THF, reaction of **33b** with activated zinc afforded **33a** in 120 hours, whilst **33a** was readily oxidised to **33b** using $PhICl_2$ within 1 hour. Although oxidation of **33a** proceeded with a similar rate to the model system, the reduction of **33b** was far more sluggish. This was attributed to steric factors (t = 120 h for **33b** *vs*. 1 h for **20b**), exacerbated by the heterogeneous nature of the reaction. The preparation of **33b** in this manner is preferable, proceeding far quicker than the reaction of **31b** with CO and avoiding the need for forcing conditions.

4.2.4. Computational analysis

To further investigate the potential to form M···H–C interactions in complexes of ^{R}**pybox**, a DFT-based computational analysis was carried out employing complexes of ^{Ph}**pybox** as models (Figure 4.18).‡ The acyclic pybox variant was used for computational simplicity, compared to the more computationally challenging rotaxane ligand.

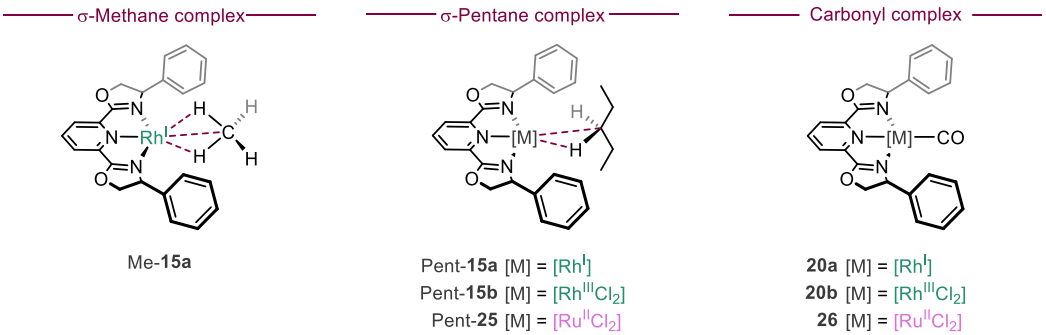

Figure 4.18. Acyclic complexes investigated with computational analysis.

As a starting point, the pybox analogue of Brookhart's σ-methane complex Me-**15a** (*cf.* **A84a**) was optimised (Figure 4.19).[271] The coordination of methane occurs by interaction of two C–H bonds (M···H = 2.022 Å) similar to Brookhart's (*cf.* **A84a** M···H = 1.869 and 2.178 Å), and the associated M···C contact of 2.378 Å is directly comparable (*cf.* **A84a** 2.380 Å). Using pentane as the substrate considerably altered the binding-mode (*viz.* Pent-**15a**). Notably, a rotation is required to avoid steric buttressing with the aryl substituents and interaction with the metal only occurs *via* one of the C–H bonds, with a corresponding increase in the M···C contact to 2.698 Å. A similar substrate binding mode was found for the rhodium(III) analogue Pent-**15b**, although the M···C contact is appreciably larger (2.972 Å). Both are associated with large M-H-C angles suggesting they may be better described as electrostatic or hydrogen bonding interactions.[248] Moreover, the ruthenium σ-pentane complex Pent-**25** could not be optimised, signifying an energetically unfavourable interaction.

‡ Computational analysis was performed by Dr Adrian Chaplin. DFT calculations were carried out at the B3PW91/6-31G**(non-metals), SDD(Rh,Ru) level of theory.

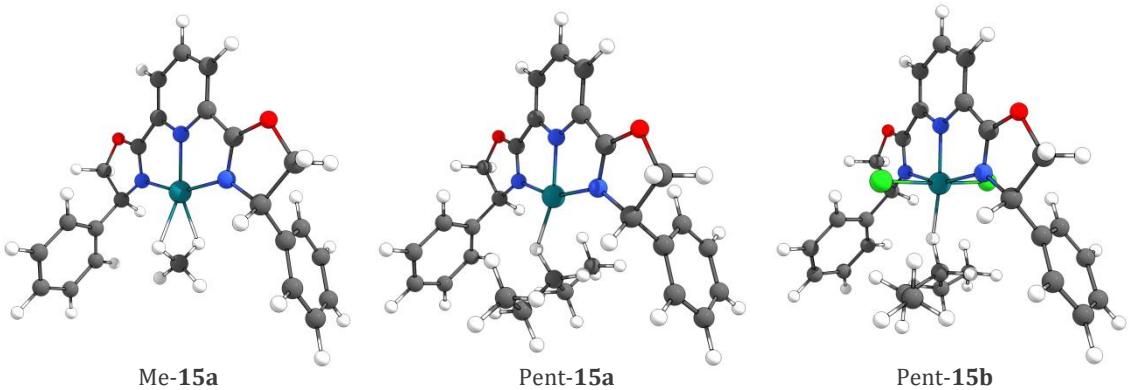

Me-**15a** Pent-**15a** Pent-**15b**

Figure 4.19. Geometry structures.

The calculated gas phase methane dissociation enthalpy of Me-**15a** is 50.2 kJ mol^{-1}, appreciably lower than **A84a** (71.3. kJ mol^{-1}) and presumably a reflection of the weaker net donor character of pybox compared with PNP ligands (Table 4.1; see Chapter 3).[271,287] Not surprisingly, binding of pentane is weaker in Pent-**15a**, and even more so for Pent-**15b**, becoming distinctly endergonic. These findings suggest that coordination of the alkyl chain to the metal in **31a** and especially **31b** is not thermodynamically possible. For comparison, formation of all the corresponding carbonyl complexes is predicted to be very exergonic, in line with the experimental findings.

Table 4.1. Calculated binding energies, free energies (kJ mol^{-1}) and structural parameters.

σ-Complex	BDE	ΔG	*r*(M–C) /Å	∠ M-H-C /°	CO-Complex	BDE	ΔG	*r*(M–C) /Å
Me-**15a**	50.2	−7.81	2.378	94.0				
Pent-**15a**	29.0	22.3	2.698	125.9	**20a**	204.8	−155.8	1.878
Pent-**15b**	2.3	47.9	2.972	151.2	**20b**	162.6	−115.5	1.940
Pent-**25**	<0	>>0	-	-	**26**	179.8	−129.6	-

4.3. Rhodium and iridium 2,2'-biphenyl complexes

The rhodium and iridium 2,2'-biphenyl (biph) complexes [Rh(biph)(dtbpm)Cl] and [Ir(biph)(COD)Cl]$_2$ have demonstrated their effectiveness as convenient precursors for the generation of M(III) ^{Ph}**pybox** complexes (*cf*. Section 3.3). The use of the robust precursors with the elaborate ^{M}**pybox** and ^{R}**pybox** ligands are described below.

4.3.1. Synthesis and characterisation of macrocyclic iridium complexes

The macrocyclic iridium(III) complex [Ir(^{M}**pybox**)(biph)Cl] (**34**) was prepared from reaction of ^{M}**pybox** and [Ir(biph)(COD)Cl]$_2$ in CD_2Cl_2 at room temperature (Scheme 4.9). Quantitative conversion to **34** was observed by ^{1}H NMR spectroscopy. Indicative signals in the spectrum included six inequivalent oxazoline resonances at δ 5.18, 5.01, 4.93, 4.54, 4.46 and 4.19, consistent with the formation of a C_1 symmetric species. HR ESI-MS confirmed the formation of **34**, which displayed a signal at 912.3354 (calcd 912.3350) m/z, attributed to the $[M-Cl]^+$ ion.

Chloride abstraction from **34** using Na[BAr$^F_4$] proceeded with quantitative conversion to give **35** within 18 hours, which is associated with adoption of time-averaged C_2 symmetry, indicating pseudorotation of the biphenyl moiety. The highly fluxional nature of the complex was indicated through extensive line broadening of the oxazoline (fwhm = 90 Hz), biphenyl and phenyl proton resonances, whilst only the pyridine signals remained sharp (Figure 4.20). Similar fluxionality was noted for the analogous ^{Ph}**pybox** complexes **22** and **24** (see Section 3.3), but in related CNC and PNP systems pseudo rotation has been blocked by use of macrocyclic variants.[252,314,315]

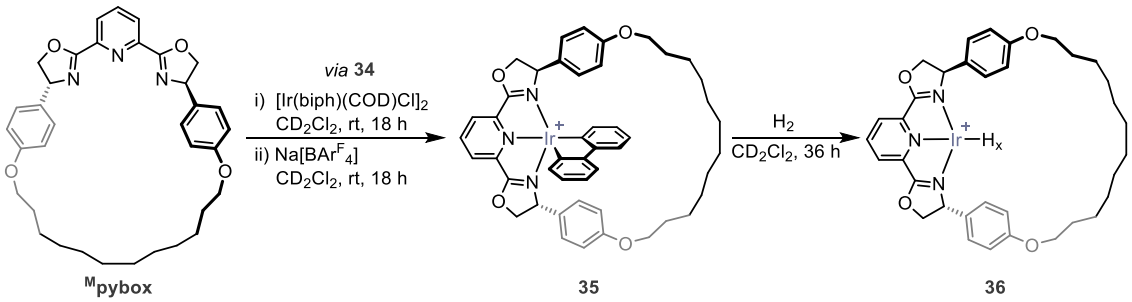

Scheme 4.9. Synthesis of macrocyclic iridium biphenyl complexes, counter anions omitted for clarity.

Generation of an iridium hydride complex **36** was attempted by hydrogenolysis of the biph ligand through reaction of **35** with dihydrogen in CD_2Cl_2 (1 atm; Scheme 4.9). After 36 hours at room temperature, near quantitative formation of **36** was observed by ^{1}H NMR spectroscopy in CD_2Cl_2 (*ca*. 80%). One main hydride signal was observed in the ^{1}H NMR spectrum; a broad singlet at −23.12 ppm (fwhm = 105 Hz), which integrated to 2H when compared with the oxazoline protons and suggested the formation of a dihydride

complex. This assignment correlated well to a related iridium(III) dihydride complex bearing an NHC-based macrocycle (*viz.* **A75**, IrH δ −24.53 in CD_2Cl_2, see Chapter 3).[252]

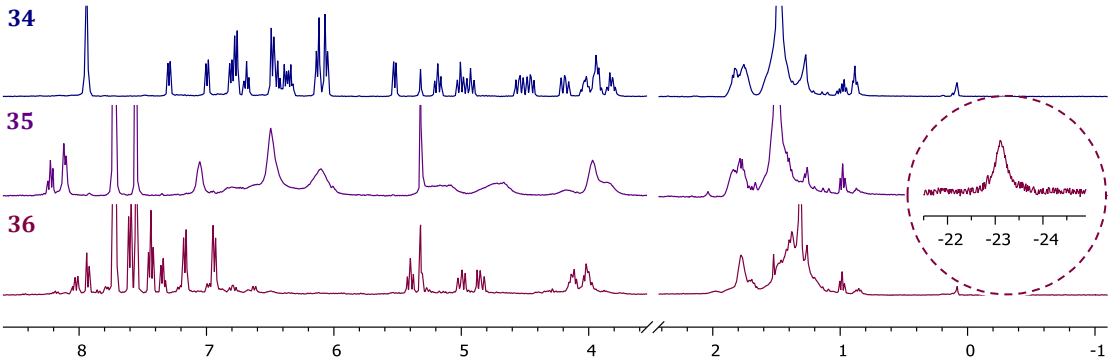

Figure 4.20. ^{1}H NMR spectra of **34**, **35** and **36**, with hydride signals of **36** shown (298 K, CD_2Cl_2, 400 MHz).

4.3.2. Attempted synthesis of rotaxane biphenyl complexes

Building upon the aforementioned work with ^{Ph}**pybox** and ^{M}**pybox**, the low coordinate complexes **38** and **40** were targeted (Scheme 4.10).

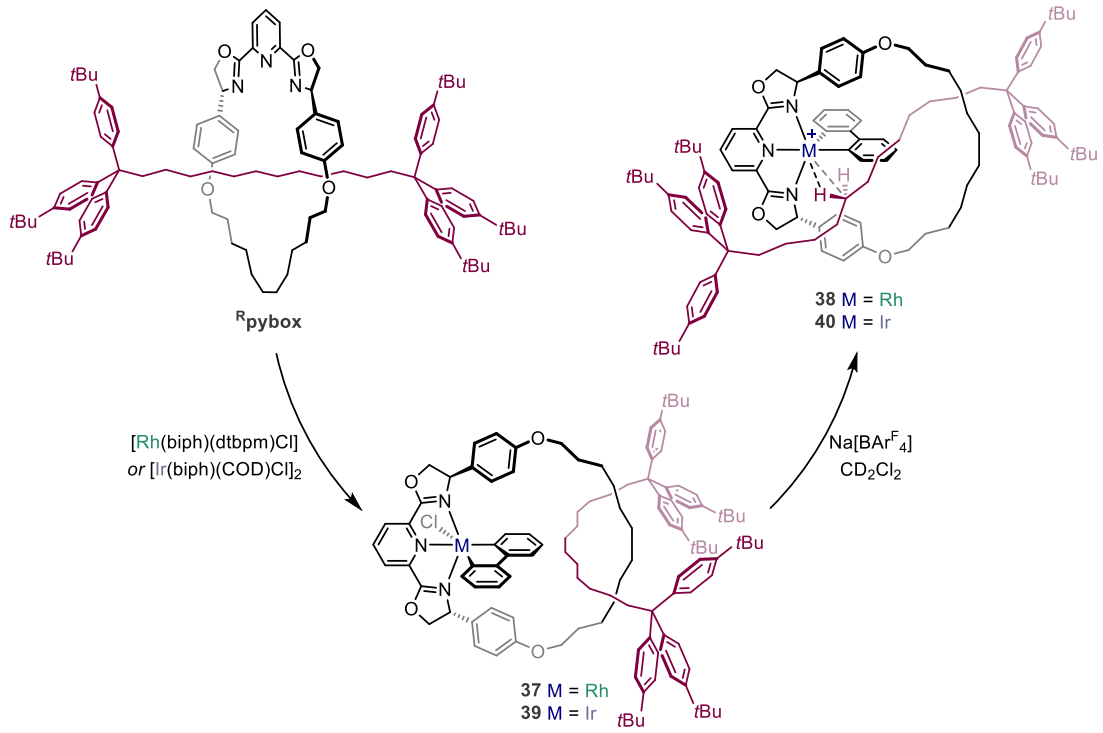

Scheme 4.10. Preparation of rotaxane complexes **38** and **40**, counter anions omitted for clarity.

Reaction of ^{R}**pybox** with [Rh(biph)(dtbpm)Cl] in MeCN at 85 °C proceeded slowly, requiring 14 days for complete consumption of the starting material. THF was probed as an alternative solvent, due to the higher solubility of ^{R}**pybox** in this solvent, however, a similar rate was observed. The slow rate and forcing conditions was similarly noted for metalation of platinum(II) rotaxane complexes.[219] Unfortunately, under these conditions several intractable decomposition products were generated, as observed by ^{1}H NMR

spectroscopy. The crude was extracted into pentane and washed with HMDSO to remove axle and unreacted **^{R}pybox** to yield impure **37** (*ca*. 83%). Purification was attempted by recrystallisation and column chromatography, however, these were ultimately unsuccessful.

Nevertheless, abstraction of the chloride using Na[BAr$^{F}_{4}$] from crude **37** in CD_2Cl_2 was investigated and yielded impure **38** (Figure 4.21). The ^{1}H NMR spectrum is notable for the adoption of C_1 symmetry, evidenced by the inequivalent oxazoline and pybox aryl signals in stark contrast to the time-averaged C_2 symmetric acyclic congener **22** (see Chapter 3): pseudorotation of the biphenyl moiety in this case appears to be prevented by the axle component. No signals below 1 ppm were observed and further interrogation by NMR spectroscopy was encumbered by the inability to purify **38**. However, further structural corroboration was possible by HR ESI-MS, where a strong molecular ion peak at 1814.0844 (calcd 1814.0832) m/z assigned to **38** was observed.

The iridium variant was similarly explored. Reaction of **^{R}pybox** with [Ir(biph)(COD)Cl]$_2$ in CD_2Cl_2 for 18 hours at room temperature yielded **39**, in *ca*. 75% purity. This complex adopted C_1 symmetry in the ^{1}H NMR spectrum, as evidenced by 6 inequivalent oxazoline resonances (Figure 4.21). Further proof of formation was obtained by ESI-MS, which displayed a signal at 1904.0 (calcd 1904.1) m/z attributed to the $[M-Cl]^+$ ion. As for **37**, purification by recrystallisation and column chromatography on silica were attempted but these were also unsuccessful. Chloride abstraction of crude **39** using Na[BAr$^{F}_{4}$] was attempted, resulting in a species characterised by extensive line broadening in ^{1}H NMR spectrum. This result, in combination with the inability to purify **39**, prevented further investigation of this iridium system.

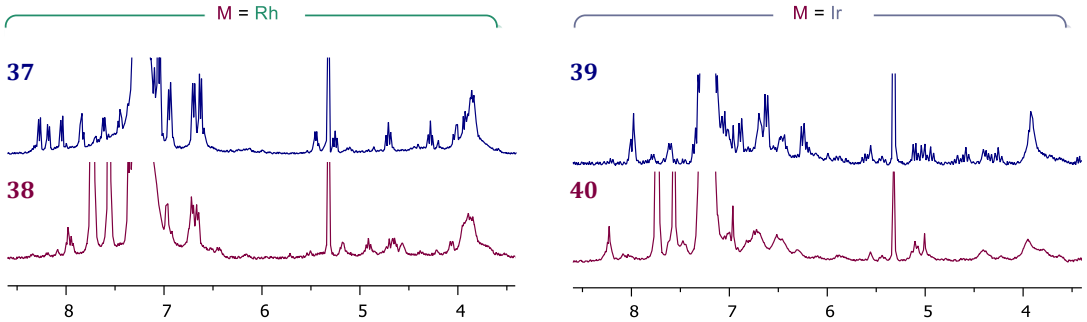

Figure 4.21. ^{1}H NMR spectra of rhodium complexes (*left*) and iridium complexes (*right*). Selected region shown for clarity (298 K, CD_2Cl_2, 400 MHz).

4.4. Ruthenium complexes

4.4.1. Synthesis and characterisation of macrocyclic complexes

Using the method established for ruthenium(II) dichloride of ^{Ph}**pybox** (*cf.* Section 3.4), macrocyclic complex **THF-41** was prepared by stirring ^{M}**pybox** with $[Ru(p\text{-cymene})Cl_2]_2$ in THF for 1 hour at room temperature (Scheme 4.11). Liberated *p*-cymene was removed by washing with hexane and **THF-41** was isolated in good yield (78%). Formation of **THF-41** was corroborated by a combination of mass spectrometry and NMR spectroscopy, with bound THF notably characterised in CD_2Cl_2 with shifted OCH_2 resonances at δ 3.77 and 3.28 compared to free THF (δ 3.68).

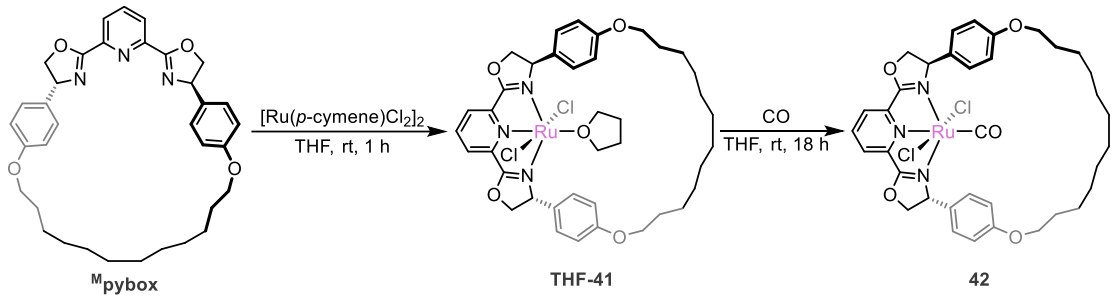

Scheme 4.11. Synthesis of macrocyclic ruthenium(II) complexes.

As for **THF-25**, the ^{1}H NMR spectrum of **THF-41** in CD_2Cl_2 revealed an equilibrium mixture between **THF-41** and the corresponding CD_2Cl_2 adduct (**DCM-41**) in a 1:1 ratio. Both complexes adopt C_2 symmetry and the position of equilibrium can be perturbed toward **THF-41** by addition of THF to the sample, facilitating assignment.

Placing a THF solution of **THF-41** under an atmosphere of carbon monoxide (1 atm) at room temperature resulted in the formation of carbonyl complex **42**, which was subsequently isolated in excellent yield (92%). Complex **42** was characterised in solution using NMR spectroscopy and by mass spectrometry. The HR ESI-MS displayed a signal at 764.2037 (calcd 764.2041) m/z, assigned to the $[M–Cl+MeOH]^+$ cation. The ^{1}H NMR spectra of **42** in CD_2Cl_2 was consistent with the adoption of C_2 symmetry in solution, with 3 unique oxazoline resonances. Furthermore, the $^{13}C\{^1H\}$ NMR spectrum featured a characteristic high frequency carbonyl resonance at δ 203.6, closely matching the acyclic congener (**26** δ 204.3). The carbonyl stretching frequency of **42** was measured to be 1980 cm^{-1} in dichloromethane and is likewise very similar to that of **26** (1977 cm^{-1}). Both suggest strongly bound CO and match literature-known NNN pincer-based complexes.[363,364] Gratifyingly, dark green crystals suitable for X-ray diffraction were obtained from diffusion of hexane into a dichloromethane solution of **42**, permitting characterisation in the solid-state (Figure 4.22).

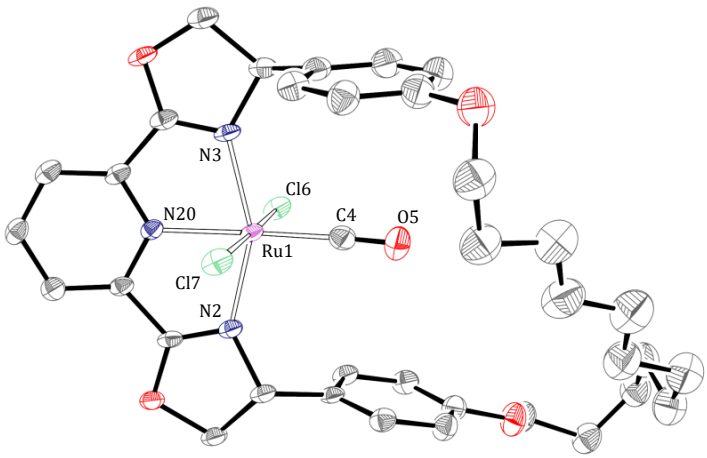

Figure 4.22. Solid-state structure of **42**. Thermal ellipsoids drawn at 40% probability. Hydrogen atoms and minor disordered components are omitted for clarity. Selected bond lengths (Å) and angles (°): Ru1-N2, 2.061(3); Ru1-N3, 2.077(3); Ru1-N20, 2.052(3); Ru1-C4, 1.878 (4); Ru1-Cl6, 2.3964(9); Ru1-Cl7, 2.3811(9); C4-O5, 1.129(5); N2-Ru1-N3, 154.06(12); N20-Ru1-C4, 174.61(14); Cl6-Ru1-Cl7, 176.88(4).

The solid-state structure of **42** is notable for twisting of the macrocycle to one side of the pincer coordination plane, although this does not appear to be a requirement to accommodate CO within the cavity and is most likely the result of crystal packing effects. The C_1 symmetry in the solid-state certainly does not persist in solution (C_2 symmetry). Comparison to the acyclic counterpart **26** showed similar metrics about the metal, although the Ru–Cl bond is slightly elongated in **42** (2.3964(9) and 2.3811(9) Å *vs* 2.33864(7) Å).

4.4.2. Attempted synthesis of rotaxane complexes

To assess the five-coordinate target **43**, both THF and MTBE were probed as solvents; the latter, in particular, being helpful for establishing the presence of coordinated solvent (Scheme 4.12).

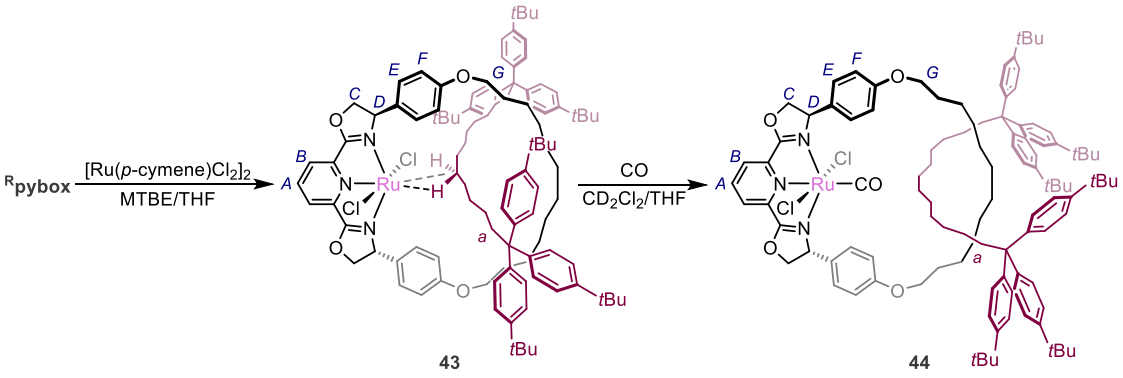

Scheme 4.12. Synthesis of interlocked ruthenium complex **43**, drawn as target σ-complex.

The synthesis of **43** by the reaction of **^{R}pybox** and [Ru(*p*-cymene)Cl_2]$_2$ in MTBE required a total of 7 days at 50 °C for full consumption of **^{R}pybox**, as evidenced by ^{1}H NMR spectroscopy. The use of THF failed to shorten the reaction time, but did remove the need

for elevated temperatures. Analysis of crude materials obtained from both reactions using ^{1}H NMR spectroscopy in CD_2Cl_2 revealed the formation of one main C_2 symmetric compound, with similar chemical shifts to the macrocyclic ruthenium complex **DCM-41**. For instance, an oxazolinyl methylene resonance ($H_{C'}$) at δ 4.51 closely matched the macrocyclic analogue (δ 4.47), whilst the *meta*-pyridine resonance (H_B) at δ 7.73 was similar to both model variants (**DCM-41**: δ 7.76, **DCM-25** δ 7.80).

Despite numerous purification attempts, a number of impurities persisted in the sample, exacerbated by comparable solubility to **43**. Therefore, **43** was characterised as an impure mixture (85%). The HR ESI-MS displayed a strong molecular ion peak at 1763.0283 (calcd 1763.0284) m/z, corroborating the successful formation of **43**. The ^{1}H NMR spectrum (CD_2Cl_2, 500 MHz) of **43** exhibited a number of high-field broad signals at room temperature, the most notable being a singlet at −1.78 ppm, although it did not integrate well with other resonances attributed to **43** (0.2H; Figure 4.23). These high-field signals instead appear to correspond to some of the broader signals in the spectrum, attributed to a 'minor' species in the mixture.

To investigate the propensity of **43** to form Ru···H–C type interactions, ^{1}H spectra were collected at 200 K and 185 K in CD_2Cl_2 (Figure 4.23). Cooling **43** to 200 K resulted in resolution of some of the diastereotopic resonances, such as the methylene protons adjacent to the oxygen of the macrocyclic tether (H_G, 200 K δ 3.72, 3.62) and the protons of the axle alpha to the triaryl stopper (H_a, 200 K δ 2.43, 2.36), but a distinctive change in overall symmetry from C_2 to C_1 could not be established. The observation of signals at −1.84 and −11.03 ppm at 200 K was noted, although we do not feel they are associated with the main product **43**.

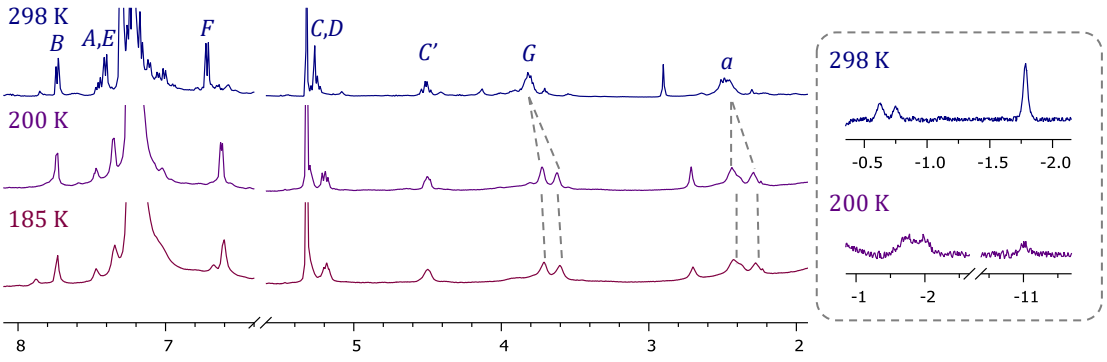

Figure 4.23. ^{1}H NMR spectra of **43** collected at different temperatures (CD_2Cl_2, 600 MHz). High-field signals displayed in the dashed square.

4.4.3. Carbon monoxide trapping

Further evidence for the synthesis of **43** was obtained by trapping experiments using carbon monoxide. Formation of the air and moisture stable carbonyl complex **44** resulted upon placing crude **43** under an atmosphere of CO (1 atm) and mixing for 72 hours at room temperature, in either THF or CD_2Cl_2, as marked visually by a colour change from deep pink to dark red solution. In this case **44** is sufficiently stable to permit purification by column chromatography, to afford **44** in 54% isolated yield and structurally corroborated by NMR spectroscopy.

The ^{1}H NMR spectrum of **44** in CD_2Cl_2 was consistent with the adoption of C_2 symmetry in solution, with 3 unique oxazoline resonances ($H_{C/D}$ δ 5.18, 5.11 and 4.48) shifted upfield compared to **43** (Figure 4.24). Interestingly, the high-field signals exhibited by **43** were not observed in the ^{1}H NMR spectrum of **44**. Furthermore, the ^{13}C{^{1}H} NMR spectrum featured a characteristic high frequency carbonyl resonance at δ 203.5, closely matching the acyclic and macrocyclic congeners (**26** δ 204.3; **42** δ 203.6).

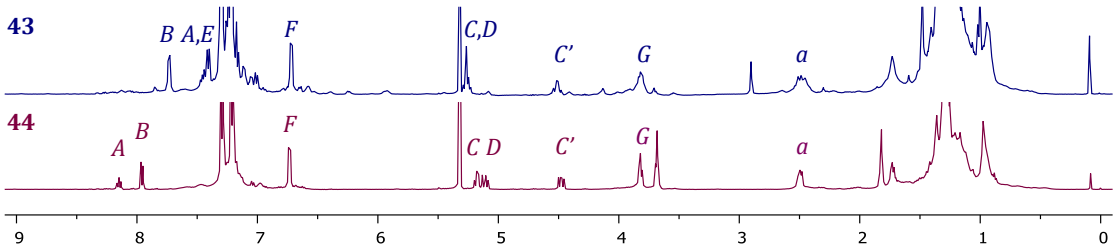

Figure 4.24. ^{1}H NMR spectra of **43** and **44** (298 K, CD_2Cl_2, 500 MHz).

The carbonyl stretching frequency of **44** was measured in dichloromethane (1993 cm^{-1}) and is notably blue-shifted with respect to the analogous macrocyclic (1980 cm^{-1}) and acyclic (1977 cm^{-1}) complexes. As for *mono*-**33a**, we attribute this to distortion of the N-Ru-CO bond from the ideal linear geometry, as a result of steric buttressing with the axle, and corresponding reductions in metal to π* (CO) backbonding.

4.5. Summary

Building on the findings in Chapter 3, macrocycle and rotaxane complexes of rhodium, iridium and ruthenium were explored, but with mixed success. Preparation of the rhodium chloride complexes **28a** and **28b** was successfully realised and subsequent halide abstraction generated the low-coordinate targets **31a** and **31b** (Scheme 4.13).

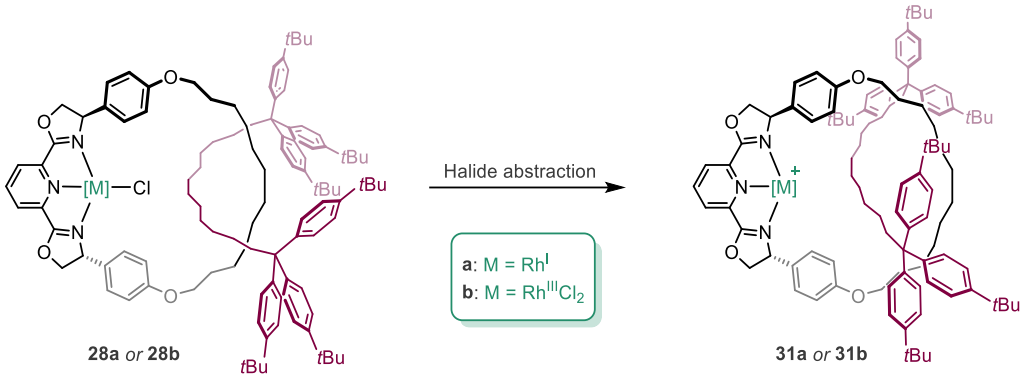

Scheme 4.13. Synthesis of low-coordinate complexes **31a** and **31b**, counter anions omitted for clarity.

Variable temperature ^{1}H NMR spectroscopy was used to probe the solution-phase structure of these reactive species. Although high-field signals were observed at low temperature, these are attributed to CH–π interactions and not the M···H–C bonding interactions of interest. Ultimately, the net donor strength of pybox appears to be insufficient for the formation of persistent M···H–C bonding interactions in solution. The incorporation of a more electron donating pincer scaffold (*e.g.* PNP) could favour such an interaction.

Trapping the low-coordinate complexes **31a** and **31b** with carbon monoxide formed the corresponding carbonyl derivatives **33a** and **33b**. Interestingly, the stretching frequencies of the rotaxane analogues are appreciably blue-shifted, compared to the acyclic and macrocyclic variants, as a consequence of steric buttressing between the carbonyl ligand and the axle. In the case of **33a**, the sterically demanding axle influences the binding orientation of the carbonyl ligand sufficiently that coordination of a second carbonyl can be facilitated. Formation of the bis-carbonyl complex (*bis*-**33a**) was in stark contrast to the non-interlocked analogues and clearly illustrates how the unique ligand architecture of the rotaxane can augment the metal coordination environment.

Chapter 5: Perspectives

The objective of this thesis was to investigate the coordination chemistry of entangled ligands derived from a pybox-based macrocycle, particularly targeting the formation of σ-complexes. These bespoke ligand architectures are designed to kinetically stabilise interaction of a mechanically interlocked hydrocarbon with a low-coordinate metal fragment. With this goal in mind, the coordination chemistry of similar acyclic and macrocyclic complexes has also been studied to help develop the necessary synthetic methodology and provide insight into the effect of substrate entanglement (Figure 5.1).

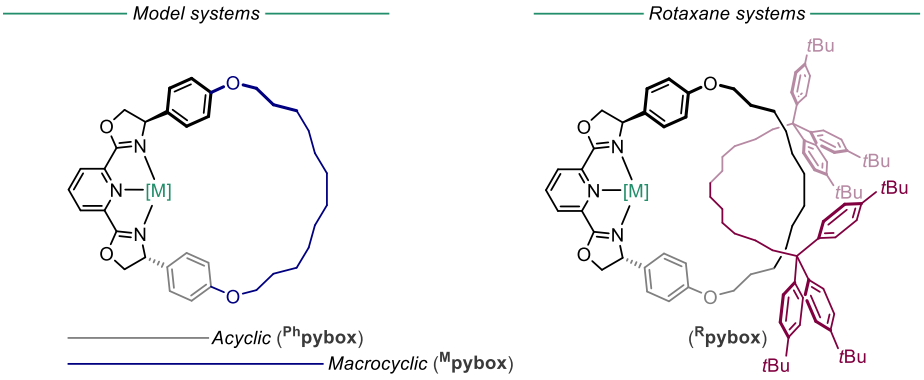

Figure 5.1. Systems of interest.

5.1. Ligand synthesis

The synthesis of the pybox-based macrocycle of interest (**Mpybox**) was achieved using a 10-step procedure adapted from literature, in an overall yield of 5%.[160] The [2]rotaxane **Rpybox** was thereafter obtained following optimisation of a reported active metal template procedure, where the interlocked architecture is captured using a nickel-catalysed C(sp^3)–C(sp^3) homocoupling reaction (Figure 5.2). A doubly threaded [3]rotaxane was also generated using this procedure, but separation of the desired interlocked species could be achieved using reverse phase (C18) column chromatography. Tandem mass spectrometry and NMR spectroscopy were used to verify formation of **Rpybox**.

The main challenge associated with preparation of **Rpybox** is the low-yielding homocoupling procedure (18%) and difficult separation from the non-interlocked axle (**3**). In combination with the arduous and low-yielding **Mpybox** synthesis, the [2]rotaxane was ultimately prepared with a low overall yield of <1%. Decomposition of the oxazoline moiety over the course of the synthesis, especially during the purification procedures, is suggested to reconcile the poor yield. Use of a more robust macrocyclic ligand could alleviate some of these difficulties. To this end, preparation of a [2]rotaxane derived from

terpyridine-based **^{M}terpy** was also attempted, however, the macrocycle proved incompatible with the homocoupling procedure.

A ditopic pybox-based [2]catenane ligand was targeted through use of nickel as a passive metal template (Figure 5.2). Ultimately, removal of the metal from the corresponding catenate proved challenging and prevented further investigation of this interlocked ligand. On reflection, further efforts seeking to exploit the redox chemistry of the nickel(II) centre would be worthwhile; reduction could facilitate removal of the metal by enforcing an unfavourable coordination geometry.

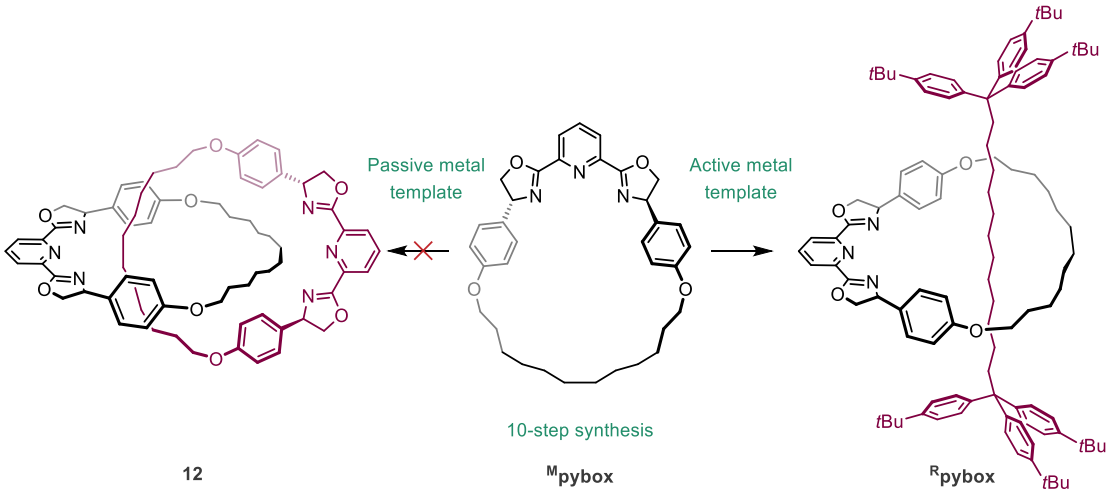

Figure 5.2. Synthesis of interlocked ligands.

5.2. Donor properties

Rhodium(I) and rhodium(III) carbonyl complexes of acyclic **^{Ph}pybox** were prepared to compare the donor properties to related PNP and CNC ligands (Figure 5.3).[310] The spectroscopic properties of rhodium carbonyl derivatives were investigated using a combination of IR and ^{13}C NMR spectroscopy.

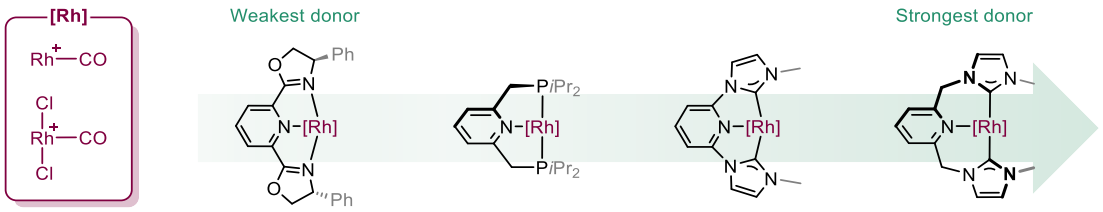

Figure 5.3. Donor properties of pincer ligands.

The carbonyl stretching frequencies of rhodium(I) complexes proved the most insightful, with ν(CO) decreasing in the order: pybox > PNP > CNC, indicating that pybox is the weakest donor ligand. The absence of persistent M···H–C bonding in rhodium(I) and rhodium(III) complexes of **^{R}pybox** can therefore be rationalised by the weak donor properties of the pybox moiety. To increase the likelihood of forming a σ-complex,

incorporation of a more strongly donating pincer scaffold into the macrocyclic component of the interlocked ligand would be required. More strongly donating ligands would, however, also increase the propensity to undergo C–H activation.

5.3. The mechanical bond

The proximity of the interlocked hydrocarbon and the unique steric profile of ^{R}**pybox** resulted in structural variations accessible only to the interlocked systems. Rhodium(I) and rhodium(III) low coordinate complexes of ^{R}**pybox** were investigated *in situ* by variable temperature ^{1}H NMR spectroscopy. Ultimately, no persistent interaction between the metal and the hydrocarbon axle was present, instead CH–π interactions were substantiated by low temperature correlation experiments (Figure 5.4).

Trapping low coordinate rhodium ^{R}**pybox** complexes with carbon monoxide resulted in formation of carbonyl derivatives, which interestingly displayed blue-shifted ν(CO) bands compared to the non-interlocked counterparts, particularly for the rhodium(I) complex (Figure 5.4). The increase in stretching frequency was attributed to distortion of the metal–carbonyl bond, induced by steric buttressing with the rotaxane axle, decreasing the magnitude of π-backdonation. Interestingly, under an atmosphere of CO the formation of a *bis*-carbonyl complex was observed. This is similarly attributed to the unique steric profile of the ligand that perturbs CO from linearity and facilitates binding of a second ligand.

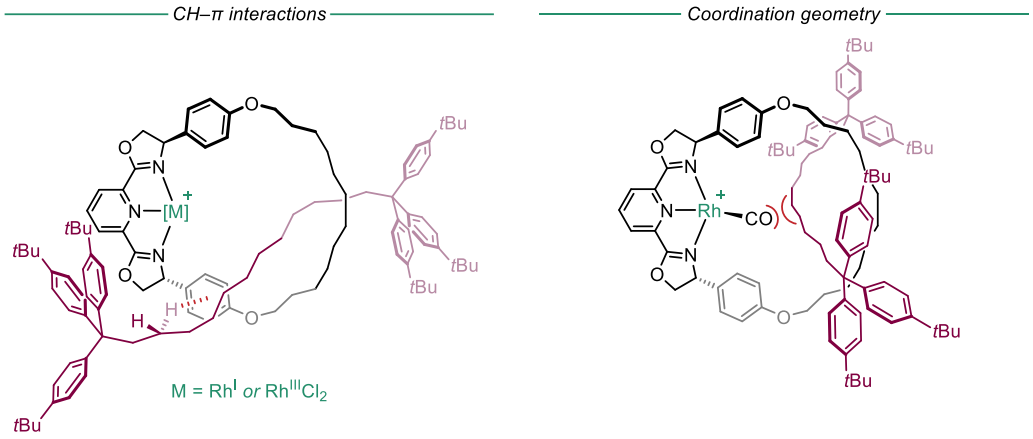

Figure 5.4. Effect of the mechanical bond on the structure of rhodium complexes.

These observations illustrate how interlocked ligand architectures can augment metal-based structure and reactivity.[217] The coordination chemistry of rotaxanes has remained relatively unexplored, with the main focus on the synthesis of interlocked ligands in appreciable quantities. The ability to exploit the mechanical bond as a means to tune the structure and reactivity of metal complexes, however, has potentially powerful applications.[223]

5.4. Towards models of σ-alkane complexes

Although M···H–C bonding interactions were not observed in the pybox-based rotaxane complexes investigated, interlocked macrocyclic pincer–alkane systems represent a potential tool to model σ-alkane complexes. The unique approach in which an alkane substrate is held in close proximity to a reactive metal centre through mechanical entanglement differs substantially to current state-of-the-art achievements in the field, which utilise low temperature and solid state methods.[271,280] Facile alkane dissociation should be circumvented, enabling isolation and the structure and reaction chemistry of σ-alkane complexes to be probed in much greater detail than has been previously possible.

Future endeavours in the Chaplin group may utilise more strongly donating tridentate pincer donors (*e.g.* PNP) incorporated into the macrocyclic component, to favour interactions between the metal and the axle (Figure 5.5). Phenyl-pybox ligand derivatives were shown to be comparatively weak donors. The addition of electron donating groups could be explored to increase the donor capacity whilst permitting efficient nickel-catalysed C(sp³)–C(sp³) homocoupling reactions within the macrocyclic cavity. Alternatively, the use of more robust pincer scaffolds (*e.g.* terpyridine) could increase yields of rotaxane and aid generation in more practical quantities to extensively probe the coordination chemistry.

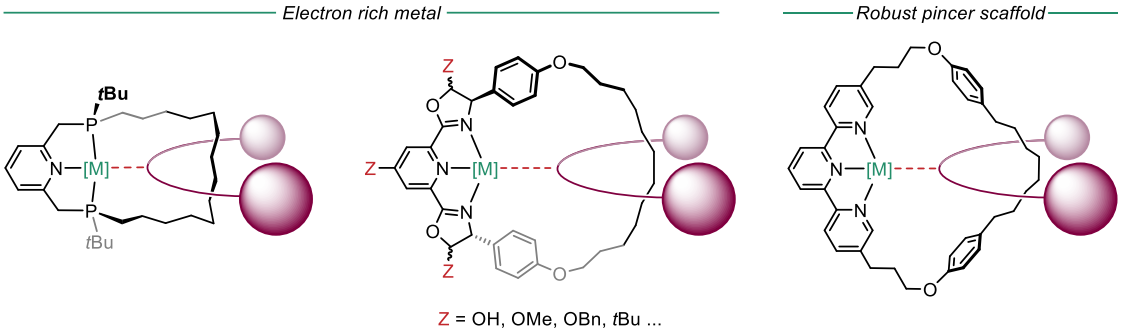

Figure 5.5. Proposed future target rotaxane complexes.

Generally speaking, interlocked ligands provide unique coordination environments and the prospect for interesting and unusual metal-based reactivity. However, the synthesis of these ligand architectures is challenging and a substantial bottleneck for realising their potential utility.

Chapter 6: Experimental Procedures

6.1. General considerations

All manipulations were performed under an inert atmosphere using standard Schlenk (nitrogen and argon) and glovebox (argon) techniques, unless otherwise stated. Glassware was oven dried at 150 °C and flame-dried under vacuum prior to use. Molecular sieves were activated by heating at 300 °C *in vacuo* overnight. CD_2Cl_2 was freeze-pump-thaw degassed and stored under an atmosphere of argon over molecular sieves (3 Å). C_6D_6 was dried over sodium, distilled, freeze-pump-thaw degassed and stored under an atmosphere of argon over molecular sieves (3 Å). Toluene-d_8 and THF-d_8 were dried over sodium, distilled, freeze-pump-thaw degassed and stored under an atmosphere of argon over molecular sieves (3 Å). 1-bromohexane, 1,6-dibromohexane, 1,12-dibromododecane, DMF and NMP were freeze-pump-thaw degassed, dried over three successive batches of molecular sieves (3 Å) and stored under an atmosphere of argon over new molecular sieves (3 Å). THF was distilled from sodium benzophenone then freeze-pump-thaw degassed and stored under an atmosphere of argon over molecular sieves (3 Å). Fluorobenzene and 1,2-difluorobenzene were pre-dried over Al_2O_3, distilled from calcium hydride then freeze-pump-thaw degassed, dried twice over molecular sieves (3 Å) and stored under an atmosphere of argon over molecular sieves (3 Å). TMS and HMDSO were dried over Na/K_2 alloy before being vacuum distilled and stored under an atmosphere of argon over molecular sieves (3 Å). All other anhydrous solvents were purchased from Acros Organics, Alfa Aesar, or Sigma-Aldrich. Solvents stored under argon were freeze-pump-thaw degassed and stored under an atmosphere of argon over molecular sieves (3 Å). Solvents stored under nitrogen were transferred from the commercially purchased anhydrous bottles and stored in catchpots without further purification.

6,6''-Dibromo-4'-phenyl-2,2':6',2''-terpyridine (**A25**),[77] tris(4-*tert*-butylphenyl)methane (**A107**),[291] $PhICl_2$,[365] $Na[BAr^F_4]$,[366] $Tl[BAr^F_4]$,[367] $[Rh(COE)_2Cl]_2$,[368] $[Rh(COE)_2(acetone)_2][PF_6]$,[369] $[Ru(p\text{-cymene})Cl]_2$,[370] $[Ir(COD)(biph)Cl]_2$ (**A108**),[312] [Rh(dtbpm)(biph)Cl] (**A109**),[311] $[Rh(Binor)PCy_3][BAr^F_4]$ (**A119**),[251] were synthesised according to literature procedures. Zinc powder was activated through reaction with 1,2-dibromoethane in THF, dried and stored under argon. All other reagents are commercial products and were used as received. Column chromatography was carried out using Silica (60 Å pore size, 230-400 mesh, 40-63 μm particle size); or C_{18} reversed phase silica gel (fully endcapped, 90 Å pore size, 230-400 mesh, 40-63 μm particle size). TLC was performed on silica gel coated (60 matrix) aluminium plates; or C_{18} silica gel coated (60 matrix) aluminium sheets and observed under UV light. Melting points (M.P.) were

measured with a Gallenkamp melting point apparatus. NMR spectra were recorded on Bruker spectrometers: Bruker Avance 300 and 500, Bruker Avance III 400 and 600, Bruker Avance III HD 300, 400, 500 MHz at 298 K unless otherwise stated. Chemical shifts are quoted in parts per million (ppm) and coupling constants (*J*) in Hertz (Hz). Abbreviations indicating multiplicity are: s = singlet, d = doublet, t = triplet, q = quartet, p = pentet, hept = heptet, m = multiplet, br = broad, vbr = very broad. Very broad signals are quoted with an associated line width (fwhm) in Hz. ^{1}H and $^{13}C\{^{1}H\}$ NMR spectra were assigned using a combination of COSY, HSQC and HMBC correlation experiments, as well as attached proton test (APT) NMR experiments. ^{1}H and $^{13}C\{^{1}H\}$ NMR spectra recorded in proteo-solvents were referenced to an internal sealed capillary containing C_6D_6. ^{1}H NMR spectra recorded in C_6H_5F were referenced using the highest intensity peak of the lowest frequency fluoroarene multiplet (δ 6.865) - referenced externally to TMS in $CDCl_3$. ^{1}H NMR spectra recorded in 1,2-$C_6H_4F_2$ were referenced using the highest intensity peak of the highest frequency fluoroarene multiplet (δ 6.865) - referenced externally to TMS in $CDCl_3$. HR ESI-MS were recorded on a Bruker MaXis mass spectrometer; LR ESI-MS were collected using an Agilent 6130B single Quad mass spectrometer. IR spectra were recorded on a PerkinElmer Spectrum 100 FT-IR using a KBr transmission cell. GC spectra were recorded on an Agilent 7820A GC System. Microanalyses were performed at the London Metropolitan University by Stephen Boyer. Solution phase effective magnetic moments were acquired using the Evans method.[299,300]

6.2. Compounds discussed in Chapter 2

6.2.1. Preparation of macrocyclic ligands

6.2.1.1. Synthesis of pybox-based macrocycle ^{M}**pybox**

(*R*)-4-Hydroxyphenylglycine methyl ester hydrochloride (**A96**)

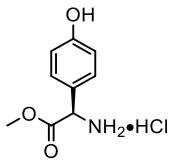

The title compound was obtained as a white powder, synthesised using a literature procedure (99%). Spectroscopic data was consistent with those published previously.[160]

^{1}H NMR (300 MHz, CD_3OD): δ 7.24 (d, $^{3}J_{HH}$ = 7.1, 2H, Ar), 6.83 (d, $^{3}J_{HH}$ = 7.4, 2H, Ar), 5.04 (s, 1H, CH), 3.81 (s, 3H, CH_3).

LR ESI-MS (CH_3CN, 180 °C, 4 kV) positive ion: 181.7 ([M−Cl]$^{+}$, calcd 182.1) *m*/*z*.

(*R*)-N-(*t*-Butoxycarbonyl)-4-hydroxyphenylglycine methyl ester (**A97**)

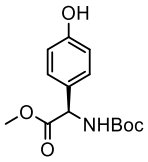

The title compound was obtained as an off-white powder, synthesised using a literature procedure (93%). Spectroscopic data was consistent with those published previously.[160]

^{1}H NMR (400 MHz, $CDCl_3$): δ 7.16 (d, $^{3}J_{HH}$ = 8.1, 2H, Ar), 6.73 (d, $^{3}J_{HH}$ = 8.6, 2H, Ar), 6.06 (s, 1H, OH), 5.58 (s, 1H, NH), 5.22 (d, $^{3}J_{HH}$ = 7.3, 1H, CH), 3.70 (s, 3H, CH_3), 1.43 (s, 9H, Boc).

LR ESI-MS (CH_3CN, 180 °C, 4 kV) positive ion: 304.2 ([M+Na]$^{+}$, calcd 304.1) *m*/*z*.

(*R*)-N-(*t*-Butoxycarbonyl)-4-(t-butyldimethylsiloxyphenyl)glycine methyl ester (**A98**)

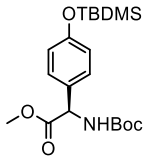

The title compound was obtained as a yellow oil, synthesised using a literature procedure (95%). Spectroscopic data was consistent with those published previously.[160]

^{1}H NMR (300 MHz, $CDCl_3$): δ 7.20 (d, $^{3}J_{HH}$ = 8.0, 2H, Ar), 6.80 (d, $^{3}J_{HH}$ = 8.0, 2H, Ar), 5.42 (d, $^{3}J_{HH}$ = 5.6, 1H, NH), 5.23 (d, $^{3}J_{HH}$ = 6.5, 1H, CH), 3.71 (s, 3H, CH_3), 1.43 (s, 9H, Boc), 0.97 (s, 9H, Si*t*Bu), 0.19 (s, 6H, SiMe).

(*R*)-4-(*t*-Butyldimethylsiloxy)phenylglycine methyl ester (**A99**)

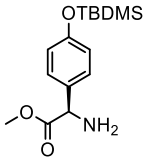

The title compound was obtained as a yellow oil, synthesised using a literature procedure (75%). Spectroscopic data was consistent with those published previously.[160]

^{1}H NMR (300 MHz, $CDCl_3$): δ 7.22 (d, $^3J_{HH}$ = 8.5, 2H, Ar), 6.80 (d, $^3J_{HH}$ = 8.6, 2H, Ar), 4.55 (s, 1H, CH), 3.70 (s, 3H, CH_3), 1.83 (br, 2H, NH_2), 0.97 (s, 9H, Si*t*Bu), 0.19 (s, 6H, SiMe).

LR ESI-MS (CH_3CN, 180 °C, 4 kV) positive ion: 296.2 ($[M+H]^+$, calcd 296.2) *m*/*z*.

A100

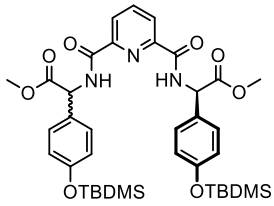

The title compound was obtained as an off-white powder, synthesised as a mixture of diastereomers using a literature procedure (95%, dr = 1:1). The major diastereomers, (*R*,*R*)-**A100**, can be obtained from column chromatography (70:30 hexane:EtOAc; *Rf* = 0.22). Yield: 53%. Spectroscopic data was consistent with those published previously.[160]

^{1}H NMR (300 MHz, $CDCl_3$): δ 8.74 (d, $^3J_{HH}$ = 7.1, 2H, NH), 8.32 (d, $^3J_{HH}$ = 7.8, 2H, py), 8.02 (t, $^3J_{HH}$ = 7.8, 1H, py), 7.37 (d, $^3J_{HH}$ = 8.0, 4H, Ar), 6.86 (d, $^3J_{HH}$ = 7.6, 4H, Ar), 5.69 (d, $^3J_{HH}$ = 7.3, 2H, CH), 3.78 (s, 6H, CH_3), 0.97 (s, 18H, Si*t*Bu), 0.20 (s, 12H, SiMe).

A101

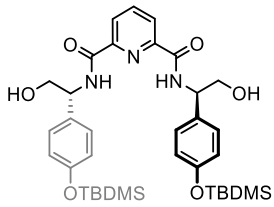

The title compound was obtained as a white powder, synthesised using a literature procedure (72% from (*R*,*R*)-**A100** or 41% from mixture of (*R*,*R*)- and *meso*-**A100** diastereomers). Spectroscopic data was consistent with those published previously.[160]

^{1}H NMR (400 MHz, $CDCl_3$): δ 8.45 (d, $^3J_{HH}$ = 7.4, 2H, NH), 8.35 (d, $^3J_{HH}$ = 7.8, 2H, py), 8.05 (t, $^3J_{HH}$ = 7.8, 1H, py), 7.26 (d, $^3J_{HH}$ = 8.5, 4H, Ar), 6.86 (d, $^3J_{HH}$ = 8.4, 4H, Ar), 5.25 – 5.16 (m, 2H, CH), 3.98 (d, $^3J_{HH}$ = 4.8, 4H, CH_2), 0.98 (s, 18H, Si*t*Bu), 0.19 (s, 12H, SiMe).

A102

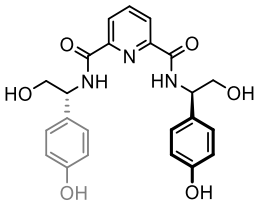

The title compound was obtained as a white powder, synthesised using a literature procedure (85%). Spectroscopic data was consistent with those published previously.[160]

^{1}H NMR (300 MHz, CD_3OD): δ 8.29 (d, $^3J_{HH}$ = 7.8, 2H, py), 8.15 (t, $^3J_{HH}$ = 7.8, 1H, py), 7.30 (d, $^3J_{HH}$ = 8.0, 4H, Ar), 6.80 (d, $^3J_{HH}$ = 8.0, 4H, Ar), 5.21 (t, $^3J_{HH}$ = 5.7, 2H, CH), 3.95 (d, $^3J_{HH}$ = 6.5, 4H, CH_2).

LR ESI-MS (CH_3CN, 180 °C, 4 kV) positive ion: 438.0 ($[M+H]^+$, calcd 438.2) *m/z*.

A103

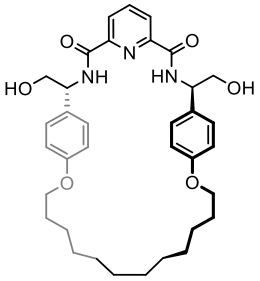

Synthesis of **A103** was modified from a literature procedure.[160] A suspension of **A102** (1.32 g, 3.0 mmol), 1,12-dibromododecane (0.99 g, 3.0 mmol) and K_2CO_3 (1.7 g, 12 mmol) in DMF (900 mL) was stirred at 100 °C for 7 d. The solvent was removed under reduced pressure, and the crude residue was re-dissolved in H_2O (50 mL) and extracted into CH_2Cl_2 (4 × 100 mL). The organic layers were combined, dried with $MgSO_4$, filtered, concentrated under reduced pressure and purified by column chromatography (silica; 1:99 CH_3OH:EtOAc) to yield the title compound as a colourless solid. Yield: 0.77 g (43%). Spectroscopic data was consistent with those published previously.[160]

^{1}H NMR (400 MHz, $CDCl_3$): δ 8.38 (d, $^3J_{HH}$ = 7.7, 2H, py), 8.19 – 7.93 (m, 3H, 1×py, 2×NH), 7.27 (d, $^3J_{HH}$ = 8.8, 4H, Ar), 6.94 (d, $^3J_{HH}$ = 8.7, 4H, Ar), 5.16 (td, $^3J_{HH}$ = 6.7, $^3J_{HH}$ = 4.1, 2H, CH), 4.11 – 3.81 (m, 8H, 4×CH_2O, 4×CH_2), 1.80 (p, $^3J_{HH}$ = 6.7, 4H, CH_2), 1.56 – 1.45 (m, 4H, CH_2), 1.43 – 1.24 (m, 12H, CH_2).

LR ESI-MS (CH_3CN, 180 °C, 4 kV) positive ion: 626.3 ($[M+Na]^+$, calcd 626.3) *m/z*.

A104

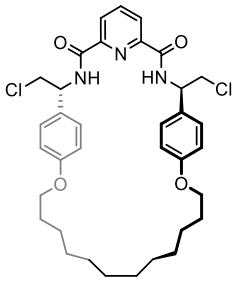

A104 was obtained as a white powder, synthesised using a literature procedure (74%). Spectroscopic data was consistent with those published previously.[160]

^{1}H NMR (400 MHz, $CDCl_3$): δ 8.38 (d, $^3J_{HH}$ = 7.8, 2H, py), 8.12 – 8.02 (m, 3H, 1×py, 2×NH), 7.33 (d, $^3J_{HH}$ = 8.6, 4H, Ar), 6.95 (d, $^3J_{HH}$ = 8.7, 4H, Ar), 5.40 (app q, J_{HH} = 6.2, 2H, CH), 4.06 – 3.88 (m, 8H, 4×CH_2O, 4×CH_2Cl), 1.80 (br, 4H, CH_2), 1.47 (br, 4H CH_2), 1.42 – 1.21 (m, 12H, CH_2).

LR ESI-MS (CH_3CN, 180 °C, 4 kV) positive ion: 662.3 ([M+Na]$^+$, calcd 662.3) *m/z*.

Ph-pybox macrocycle (**^{M}pybox**)

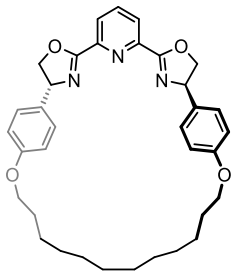

Synthesis of **^{M}pybox** was modified from a literature procedure.[160] TBAF (1M in THF, 11.1 mL, 11.1 mmol) was added to a solution of **A104** (1.422 g, 2.22 mmol) in THF (30 mL) and stirred at rt for 18 h, after which the solvent was removed under reduced pressure. The product was extracted into CH_2Cl_2 (50 mL) and Et_2O (50 mL), washed with sodium citrate (aq.) (3 × 50 mL), NH_4Cl (aq.) (2 × 50 mL), brine (50 mL), dried over $MgSO_4$, filtered and concentrated under reduced pressure to afford the title compound as a colourless solid. Yield: 0.924 g (73%). Spectroscopic data was consistent with those published previously.[160]

M.P. 79.3 – 80.1 °C.

^{1}H NMR (500 MHz, $CDCl_3$): δ 8.11 (d, $^3J_{HH}$ = 7.9, 2H, py), 7.92 (t, $^3J_{HH}$ = 7.8, 1H, py), 7.20 (d, $^3J_{HH}$ = 8.6, 4H, Ar), 6.85 (d, $^3J_{HH}$ = 8.6, 4H, Ar), 5.38 (dd, $^3J_{HH}$ = 9.9, $^3J_{HH}$ = 6.2, 2H, ox{CH}), 4.76 (dd, $^3J_{HH}$ = 9.9, $^2J_{HH}$ = 8.6, 2H, ox{CH_2}), 4.51 (dd, $^2J_{HH}$ = 8.5, $^3J_{HH}$ = 6.2, 2H, ox{CH_2}), 4.01

(t, $^3J_{HH}$ = 6.9, 4H, CH_2O), 1.70 (p, $^3J_{HH}$ = 6.9, 4H, CH_2), 1.40 – 1.32 (m, 4H, CH_2), 1.23 (br, 12H, CH_2).

$^{13}C\{^1H\}$ NMR (126 MHz, $CDCl_3$): δ 162.9 (ox{OCN}), 158.4 (Ar), 147.2 (py), 137.6 (py), 134.1 (Ar), 128.1 (Ar), 125.6 (py), 115.4 (Ar), 75.4 (ox{CH_2}), 69.6 (ox{CH}), 68.0 (CH_2O), 30.1 (CH_2), 29.8 (CH_2), 29.2 (CH_2), 28.6 (CH_2), 25.9 (CH_2).

HR ESI-MS (CH_3OH, 180 °C, 4 kV) positive ion: 568.3173 ([M+H]$^+$, calcd 568.3170) *m*/*z*.

6.2.1.2. Synthesis of terpy-based macrocycle ^{M}**terpy**

4-Hydroxyphenyl terpyridine (**1**)

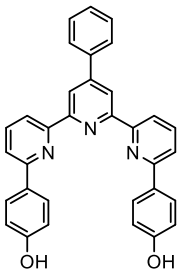

Synthesis used was modified from a literature procedure.[71] Under argon, a solution of 6,6''-dibromo-4'-phenyl-2,2':6',2''-terpyridine (1.13 g, 2.4 mmol), 4-hydroxyphenylboronic acid (0.73 g, 5.0 mmol), sodium carbonate (1.12 g, 10.6 mmol) and [$Pd(PPh_3)_4$] (0.14 g, 0.12 mmol) in 1,4-dioxane (24 mL) and H_2O (4.8 mL) was heated to 100 °C for 72 h. The reaction was cooled to rt, water (100 mL) was added and the product extracted into CH_2Cl_2 (3 × 50 mL). The organic layers were combined, dried over $MgSO_4$, filtered and concentrated under reduced pressure. The crude product was purified by precipitation from CH_3OH/CH_2Cl_2 to afford the title compound as an off white solid. Yield: 0.99 g (84%).

^1H NMR (500 MHz, CD_3OD): δ 8.83 (s, 2H, py), 8.54 (d, $^3J_{HH}$ = 7.7, 2H, py), 8.07 (d, $^3J_{HH}$ = 8.7, 4H, Ar), 7.97 (t, $^3J_{HH}$ = 7.8, 2H, py), 7.93 (d, $^3J_{HH}$ = 7.2, 2H, Ar), 7.84 (d, $^3J_{HH}$ = 7.9, 2H, py), 7.62 (t, $^3J_{HH}$ = 7.6, 2H, Ar), 7.53 (t, $^3J_{HH}$ = 7.4, 1H, Ar), 6.95 (d, $^3J_{HH}$ = 8.6, 4H, Ar).

^1H NMR (500 MHz, $(CD_3)_2SO$): δ 9.80 (s, 2H, OH), 8.81 (s, 2H, py), 8.55 (d, $^3J_{HH}$ = 7.7, 2H, py), 8.13 (d, $^3J_{HH}$ = 8.2, 4H, Ar), 8.05 (t, $^3J_{HH}$ = 7.8, 2H, py), 7.98 (app d, J_{HH} = 7.6, 4H, 2×Ar, 2×py), 7.71 – 7.53 (m, 3H, Ar), 6.94 (d, $^3J_{HH}$ = 8.3, 4H, Ar).

$^{13}C\{^1H\}$ NMR (126 MHz, CD_3OD): δ 160.1 (Ar), 158.1 (py), 157.7 (py), 156.8 (py), 151.7 (py), 140.2 (Ar), 139.0 (py), 132.0 (Ar), 130.4 (Ar), 130.3 (Ar), 129.4 (Ar), 128.2 (Ar), 120.9 (py), 119.9 (py), 119.8 (py), 116.6 (Ar).

HR ESI-MS (CH_3OH, 180 °C, 4 kV) positive ion: 494.1862 ([M+H]$^+$, calcd 494.1863) *m*/*z*.

Macrocyclic-terpyridine (**^{M}terpy**)

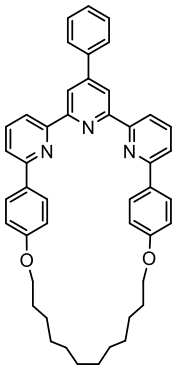

To a solution of **1** (25 mg, 51 μmol) and 1,12-dibromododecane (17 mg, 51 μmol) in DMF (15 mL) was added K_2CO_3 (280 mg, 2.0 mmol). The suspension was stirred at 100 °C for 120 h. The solvent was removed under reduced pressure, and the crude residue was redissolved in H_2O (100 mL) and extracted into CH_2Cl_2 (3 × 300 mL). The organic layers were combined, dried over $MgSO_4$, filtered and concentrated under reduced pressure. The resulting residue was extracted into refluxing CH_2Cl_2 (50 mL), filtered and the filtrate concentrated to dryness *in vacuo* to yield the title compound as a yellow solid in *ca*. 90% purity. Yield: 10 mg (29%).

^{1}H NMR (500 MHz, $CDCl_3$): δ 8.91 – 8.84 (m, 2H, py), 8.60 – 8.51 (m, 2H, py), 8.21 – 8.03 (m, 4H, Ar), 7.96 – 7.80 (m, 4H, 2×Ar, 2×py), 7.77 – 7.65 (m, 2H, py), 7.65 – 7.41 (m, 3H, Ar), 7.06 – 6.97 (m, 4H, Ar), 4.04 (t, $^{3}J_{HH}$ = 6.6, 4H, CH_2O), 1.82 (br, 4H, CH_2), 1.48 (br, 4H, CH_2), 1.34 (br, 12H, CH_2).

^{13}C{^{1}H} NMR (126 MHz, $CDCl_3$): δ 160.3 (Ar), 160.2 (py), 156.3 (py), 155.9 (py), 150.4 (py), 139.5 (Ar), 137.6 (py), 132.0 (Ar), 129.2 (Ar), 129.0 (Ar), 128.4 (Ar), 127.6 (Ar), 119.7 (py), 119.3 (py), 119.1 (py), 114.8 (Ar), 68.3 (CH_2O), 29.7 (CH_2), 29.6 (CH_2), 29.4 (CH_2) 26.2 (CH_2), 26.1 (CH_2).

HR ESI-MS (CH_3CN, 180 °C, 4 kV) positive ion: 660.3586 ([M+H]$^{+}$, calcd 660.3585) *m*/*z*.

6.2.2. Preparation of acyclic ligands

(*R*,*R*)-2,6-Bis(4-phenyl-2-oxazolinyl)pyridine (**^{Ph}pybox**)

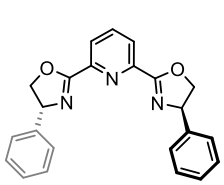

The title compound was synthesised using an adapted literature procedure.[101,114] 2,6-Pyridinedicarboxylic acid (12.2 g, 73 mmol) was refluxed in $SOCl_2$ (15 mL) for 15 h. The volatiles were removed *in vacuo* to give the acid chloride as a white solid. To a solution of

(*R*)-phenylglycinol (25 g, 180 mmol) and NEt_3 (61 mL, 440 mmol) in CH_2Cl_2 (200 mL) at 0 °C was slowly added dropwise a solution of the acid chloride (14.9 g, 73 mmol) in CH_2Cl_2 (100 mL), and stirred at rt for 15 h. $SOCl_2$ (15 mL) was added at 0 °C and the resulting solution heated at reflux for 2 h. The solution was poured onto ice, the organic layer was collected, washed with brine (100 mL), saturated Na_2CO_3 (aq.) (100 mL), dried over $MgSO_4$, filtered and concentrated under reduced pressure. Purification by column chromatography (silica; CH_2Cl_2/ether, 9:1) gave the bis-chloroamide intermediate as a yellow solid, which was treated with a solution of NaOH (3.8 g, 95 mmol) in H_2O (100 mL) and CH_3OH (200 mL) and stirred at rt for 72 h. The crude residue was extracted with CH_2Cl_2 (100 mL), washed with brine (100 mL) and concentrated under reduced pressure. Recrystallisation from hot EtOH afforded the title compound as an off-white microcrystalline solid. Yield: 10.2 g (38%). Spectroscopic data were consistent with those published previously.[114,290]

M.P. 175.0 – 176.4 °C.

^{1}H NMR (400 MHz, $CDCl_3$): δ 8.35 (d, $^3J_{HH}$ = 7.8, 2H, py), 7.92 (t, $^3J_{HH}$ = 7.9, 1H, py), 7.40 – 7.27 (m, 10H, Ar), 5.46 (dd, $^2J_{HH}$ = 10.3, $^3J_{HH}$ = 8.6, 2H, ox{CH_2}), 4.93 (dd, $^2J_{HH}$ = 10.4, $^3J_{HH}$ = 8.6, 2H, ox{CH_2}), 4.43 (app t, J_{HH} = 8.6, 2H, ox{CH}).

LR ESI-MS (CH_3CN) positive ion: 370.7 ([M+H]$^+$, calcd 370.2) *m*/*z*.

2,6-bis-(6-phenyl-2-pyridyl)-4-phenylpyridine (**^{Ph}terpy**)

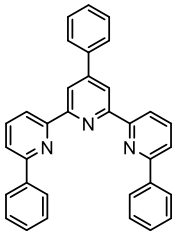

The title compound was synthesised using an adapted literature procedure.[71] Under argon, a solution of 6,6''-dibromo-4'-phenyl-2,2':6',2''-terpyridine (1.68 g, 3.6 mmol), phenyl boronic acid (0.96 g, 7.9 mmol), Na_2CO_3 (1.7 g, 15.8 mmol), and $[Pd(PPh_3)_4]$ (0.21 g, 0.18 mmol) in 1,4-dioxane (35 mL) and H_2O (7 mL) was heated at 100 °C for 48 h. The suspension was extracted from H_2O (50 mL) with CH_2Cl_2 (3 × 50 mL). The organic layers were combined, dried over $MgSO_4$, filtered and concentrated under reduced pressure. The crude product was purified by precipitation from CH_2Cl_2/CH_3OH at rt to afford the title compound as a white solid. Yield: 1.2 g (72%). The melting point was consistent with data published previously.[72]

M.P. 201.7 – 203.6 °C.

^{1}H NMR (500 MHz, $CDCl_3$): δ 8.92 (s, 2H, py), 8.67 (d, $^{3}J_{HH}$ = 7.7, 2H, py), 8.20 (d, $^{3}J_{HH}$ = 7.4, 4H, Ar), 7.96 (t, $^{3}J_{HH}$ = 7.8, 2H, py), 7.92 (d, $^{3}J_{HH}$ = 7.4, 2H, Ar), 7.83 (d, $^{3}J_{HH}$ = 7.7, 2H, py), 7.61 – 7.44 (m, 9H, Ar).

^{13}C{^{1}H} NMR (126 MHz, $CDCl_3$): δ 156.6 (py), 156.2 (py), 156.1 (py), 150.5 (py), 139.56 (Ar), 139.4 (Ar), 137.8 (py), 129.2 (Ar), 129.0 (Ar), 128.9 (Ar), 127.6 (py), 127.2 (Ar), 120.6 (py), 119.8 (py), 119.5 (py).

HR ESI-MS (CH_3CN, 180 °C, 4 kV) positive ion: 462.1943 ($[M+H]^+$, calcd 462.1925) *m/z*.

6.2.3. Preparation of axle components

Half axle (**2**)

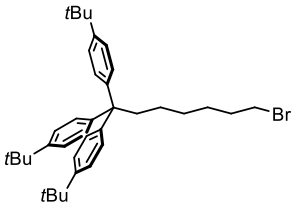

A solution of *n*-BuLi (1.6 M in hexanes, 18 mL, 29 mmol) was added to tris(4-*tert*-butylphenyl)methane (**A107**) (5.97 g, 14.5 mmol) in THF:HMPA (200 : 50 mL) at –78 °C, and stirred for 1 h at rt. Over 5 h the solution was added dropwise to 1,6-dibromohexane (150 mL, 0.97 mol) at 0 °C and stirred at rt for a further 18 h. The reaction was washed with 1 M HCl (aq.) (3 x 100 mL) and subsequently the solvent and 1,6-dibromohexane were removed *via* vacuum distillation. Purification by column chromatography (silica; hexanes *Rf* = 0.16) yielded the title compound as a white powder. Yield: 6.68 g (80%).

M.P. 180.3 – 181.4 °C.

^{1}H NMR (500 MHz, $CDCl_3$): δ 7.24 (d, $^{3}J_{HH}$ = 8.5, 6H, Ph), 7.14 (d, $^{3}J_{HH}$ = 8.5, 6H, Ph), 3.34 (t, $^{3}J_{HH}$ = 6.9, 2H, CH_2Br), 2.53 – 2.47 (m, 2H, {Ar_3C}CH_2), 1.76 (p, $^{3}J_{HH}$ = 6.9, 2H, CH_2), 1.38 – 1.31 (m, 2H, CH_2), 1.30 (s, 27H, *t*Bu), 1.28 – 1.23 (m, 2H, CH_2), 1.10 (q, $^{3}J_{HH}$ = 8.0, 2H, CH_2).

^{13}C{^{1}H} NMR (126 MHz, $CDCl_3$): δ 148.2 (Ph), 144.9 (Ph), 128.9 (Ph), 124.6 (Ph), 55.5 (CAr_3), 40.6 ({Ar_3C}CH_2), 34.4 ($BrCH_2$), 34.2 (*t*Bu{C}), 33.0 (CH_2), 31.5 (*t*Bu{CH_3}), 29.7 (CH_2), 28.2 (CH_2), 25.6 (CH_2).

HR ESI-MS (CH_3CN, 180 °C, 4 kV) positive ion: 613.2802 ($[M+K]^+$, calcd 613.2806) *m/z*.

Axle (**3**)

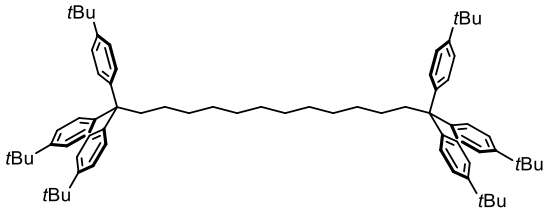

Synthesis of axle was modified from a literature procedure.[291] A solution of *n*-BuLi (1.6 M in hexanes, 375 µL, 0.6 mmol) was added to tris(4-*tert*-butylphenyl)methane (**A107**) (206 mg, 0.5 mmol) in THF:HMPA (2.5 mL : 0.5 mL) at –78 °C and stirred at rt for 1 h. 1,12-dibromododecane (65.6 mg, 0.2 mmol) in THF (1 mL) was added to the solution at 0 °C, warmed to rt and then stirred for a further 18 h. The reaction was quenched with H_2O (20 mL) and extracted with CH_2Cl_2 (3 × 10 mL), the organic layers were combined, dried over $MgSO_4$, filtered and concentrated under reduced pressure. The residue was taken up in a minimal amount of CH_2Cl_2 (1 mL) and the product precipitated *via* addition of excess CH_3OH, yielding the crude product. Purification by column chromatography (silica; hexanes/EtOAc, 99:1; *Rf* = 0.37) afforded the title compound as a white powder. Yield: 144 mg (73%).

M.P. 251.0 – 252.3 °C.

^{1}H NMR (500 MHz, $CDCl_3$): δ 7.23 (d, $^3J_{HH}$ = 8.6, 12H, Ph), 7.14 (d, $^3J_{HH}$ = 8.6, 12H, Ph), 2.54 – 2.43 (m, 4H, {Ar_3C}CH_2), 1.30 (s, 54H, *t*Bu), 1.28 – 1.22 (m, 6H, CH_2), 1.17 (s, 10H, CH_2), 1.11 – 1.01 (m, 4H, CH_2).

^{13}C{^{1}H} NMR (126 MHz, $CDCl_3$): δ 148.1 (Ph), 145.1 (Ph), 129.0 (Ph), 124.5 (Ph), 55.5 (CAr_3), 40.7 ({Ar_3C}CH_2), 34.4 (*t*Bu{C}), 31.5 (*t*Bu{CH_3}), 30.7 (CH_2), 29.9 (CH_2), 29.8 (CH_2), 29.7 (CH_2), 25.8 (CH_2).

HR ESI-MS (CH_3CN, 180 °C, 4 kV) positive ion: 1029.7601 ([M+K]$^+$, calcd 1029.7613) *m*/*z*.

6.2.4. Preparation of rotaxanes

General procedure for C(sp^3)–C(sp^3) homocoupling reactions

A solution of ^{Ph}**pybox** (2.2 mg, 6 µmol), ^{Ph}**terpy** (2.8 mg, 6 µmol), or ^{M}**pybox** (3.4 mg, 6 µmol); and [$NiCl_2$(glyme)] (1.2 mg, 5.5 µmol) in THF:NMP (1:1), THF:DMF (1:1), NMP:DMF (1:1), NMP, DMF or THF (1, 2 or 4 mL total solvent volume); was transferred to activated Zn (35 mg, 550 µmol) under argon. The resulting suspension was sonicated for 30 min and the unactivated bromide (1-bromohexane or **2**; 15 µL, 110 µmol) was added. The suspension was stirred at room temperature for 18 h. The reaction mixture was quenched with saturated NH_4Cl (aq.) (5 mL) and extracted with pentane (4 × 5 mL). After passing

through a silica plug (pentane) the sample was analysed by GC (1 mL) or ^{1}H NMR spectroscopy.

[2]Rotaxane (**^{R}pybox**)

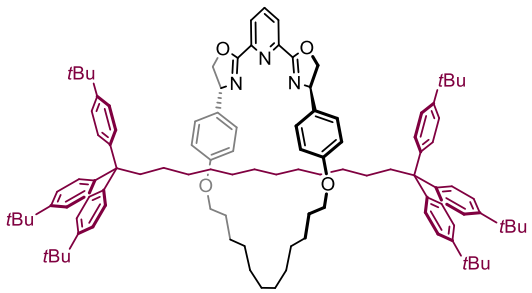

A solution of **^{M}pybox** (100 mg, 176 μmol) and [$NiCl_2$(glyme)] (36.0 mg, 163 μmol) in THF:NMP (2 mL : 2 mL) was transferred to activated Zn (115 mg, 1.8 mmol) under argon. The resulting suspension was sonicated for 5 min after which the half-axle (**2**) was added (304 mg, 528 μmol). The suspension was stirred at rt for 5 h. The reaction mixture was diluted with EtOAc (120 mL) and extracted with 17.5% NH_3(aq.) saturated with EDTA (3 × 100 mL portions), H_2O (3 × 100 mL) and brine (100 mL). The organic layer was dried over $MgSO_4$, filtered and concentrated under reduced pressure. The residue was diluted with CH_3CN (100 mL) and extracted with *n*-hexane (3 × 20 mL). The *n*-hexane layer was isolated and concentrated, purification of the crude mixture by column chromatography (C_{18} end capped reversed-phase silica; gradient elution; CH_3OH:THF, 1:0 to 7:3; *Rf* = 0.19 (7:3)) to yield the title compound as a white solid in 90% purity. Yield: 49.6 mg (18%).

^{1}H NMR (500 MHz, $CDCl_3$): δ 7.99 (d, $^{3}J_{HH}$ = 7.8, 2H, py), 7.57 (t, $^{3}J_{HH}$ = 7.8, 1H, py), 7.23 (d, $^{3}J_{HH}$ = 8.3, 12H, Ar{axle}), 7.09 (d, $^{3}J_{HH}$ = 8.4, 12H, Ar{axle}), 7.08 – 7.04 (m, 4H, Ar{macro}), 6.70 (d, $^{3}J_{HH}$ = 8.3, 4H, Ar{macro}), 5.34 (dd, $^{3}J_{HH}$ = 9.7, $^{3}J_{HH}$ = 5.4, 2H, ox{CH}), 4.66 (app t, J_{HH} = 9.2, 2H, ox{CH_2}), 4.42 (dd, $^{2}J_{HH}$ = 8.6, $^{3}J_{HH}$ = 5.4, 2H, ox{CH_2}), 3.90 (app t, J_{HH} = 6.9, 4H, CH_2O), 2.35 – 2.28 (m, 4H, {Ar_3C}CH_2), 1.67 – 1.56 (m, 4H, CH_2), 1.43 (s, 12H, CH_2), 1.31 – 1.27 (m, 54H, *t*Bu), 1.27 – 1.23 (m, 4H, CH_2), 1.23 – 1.12 (m, 12H, CH_2), 0.98 – 0.85 (m, 4H, CH_2), 0.80 – 0.66 (m, 4H, CH_2).

^{13}C{^{1}H} NMR (126 MHz, $CDCl_3$): δ 162.6 (ox{OCN}), 158.2 (Ar{macro}), 148.1 (Ar{axle}), 147.0 (py), 145.1 (Ar{axle}), 137.2 (py), 134.5 (Ar{macro}), 129.0 (Ar{axle}), 127.8 (Ar{macro}), 125.4 (py), 124.5 (Ar{axle}), 115.1 (Ar{macro}), 75.1 (ox{CH_2}), 69.3 (ox{CH}), 67.9 (CH_2O), 55.4 (Ar_3C), 40.8 ({Ar_3C}CH_2), 34.4 (*t*Bu{C}), 31.6 (*t*Bu{CH_3}), 30.9 (CH_2), 30.5 (CH_2), 30.3 (CH_2), 30.1 (CH_2), 29.9 (CH_2), 29.8 (CH_2), 29.8 (CH_2), 29.3 (CH_2), 28.6 (CH_2), 26.2 (CH_2), 26.0 (CH_2).

HR ESI-MS (CH_3CN, 180 °C, 4 kV) positive ion: 1581.0994 ([M+Na]$^+$, calcd 1581.0971) *m*/*z*.

HR ESI-MS/MS (1581.0994) (CH_3CN, 180 °C, 100 eV) positive ion: 590.2992 ([^{M}**pybox**+Na]$^+$, calcd 590.2989) *m*/*z*.

[3]Rotaxane (^{R*}**pybox**)

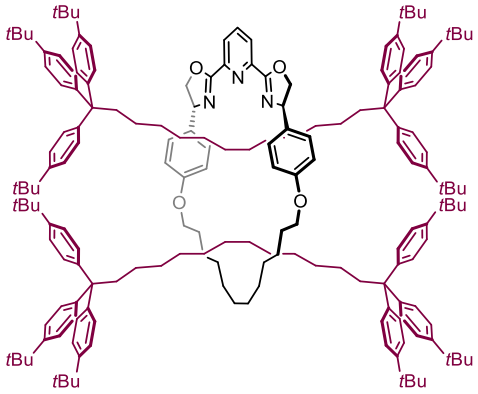

A solution of ^{M}**pybox** (50.0 mg, 88 μmol) and [$NiCl_2$(glyme)] (18.4 mg, 84 μmol) in THF:NMP (1 mL : 1 mL) was transferred to activated Zn (55.0 mg, 840 μmol) under argon. The resulting suspension was sonicated for 5 min after which the half-axle (**2**) was added (250 mg, 434 μmol). The suspension was stirred at rt for 15 h. The reaction mixture was diluted with EtOAc (100 mL) and washed with 17.5% NH_3(aq.) saturated with EDTA (3 × 100 mL portions), H_2O (3 × 100 mL) and brine (100 mL). The organic layer was dried over $MgSO_4$, filtered and concentrated under reduced pressure. The residue was diluted with CH_3CN (100 mL) and extracted with *n*-hexane (3 × 20 mL). The *n*-hexane layer was isolated and concentrated, purification of the crude mixture by column chromatography (C_{18} end capped reversed-phase silica; gradient elution; CH_3OH:THF, 1:0 to 6:4; *Rf* = 0.17 (6:4)) afforded the title compound as a white solid. Yield: 20.1 mg (9%). (These conditions also yielded [2]rotaxane (^{R}**pybox**) 10.4 mg (8%).

^{1}H NMR (500 MHz, $CDCl_3$): δ 7.86 (d, $^3J_{HH}$ = 7.8, 2H, py), 7.45 (t, $^3J_{HH}$ = 7.9, 1H, py), 7.19 (d, $^3J_{HH}$ = 8.2, 24H, Ar{axle}), 7.12 (d, $^3J_{HH}$ = 8.3, 24H, Ar{axle}), 6.98 (d, $^3J_{HH}$ = 8.0, 4H, Ar{macro}), 6.59 (d, $^3J_{HH}$ = 8.2, 4H, Ar{macro}), 5.36 (dd, $^3J_{HH}$ = 10.0, $^3J_{HH}$ = 5.9, 2H, ox{CH}), 4.66 (app t, J_{HH} = 9.3, 2H, ox{CH_2}), 4.52 (dd, $^2J_{HH}$ = 8.7, $^3J_{HH}$ = 5.9, 2H, ox{CH_2}), 3.76 (dq, $^2J_{HH}$ = 11.6, $^3J_{HH}$ = 7.8, 7.3, 4H, CH_2O), 2.46 – 2.32 (m, 8H, {Ar_3C}CH_2), 1.68 (t, $^3J_{HH}$ = 6.8, 4H, CH_2), 1.37 – 1.16 (m, 136H, CH_2), 0.99 – 0.83 (m, 12H, CH_2), 0.67 – 0.54 (m, 10H, CH_2), 0.54 – 0.41 (m, 6H, CH_2).

^{13}C{^{1}H} NMR (126 MHz, $CDCl_3$): δ 161.8 (ox{OCN}), 158.7 (Ar{macro}), 148.0 (Ar{axle}), 147.4 (py), 145.1 (Ar{axle}), 137.2 (py), 134.0 (Ar{macro}), 129.0 (Ar{axle}), 128.2

(Ar{macro}), 125.3 (py), 124.5 (Ar{axle}), 115.0 (Ar{macro}), 73.8 (ox{CH_2}), 69.3 (ox{CH}), 68.0 (CH_2O), 55.4 (Ar_3C), 40.8 ({Ar_3C}CH_2), 34.4 (*t*Bu{C}), 31.6 (*t*Bu{CH_3}), 30.9 (CH_2), 30.6 (CH_2), 30.5 (CH_2), 30.4 (CH_2), 30.2 (CH_2), 29.9 (CH_2), 29.8 (CH_2), 29.7 (CH_2), 29.7 (CH_2), 29.5 (CH_2), 26.3 (CH_2), 25.5 (CH_2).

HR ESI-MS (CH_3CN, 180 °C, 4 kV) positive ion: 2549.9143 ([M+H]$^+$, calcd 2549.9133) *m*/*z*.

6.2.5. Preparation of model nickel complex

[Ni(**^{Ph}pybox**)$_2$][BF_4]$_2$ (**4**)

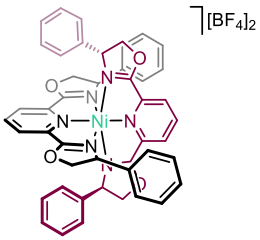

A solution of [$NiCl_2$(glyme)] (43.9 mg, 0.20 mmol) and **^{Ph}pybox** (147.8 mg, 0.40 mmol) in CH_2Cl_2 (10 mL) was stirred at rt for 18 h under argon and then washed with 0.1 M $NH_4[BF_4]$ (10 × 10 mL). The solution was then concentrated under reduced pressure to yield the title compound as a grey-purple microcrystalline solid. Yield: 112 mg (58%). Crystals suitable for X-ray diffraction were attained from a CH_2Cl_2/hexane layer at rt.

^{1}H NMR (500 MHz, CD_3CN): δ 67.04 (vbr, fwhm = 340), 19.44 (vbr, fwhm = 82), 16.87 (vbr, fwhm = 110), 7.60 (vbr, fwhm = 30), 7.32 (vbr, fwhm = 50), 6.02 (vbr, fwhm = 260), 2.71 (vbr, fwhm = 130). Signals could not be unambiguously assigned due to the paramagnetic nature of the complex.

^{13}C{^{1}H} NMR (126 MHz, CD_3CN): δ 167.3, 130.8, 129.9, 76.1, 70.9. Other peaks not observed due to paramagnetic broadening.

HR ESI-MS (CH_3CN, 180 °C, 4 kV) positive ion: 883.2343 ([M+BF_4]$^+$, calcd 883.2337) *m*/*z*.

μ_{eff} = 2.71 μ_B (Evans method, in CD_3CN).

6.2.6. Preparation of terminal alkene pybox **10**

5

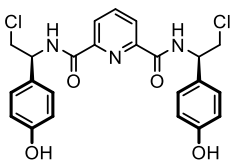

To a solution of *meso*-**A101** (346 mg, 0.52 mmol) in CH_2Cl_2 (5 mL) was added $SOCl_2$ (0.38 mL, 5.2 mmol). The resulting solution was heated at reflux for 48 h. The solvent was

removed under reduced pressure and the crude residue was purified by column chromatography (silica; EtOAc:CH_2Cl_2, 1:2) to yield the title compound as a yellow solid. Yield: 216 mg (88%).

^{1}H NMR (300 MHz, CD_3OD): δ 8.32 (d, $^3J_{HH}$ = 7.7, 2H, py), 8.24 – 8.14 (m, 1H, py), 7.32 (d, $^3J_{HH}$ = 8.3, 4H, Ar), 6.82 (d, $^3J_{HH}$ = 8.3, 4H, Ar), 5.42 (t, $^3J_{HH}$ = 7.2, 2H, CH), 4.00 (d, $^3J_{HH}$ = 7.1, 4H, CH_2).

LR ESI-MS (CH_3CN) positive ion: 474.0 ([M+H]$^+$, calcd 474.1) *m/z*.

meso-Phenol-pybox (**6**)

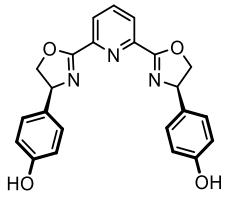

TBAF (1M in THF, 5.8 mL, 5.8 mmol) was added to a solution of **5** (0.691 g, 1.46 mmol) in THF (10 mL) and stirred for 72 h at room temperature, after which the solvent was removed under reduced pressure. The product was extracted into CH_2Cl_2 (20 mL) and Et_2O (20 mL), washed with sodium citrate (aq.) (3 × 20 mL), NH_4Cl (aq.) (2 × 20 mL), brine (20 mL), dried over $MgSO_4$, filtered and concentrated under reduced pressure, to yield the title compound in *ca*. 50% purity.

^{1}H NMR (300 MHz, CD_3OD, selected data): δ 8.22 (d, $^3J_{HH}$ = 8.0, 2H, py), 8.10 (t, $^3J_{HH}$ = 7.6, 1H, py), 7.18 (d, $^3J_{HH}$ = 8.1, 4H, Ar), 6.79 (d, $^3J_{HH}$ = 8.4, 4H, Ar), 5.40 (app t, J_{HH} = 9.2, 2H, ox), 4.94 (obsc t, J_{HH} = 9.6, 2H, ox), 4.37 (app t, J_{HH} = 8.5, 2H, ox).

HR ESI-MS (CH_3OH, 180 °C, 4 kV) positive ion: 402.1431 ([M+H]$^+$, calcd 402.1448) *m/z*.

7

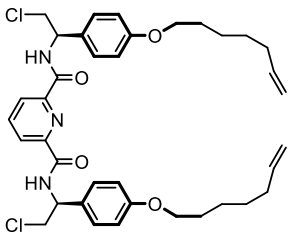

A suspension of **5** (216 mg, 0.46 mmol), 7-bromo-1-heptene (208 µL, 1.37 mmol) and K_2CO_3 (315 mg, 2.28 mmol) in DMF (50 mL) was heated at 50 °C for 48 h. The solvent was removed under reduced pressure, the resulting residue was re-dissolved in H_2O (20 mL) and extracted into CH_2Cl_2 (4 × 20 mL). The combined organic layers were dried over $MgSO_4$, filtered, concentrated under reduced pressure and purified by column

chromatography (silica; 1:99 CH_3OH:CH_2Cl_2) to yield the title compound as a yellow waxy solid. NMR spectroscopy was unassigned as a consequence of the low purity (*ca*. 70%).

HR ESI-MS (CH_3CN, 180 °C, 4 kV) positive ion: 688.2668 ($[M+Na]^+$, calcd 688.2679) *m*/*z*.

Hydroxy-catenane precursor (**8**)

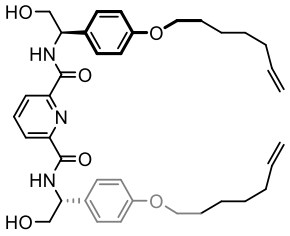

A suspension of (*R*,*R*)-**A102** (605 mg, 1.38 mmol), 7-bromo-1-heptene (630 µL, 4.14 mmol) and K_2CO_3 (1.0 g, 6.9 mmol) in DMF (100 mL) was heated at 50 °C for 72 h. The solvent was removed under reduced pressure, and the resulting residue re-dissolved in H_2O (50 mL) and the product extracted into CH_2Cl_2 (4 × 50 mL). The organic layers were combined, dried over $MgSO_4$, filtered, concentrated under reduced pressure and purified by column chromatography (silica; 5:95 CH_3OH:CH_2Cl_2; *Rf* = 0.2) to yield the title compound as a colourless solid. Yield: 470 mg (54%).

^{1}H NMR (500 MHz, $CDCl_3$): δ 8.44 (d, $^3J_{HH}$ = 7.2, 2H, NH), 8.35 (d, $^3J_{HH}$ = 7.8, 2H, py), 8.05 (t, $^3J_{HH}$ = 7.8, 1H, py), 7.30 (d, $^3J_{HH}$ = 8.6, 4H, Ar), 6.91 (d, $^3J_{HH}$ = 8.6, 4H, Ar), 5.81 (ddt, $^3J_{HH}$ = 16.9, $^3J_{HH}$ = 10.2, $^3J_{HH}$ = 6.7, 2H, C<u>H</u>=CH_2), 5.20 (q, $^3J_{HH}$ = 5.2, 2H, C<u>H</u>NH), 5.02 – 4.99 (m, 2H, C<u>H</u>$_2$=CH), 4.96 – 4.94 (m, 2H, C<u>H</u>$_2$=CH), 3.99 (br, 4H, C<u>H</u>$_2$OH), 3.95 (t, $^3J_{HH}$ = 6.5, 4H, CH_2OPh), 2.46 (t, $^3J_{HH}$ = 6.1, 2H, OH), 2.08 (d, $^3J_{HH}$ = 6.7, 4H, C<u>H</u>$_2$CH=CH_2), 1.83 – 1.74 (m, 4H, CH_2), 1.49 – 1.44 (m, 8H, CH_2).

^{13}C{^{1}H} NMR (126 MHz, $CDCl_3$): δ 163.6 (C=O), 159.1 (Ar), 148.7 (py), 139.5 (py), 138.9 (<u>C</u>H=CH_2), 130.6 (Ar), 127.9 (Ar), 125.3 (py), 115.2 (Ar), 114.6 (<u>C</u>H$_2$=CH), 68.1 (CH_2OPh), 67.0 (CH_2OH), 55.6 (CHNH), 33.8 (<u>C</u>H$_2$CH=CH_2), 29.2 (CH_2), 28.8 (CH_2), 25.7 (CH_2).

HR ESI-MS (CH_3CN, 180 °C, 4 kV) positive ion: 652.3364 ($[M+Na]^+$, calcd 652.3363) *m*/*z*.

Chloro-catenane precursor (**9**)

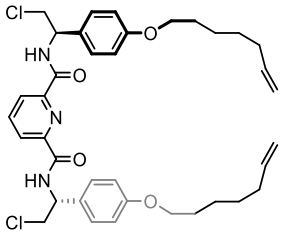

$SOCl_2$ (0.6 mL, 7.3 mmol) was added to a stirring solution of **8** (470 mg, 0.75 mmol) in $CHCl_3$ (20 mL) and the resulting solution was heated at 50 °C for 48 h. The solvent was removed under reduced pressure and purified by column chromatography (silica; 1:99 CH_3OH:CH_2Cl_2; *Rf* = 0.3) to yield the title compound as a waxy yellow solid. Yield: 421 mg (85%).

^{1}H NMR (500 MHz, $CDCl_3$): δ 8.42 (d, $^3J_{HH}$ = 8.2, 2H, NH), 8.36 (d, $^3J_{HH}$ = 7.7, 2H, py), 8.06 (t, $^3J_{HH}$ = 7.8, 1H, py), 7.32 (d, $^3J_{HH}$ = 8.6, 4H, Ar), 6.90 (d, $^3J_{HH}$ = 8.7, 4H, Ar), 5.81 (ddt, $^3J_{HH}$ = 17.0, $^3J_{HH}$ = 10.3, $^3J_{HH}$ = 6.7, 2H, C<u>H</u>=CH_2), 5.49 (dt, $^3J_{HH}$ = 8.3, $^3J_{HH}$ = 4.9, 2H, C<u>H</u>NH), 5.00 (dd, $^3J_{HH}$ = 17.1, $^3J_{HH}$ = 1.8, 2H, C<u>H</u>$_2$=CH), 4.94 (d, $^3J_{HH}$ = 10.2, 2H, C<u>H</u>$_2$=CH), 3.98 (t, $^3J_{HH}$ = 4.8, 4H, CH_2Cl), 3.94 (t, $^3J_{HH}$ = 6.6, 4H, CH_2O), 2.08 (q, $^3J_{HH}$ = 6.5, 4H, C<u>H</u>$_2$CH=CH_2), 1.78 (p, $^3J_{HH}$ = 6.9, 4H, CH_2), 1.50 – 1.42 (m, 8H, CH_2).

^{13}C{^{1}H} NMR (126 MHz, $CDCl_3$): δ 162.8 (C=O), 159.2 (Ar), 148.6 (py), 139.5 (py), 138.9 (<u>C</u>H=CH_2), 130.2 (Ar), 127.9 (Ar), 125.5 (py), 115.0 (Ar), 114.6 (<u>C</u>H_2=CH), 68.1 (CH_2O), 53.2 (CHNH), 48.7 (CH_2Cl), 33.8 (<u>C</u>H_2CH=CH_2), 29.2 (CH_2), 28.8 (CH_2), 25.7 (CH_2).

HR ESI-MS (CH_3CN, 180 °C, 4 kV) positive ion: 688.2677 ([M+Na]$^+$, calcd 688.2679) *m/z*.

(*R*,*R*)-bis(6-heptenyl)-phenol-pybox (**10**)

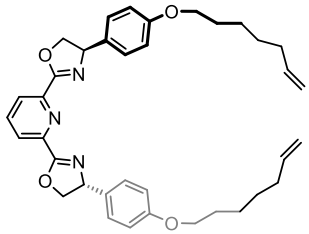

TBAF (1M in THF, 2.5 mL, 2.5 mmol) was added to a solution of **9** (421 mg, 0.63 mmol) in THF (20 mL) and the resulting solution was stirred at rt for 72 h. The solvent was removed under reduced pressure, subsequently the crude residue was re-dissolved in CH_2Cl_2 (20 mL) and Et_2O (20 mL) and washed with saturated trisodium citrate (aq.) (3 × 50 mL), saturated NH_4Cl (aq.) (2 × 50 mL), brine (50 mL). The organic layer was dried over $MgSO_4$, filtered and concentrated under reduced pressure, to yield the title compound as an off-white solid. Yield: 503 mg (80%).

^{1}H NMR (500 MHz, $CDCl_3$): δ 8.33 (d, $^3J_{HH}$ = 7.9, 2H, py), 7.90 (t, $^3J_{HH}$ = 7.8, 1H, py), 7.23 (d, $^3J_{HH}$ = 8.7, 4H, Ar), 6.88 (d, $^3J_{HH}$ = 8.7, 4H, Ar), 5.81 (ddt, $^3J_{HH}$ = 17.0, $^3J_{HH}$ = 10.2, $^3J_{HH}$ = 6.7, 2H, C<u>H</u>=CH_2), 5.40 (dd, $^3J_{HH}$ = 10.3, $^3J_{HH}$ = 8.6, 2H, ox{CH}), 5.01 (dd, $^2J_{HH}$ = 17.2, $^3J_{HH}$ = 1.8, 2H, C<u>H</u>$_2$=CH), 4.95 (d, $^3J_{HH}$ = 10.2, 2H, C<u>H</u>$_2$=CH), 4.89 (dd, $^3J_{HH}$ = 10.3, $^2J_{HH}$ = 8.7, 2H, ox{CH_2}), 4.40 (app t, J_{HH} = 8.6, 2H, ox{CH_2}), 3.94 (t, $^3J_{HH}$ = 6.5, 4H, CH_2O), 2.13 – 2.03 (m, 4H, C<u>H</u>$_2$CH=CH_2), 1.78 (p, $^3J_{HH}$ = 6.8, 4H, CH_2), 1.54 – 1.40 (m, 8H, CH_2).

^{13}C{^{1}H} NMR (126 MHz, $CDCl_3$): δ 163.3 (ox{OCN}), 158.9 (Ar), 146.9 (py), 139.0 (<u>C</u>H=CH_2), 137.6 (py), 133.8 (Ar), 128.1 (Ar), 126.4 (py), 114.6 (Ar), 114.6 (C<u>H</u>$_2$=CH), 75.7 (ox{CH_2}), 70.0 (ox{CH}), 68.1 (CH_2O), 33.8 (<u>C</u>H_2CH=CH_2), 29.2 (CH_2), 28.8 (CH_2), 25.7 (CH_2).

HR ESI-MS (CH_3CN, 180 °C, 4 kV) positive ion: 616.3150 ([M+Na]$^+$, calcd 616.3146) m/z.

6.2.7. Attempted nickel-templated catenane synthesis

<u>[Ni((*R*,*R*)-bis(6-heptenyl)-phenol-pybox)$_2$][BF_4]$_2$ (**11**)</u>

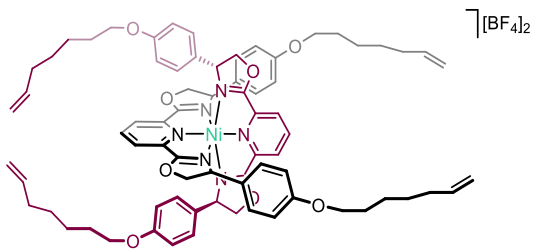

A solution of [$NiCl_2$(glyme)] (92.5 mg, 0.42 mmol) and (*R*,*R*)-bis(6-heptenyl)-phenol pybox (**10**) (500 mg, 0.84 mmol) in CH_2Cl_2 (50 mL) was stirred at rt for 18 h under argon and then washed with 0.1 M $NH_4[BF_4]$ (aq.) (10 × 10 mL). The solution was then concentrated under reduced pressure and washed with pentane (3 × 10 mL) to yield the title compound as a yellow-green microcrystalline solid. Yield: 548 mg (92%). Crystals suitable for X-ray crystallography were obtained from diffusion of *n*-hexane into a CH_2Cl_2 solution at rt.

^{1}H NMR (500 MHz, CD_3CN): δ 66.93 (vbr, fwhm = 460), 19.38 (vbr, fwhm = 120), 17.68 (vbr, fwhm = 150), 6.83 (vbr, fwhm = 110), 6.34 – 5.61 (vbr m, fwhm = 42), 5.12 (br d, J_{HH} = 16.7, 4H, CH=CH_2), 5.02 (br d, J_{HH} = 9.9, 4H, CH=CH_2), 4.23 (vbr d, J_{HH} = 48, 8H, CH_2), 2.29 (vbr s, fwhm = 25), 2.06 (vbr s, fwhm = 34), 1.87 – 1.56 (m). Signals could not be unambiguously fully assigned due to the paramagnetic nature of the complex.

^{13}C{^{1}H} NMR (126 MHz, CD_3CN): δ 160.1, 140.1, 115.1, 69.2, 34.5, 29.9, 29.6, 26.5. Other peaks not observed due to paramagnetic broadening.

HR ESI-MS (CH_3CN, 180 °C, 4 kV) positive ion: 1331.5905 ([M−BF_4]$^+$, calcd 1331.5896) m/z.

μ_{eff} = 2.93 μ_B (Evans method, in CD_3CN).

[2]Catenate (**Ni-12**)

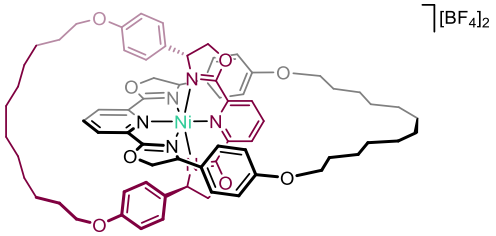

A solution of nickel complex **11** (502 mg, 0.35 mmol) and Grubbs I (14.5 mg, 0.018 mmol) in CH_2Cl_2 (350 mL) was stirred at rt for 18 h. A further 6 portions of Grubbs I (14.5 mg, 0.018 mmol) were added every 18 h until ESI-MS indicated the reaction had gone to completion. The solution was then concentrated under reduced pressure to yield the crude alkene precursor as a brown solid, the product was used without further purification. A solution of the crude alkene precursor in 1,2-dichloroethane (20 mL) was charged with palladium on carbon (10 wt % Pd, 150 mg, 0.14 mmol) and the solution was placed under H_2 (4 bar) and reacted at 100 °C for 72 h. The resulting suspension was filtered and the volatiles were removed *in vacuo*. The residue was extracted into CH_2Cl_2 (50 mL) and concentrated to dryness, followed by extraction into acetone (50 mL) and again concentrated *in vacuo*. The resulting solid was washed with cold Et_2O (2 × 10 mL) and dried *in vacuo* to yield the crude product as a brown solid. Crude yield: 271 mg. The purity of **12** could not be determined due to the paramagnetic broadness of the ^{1}H NMR spectrum which consequently prevented characterisation by NMR spectroscopy.

Pre-hydrogenated Ni-12: HR ESI-MS (CH_3CN, 180 °C, 4 kV) positive ion: 1275.5293 ($[M-BF_4]^+$, calcd 1275.5269) *m*/*z*.

Ni-12: HR ESI-MS (CH_3CN, 180 °C, 4 kV) positive ion: 1279.5565 ($[M-BF_4]^+$, calcd 1279.5577) *m*/*z*.

[2]Catenane (**12**)

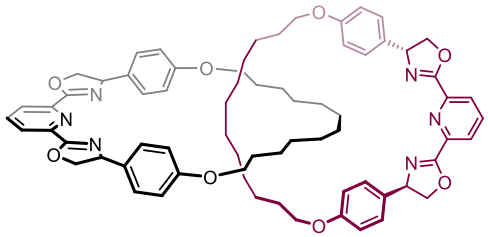

General procedure for attempted demetalation reactions

A solution of **Ni-12** (generated as crude mixture as described above) was treated with the chosen demetalation reagent (Na_2EDTA, Na_4EDTA or KCN) in CH_3CN/EtOAc. The reaction progress was monitored using HR ESI-MS and ^1H NMR spectroscopy. ^1H NMR spectroscopy data obtained after demetalation attempts were unsatisfactory to assign to **12**, paramagnetic broadening of **Ni-12** and other impurities obscured any signals associated with **12**. However, trace **12** was observed by mass spectrometry.

HR ESI-MS (CH_3CN, 180 °C, 4 kV) positive ion: 1193.6301 ($[M+2H_2O+Na]^+$, calcd 1193.6298) *m*/*z*.

HR ESI-MS/MS(1993.6301) (CH_3CN, 180 °C, 40 eV) positive ion: 590.2978 ($[^{M}$**pybox**$+Na]^+$, calcd 590.2989) *m*/*z*.

Method A: A solution of **Ni-12** (126 µmol, generated *in situ*) in EtOAc (50 mL) was washed with 17.5% NH_3(aq.) saturated with Na_2EDTA (5 × 50 mL), H_2O (3 × 50 mL) and brine (50 mL). The organic layer was dried over $MgSO_4$, filtered and dried *in vacuo* to give a brown solid. The residue was subjected to column chromatography (C_{18} end capped reversed-phase silica; gradient elution; CH_3OH:THF, 1:0 to 7:3). The title compound could not be isolated from the crude mixture.

Method B: A saturated solution of Na_2EDTA or Na_4EDTA (aq.) was added to **Ni-12** (10 µmol, generated *in situ*) in CH_3CN (10 mL) and the resulting suspension was heated at 90°C for 48 h. The solution was washed with H_2O (3 × 10 mL), brine (10 mL) and dried *in vacuo* to give a brown solid. The title compound could not be isolated from the crude mixture.

Method C: A suspension of KCN (33 µmol) in H_2O (1 mL) was added to **Ni-12** (22 µmol, generated *in situ*) in CH_3CN (10 mL) and the resulting suspension was heated at 90°C for 72 h. The sample was diluted with H_2O (50 mL) and extracted with CH_2Cl_2 (3 × 20 mL). The organic layers were combined, washed with H_2O (20 mL) and brine (20 mL), before being dried over $MgSO_4$, filtered and concentrated under reduced pressure to give a brown solid. The title compound could not be isolated from the crude mixture.

6.3. Compounds discussed in Chapter 3

6.3.1. Synthesis of rhodium complexes

6.3.1.1. Preparation of rhodium chloride complexes

[Rh(**^{Ph}pybox**)Cl] (**13a**)

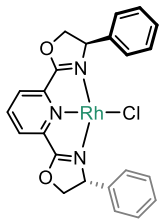

A solution of **^{Ph}pybox** (443 mg, 1.2 mmol) and $[Rh(COE)_2Cl]_2$ (431 mg, 0.6 mmol) in THF (50 mL) was stirred at rt for 1 h. The suspension was left to settle for 48 h, before the solid was isolated by filtration and washed with cold THF (3 × 10 mL, –78 °C) to afford the title compound as a dark sparingly soluble blue-black solid. Yield: 526 mg (86%).

^{1}H NMR (400 MHz, C_6D_6): δ 7.64 (t, $^3J_{HH}$ = 7.8, 1H, py), 7.51 (d, $^3J_{HH}$ = 7.3, 4H, Ph), 7.10 (app t, J_{HH} = 7.8, 4H, Ph), 7.01 (t, $^3J_{HH}$ = 7.4, 2H, Ph), 6.85 (d, $^3J_{HH}$ = 7.8, 2H, py), 5.46 (dd, $^3J_{HH}$ = 9.6, $^3J_{HH}$ = 5.0, 2H, ox{CH}), 4.22 (dd, $^2J_{HH}$ = 8.8, $^3J_{HH}$ = 5.0, 2H, ox{CH_2}), 4.10 (app t, J_{HH} = 9.2, 2H, ox{CH_2}).

^{1}H NMR (300 MHz, THF, selected data): δ 8.93 – 8.81 (m, 1H, py), 7.86 (d, $^3J_{HH}$ = 7.3, 4H), 7.78 (d, $^3J_{HH}$ = 7.7, 2H, py), 7.61 – 7.45 (m, 6H, Ph), 6.13 – 6.02 (m, 2H, ox), 5.53 (app t, J_{HH} = 9.2, 2H, ox), 5.35 – 5.26 (m, 2H, ox).

Acquisition of ^{13}C NMR data was encumbered by low solubility in C_6D_6.

HR ESI-MS (CH_3OH, 180 °C, 3 kV) positive ion: 508.0293 ($[M+H]^+$, calcd 508.0294) m/z.

Anal. Calcd for $C_{23}H_{19}ClN_3O_2Rh$ (507.78 $gmol^{-1}$): C, 54.40; H, 3.77; N, 8.28. Found: C, 54.16; H, 4.07; N, 8.13.

[Rh(**^{Ph}pybox**)Cl_3] (**13b**)

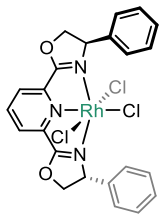

A solution of **13a** (50 mg, 98 µmol) and $PhICl_2$ (27 mg, 98 µmol) in CH_2Cl_2 (10 mL) was stirred at rt for 18 h. The product was precipitated through addition of pentane (20 mL), isolated by filtration, and washed with pentane (3 × 10 mL) to afford the title compound as

a dark orange solid. Yield: 45 mg (79%). The spectroscopic data is consistent with literature.[114]

^{1}H NMR (500 MHz, CD_2Cl_2): δ 8.36 (t, $^3J_{HH}$ = 8.0, 1H, py), 8.17 (d, $^3J_{HH}$ = 8.1, 2H, py), 7.53 – 7.45 (m, 4H, Ph), 7.38 – 7.32 (m, 6H, Ph), 5.54 (app t, J_{HH} = 10.5, 2H, ox{CH}), 5.42 (app t, J_{HH} = 10.5, 2H, ox{CH_2}), 4.92 (app t, J_{HH} = 8.9, 2H, ox{CH_2}).

[Rh(**^{Ph}pybox**)Cl_2(CH_2Cl)] (**14**)

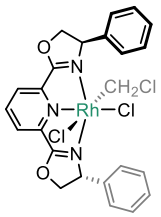

A solution of **13a** (5.1 mg, 10 μmol) in CH_2Cl_2 (0.5 mL) was stirred at rt for 18 h. The volatiles were removed *in vacuo* to afford the title compound as a bright yellow solid. Yield: 4.7 mg (84%).

^{1}H NMR (500 MHz, CD_2Cl_2): δ 8.25 (t, $^3J_{HH}$ = 8.0, 1H, py), 8.06 (d, $^3J_{HH}$ = 8.0, 1H, py), 8.01 (d, $^3J_{HH}$ = 8.0, 1H, py), 7.61 (d, $^3J_{HH}$ = 6.1, 2H, Ph), 7.49 – 7.44 (m, 2H, Ph), 7.40 – 7.31 (m, 6H, Ph), 5.49 – 5.41 (m, 1H, ox{CH}), 5.42 – 5.28 (m, 3H, 1×ox{CH}, 2×ox{CH_2}), 5.07 (dd, $^2J_{HH}$ = 9.1, $^3J_{HH}$ = 6.5, 1H, ox{CH_2}), 4.75 (app t, J_{HH} = 8.7, 1H, ox{CH_2}), 4.34 (dd, $^2J_{HH}$ = 5.3, $^2J_{RhH}$ = 3.2, 1H, CH_2), 3.89 (dd, $^2J_{HH}$ = 5.2, $^2J_{RhH}$ = 3.1, 1H, CH_2).

^{13}C{^{1}H} NMR (126 MHz, CD_2Cl_2): δ 168.4 (d, $^2J_{RhC}$ = 2.7, ox{OCN}), 167.1 (d, $^2J_{RhC}$ = 2.8, ox{OCN}), 146.8 (d, $^2J_{RhC}$ = 4.1, py), 139.1 (py), 138.1 (Ph), 137.7 (Ph), 129.7 (Ph), 129.2 (Ph), 129.1 (Ph), 128.9 (Ph), 128.8 (Ph), 128.7 (Ph), 127.1 (py), 126.9 (py), 80.9 (ox{CH_2}), 80.6 (ox{CH_2}), 67.5 (ox{CH}), 67.2 (ox{CH}), 39.3 (d, $^1J_{RhC}$ = 26, CH_2Cl).

HR ESI-MS (CH_3OH, 180 °C, 3 kV) positive ion: 556.0051 ([M−Cl]$^+$, calcd 556.0060) m/z.

6.3.1.2. Generation of cationic rhodium complexes

Generation of [Rh(**^{Ph}pybox**)][BAr^F_4] (**15a**)

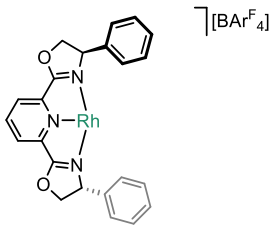

In C_6H_5F: A solution of **13a** (5.1 mg, 10 µmol) and Na[BAr^F_4] (8.9 mg, 10 µmol) in C_6H_5F (0.5 mL) was stirred for 5 min at rt to afford the title compound in quantitative spectroscopic yield.

^{1}H NMR (300 MHz, C_6H_5F, selected data): δ 4.50 – 4.29 (m, 4H, ox), 4.06 (dd, J_{HH} = 8.4, J_{HH} = 4.8, 2H, ox).

In THF: A solution of **13a** (10.2 mg, 20 µmol) and Tl[BAr^F_4] (21.4 mg, 20 µmol) were stirred in THF (0.5 mL) at rt for 5 min to afford the title compound in quantitative spectroscopic yield.

^{1}H NMR (300 MHz, THF, selected data): δ 8.72 (br, 1H, py), 8.19 (br, 1H, py), 8.04 (br, 8H, Ar^F), 7.82 (s, 4H, Ar^F), 7.68 (d, $^3J_{HH}$ = 7.5, 4H, Ph), 7.41 (br, 4H, Ph), 7.04 (br, 2H, Ph), 6.11 (br, 2H, ox), 5.62 (br, 2H, ox), 5.46 (br, 2H, ox).

Generation of [Rh(**^{Ph}pybox**)Cl_2][BAr^F_4] (**15b**)

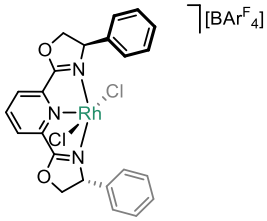

In C_6H_5F: A solution of **13b** (10.0 mg, 17 µmol) and Na[BAr^F_4] (15.3 mg, 17 µmol) in C_6H_5F (0.5 mL) was stirred for 5 min at rt to afford the title compound in quantitative spectroscopic yield.

^{1}H NMR (300 MHz, C_6H_5F, selected data): δ 5.02 – 4.92 (m, 2H, ox), 4.81 – 4.74 (m, 2H, ox), 4.54 – 4.47 (m, 2H, ox).

In CD_2Cl_2: A solution of **13b** (30.0 mg, 52 µmol) and Na[BAr^F_4] (48.0 mg, 54 µmol) were stirred in CD_2Cl_2 (0.5 mL) at rt for 5 min to afford the title compound in quantitative spectroscopic yield.

^{1}H NMR (300 MHz, CD_2Cl_2): δ 8.43 (dd, $^3J_{HH}$ = 8.6, $^3J_{HH}$ = 7.4, 1H, py), 8.24 (d, $^3J_{HH}$ = 8.0, 2H, py), 7.73 (br, 8H, Ar^F), 7.56 (s, 4H, Ar^F), 7.51 – 7.32 (m, 10H, Ph), 5.51 – 5.36 (m, 4H, ox), 5.10 – 4.92 (m, 2H, ox).

Generation of [Rh(**^{Ph}pybox**)(C_6H_4F)(H)][BAr^F_4] (**16**)

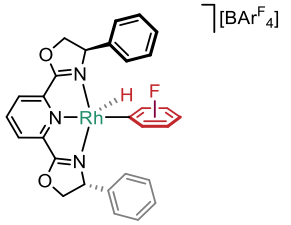

A solution of **13a** (5.1 mg, 10 μmol) and Na[BAr^F_4] (8.9 mg, 10 μmol) were stirred in C_6H_5F (0.5 mL) at rt for 18 h to afford the title compound in quantitative spectroscopic yield. Characterised *in situ* as a mixture of isomers (*ca*. 1:1) in C_6H_5F.

^{1}H NMR (300 MHz, C_6H_5F, selected data): δ 5.51 – 5.40 (m, 2H, ox), 5.31 (dd, $^2J_{HH}$ = 9.4, $^3J_{HH}$ = 5.3, 1H, ox), 5.16 – 5.03 (m, 1H, ox), 5.01 – 4.81 (m, 2H, ox), 4.70 (app t, J_{HH} = 9.4, 1H, ox), 4.61 (app t, J_{HH} = 10.0, 1H, ox), 4.30 – 4.19 (m, 1H, ox), 4.11 (obsc, 2H, ox), 3.86 – 3.72 (m, 1H, ox), −24.22 (d, $^1J_{RhH}$ = 22.4, 1H, RhH), −24.33 (d, $^1J_{RhH}$ = 23.3, 1H, RhH).

Preparation of [Rh(**^{Ph}pybox**)(PCy_3)][BAr^F_4] (**17**)

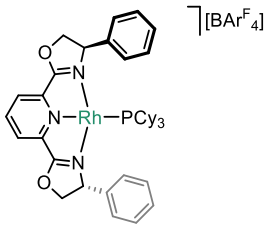

Method A: A solution of **^{Ph}pybox** (1.9 mg, 5 μmol) and [Rh(Binor)PCy_3][BAr^F_4] (7.2 mg, 5 μmol) were stirred in 1,2-$C_6H_4F_2$ (0.6 mL) at rt for 18 h to afford the title compound in quantitative spectroscopic yield.

^{1}H NMR (300 MHz, 1,2-$C_6H_4F_2$): δ 8.15 (s, 8H, Ar^F), 7.93 (t, $^3J_{HH}$ = 8.0, 1H, py), 7.53 (obsc d, 2H, py), 7.50 (s, 4H, Ar^F), 5.14 (d, $^3J_{HH}$ = 8.2, 2H, ox), 4.73 (t, $^3J_{HH}$ = 8.6, 2H, ox), 4.42 (d, $^3J_{HH}$ = 8.7, 2H, ox), 1.90 – 0.95 (m, 33H, Cy).

^{31}P{^{1}H} NMR (121 MHz, 1,2-$C_6H_4F_2$): δ 36.14 (d, $^1J_{RhP}$ = 166.9).

Method B: A solution of **13a** (31.4 mg, 62 μmol), Na[BAr^F_4] (54.9 mg, 62 μmol) and PCy_3 (17.3 mg, 62 μmol) were stirred in C_6H_5F (10 mL) at rt for 18 h. The suspension was filtered followed by removal of the volatiles *in vacuo* to afford the title compound as a foamy dark pink solid. Yield: 79 mg (79%).

^{1}H NMR (500 MHz, CD_2Cl_2): δ 8.27 (t, $^{3}J_{HH}$ = 7.9, 1H, py), 7.89 (d, $^{3}J_{HH}$ = 7.9, 2H, py), 7.72 (s, 8H, Ar^F), 7.56 (s, 4H, Ar^F), 7.46 – 7.34 (m, 6H, Ph), 7.23 – 7.10 (m, 4H, Ph), 5.18 (dd, $^{3}J_{HH}$ = 8.5, $^{3}J_{HH}$ = 2.2, 2H, ox{CH}), 4.95 (app t, J_{HH} = 8.5, 2H, ox{CH_2}), 4.70 (dd, $^{2}J_{HH}$ = 8.7, $^{3}J_{HH}$ = 2.2, 2H, ox{CH_2}), 1.93 – 1.39 (m, 15H, Cy), 1.36 – 1.01 (m, 15H, Cy), 0.42 – 0.22 (m, 3H, Cy).

^{1}H NMR (300 MHz, C_6H_5F, selected data): δ 5.03 (app d, J_{HH} = 8.4, 2H, ox), 4.50 (app t, J_{HH} = 8.6, 2H, ox), 4.27 (app d, J_{HH} = 8.7, 2H, ox), 1.89 – 0.92 (m, 33H, Cy).

^{13}C{^{1}H} NMR (126 MHz, CD_2Cl_2): δ 169.7 (ox{OCN}), 162.3 (q, $^{1}J_{CB}$ = 50, Ar^F), 144.2 (py), 139.31 (Ph), 136.9 (py), 135.4 (Ar^F), 130.1 (Ph), 129.8 (Ph), 129.2 (qq, $^{2}J_{FC}$ = 32, $^{3}J_{CB}$ = 3, Ar^F), 126.4 (Ph), 125.7 (py), 125.0 (q, $^{1}J_{FC}$ = 272, Ar^F), 118.1 (sept, $^{3}J_{FC}$ = 4, Ar^F), 80.1 (ox{CH_2}), 69.0 (ox{CH}), 35.0 (d, $^{1}J_{PC}$ = 19.7, Cy), 30.8 (Cy), 30.4 (Cy), 28.0 (d, $^{2}J_{PC}$ = 10.1, Cy), 27.2 (d, $^{2}J_{PC}$ = 10.0, Cy), 26.6 (Cy).

^{31}P{^{1}H} NMR (121 MHz, CD_2Cl_2): δ 36.55 (d, $^{1}J_{RhP}$ = 166.2).

^{31}P{^{1}H} NMR (121 MHz, C_6H_5F): δ 36.28 (d, $^{1}J_{RhP}$ = 167.0).

HR ESI-MS (CH_3OH, 180 °C, 3 kV) positive ion: 752.2847 ([M]$^+$, calcd 752.2847) m/z.

Anal. Calcd for $C_{73}H_{64}BF_{24}N_3O_2PRh$ (1615.98 gmol^{-1}): C, 54.26; H, 3.99; N, 2.60. Found: C, 54.42; H, 3.93; N, 2.45.

Generation of [Rh(^{Ph}**pybox**)(CH_3CN)][PF_6] (**18**)

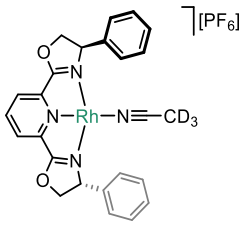

A suspension of ^{Ph}**pybox** (3.7 mg, 10 µmol) and [Rh(COE)$_2$(acetone)$_2$][PF_6] (5.8 mg, 10 µmol) was stirred in CD_3CN (0.6 mL) at rt for 1 h to afford the title compound in quantitative spectroscopic yield.

^{1}H NMR (300 MHz, CD_3CN): δ 8.20 (t, $^{3}J_{HH}$ = 8.0, 1H, py), 7.70 (d, $^{3}J_{HH}$ = 8.1, 2H, py), 7.39 (br s, 10H, Ph), 5.42 – 5.26 (m, 4H, ox), 4.83 – 4.69 (m, 2H, ox).

6.3.1.3. Preparation of carbonyl derivatives

[Rh(**^{Ph}pybox**)(CO)][BAr$^F_4$] (**20a**)

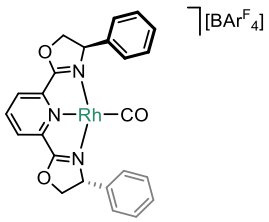

A suspension of **13a** (34 mg, 67 μmol) and Na[BAr$^F_4$] (63 mg, 70 μmol) in C_6H_5F (10 mL) was prepared and immediately freeze-pump-thaw degassed, placed under an atmosphere of CO and then stirred at rt for 30 min. The solution was filtered and the volatiles were removed *in vacuo* to give an oily residue, from which the product was extracted using CH_2Cl_2 (10 mL). The title compound was obtained as a foamy dark green solid on removal of the solvent, azeotroping with Et_2O. Yield: 64 mg (85%).

^{1}H NMR (500 MHz, CD_2Cl_2): δ 8.19 (t, $^3J_{HH}$ = 8.0, 1H, py), 7.92 (d, $^3J_{HH}$ = 8.0, 2H, py), 7.78 – 7.66 (m, 8H, Ar^F), 7.56 (br, 4H, Ar^F), 7.48 – 7.35 (m, 6H, Ph), 7.27 – 7.21 (m, 4H, Ph), 5.32 (app t, J_{HH} = 10.4, 2H, ox{CH_2}), 5.12 (app t, J_{HH} = 9.9, 2H, ox{CH}), 4.86 (app t, J_{HH} = 9.4, 2H, ox{CH_2}).

^{1}H NMR (300 MHz, C_6H_5F, selected data): δ 5.00 (app t, J_{HH} = 9.4, 2H, ox{CH_2}), 4.77 (app t, J_{HH} = 10.3, 2H, ox{CH}), 4.49 (app t, J_{HH} = 8.9, 2H, ox{CH_2}).

^{1}H NMR (300 MHz, MTBE, selected data): δ 8.80 (t, $^3J_{HH}$ = 8.2, 1H, py), 8.59 (d, $^3J_{HH}$ = 8.8, 2H), 8.33 (br, 8H, Ar^F), 8.06 (s, 4H, Ar^F), 7.99 – 7.90 (m, 6H, Ph), 7.90 – 7.79 (m, 4H, Ph), 5.93 (app t, J_{HH} = 9.9, 2H, ox{CH_2}), 5.77 (app t, J_{HH} = 9.8, 2H, ox{CH}), 5.42 (app t, J_{HH} = 10.2, 2H, ox{CH_2}).

^{13}C{^{1}H} NMR (126 MHz, CD_2Cl_2): δ 188.1 (d, $^1J_{RhC}$ = 77, RhCO), 167.5 (ox{OCN}), 162.1 (q, $^1J_{CB}$ = 50, Ar^F), 146.5 (py), 143.3 (py), 136.8 (Ph), 135.2 (Ar^F), 130.2 (Ph), 129.8 (Ph), 129.2 (qq, $^2J_{FC}$ = 32, $^3J_{CB}$ = 3, Ar^F), 128.0 (Ph), 125.5 (py), 125.0 (q, $^1J_{FC}$ = 272, Ar^F), 117.8 (sept, $^3J_{FC}$ = 4, Ar^F), 80.1 (ox{CH_2}), 69.8 (ox{CH}).

HR ESI-MS (CH_3OH, 180 °C, 3 kV) positive ion: 500.0518 ([M]$^+$, calcd 500.0521) *m/z*.

Anal. Calcd for $C_{56}H_{31}BF_{24}N_3O_3Rh$ (1363.56 gmol^{-1}): C, 49.33; H, 2.29; N, 3.08. Found: C, 49.17; H, 2.38; N, 3.03.

FT-IR (CH_2Cl_2): ν(CO) 2019 cm^{-1}.

Rh(**^{Ph}pybox**)Cl_2(CO)][BAr^F_4] (**20b**)

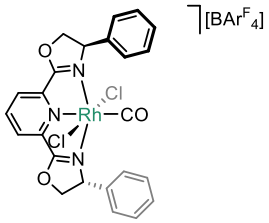

A suspension of **13b** (21 mg, 36 μmol) and Na[BAr^F_4] (34 mg, 38 μmol) in C_6H_5F (10 mL) was prepared and immediately freeze-pump-thaw degassed, placed under an atmosphere of CO and then stirred vigorously at rt for 18 h. The volatiles were removed *in vacuo* to give an oily residue, from which the crude product was extracted using CH_2Cl_2 (10 mL). The resulting solution was concentrated *in vacuo* and excess pentane (10 mL) added to precipitate the product, which was isolated by filtration, washed with pentane (3 × 10 mL) and dried to afford the title compound as a foamy lime green solid. Yield: 37 mg (72%). Crystals suitable for X-ray crystallography were obtained from diffusion of *n*-hexane into a CH_2Cl_2 solution at rt.

^{1}H NMR (500 MHz, CD_2Cl_2): δ 8.67 (t, $^3J_{HH}$ = 8.1, 1H, py), 8.40 (d, $^3J_{HH}$ = 8.1, 2H, py), 7.76 – 7.70 (m, 8H, Ar^F), 7.56 (br, 4H, Ar^F), 7.54 – 7.38 (m, 10H, Ph), 5.58 (app t, J_{HH} = 9.9, 2H, ox{CH_2}), 5.43 (app t, J_{HH} = 11.6, 2H, ox{CH}), 5.04 (dd, $^2J_{HH}$ = 12.0, $^3J_{HH}$ = 9.4, 2H, ox{CH_2}).

^{1}H NMR (300 MHz, C_6H_5F, selected data): δ 4.99 (app t, J_{HH} = 10.8, 2H, ox{CH_2}), 4.75 (app t, J_{HH} = 9.8, 2H, ox{CH}), 4.37 (dd, $^2J_{HH}$ = 12.2, $^3J_{HH}$ = 9.5, 2H, ox{CH_2}).

^{13}C{^{1}H} NMR (126 MHz, CD_2Cl_2): δ 171.8 (d, $^1J_{RhC}$ = 55, RhCO), 168.2 (ox{OCN}), 162.2 (q, $^1J_{CB}$ = 50, Ar^F), 145.3 (py), 145.1 (py), 135.2 (Ar^F), 132.9 (Ph), 131.3 (Ph), 130.0 (Ph), 129.8 (py), 129.6 (Ph), 129.3 (qq, $^2J_{FC}$ = 32, $^3J_{CB}$ = 3, Ar^F), 125.0 (q, $^1J_{FC}$ = 272, Ar^F), 117.9 (sept, $^3J_{FC}$ = 4, Ar^F), 80.6 (ox{CH_2}), 69.4 (ox{CH}).

HR ESI-MS (CH_3OH, 180 °C, 3 kV) positive ion: 623.9939 ([M+NaOMe]$^+$, calcd 623.9935) *m*/*z*.

Anal. Calcd for $C_{56}H_{31}BCl_2F_{24}N_3O_3Rh$ (1434.46 gmol^{-1}): C, 46.89; H, 2.18; N, 2.93. Found: C, 47.11; H, 2.10; N, 2.86.

FT-IR (CH_2Cl_2): ν(CO) 2151 cm^{-1}.

Redox shuttling between carbonyl complexes **20a** and **20b**

Oxidation of **20a**: In a J. Young valve NMR tube a solution of **20a** (6.9 mg, 5.0 μmol) and $PhICl_2$ (1.4 mg, 5.0 μmol) in THF (0.5 mL) was mixed at rt for 1 h to afford **20b** in quantitative spectroscopic yield.

^{1}H NMR (300 MHz, THF, selected data): δ 9.17 (t, $^3J_{HH}$ = 8.2, 1H, py), 9.01 (d, $^3J_{HH}$ = 8.1, 2H, py), 7.85 – 7.70 (m, 10H, Ph), 5.99 (app t, J_{HH} = 9.6, 2H, ox{CH_2}), 5.82 (app t, J_{HH} = 11.1, 2H, ox{CH}), 5.41 (dd, $^2J_{HH}$ = 11.4, $^3J_{HH}$ = 9.1, 2H, ox{CH_2}).

Reduction of **20b**: In a J. Young valve NMR tube a solution of **20b** (7.2 mg, 5.0 μmol) and activated Zn powder (0.6 mg, 10.7 μmol) in THF (0.5 mL) was mixed at rt for 1 h to afford **20a** in quantitative spectroscopic yield.

^{1}H NMR (300 MHz, THF, selected data): δ 8.71 (t, $^3J_{HH}$ = 7.9, 1H, py), 8.47 (d, $^3J_{HH}$ = 7.9, 2H, py), 7.76 – 7.60 (m, 10H, Ph), 5.73 (app t, J_{HH} = 9.6, 2H, ox{CH_2}), 5.55 (app t, J_{HH} = 9.8, 2H, ox{CH}), 5.22 (app t, J_{HH} = 9.1, 2H, ox{CH_2}).

6.3.2. Synthesis of rhodium and iridium 2,2'-biphenyl complexes

[Rh(^{Ph}**pybox**)(biph)Cl] (**21**)

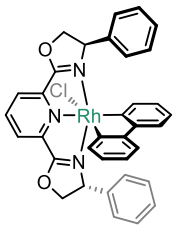

A solution of ^{Ph}**pybox** (31 mg, 84 μmol) and [Rh(dtbpm)(biph)Cl] (50 mg, 84 μmol) in CH_3CN (10 mL) was stirred at 85 °C for 48 h, before cooling to rt and removal of volatiles *in vacuo*. The residue was re-dissolved in CH_2Cl_2 (2 mL) and precipitated with pentane (10 mL), filtered and then washed with pentane (3 × 10 mL) to afford the crude product. The crude compound was purified by column chromatography (silica; 95:5 CH_2Cl_2:CH_3OH) to yield the title compound as a dark red solid. Yield: 41 mg (74%).

^{1}H NMR (500 MHz, CD_2Cl_2): δ 8.32 (t, $^3J_{HH}$ = 8.0, 1H, py), 8.19 (d, $^3J_{HH}$ = 10.5, 1H, py), 8.17 (d, $^3J_{HH}$ = 10.3, 1H, py), 7.83 (d, $^3J_{HH}$ = 8.7, 1H, biph), 7.18 – 7.13 (m, 1H, Ph), 7.10 (app t, $^3J_{HH}$ = 7.3, 2H, Ph), 7.00 (d, $^3J_{HH}$ = 7.5, 2H, Ph), 6.89 – 6.81 (m, 3H, 3×biph), 6.68 (t, $^3J_{HH}$ = 6.7, 1H, biph), 6.65 – 6.60 (m, 3H, Ph), 6.51 – 6.44 (m, 2H, 2×biph), 6.18 (d, $^3J_{HH}$ = 6.8, 2H, Ph), 5.75 (d, $^3J_{HH}$ = 7.4, 1H, biph), 5.11 (dd, $^3J_{HH}$ = 10.7, $^2J_{HH}$ = 9.1, 1H, ox{CH_2}), 4.94 (dd, $^3J_{HH}$ = 10.6, $^2J_{HH}$ = 9.0, 1H, ox{CH_2}), 4.82 (dd, $^3J_{HH}$ = 10.6, $^3J_{HH}$ = 8.5, 1H, ox{CH}), 4.55 (app t, J_{HH} = 8.8,

1H, ox{CH_2}), 4.51 (dd, $^3J_{HH}$ = 10.4, $^2J_{HH}$ = 9.1, 1H, ox{CH_2}), 4.28 (app t, J_{HH} = 10.5, 1H, ox{CH}).

^{13}C{^{1}H} NMR (126 MHz, CD_2Cl_2): δ 169.0 (d, $^1J_{RhC}$ = 30.0, biph), 166.8 (ox{OCN}), 166.1 (ox{OCN}), 160.7 (d, $^1J_{RhC}$ = 31.3, biph), 155.7 (biph), 152.1 (biph), 145.0 (py), 144.9 (py), 138.7 (py), 138.2 (biph), 137.2 (Ph), 136.6 (Ph), 131.6 (biph), 128.6 (Ph), 128.5 (Ph), 128.3 (Ph), 128.2 (biph), 127.7 (biph), 127.4 (Ph), 125.9 (py), 125.9 (py), 124.8 (biph), 124.4 (biph), 122.8 (biph), 121.6 (Ph), 119.6 (biph), 118.9 (biph), 80.2 (ox{CH_2}), 79.7 (ox{CH_2}), 68.2 (ox{CH}), 68.0 (ox{CH}).

HR ESI-MS (CH_3CN, 180 °C, 3 kV) positive ion: 624.1156 ([M–Cl]$^+$, calcd 624.1153) *m*/*z*.

Rh(**^{Ph}pybox**)(biph)][BAr^F_4] (**22**)

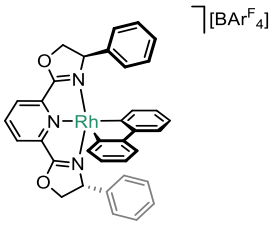

A solution of **21** (64 mg, 0.097 mmol) and Na[BAr^F_4] (95 mg, 0.107 mmol) in CH_2Cl_2 (10 mL) was stirred for at rt 18 h. The resulting suspension was filtered and the filtrate concentrated to dryness *in vacuo* to afford the title compound as a dark orange solid. Yield: 114 mg (79%).

^{1}H NMR (500 MHz, CD_2Cl_2): δ 8.51 (t, $^3J_{HH}$ = 8.0, 1H, py), 8.30 (d, $^3J_{HH}$ = 8.0, 2H, py), 7.74 (s, 8H, Ar^F), 7.56 (s, 4H, Ar^F), 7.12 (t, $^3J_{HH}$ = 7.6, 2H, Ph), 7.00 (d, $^3J_{HH}$ = 7.5, 2H, biph), 6.97 – 6.84 (m, 6H, 2×biph, 4×Ph), 6.64 (t, $^3J_{HH}$ = 7.4, 2H, biph), 6.42 (br d, $^3J_{HH}$ = 7.6, 4H, Ph), 6.18 (br, 2H, biph), 5.10 (app t, J_{HH} = 10.2, 2H, ox{CH_2}), 4.90 (app t, J_{HH} = 8.9, 2H, ox{CH_2}), 4.53 (br app t, J_{HH} = 9.5, 2H, ox{CH}).

^{13}C{^{1}H} NMR (126 MHz, CD_2Cl_2): δ 168.4 (ox{OCN}), 162.3 (q, $^1J_{CB}$ = 49.8, Ar^F), 151.8 (assigned from HMBC, biph), 145.2 (py), 142.2 (py), 135.4 (Ar^F), 135.2 (Ph), 132.2 (located from HMBC, biph), 129.4 (qq, $^2J_{FC}$ = 31.2; $^2J_{CB}$ = 2.8, Ar^F), 129.4 (Ph), 129.2 (Ph), 128.8 (Ph), 128.0 (Ph), 127.8 (py), 126.2 (biph), 125.2 (q, $^1J_{FC}$ = 272, Ar^F), 124.5 (biph), 121.4 (biph), 118.0 (sept, $^3J_{FC}$ = 4, Ar^F), 80.4 (ox{CH_2}), 67.9 (ox{CH}).

HR ESI-MS (CH_3CN, 180 °C, 3 kV) positive ion: 624.1150 ([M]$^+$, calcd 624.1153) *m*/*z*.

225K ^{1}H NMR (600 MHz, CD_2Cl_2): δ 8.46 (t, $^3J_{HH}$ = 8.1, 1H, py), 8.27 (d, $^3J_{HH}$ = 8.1, 1H, py), 8.24 (d, $^3J_{HH}$ = 8.1, 1H, py), 7.74 (s, 8H, Ar^F), 7.56 (s, 4H, Ar^F), 7.27 (br, 1H, Ph), 7.15 (br, 2H, Ph), 7.02 (d, $^3J_{HH}$ = 7.6, 1H, Ph), 6.96 (d, $^3J_{HH}$ = 6.0, 1H, Ph), 6.94 – 6.85 (m, 2H, biph), 6.81

(d, $^3J_{HH}$ = 7.5, 1H, Ph), 6.77 – 6.67 (m, 2H, biph), 6.65 – 6.55 (m, 4H, 2×Ph, 2×biph), 6.46 (t, $^3J_{HH}$ = 7.4, 1H, biph), 6.12 (d, $^3J_{HH}$ = 7.6, 2H, Ph), 5.26 (d, $^3J_{HH}$ = 7.7, 1H, biph), 5.18 (t, J_{HH} = 10.0, 1H, ox), 5.02 (app t, J_{HH} = 10.4, 1H, ox), 4.96 (app t, J_{HH} = 9.0, 1H, ox), 4.78 (t, J_{HH} = 8.7, 1H, ox), 4.73 (app t, J_{HH} = 8.9, 1H, ox), 4.27 (app t, J_{HH} = 9.3, 1H, ox).

HR ESI-MS (CH_3CN, 180 °C, 3 kV) positive ion: 624.1150 ([M–Cl]$^+$, calcd 624.1153) *m/z*.

Anal. Calcd for $C_{67}H_{39}BF_{24}N_3O_2Rh$ (1487.75 gmol^{-1}): C, 54.09; H, 2.64; N, 2.82. Found: C, 54.12; H, 2.59; N, 2.92.

[Ir(**^{Ph}pybox**)(biph)Cl] (**23**)

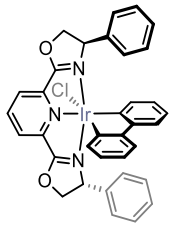

A solution of **^{Ph}pybox** (75.6 mg, 0.205 mmol) and [Ir(COD)(biph)Cl]$_2$ (100 mg, 0.102 mmol) in CH_2Cl_2 (10 mL) was stirred at rt for 18 h. The volatiles were removed *in vacuo* and the residue washed with hexane (3 × 10 mL) to afford the title compound as a brown solid. Yield: 127 mg (85%).

^{1}H NMR (500 MHz, CD_2Cl_2): δ 8.00 – 7.94 (m, 3H, 3×py), 7.45 (d, $^3J_{HH}$ = 7.4, 1H, biph), 7.18 (t, $^3J_{HH}$ = 7.4, 1H, Ph), 7.10 (app t, J_{HH} = 8, 2H, Ph), 6.95 (d, $^3J_{HH}$ = 7.6, 2H, Ph), 6.89 (d, $^3J_{HH}$ = 7.4, 1H, biph), 6.85 (t, $^3J_{HH}$ = 7.5, 1H, Ph), 6.82 (d, $^3J_{HH}$ = 7.5, 1H, biph), 6.60 (app t, $^3J_{HH}$ = 8, 2H, Ph), 6.58 – 6.52 (m, 2H, 2×biph), 6.47 (app t, $^3J_{HH}$ = 7, 1H, biph), 6.39 (app t, $^3J_{HH}$ = 7, 1H, biph), 6.21 (d, $^3J_{HH}$ = 7.7, 2H, Ph), 5.45 (d, $^3J_{HH}$ = 7.2, 1H, biph), 5.22 (dd, $^3J_{HH}$ = 10.5, $^2J_{HH}$ = 9.2, 1H, ox{CH_2}), 5.02 (dd, $^3J_{HH}$ = 10.5, $^2J_{HH}$ = 9.2, 1H, ox{CH_2}), 4.87 (dd, $^3J_{HH}$ = 10.5, $^3J_{HH}$ = 8.3, 1H, ox{CH}), 4.68 (app t, J_{HH} = 10, 1H, ox{CH_2}), 4.66 (app t, J_{HH} = 9, 1H, ox{CH_2}), 4.27 (app t, J_{HH} = 10, 1H, ox{CH}).

^{13}C{^{1}H} NMR (126 MHz, CD_2Cl_2): δ 172.6 (ox{OCN}), 172.1 (ox{OCN}), 157.5 (biph), 152.9 (biph), 151.4 (biph), 145.7 (py), 145.7 (py), 140.5 (biph), 136.8 (py), 136.7 (biph), 136.6 (Ph), 136.1 (Ph), 130.2 (biph), 128.9 (Ph), 128.5 (Ph), 128.4 (Ph), 128.2 (Ph), 127.8 (Ph), 127.6 (Ph), 125.7 (py), 125.63 (py), 124.8 (biph), 124.4 (biph), 122.3 (biph), 121.4 (biph), 119.2 (biph), 118.8 (biph), 80.4 (ox{CH_2}), 79.7 (ox{CH_2}), 69.4 (ox{CH}), 69.2 (ox{CH}).

HR ESI-MS (CH_3CN, 180 °C, 3 kV) positive ion: 714.1729 ([M–Cl]$^+$, calcd 714.1727) *m/z*.

Anal. Calcd for $C_{35}H_{27}ClIrN_3O_2 \cdot 0.1(C_6H_{14})$ (757.90 gmol^{-1}): C, 56.42; H, 3.78; N, 5.54. Found: C, 56.13; H, 4.14; N, 5.62.

[Ir(**^{Ph}pybox**)(biph)Cl][BAr^F_4] (**24**)

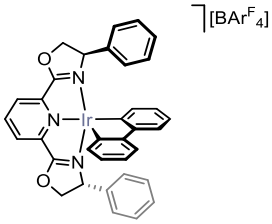

A solution of **23** (103 mg, 0.137 mmol) and Na[BAr^F_4] (127 mg, 0.143 mmol) in CH_2Cl_2 (10 mL) was stirred at rt for 18 h. The suspension was filtered and the filtrate concentrated to dryness *in vacuo* to afford the title compound as a brown solid. Yield: 154 mg (71%).

^{1}H NMR (500 MHz, CD_2Cl_2): δ 8.25 (t, $^3J_{HH}$ = 8.0, 1H, py), 8.16 (br s, 2H, py), 7.74 (s, 8H, Ar^F), 7.57 (s, 4H, Ar^F), 7.32 (br, 1H, Ph), 7.21 (br, 2H, Ph), 7.12 (br d, $^3J_{HH}$ = 7.2, 1H, Ph), 6.91 (br, 1H, biph), 6.87 (br, 3H, Ph), 6.81 (br d, $^3J_{HH}$ = 6.9, 1H, Ph), 6.72 (br d, $^3J_{HH}$ = 7.2, 2H, Ph), 6.67 (br, 1H, biph), 6.62 (br t, $^3J_{HH}$ = 7.4, 2H, biph), 6.45 (br t, $^3J_{HH}$ = 7.6, 1H, biph), 6.21 (br d, $^3J_{HH}$ = 7.6, 2H, biph), 5.33 (s, 1H, ox{CH_2}), 5.11 (br t, $^3J_{HH}$ = 9.8, 2H, ox{CH_2}), 4.91 (br, 2H, 1×ox{CH_2}; 1×biph), 4.84 (br app t, J_{HH} = 9.1, 1H, ox{CH}), 4.27 (br app t, J_{HH} = 9.6, 1H, ox{CH}).

^{13}C{^{1}H} NMR (126 MHz, CD_2Cl_2): δ 174.0 (ox{OCN}), 173.5 (ox{OCN}), 162.3 (q, $^1J_{CB}$ = 49.8, Ar^F), 155.2 (biph), 151.0 (Ph), 147.6 (Ph), 146.4 (py), 141.1 (py), 135.4 (Ar^F), 134.1 (Ph), 130.2 (Ph), 129.8 (Ph), 129.6 (biph), 129.4 (qq, $^2J_{FC}$ = 31.2, $^2J_{CB}$ = 2.8, Ar^F), 128.9 (Ph), 128.8 (Ph), 128.4 (py), 127.8 (biph), 127.6 (Ph), 126.8 (biph), 126.4 (Ph), 126.2 (Ph), 125.4 (biph), 125.2 (q, $^1J_{FC}$ = 272.4, Ar^F), 124.9 (biph), 123.8 (biph), 120.9 (Ph), 120.8 (Ph), 118.5 – 117.6 (m, Ar^F), 81.2 (ox{CH_2}), 79.8 (ox{CH_2}), 70.1 (ox{CH}), 68.2 (ox{CH}).

HR ESI-MS (CH_3CN, 180 °C, 3 kV) positive ion: 714.1734 ($[M]^+$, calcd 714.1727) *m/z*.

Anal. Calcd for $C_{67}H_{39}BF_{24}IrN_3O_2$ (1577.06 $gmol^{-1}$): C, 51.03; H, 2.49; N, 2.66. Found: C, 50.86; H, 2.40; N, 2.85.

6.3.3. Synthesis of ruthenium complexes

Preparation of [Ru(**^{Ph}pybox**)Cl_2(THF)] (**THF-25**)

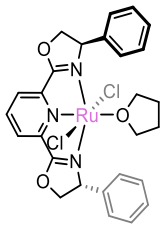

A solution of **^{Ph}pybox** (14.8 mg, 40 µmol) and [Ru(*p*-cymene)Cl_2]$_2$ (12.2 mg, 20 µmol) in THF (10 mL) was stirred at rt for 1 h. The volatiles were removed *in vacuo* and the

resulting residue washed with hexane (3 × 10 mL) to yield the title compound as a as a dark purple solid. Yield: 23 mg (93%). Crystals suitable for X-ray crystallography were obtained from diffusion of *n*-hexane into a THF solution at rt.

^{1}H NMR (400 MHz, THF): δ 8.01 (d, $^{3}J_{HH}$ = 7.9, 2H, py), 7.93 (d, $^{3}J_{HH}$ = 7.5, 4H, Ph), 7.74 (t, $^{3}J_{HH}$ = 7.8, 1H, py), 7.61 – 7.49 (m, 6H, Ph), 5.72 – 5.59 (m, 4H, 2×ox{CH_2}, 2×ox{CH}), 4.81 – 4.68 (m, 2H, ox{CH_2}).

Characterised in CD_2Cl_2 as approximately a 2:3 mixture of **THF-25** to **DCM-25**.

^{1}H NMR (600 MHz, CD_2Cl_2): δ 7.74 (d, $^{3}J_{HH}$ = 7.9, 2H, py), 7.51 (d, $^{3}J_{HH}$ = 7.4, 4H, Ph), 7.49 – 7.43 (obsc, 1H, py), 7.38 – 7.27 (m, 6H, Ph), 5.32 – 5.26 (m, 4H, 2×ox{CH_2}, 2×ox{CH}), 4.55 (dd, $^{3}J_{HH}$ = 10.7, $^{2}J_{HH}$ = 7.6, 2H, ox{CH_2}), 3.62 (q, $^{3}J_{HH}$ = 6.8, 2H, THF), 3.50 (q, $^{3}J_{HH}$ = 6.9, 2H, THF), 1.24 – 1.15 (m, 2H, THF), 1.10 – 1.02 (m, 2H, THF).

^{13}C{^{1}H} NMR (151 MHz, CD_2Cl_2): δ 169.2 (ox{OCN}), 154.7 (py), 138.7 (Ph), 129.1 (Ph), 129.0 (Ph) , 128.9 (Ph), 125.1 (py), 124.2 (py), 79.1 (ox{CH_2}), 73.6 (THF), 70.0 (ox{CH}), 25.4 (THF).

HR ESI-MS (CH_3OH, 180 °C, 3 kV) positive ion: 507.0284 ([M–Cl–THF+H]$^{+}$, calcd 507.0285) *m*/*z*.

Generation of [Ru(**^{Ph}pybox**)Cl_2(CD_2Cl_2)] (**DCM-25**)

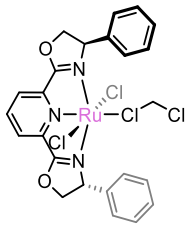

Generated from **THF-25** (*vide supra*).

^{1}H NMR (600 MHz, CD_2Cl_2): δ 7.80 (d, $^{3}J_{HH}$ = 7.9, 2H, py), 7.62 (t, $^{3}J_{HH}$ = 8.1, 1H, py), 7.49 – 7.43 (m, 4H, Ph), 7.38 – 7.27 (m, 6H, Ph), 5.39 – 5.32 (m, 4H, 2×ox{CH_2}, 2×ox{CH}), 4.73 – 4.66 (m, 2H, ox{CH_2}).

^{13}C{^{1}H} NMR (151 MHz, CD_2Cl_2): δ 168.1 (ox{OCN}), 153.8 (py), 138.4 (Ph), 129.4 (Ph), 129.0 (Ph), 128.7 (py), 128.6 (Ph), 124.3 (py), 79.6 (ox{CH_2}), 69.9 (ox{CH}).

Generation of [Ru(**^{Ph}pybox**)(MTBE)Cl_2] (**MTBE-25**)

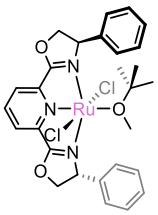

A solution of **^{Ph}pybox** (3.7 mg, 10 μmol) and [Ru(*p*-cymene)Cl_2]$_2$ (3.1 mg, 5 μmol) in MTBE (0.5 mL) was stirred at rt for 1 h. The product was sparingly soluble in MTBE and precipitated out as a dark pink solid.

^{1}H NMR (400 MHz, MTBE): δ 8.24 (d, $^3J_{HH}$ = 7.8, 2H, py), 8.13 (d, $^3J_{HH}$ = 7.6, 4H, Ph), 7.93 (t, $^3J_{HH}$ = 7.5, 1H, py), 7. 84 – 7.71 (m, 6H, Ph), 5.96 – 5.79 (m, 4H, ox), 5.05 (app t, J_{HH} = 7.2, 2H, ox).

Preparation of [Ru(**^{Ph}pybox**)Cl_2(CO)] (**26**)

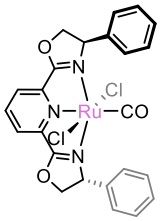

A solution of [Ru(*p*-cymene)Cl_2]$_2$ (6.1 mg, 10 μmol) and **^{Ph}pybox** (7.4 mg, 20 μmol) in THF (0.5 mL) was stirred at rt for 1 h. The purple solution was freeze-pump-thaw degassed, placed under an atmosphere of CO, and then stirred at rt for 18 h. The volatiles were removed *in vacuo*. The product was isolated as dark brown-red crystals following recrystallisation from CH_2Cl_2/hexane. Yield: 10.2 mg (89%). Crystals grown in this way were suitable for single crystal X-ray diffraction.

^{1}H NMR (500 MHz, CD_2Cl_2): δ 8.21 (t, $^3J_{HH}$ = 8.1, 1H, py), 8.02 (d, $^3J_{HH}$ = 8.0, 2H, py), 7.38 (s, 10H, Ph), 5.28 (app t, J_{HH} = 9.6, 2H, ox{CH_2}), 5.13(app t, J_{HH} = 11.0, 2H, ox{CH}), 4.66 (app t, J_{HH} = 10.1, 2H, ox{CH_2}).

^{13}C{^{1}H} NMR (126 MHz, CD_2Cl_2): δ 204.4 (RuCO), 165.5 (ox{OCN}), 147.8 (py), 140.1 (py), 136.9 (Ph), 129.4 (Ph), 129.3 (Ph), 129.1 (Ph), 124.6 (py), 79.4 (ox{CH_2}), 71.0 (ox{CH}).

HR ESI-MS (CH_3OH, 180 °C, 3 kV) positive ion: 591.9740 ([M+Na]$^+$, calcd 591.9740) *m/z*.

FT-IR (CH_2Cl_2): ν(CO) 1977 cm^{-1}.

6.4. Compounds discussed in Chapter 4

6.4.1. Synthesis of rhodium complexes

6.4.1.1. Preparation of rhodium chloride complexes

[Rh(**ᴹpybox**)Cl] (**27a**)

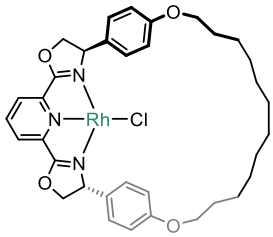

A solution of **ᴹpybox** (30.0 mg, 53 μmol) and $[Rh(COE)_2Cl]_2$ (19.0 mg, 26 μmol) in MTBE (10 mL) was stirred at rt for 48 h. The suspension was left to settle before the solid was isolated by filtration and washed with cold MTBE (3 × 5 mL, –78 °C) to afford the product as a dark black solid. Yield: 27 mg (73%). Characterised by NMR spectroscopy as a mixture of outer- and inner-sphere chloride complex (*ca*. 1:9).

Major species:

^{1}H NMR (600 MHz, THF-d_8): δ 8.41 (t, $^3J_{HH}$ = 7.8, 1H, py), 7.34 (d, $^3J_{HH}$ = 8.4, 4H, Ph), 7.27 (d, $^3J_{HH}$ = 7.8, 2H, py), 6.75 (d, $^3J_{HH}$ = 8.6, 4H, Ph), 5.68 (app t, J_{HH} = 10.2, 2H, ox{CH}), 5.26 (dd, $^3J_{HH}$ = 10.1, $^2J_{HH}$ = 8.3, 2H, ox{CH_2}), 4.47 (dd, $^3J_{HH}$ = 10.4, $^2J_{HH}$ = 8.3, 2H, ox{CH_2}), 4.11 – 4.06 (m, 2H, CH_2), 4.06 – 3.97 (m, 2H, CH_2), 1.72 – 1.53 (m, 4H, CH_2), 1.41 – 1.26 (m, 6H, CH_2), 1.26 – 1.13 (m, 10H, CH_2).

^{13}C{^{1}H} NMR (151 MHz, THF-d_8): δ 170.0 (d, $^2J_{RhC}$ = 4.3, ox{OCN}), 159.5 (Ph), 144.0 (py), 132.9 (Ph), 130.5 (Ph), 126.1 (py), 121.9 (py), 116.2 (Ph), 80.1 (ox{CH_2}), 69.8 (ox{CH}), 68.5 (CH_2), 30.9 (CH_2), 30.6 (CH_2), 30.0 (CH_2), 29.3 (CH_2), 26.5 (CH_2).

Minor species:

^{1}H NMR (600 MHz, THF-d_8, selected data): δ 8.50 (t, $^3J_{HH}$ = 7.8, 1H, py), 7.37 (d, $^3J_{HH}$ = 7.8, 2H, py), 6.73 (obsc, 4H, Ph), 5.68 (obsc, 2H, ox{CH}), 5.32 (app t, J_{HH} = 9.4, 2H, ox{CH_2}), 4.55 (dd, $^3J_{HH}$ = 10.4, $^2J_{HH}$ = 8.4, 2H, ox{CH_2}), 4.21 (t, $^3J_{HH}$ = 7.0, 2H, CH_2).

HR ESI-MS (CH_3OH, 180 °C, 3 kV) positive ion: 670.2147 ($[M–Cl]^+$, calcd 670.2147) *m*/*z*.

[Rh(**ᴹpybox**)Cl_3] (**27b**)

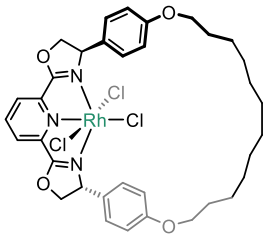

A solution of **27a** (7.1 mg, 10 μmol) and $PhICl_2$ (2.7 mg, 10 μmol) in THF (0.5 mL) was stirred at rt for 1 h. The volatiles were removed *in vacuo* and the resulting residue washed with hexane (3 × 1 mL) to afford the crude product. The crude compound was purified by column chromatography (silica; 95:5 CH_2Cl_2:CH_3OH) to yield the title compound as a bright orange solid. Yield: 5.5 mg (71%).

^{1}H NMR (500 MHz, CD_2Cl_2): δ 8.34 (t, $^3J_{HH}$ = 8.0, 1H, py), 8.15 (d, $^3J_{HH}$ = 8.0, 2H, py), 7.37 (d, $^3J_{HH}$ = 8.6, 4H, Ph), 6.83 (d, $^3J_{HH}$ = 8.6, 4H, Ph), 5.48 (dd, $^3J_{HH}$ = 13.2, $^3J_{HH}$ = 10.2, 2H, ox{CH}), 5.38 (dd, $^3J_{HH}$ = 10.2, $^2J_{HH}$ = 8.7, 2H, ox{CH_2}), 4.73 (dd, $^3J_{HH}$ = 13.1, $^2J_{HH}$ = 8.7, 2H, ox{CH_2}), 4.10 – 3.96 (m, 4H, CH_2), 1.78 – 1.66 (m, 4H, CH_2), 1.46 – 1.18 (m, 16H, CH_2).

^{13}C{^{1}H} NMR (126 MHz, CD_2Cl_2): δ 168.3 (d, $^2J_{RhC}$ = 2.1, ox{OCN}), 159.9 (Ph), 147.7 (py), 140.6 (py), 130.8 (Ph), 127.6 (py), 127.2 (Ph), 115.3 (Ph), 79.8 (ox{CH_2}), 68.7 (ox{CH}), 68.4 (CH_2), 30.0 (CH_2), 29.9 (CH_2), 29.4 (CH_2), 28.9 (CH_2), 26.0 (CH_2).

HR ESI-MS (CH_3CN, 180 °C, 3 kV) positive ion: 798.1113 ([M+Na]$^+$, calcd 798.1110) *m*/*z*.

[Rh(**ᴿpybox**)Cl] (**28a**)

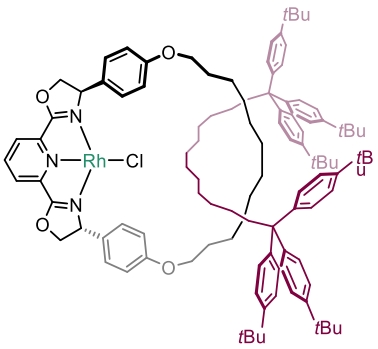

A solution of **ᴿpybox** (15.6 mg, 10.1 μmol) and $[Rh(COE)_2Cl]_2$ (3.6 mg, 5.1 μmol) in THF (0.5 mL) was stirred at rt for 48 h. The volatiles were removed *in vacuo* and the resulting residue washed with TMS (6 × 1 mL, with sonication) to afford the title compound as a dark black solid. Yield: 13.8 mg (80%). Characterised by NMR spectroscopy as a mixture of outer- and inner-sphere chloride complex (14:86, THF-d_8).

Major species:

^{1}H NMR (500 MHz, THF-d_8): δ 8.39 (t, $^{3}J_{HH}$ = 7.8, 1H, py), 7.29 – 7.19 (m, 18H, 2×py, 12× Ar{axle}, 4×Ar{macro}), 7.14 (d, $^{3}J_{HH}$ = 8.4, 12H, Ar{axle}), 6.57 (d, $^{3}J_{HH}$ = 8.3, 4H, Ar{macro}), 5.50 (dd, $^{3}J_{HH}$ = 13.3, $^{3}J_{HH}$ = 9.6, 2H, ox{CH}), 5.23 (app t, J_{HH} = 8.8, 2H, ox{CH_2}), 4.32 (dd, $^{3}J_{HH}$ = 13.3, $^{2}J_{HH}$ = 8.1, 2H, ox{CH_2}), 3.85 (td, 2H, $^{2}J_{HH}$ = 9.1, $^{3}J_{HH}$ = 5.9, CH_2), 3.75 (td, $^{2}J_{HH}$ = 8.8, $^{3}J_{HH}$ = 6.0, 2H, CH_2), 2.59 – 2.32 (br m, 4H, {Ar_3C}CH_2), 1.47 – 0.80 (m, 94H, 40×CH_2, 54×*t*Bu).

^{1}H NMR (400 MHz, MTBE, selected data): δ 8.73 (t, $^{3}J_{HH}$ = 7.9, 1H, py), 7.85 (d, $^{3}J_{HH}$ = 8.5, 4H, Ar{macro}), 7.76 (d, $^{3}J_{HH}$ = 8.1, 12H, Ar{axle}), 7.68 (d, $^{3}J_{HH}$ = 8.3, 12H, Ar{axle}), 7.55 (d, $^{3}J_{HH}$ = 7.8, 2H, py), 7.18 (obsc, 4H, Ar{macro}), 6.06 (br, 2H, ox), 5.74 (app t, J_{HH} = 8.7, 2H, ox), 4.74 (br, 2H, ox), 4.50 – 4.28 (m, 4H, CH_2).

^{13}C{^{1}H} NMR (126 MHz, THF-d_8): δ 170.6 (d, $^{2}J_{RhC}$ = 4.1, ox{OCN}), 160.4 (Ar{macro}), 148.4 (Ar{axle}), 146.6 (Ar{axle}), 144.0 (py), 131.1 (Ar{macro}), 130.3 (Ar{macro}), 130.1 (Ar{axle}), 129.9 (d, $^{3}J_{RhC}$ = 1.7, py), 125.3 (Ar{axle}), 121.7 (d, $^{4}J_{RhC}$ = 1.2, py), 115.0 (Ar{macro}), 79.5 (ox{CH_2}), 71.3 (ox{CH}), 67.7 (CH_2), 56.4, (Ar_3C), 42.37 ({Ar_3C}CH_2), 35.0 (*t*Bu{C}), 32.3 (CH_2), 31.9 (*t*Bu{CH_3}), 31.5 (CH_2), 31.3 (CH_2), 31.2 (CH_2), 31.1 (CH_2), 30.6 (CH_2), 29.9 (CH_2), 29.2 (CH_2), 27.7 (CH_2), 26.1 (CH_2).

Minor species:

^{1}H NMR (500 MHz, THF-d_8, selected data): δ 8.48 (t, $^{3}J_{HH}$ = 7.8, 1H, py), 7.39 (d, $^{3}J_{HH}$ = 7.9, 2H, py), 5.59 (app t, J_{HH} = 5.6, 2H, ox{CH}), 5.26 (obsc, 2H, ox{CH_2}), 4.38 (dd, $^{3}J_{HH}$ = 13.4, $^{2}J_{HH}$ = 8.3, 2H, ox{CH_2}).

^{13}C{^{1}H} NMR (126 MHz, THF-d_8, selected data): δ 148.9 (Ar{axle}), 146.1 (Ar{axle}), 144.1 (py), 131.0 (Ar{macro}), 125.3 (Ar{axle}), 115.1 (Ar{macro}), 35.0 (*t*Bu{C}).

HR ESI-MS (CH_3OH, 180 °C, 3 kV) positive ion: 1661.0127 ([M–Cl]$^{+}$, calcd 1661.0128) *m*/*z*.

[Rh(**R**-**pybox**)Cl_3] (**28b**)

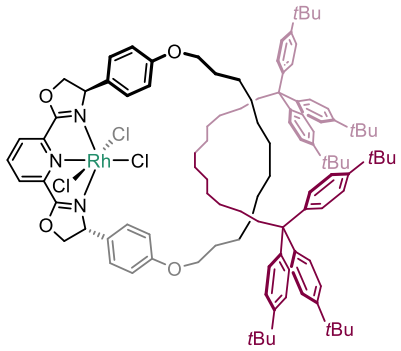

A solution of **28a** (9.6 mg, 5.7 µmol) and $PhICl_2$ (1.6 mg, 5.7 µmol) in THF (0.5 mL) was stirred at rt for 1 h. The volatiles were removed *in vacuo*. The crude compound was purified by column chromatography (silica; 99:1 CH_2Cl_2:CH_3OH, *Rf* = 0.14) to yield the title compound as a bright orange solid. Yield: 7.1 mg (70%).

^{1}H NMR (500 MHz, CD_2Cl_2): δ 8.30 (t, $^3J_{HH}$ = 8.1, 1H, py), 8.13 (d, $^3J_{HH}$ = 8.0, 2H, py), 7.30 – 7.27 (m, 12H, Ar{axle}), 7.25 (d, $^3J_{HH}$ = 8.6, 4H, Ar{macro}), 7.23 – 7.20 (m, 12H, Ar{axle}), 6.65 (d, $^3J_{HH}$ = 8.7, 4H, Ar{macro}), 5.46 (dd, $^3J_{HH}$ = 14.4, $^3J_{HH}$ = 9.8, 2H, ox{CH}), 5.27 (app t, J_{HH} = 9.3, 2H, ox{CH_2}), 4.65 (dd, $^3J_{HH}$ = 14.4, $^2J_{HH}$ = 8.8, 2H, ox{CH_2}), 3.88 – 3.73 (m, 4H, CH_2), 2.53 – 2.43 (m, 4H, {Ar_3C}CH_2), 1.69 (p, $^3J_{HH}$ = 7.0, 4H, CH_2), 1.47 – 1.06 (m, 82H, 28×CH_2, 54×*t*Bu), 1.03 – 0.88 (m, 8H, CH_2).

^{1}H NMR (400 MHz, THF-d_8): δ 8.42 (t, $^3J_{HH}$ = 8.0, 1H, py), 8.29 (d, $^3J_{HH}$ = 7.9, 2H, py), 7.36 (d, $^3J_{HH}$ = 8.1, 4H, Ar{macro}), 7.29 (d, $^3J_{HH}$ = 8.2, 12H, Ar{axle}), 7.22 (d, $^3J_{HH}$ = 8.2, 12H, Ar{axle}), 6.65 (d, $^3J_{HH}$ = 8.2, 4H, Ar{macro}), 5.55 (dd, $^3J_{HH}$ = 14.3, $^3J_{HH}$ = 9.8, 2H, ox{CH}), 5.36 (app t, J_{HH} = 9.2, 2H, ox{CH_2}), 4.63 (dd, $^3J_{HH}$ = 14.4, $^2J_{HH}$ = 8.5, 2H, ox{CH_2}), 3.89 – 3.74 (m, 4H, CH_2), 2.63 – 2.36 (m, 4H, {Ar_3C}CH_2), 1.67 (p, $^3J_{HH}$ = 6.7, 4H, CH_2), 1.41 – 0.87 (m, 90H, 36×CH_2, 54×*t*Bu).

^{13}C{^{1}H} NMR (126 MHz, CD_2Cl_2): δ 168.76 (d, $^2J_{RhC}$ = 1.6, ox{OCN}), 160.2 (Ar{macro}), 148.6 (Ar{axle}), 147.8 (py), 146.0 (Ar{axle}), 140.1 (py), 131.0 (Ar{macro}), 129.5 (Ar{axle}), 127.4 (py), 126.3 (Ar{macro}), 125.0 (Ar{axle}), 115.0 (Ar{macro}), 79.4 (ox{CH_2}), 69.2 (ox{CH}), 68.1 (CH_2), 56.1 (Ar_3C), 40.8 ({Ar_3C}CH_2), 34.7 (*t*Bu{C}), 31.7 (*t*Bu{CH_3}), 31.4 (CH_2), 30.9 (CH_2), 30.7 (CH_2), 30.6 (CH_2), 30.3 (CH_2), 30.2 (CH_2), 29.6 (CH_2), 29.3 (CH_2), 26.7 (CH_2), 25.8 (CH_2).

HR ESI-MS (CH_3OH, 180 °C, 3 kV) positive ion: 1788.9086 ([M+Na]$^+$, calcd 1788.9091) *m*/*z*.

[Rh(**R pybox**)$Cl_2(CD_2Cl)$] (**29**)

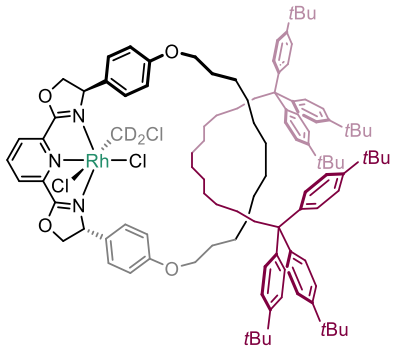

A solution of **28a** (5.9 mg, 3.5 μmol) in CD_2Cl_2 (0.5 mL) was stirred at rt for 1 h to afford the title compound in *ca*. 87% purity.

^{1}H NMR (500 MHz, CD_2Cl_2): δ 8.21 (t, $^3J_{HH}$ = 8.0, 1H, py), 8.00 (d, $^3J_{HH}$ = 8.8, 2H, py), 7.46 – 7.00 (m, 28H, 24×Ar{axle}, 4×Ar{macro}), 6.69 (d, $^3J_{HH}$ = 8.4, 2H, Ar{macro}), 6.65 (d, $^3J_{HH}$ = 8.6, 2H, Ar{macro}), 5.49 – 5.40 (m, 1H, ox{CH}), 5.30 – 5.13 (m, 3H, 1×ox{CH_2}, 2×ox{CH_2}), 4.76 (dd, $^2J_{HH}$ = 12.6, $^3J_{HH}$ = 9.0, 1H, ox{CH_2}), 4.51 (dd, $^2J_{HH}$ = 14.6, $^3J_{HH}$ = 8.2, 1H, ox{CH_2}), 3.93 – 3.71 (m, 4H, CH_2), 2.64 – 2.36 (m, 4H, CH_2), 1.81 – 1.62 (m, 6H, CH_2), 1.52 – 0.65 (m, 88H, 34×CH_2, 54×*t*Bu).

^{13}C{^{1}H} NMR (126 MHz, CD_2Cl_2, selected peaks): δ 169.4 (ox{OCN}), 167.6 (ox{OCN}), 160.4 (Ar{macro}), 160.2 (Ar{macro}), 148.8 (Ar{axle}), 148.7 (Ar{axle}), 148.6 (Ar{axle}), 147.1 (py), 146.8 (py), 145.9 (Ar{axle}), 145.8 (Ar{axle}), 145.6 (Ar{axle}), 138.5 (py), 131.02 (Ar{macro}), 130.98 (Ar{macro}), 129.5 (Ar{axle}), 129.4 (Ar{axle}), 129.3 (Ar{axle}), 128.7 (Ar{macro}), 127.5 (Ar{macro}), 126.6 (py), 125.8 (py), 125.1 (Ar{axle}), 125.04 (Ar{axle}), 125.01 (Ar{axle}), 124.9 (Ar{macro}), 115.04 (Ar{macro}), 114.96 (Ar{macro}), 79.5 (ox{CH_2}), 78.7 (ox{CH_2}), 69.3 (ox{CH}), 69.1 (ox{CH}), 68.3 (CH_2), 68.0 (CH_2), 56.1 (Ar_3C), 56.0 (Ar_3C), 55.95 (Ar_3C), 40.9 (app d, $^1J_{RhC}$ = 21, CD_2Cl), 40.4 ({Ar_3C}CH_2), 34.8 (*t*Bu{C}), 34.73 (*t*Bu{C}), 34.72 (*t*Bu{C}), 31.73 (*t*Bu{CH_3}), 31.7 (*t*Bu{CH_3}), 31.67 (*t*Bu{CH_3}), 31.6 (CH_2), 31.4 (CH_2), 31.0 (CH_2), 30.9 (CH_2), 30.8 (CH_2), 30.74 (CH_2), 30.71 (CH_2), 30.7 (CH_2), 30.6 (CH_2), 30.3 (CH_2), 30.2 (CH_2), 30.2 (CH_2), 30.1 (CH_2), 29.7 (CH_2), 29.3 (CH_2), 29.0 (CH_2), 26.8 (CH_2), 26.6 (CH_2), 26.0 (CH_2), 25.8 (CH_2), 25.7 (CH_2).

HR ESI-MS (CH_3OH, 180 °C, 3 kV) positive ion: 1746.9733 ([M–Cl]$^+$, calcd 1746.9793) *m*/*z*.

6.4.1.2. Generation of low coordinate complexes

General procedure for the preparation of samples for VT NMR measurements

In an argon filled glovebox, a J. Young valve NMR tube was charged with **27a**, **27b**, **28a** or **28b**, and Tl[BAr^F_4] or Na[BAr^F_4]. Deuterated solvent (CD_2Cl_2, THF-d_8, toluene-d_8, MTBE-d_{12}) was added shortly before measurements, inverted twice and kept at −78 °C at all times. The samples were then placed into a NMR spectrometer, pre-equilibrated to the required temperature and measured by ^{1}H NMR spectroscopy (600/500 MHz, 185 – 298 K).

[Rh(**^{M}pybox**)][BAr^F_4] (**30a**)

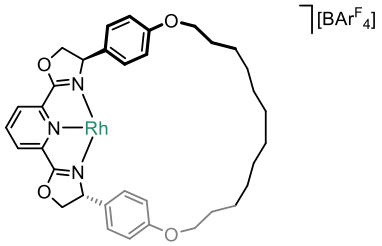

In a J. Young valve NMR tube a solution of **27a** (6.7 mg, 9.5 µmol) and Tl[BAr^F_4] (10.1 mg, 9.5 µmol) in THF-d_8 (0.475mL) was inverted twice to afford the title compound in quantitative spectroscopic yield. Characterised *in situ*.

^{1}H NMR (600 MHz, THF-d_8, 200 K): δ 8.40 (t, $^3J_{HH}$ = 8.0, 1H, py), 7.89 (br, 8H, Ar^F), 7.80 (d, $^3J_{HH}$ = 8.0, 2H, py), 7.74 (s, 4H, Ar^F), 7.46 (d, $^3J_{HH}$ = 7.9, 4H, Ph), 6.97 (d, $^3J_{HH}$ = 8.4, 4H, Ph), 5.58 – 5.49 (m, 4H, ox), 4.57 (dd, J_{HH} = 12.0, J_{HH} = 8.1, 2H, ox), 4.19 (dt, $^2J_{HH}$ = 11.3, $^3J_{HH}$ = 5.8, 2H, CH_2), 3.93 (dt, $^2J_{HH}$ = 10.6, $^3J_{HH}$ = 6.8, 2H, CH_2), 1.64 – 1.03 (m, 20H, CH_2).

^{1}H NMR (400 MHz, THF, selected data, 298 K): δ 8.63 (t, $^3J_{HH}$ = 7.9, 1H, py), 7.96 (d, $^3J_{HH}$ = 7.9, 2H, py), 7.70 (d, $^3J_{HH}$ = 8.1, 4H, Ph), 7.23 (d, $^3J_{HH}$ = 8.1, 4H, Ph), 5.88 – 5.69 (m, 4H, ox), 4.89 – 4.80 (m, 2H, ox).

^{1}H NMR (400 MHz, MTBE, selected data, 298 K): δ 8.74 (t, $^3J_{HH}$ = 8.5, 1H, py), 8.47 (d, $^3J_{HH}$ = 7.5, 2H, py), 8.33 (br, 8H, Ar^F), 8.07 (s, 4H, Ar^F), 7.74 (d, $^3J_{HH}$ = 7.8, 4H, Ph), 7.50 (d, $^3J_{HH}$ = 9.1, 4H, Ph).

[Rh(**ᴹpybox**)Cl_2][$BAr^F{}_4$] (**30b**)

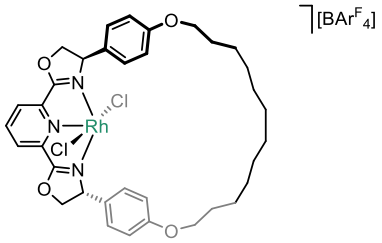

In a J. Young valve NMR tube a solution of **27b** (7.4 mg, 9.5 μmol) and Na[$BAr^F{}_4$] (8.4 mg, 9.5 μmol) in CD_2Cl_2 (0.635 mL) was inverted twice to afford the title compound in quantitative spectroscopic yield. Characterised *in situ*.

^{1}H NMR (600 MHz, CD_2Cl_2, 298 K): δ 8.43 (t, $^3J_{HH}$ = 8.0, 1H, py), 8.22 (d, $^3J_{HH}$ = 8.0, 2H, py), 7.73 (br, 8H, Ar^F), 7.56 (s, 4H, Ar^F), 7.40 (d, $^3J_{HH}$ = 8.2, 4H, Ph), 6.91 (d, $^3J_{HH}$ = 8.5, 4H, Ph), 5.50 – 5.40 (m, 4H, ox), 4.88 – 4.74 (m, 2H, ox), 4.16 – 3.93 (m, 4H, CH_2), 1.73 (p, $^3J_{HH}$ = 6.9, 4H, CH_2), 1.55 – 1.12 (m, 16H, CH_2).

[Rh(**ᴿpybox**)][$BAr^F{}_4$] (**31a**)

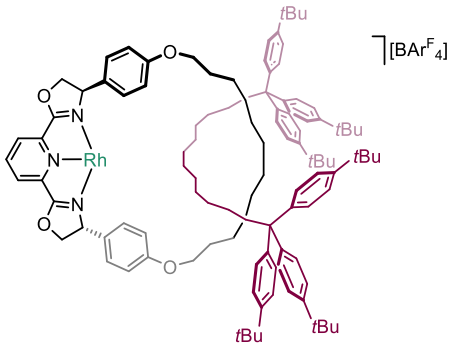

Method A: In a J. Young valve NMR tube a solution of **28a** (11.5 mg, 6.8 μmol) and Tl[$BAr^F{}_4$] (7.3 mg, 6.8 μmol) in THF-d_8 (0.450 mL) was inverted twice to afford the title compound in quantitative spectroscopic yield. Characterised *in situ*.

^{1}H NMR (600 MHz, THF-d_8, 298 K): δ 8.43 (t, $^3J_{HH}$ = 8.0, 1H, py), 7.89 (d, $^3J_{HH}$ = 7.9, 2H, py), 7.79 (br, 8H, Ar^F), 7.58 (s, 4H, Ar^F), 7.28 (d, $^3J_{HH}$ = 8.4, 12H, Ar{axle}), 7.22 (d, $^3J_{HH}$ = 8.6, 2H, Ar{macro}), 7.18 (d, $^3J_{HH}$ = 8.5, 12H, Ar{axle}), 7.14 (d, $^3J_{HH}$ = 8.5, 2H, Ar{macro}), 6.68 (d, $^3J_{HH}$ = 8.3, 4H, Ar{macro}), 5.46 – 5.31 (m, 4H, ox), 4.67 – 4.43 (m, 2H, ox), 3.93 – 3.84 (m, 2H, CH_2), 3.82 – 3.73 (m, 2H, CH_2), 2.65 – 2.41 (m, 4H, {Ar_3C}CH_2), 1.80 – 1.73 (obsc m, 4H, CH_2), 1.48 – 0.85 (m, 90H, 36×CH_2, 54×*t*Bu).

^{1}H NMR (600 MHz, THF-d_8, 185 K, selected data): δ 8.54 (t, $^3J_{HH}$ = 8.1, 1H, py), 8.10 (d, $^3J_{HH}$ = 7.8, 2H, py), 7.91 (br, 8H, Ar^F), 7.79 (s, 4H, Ar^F), 7.49 – 6.96 (m, 28H, Ar), 6.79 (br, 2H, Ar), 6.55 (br, 2H, Ar), 5.66 – 5.52 (m, 2H, ox), 5.42 (br, 1H, ox), 5.05 (br, 1H, ox), 4.65 (br, 2H, ox), 4.09 – 3.86 (m, 3H, CH_2), 3.44 (br, 1H, CH_2), 2.82 (br, 1H, CH_2), 2.53 (s, 3H,

{Ar_3C}CH_2), 2.30 (s, 1H, {Ar_3C}CH_2), 1.28 (br, 36×CH_2, 54×*t*Bu), 0.48 (br, 1H, CH_2), 0.37 (br, 1H, CH_2).

^{1}H NMR (600 MHz, toluene-d_8, 298 K): δ 8.33 (br, 8H, Ar^F), 7.66 (s, 4H, Ar^F), 7.46 –7.14 (m, 32H, 24×Ar{axle}, 8×Ar{macro}), 6.77 (br, 2H, py), 6.60 (br, 1H, py), 4.61 (s, 2H, ox{CH}), 4.29 (br, 2H, ox{CH_2}), 3.88 (q, $^3J_{HH}$ = 8.4, 2H, CH_2), 3.81 – 3.55 (m, 4H, 2×CH_2, 2×ox{CH_2}), 2.93 – 2.49 (m, 4H, {Ar_3C}CH_2), 1.77 (s, 2H, CH_2), 1.59 – 0.81 (m, 38×CH_2, 54×*t*Bu).

^{1}H NMR (400 MHz, MTBE, 298 K, selected data): δ 8.81 (t, $^3J_{HH}$ = 8.0, 1H), 8.33 (br, 8H, Ar^F), 8.32 (obsc, 2H, py), 8.06 (s, 4H, Ar^F), 7.91 – 7.57 (m, 28H, 4×Ar{macro}, 24×Ar{axle}), 7.25 (d, $^3J_{HH}$ = 8.1, 4H, Ar{macro}), 5.96 – 5.81 (m, 4H, ox), 5.18 – 5.00 (m, 2H, ox).

Method B: In a J. Young valve NMR tube a solution of **^{R}pybox** (7.2 mg, 4.6 μmol) and [Rh(Binor)PCy_3][BAr^F_4] (6.6 mg, 4.6 μmol) was mixed in C_6H_5F (0.5 mL) at rt for 18 h to afford the title compound in quantitative spectroscopic yield.

^{1}H NMR (300 MHz, C_6H_5F, selected data): δ 8.31 (br, 8H, Ar^F), 7.62 (s, 4H, Ar^F), 4.19 – 3.63 (m, 4H, CH_2), 2.80 – 2.48 (m, 4H, {Ar_3C}CH_2).

^{1}H NMR (300 MHz, THF, selected data): δ 8.72 (t, $^3J_{HH}$ = 7.4, 1H), 8.11 (br, 8H, Ar^F), 7.98 (d, $^3J_{HH}$ = 7.9, 2H, py), 7.88 (s, 4H, Ar^F), 7.65 – 7.35 (m, 28H, 4×Ar{macro}, 24×Ar{axle}), 6.99 (d, $^3J_{HH}$ = 8.3, 4H, Ar{macro}), 5.86 – 5.64 (m, 4H, ox), 4.94 – 4.75 (m, 2H, ox).

[Rh(**^{R}pybox**)Cl_2][BAr^F_4] (**31b**)

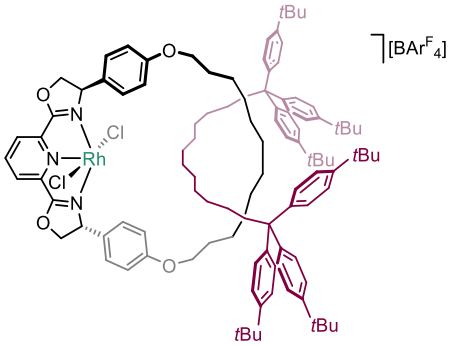

In a J. Young valve NMR tube a solution of **28b** (15.9 mg, 9.0 μmol) and Na[BAr^F_4] (8.0 mg, 9.0 μmol) in CD_2Cl_2 (0.600 mL) was inverted twice to afford the title compound in quantitative spectroscopic yield. Characterised *in situ*.

^{1}H NMR (600 MHz, CD_2Cl_2, 298 K): δ 8.37 (t, $^3J_{HH}$ = 8.0, 1H, py), 8.16 (d, $^3J_{HH}$ = 7.9, 2H, py), 7.74 (br, 8H, Ar^F), 7.56 (s, 4H, Ar^F), 7.31 (d, $^3J_{HH}$ = 8.1, 12H, Ar{axle}), 7.29 – 7.22 (m, 2H, Ar{macro}), 7.19 (d, $^3J_{HH}$ = 8.2, 14H, 2×Ar{macro}, 12×Ar{axle}), 6.81 (d, $^3J_{HH}$ = 8.1, 4H, Ar{macro}), 5.45 – 5.29 (obsc m, 4H, ox), 4.72 (br, 2H, ox), 4.00 – 3.84 (m, 4H, CH_2), 2.56 (br, 4H, {Ar_3C}CH_2), 1.75 (br, 4H, CH_2), 1.30 (br, 90, 36×CH_2, 54×*t*Bu).

^{1}H NMR (600 MHz, CD_2Cl_2, 185 K): δ 8.32 (t, $^3J_{HH}$ = 8.2, 1H, py), 8.25 – 7.97 (m, 2H, py), 7.75 (br, 8H, Ar^F), 7.52 (s, 4H, Ar^F), 7.44 – 6.35 (m, 32H, Ar), 5.45 – 5.27 (m, 4H, ox), 4.78 (br, 1H, ox), 4.59 (br, 1H, ox), 3.98 (br, 1H, CH_2), 3.63 (br, 3H, CH_2), 2.65 (br, 1H, CH_2), 2.43 (br, 4H, {Ar_3C}CH_2), 1.91 (s, 1H, CH_2), 1.71 (s, 2H, CH_2), 1.19 (s, 90H, 35×CH_2, 54×*t*Bu), −0.15 (br, 1H, CH_2).

^{1}H NMR (600 MHz, THF-d_8, 298 K): δ 8.60 (t, $^3J_{HH}$ = 8.0, 1H, py), 8.47 (d, $^3J_{HH}$ = 8.0, 2H, py), 7.79 (br, 8H, Ar^F), 7.57 (s, 4H, Ar^F), 7.40 (d, $^3J_{HH}$ = 8.3, 4H, Ar{macro}), 7.28 (d, $^3J_{HH}$ = 8.3, 12H, Ar{axle}), 7.18 (d, $^3J_{HH}$ = 8.4, 12H, Ar{axle}), 6.79 (d, $^3J_{HH}$ = 8.3, 4H, Ar{macro}), 5.58 (dd, $^2J_{HH}$ = 14.2, $^3J_{HH}$ = 9.8, 2H, ox), 5.51 (app t, J_{HH} = 9.2, 2H, ox), 4.88 (dd, $^2J_{HH}$ = 14.2, $^3J_{HH}$ = 8.7, 2H, ox), 3.90 (app q, J_{HH} = 7.7, 4H, CH_2), 2.59 – 2.48 (m, 4H, {Ar_3C}CH_2), 1.81 – 1.73 (m, 2H, CH_2), 1.48 – 1.01 (m, 92H, 38×CH_2, 54×*t*Bu).

Preparation of MTBE-d_{12}

The title compound was synthesised using an adapted literature procedure.[358] Under nitrogen, concentrated sulphuric acid-d_2 (2.85 g, 28.5 mmol) was added to ice-cooled methanol-d_4 (6.43 g, 178 mmol). The mixture was warmed to rt after which *tert*-butyl alcohol-d_{10} (15 g, 178 mmol) was added and the resulting solution heated at reflux for 3 h. The mixture was quenched with D_2O (25 mL) distilled though a Vigreux column and the fraction of b.p. 51—56 °C collected. This was dried over two batches of 4 Å sieves, followed by drying over sodium and then stored over fresh 3 Å molecular sieves, under argon. Yield: 2.23 g (12%).

^{1}H NMR (300 MHz, MTBE-d_{12}): δ 3.16 (p, $^2J_{DH}$ = 1.6, CH_3), 1.16 (p, $^2J_{DH}$ = 2.0, *t*Bu). ^{1}H NMR spectrum was referenced to TMS (δ 0 ppm).

6.4.1.3. Preparation of carbonyl derivatives

[Rh(**^{M}pybox**)(CO)][BAr^F_4] (**32a**)

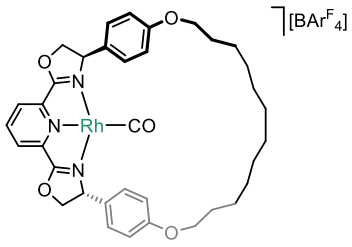

A suspension of **27a** (7.1 mg, 10 µmol) and Tl[BAr^F_4] (10.7 mg, 10 µmol) in MTBE (0.5 mL) was stirred at rt for 1 h. The suspension was freeze-pump-thaw degassed, placed under an atmosphere of CO and then stirred at rt for 30 min. The suspension was filtered and the volatiles were removed *in vacuo* to yield the title compound as a foamy dark green solid. Yield: 13.9 mg (76%).

^{1}H NMR (500 MHz, CD_2Cl_2): δ 8.16 (t, $^{3}J_{HH}$ = 8.0, 1H, py), 7.88 (d, $^{3}J_{HH}$ = 8.0, 2H, py), 7.72 (br, 8H, Ar^F), 7.55 (s, 4H, Ar^F), 7.18 – 7.13 (m, 4H, Ph), 6.95 – 6.89 (m, 4H, Ph), 5.35 (app t, J_{HH} = 9.9, 2H, ox{CH_2}), 5.12 (dd, $^{3}J_{HH}$ = 12.6, $^{3}J_{HH}$ = 10.1, 2H, ox{CH}), 4.67 (dd, $^{3}J_{HH}$ = 12.6, $^{2}J_{HH}$ = 9.4, 2H, ox{CH_2}), 4.13 – 4.05 (m, 2H, CH_2), 4.05 – 3.97 (m, 2H, CH_2), 1.71 (p, $^{3}J_{HH}$ = 6.8, 4H, CH_2), 1.44 – 1.35 (m, 4H, CH_2), 1.35 – 1.19 (m, 12H, CH_2).

^{13}C{^{1}H} NMR (126 MHz, CD_2Cl_2): δ 187.5 (d, $^{1}J_{RhC}$ = 76, RhCO), 167.8 (app d, $^{2}J_{RhC}$ = 3.1, ox{OCN}), 162.1 (q, $^{1}J_{CB}$ = 50, Ar^F), 160.8 (Ph), 147.1 (py), 143.3 (py), 135.4 (Ar^F), 130.1 (Ph), 129.4 (qq, $^{2}J_{FC}$ = 32, $^{3}J_{CB}$ = 3, Ar^F), 127.2 (Ph), 125.0 (q, $^{1}J_{FC}$ = 272, Ar^F), 125.3 (py), 118.1 (sept, $^{3}J_{FC}$ = 4, Ar^F), 116.3 (Ph), 79.9 (ox{CH_2}), 69.9 (d, $^{2}J_{RhC}$ = 2.5, ox{CH}), 68.5 (CH_2), 29.4 (CH_2), 28.8 (CH_2), 28.4 (CH_2), 25.6 (CH_2), 23.2 (CH_2).

HR ESI-MS (CH_3OH, 180 °C, 3 kV) positive ion: 670.2145 ([M–CO]$^+$, calcd 670.2147) *m*/*z*.

FT-IR (CH_2Cl_2): ν(CO) 2022 cm^{-1}.

[Rh(**^{M}pybox**)Cl_2(CO)][BAr^F_4] (**32b**)

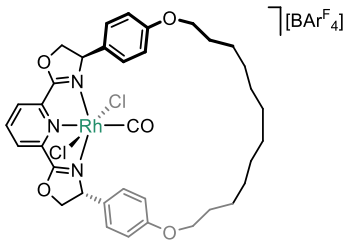

A suspension of **27b** (7.8 mg, 10 μmol) and Na[BAr^F_4] (8.9 mg, 10 μmol) in CD_2Cl_2 (0.5 mL) was stirred at rt for 1 h. The suspension was freeze-pump-thaw degassed, placed under an atmosphere of CO and then heated at 50 °C for 18 h. The resulting suspension was filtered and volatiles removed *in vacuo* to yield the title compound as a yellow glassy solid. Yield: 9.4 mg (59%).

^{1}H NMR (500 MHz, CD_2Cl_2): δ 8.64 (t, $^{3}J_{HH}$ = 8.1, 1H, py), 8.37 (d, $^{3}J_{HH}$ = 8.1, 2H, py), 7.73 (br, 8H, Ar^F), 7.56 (s, 4H, Ar^F), 7.38 – 7.31 (m, 4H, Ph), 6.99 – 6.92 (m, 4H, Ph), 5.54 (app t, J_{HH} = 9.6, 2H, ox{CH_2}), 5.41 (dd, $^{3}J_{HH}$ = 13.9, $^{3}J_{HH}$ = 9.9, 2H, ox{CH}), 4.94 (dd, $^{3}J_{HH}$ = 13.8, $^{2}J_{HH}$ = 9.2, 2H, ox{CH_2}), 4.10 – 3.94 (m, 4H, CH_2), 1.83 – 1.66 (m, 4H, CH_2), 1.52 – 1.12 (m, 16H, CH_2).

^{13}C{^{1}H} NMR (126 MHz, CD_2Cl_2): δ 171.3 (d, $^{1}J_{RhC}$ = 54, RhCO), 168.3 (ox{OCN}), 162.3 (q, $^{1}J_{CB}$ = 50, Ar^F), 161.70 (Ph), 145.8 (py), 145.1 (py), 135.4 (Ar^F), 131.4 (Ph), 129.7 (py), 129.4 (qq, $^{2}J_{FC}$ = 32, $^{3}J_{CB}$ = 3, Ar^F), 125.0 (q, $^{1}J_{FC}$ = 272, Ar^F), 123.5 (Ph), 118.1 (sept, $^{3}J_{FC}$ = 4, Ar^F), 116.2 (Ph), 80.1 (ox{CH_2}), 69.6 (ox{CH}), 68.6 (CH_2), 29.4 (CH_2), 29.1 (CH_2), 28.7 (CH_2), 28.5 (CH_2), 25.7 (CH_2).

HR ESI-MS (CH_3OH, 180 °C, 3 kV) positive ion: 822.1548 ([M+NaOMe]$^+$, calcd 822.1554) *m*/*z*.

FT-IR (CH_2Cl_2): ν(CO) 2150 cm^{-1}.

[Rh(**^{R}pybox**)(CO)][BAr^F_4] (*mono*-**33a**)

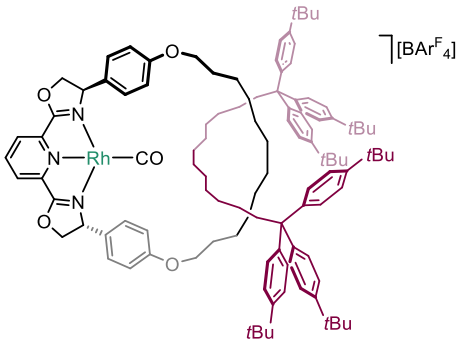

A suspension of **28a** (9.1 mg, 5.4 μmol) and Tl[BAr^F_4] (5.8 mg, 5.4 μmol) in THF (0.5 mL) was stirred for at rt for 1 h. The suspension was freeze-pump-thaw degassed, placed under an atmosphere of CO and then stirred at rt for 30 min. The resulting suspension was filtered and the volatiles were removed *in vacuo*. The sample was then dissolved in CH_2Cl_2 and dried (10 × 5 mL) to remove all traces of *bis*-**33a**, to yield the title compound as a foamy dark green solid. Yield: 10.2 mg (74%).

^{1}H NMR (500 MHz, CD_2Cl_2): δ 8.17 (t, $^3J_{HH}$ = 8.0, 1H, py), 7.88 (d, $^3J_{HH}$ = 8.0, 2H, py), 7.73 (br, 8H, Ar^F), 7.56 (s, 4H, Ar^F), 7.35 (d, $^3J_{HH}$ = 8.4, 12H, Ar{axle}), 7.24 (d, $^3J_{HH}$ = 8.3, 12H, Ar{axle}), 7.00 (d, $^3J_{HH}$ = 8.3, 4H, Ar{macro}), 6.70 (d, $^3J_{HH}$ = 8.4, 4H, Ar{macro}), 5.26 (app t, J_{HH} = 9.4, 2H, ox{CH_2}), 5.06 (dd, $^3J_{HH}$ = 14.3, $^3J_{HH}$ = 9.6, 2H, ox{CH}), 4.51 (dd, $^3J_{HH}$ = 14.3, $^2J_{HH}$ = 9.2, 2H, ox{CH_2}), 3.76 (t, $^3J_{HH}$ = 7.5, 4H, CH_2), 2.56 – 2.42 (m, 4H, {Ar_3C}CH_2), 1.74 (p, $^3J_{HH}$ = 7.2, 4H, CH_2), 1.40 – 1.17 (m, 74H, 20×CH_2, 54×*t*Bu), 1.10 – 0.76 (m, 16H, CH_2).

^{1}H NMR (500 MHz, THF-d_8): δ 8.40 (t, $^3J_{HH}$ = 8.0, 1H, py), 8.16 (d, $^3J_{HH}$ = 8.0, 2H, py), 7.79 (br, 8H, Ar^F), 7.57 (s, 4H, Ar^F), 7.31 (d, $^3J_{HH}$ = 8.4, 12H, Ar{axle}), 7.18 (d, $^3J_{HH}$ = 8.5, 12H, Ar{axle}), 7.11 (d, $^3J_{HH}$ = 8.3, 4H, Ar{macro}), 6.73 (d, $^3J_{HH}$ = 8.3, 4H, Ar{macro}), 5.39 (app t, J_{HH} = 9.3, 2H, ox{CH_2}), 5.18 (dd, $^3J_{HH}$ = 14.1, $^3J_{HH}$ = 9.6, 2H, ox{CH}), 4.58 (dd, $^3J_{HH}$ = 14.2, $^2J_{HH}$ = 9.0, 2H, ox{CH_2}), 3.88 – 3.74 (m, 4H, CH_2), 2.57 – 2.44 (m, 4H, {Ar_3C}CH_2), 1.57 – 0.77 (m, 94H, 40×CH_2, 54×*t*Bu).

^{13}C{^{1}H} NMR (126 MHz, CD_2Cl_2): δ 187.8 (d, $^1J_{RhC}$ = 75, RhCO), 168.8 (d, $^2J_{RhC}$ = 3, ox{OCN}), 162.2 (q, $^1J_{CB}$ = 50, Ar^F), 161.1 (Ar{macro}), 149.5 (Ar{axle}), 147.0 (py), 146.3 (Ar{axle}), 143.4 (py), 135.4 (Ar^F), 130.1 (Ar{macro}), 129.4 (qq, $^2J_{FC}$ = 32, $^3J_{CB}$ = 3, Ar^F), 129.5 (Ar{axle}), 125.5 (Ar{axle}), 125.4 (py), 125.4 (Ar{macro}), 125.2 (q, $^1J_{FC}$ = 272, Ar^F), 118.1 (sept, $^3J_{FC}$ = 4, Ar^F), 115.9 (Ar{macro}), 79.7 (ox{CH_2}), 70.9 (ox{CH}), 68.1 (CH_2), 56.1

(Ar_3C), 40.7 ({Ar_3C}CH_2), 34.8 (*t*Bu{C}), 31.7 (*t*Bu{CH_3}), 31.4 (CH_2), 30.6 (CH_2), 30.5 (CH_2), 30.4 (CH_2), 30.3 (CH_2), 29.9 (CH_2), 29.2 (CH_2), 28.4 (CH_2), 26.7 (CH_2), 25.2 (CH_2).

HR ESI-MS (CH_3OH, 180 °C, 3 kV) positive ion: 1689.0043 ($[M]^+$, calcd 1689.0077) *m*/*z*.

FT-IR (CH_2Cl_2): ν(CO) 2030 cm^{-1}.

Generation of [Rh(**R pybox**)(CO)][BAr^F_4] (*bis*-**33a**)

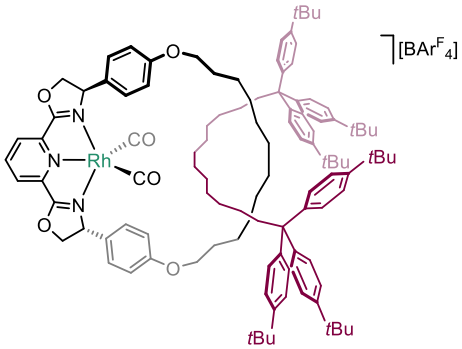

A solution of *mono*-**33a** (30.3 mg, 11.9 µmol) and CD_2Cl_2 (0.5 mL) in a J. Young valve NMR tube was freeze-pump-thaw degassed and placed under an atmosphere of CO to afford the title compound in quantitative spectroscopic yield.

^{1}H NMR (500 MHz, CD_2Cl_2/CO, 298 K): δ 8.22 (br, 2H, py), 8.08 (br, 1H, py), 7.73 (br, 8H, Ar^F), 7.56 (s, 4H, Ar^F), 7.44 – 6.97 (m, 28H, 24×Ar{axle}, 4×Ar{macro}), 6.79 (br, 4H, Ar{macro}), 5.53 (app t, J_{HH} = 10.4, 1H, ox{CH}), 5.34 (obsc, 2H, 1×ox{CH_2}, 1×ox{CH}), 4.96 (br, 2H, 2×ox{CH_2}), 4.55 (app t, J_{HH} = 9.5, 1H, ox{CH_2}), 4.16 (br, 1H, CH_2), 3.99 – 3.79 (m, 3H, CH_2), 2.59 – 2.22 (m, 4H, {Ar_3C}CH_2), 1.84 – 1.65 (m, 4H, CH_2), 1.54 – 0.59 (m, 90H, 36×CH_2, 54×*t*Bu).

^{1}H NMR (400 MHz, THF-d_8/CO, 298 K): δ 8.49 (br, 1H, py), 8.34 (br, 2H, py), 7.79 (m, 8H, Ar^F), 7.57 (s, 4H, Ar^F), 7.44 – 6.98 (m, 28H, 24×Ar{axle}, 4×Ar{macro}), 6.80 (br, 4H, Ar{macro}), 5.64 – 5.29 (m, 3H, ox), 5.03 (br, 2H, ox), 4.54 (br, 1H, ox), 3.91 (s, 4H, CH_2), 2.78 – 2.23 (m, 4H, {Ar_3C}CH_2), 1.28 (s, 94H, 40×CH_2, 54×*t*Bu).

^{1}H NMR (600 MHz, THF-d_8/CO, 185 K, selected data): δ 8.52 (t, $^3J_{HH}$ = 8.0, 1H, py), 8.37 (d, $^3J_{HH}$ = 7.9, 2H, py), 7.46 – 7.05 (m, 28H, 24×Ar{axle}, 4×Ar{macro}), 7.01 – 6.60 (m, 4H, Ar{macro}), 5.49 (br, 2H, ox), 5.11 (br, 2H, ox), 4.64 (br, 2H, ox).

^{13}C{^{1}H} NMR (126 MHz, CD_2Cl_2/CO, 298 K, selected data): δ 162.2 (q, $^1J_{CB}$ = 50, Ar^F), 159.5 (Ar{macro}), 149.1 (Ar{axle}), 145.6 (Ar{axle}), 143.8 (py), 135.4 (Ar^F), 129.8 (py), 129.4 (qq, $^2J_{FC}$ = 32, $^3J_{CB}$ = 3, Ar^F), 125.2 (q, $^1J_{FC}$ = 272, Ar^F), 118.1 (sept, $^3J_{FC}$ = 4, Ar^F), 116.4 (Ar{macro}), 115.3 (Ar{macro}), 80.5 (ox{CH_2}), 75.1 (ox{CH_2}), 71.1 (ox{CH}), 70.0

(ox{CH}), 68.2 (CH_2), 56.0 (Ar_3C), 40.7 ({Ar_3C}CH_2), 34.8 (*t*Bu{C}), 31.7 (*t*Bu{CH_3}), 30.6 (CH_2), 29.5 (CH_2), 26.4 (CH_2).

FT-IR (CH_2Cl_2/CO): ν(CO) 2041, 2101 cm^{-1}.

[Rh(**^{R}pybox**)Cl_2(CO)][BAr^F_4] (**33b**)

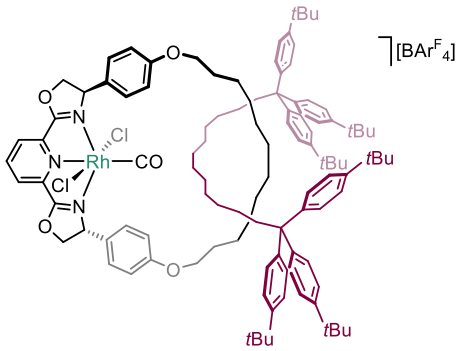

A suspension of **28b** (15.9 mg, 9 µmol) and Na[BAr^F_4] (8.0 mg, 9 µmol) in CD_2Cl_2 (0.5 mL) was stirred for at rt for 1 h. The suspension was freeze-pump-thaw degassed, placed under an atmosphere of CO and then stirred at 50 °C for 7 d. The resulting suspension was filtered and the volatiles were removed *in vacuo* to yield the title compound as a glassy yellow solid. Yield: 21.2 mg (89%).

^{1}H NMR (500 MHz, CD_2Cl_2): δ 8.64 (t, $^3J_{HH}$ = 8.1, 1H, py), 8.38 (d, $^3J_{HH}$ = 8.1, 2H, py), 7.73 (br, 8H, Ar^F), 7.57 (s, 4H, Ar^F), 7.32 – 7.28 (m, 12H, Ar{axle}), 7.25 (d, $^3J_{HH}$ = 8.3, 4H, Ar{macro}), 7.22 – 7.18 (m, 12H, Ar{axle}), 6.80 (d, $^3J_{HH}$ = 8.2, 4H, Ar{macro}), 5.50 – 5.41 (m, 4H, 2×ox{CH}, 2×ox{CH_2}), 4.87 – 4.77 (m, 2H, ox{CH_2}), 3.81 (t, $^3J_{HH}$ = 7.4, 4H, CH_2), 2.52 – 2.46 (m, 4H, {Ar_3C}CH_2), 1.84 – 1.68 (m, 4H, CH_2), 1.44 – 1.15 (m, 78H, 24×CH_2, 54×*t*Bu), 1.08 – 0.81 (m, 12H, CH_2).

^{13}C{^{1}H} NMR (126 MHz, CD_2Cl_2): δ 172.7 (d, $^1J_{RhC}$ = 55, RhCO), 169.3 (d, $^2J_{RhC}$ = 1.6, ox{OCN}), 162.3 (q, $^1J_{CB}$ = 50, Ar^F), 161.9 (Ar{macro}), 148.9 (Ar{axle}), 145.8 (py), 145.6 (Ar{axle}), 145.2 (py), 135.4 (Ar^F), 131.0 (Ar{macro}), 129.8 (py), 129.4 (qq, $^2J_{FC}$ = 32, $^3J_{CB}$ = 3, Ar^F), 129.3 (Ar{axle}), 125.2 (q, $^1J_{FC}$ = 272, Ar^F), 125.1 (Ar{axle}), 122.9 (Ar{macro}), 118.1 (sept, $^3J_{FC}$ = 4, Ar^F), 116.3 (Ar{macro}), 79.9 (ox{CH_2}), 70.3 (ox{CH}), 68.3 (CH_2), 55.9 (Ar_3C), 40.8 ({Ar_3C}CH_2), 34.8 (*t*Bu{C}), 31.7 (*t*Bu{CH_3}), 31.4 (CH_2), 30.8 (CH_2), 30.5 (CH_2), 30.4 (CH_2), 30.3 (CH_2), 29.9 (CH_2), 29.2 (CH_2), 28.7 (CH_2), 26.6 (CH_2), 25.2 (CH_2).

HR ESI-MS (CH_3OH, 180 °C, 3 kV) positive ion: 1748.9624 ([M−CO+H_2O]$^+$, calcd 1748.9611) *m*/*z*.

FT-IR (CH_2Cl_2): ν(CO) 2154 cm^{-1}.

Redox shuttling between carbonyl complexes **33a** and **33b**

Oxidation of **33a**: In a J. Young valve NMR tube a solution of *mono*-**33a** (11.0 mg, 4.3 μmol) and $PhICl_2$ (1.2 mg, 4.3 μmol) in MTBE (0.5 mL) was mixed at rt for 1 h to afford **33b** in quantitative spectroscopic yield.

^{1}H NMR (400 MHz, MTBE, selected data): δ 9.24 (t, $^3J_{HH}$ = 8.0, 1H, py), 9.10 (d, $^3J_{HH}$ = 8.0, 2H, py), 8.25 (d, $^3J_{HH}$ = 7.8, 4H, Ar{macro}), 7.82 (d, $^3J_{HH}$ = 8.3, 12H, Ar{axle}), 7.71 (d, $^3J_{HH}$ = 8.3, 12H, Ar{axle}), 7.35 (d, $^3J_{HH}$ = 8.2, 4H, Ar{macro}), 6.24 – 5.98 (m, 4H, ox), 5.44 (dd, J_{HH} = 13.7, J_{HH} = 7.1, 2H, ox).

Reduction of **33b**: In a J. Young valve NMR tube a solution of **33b** (21.8 mg, 8.3 μmol) and activated Zn powder (1.1 mg, 16.6 μmol) in MTBE (0.5 mL) was mixed at rt for 120 h to afford *mono*-**33a** in quantitative spectroscopic yield.

^{1}H NMR (400 MHz, MTBE, selected data): δ 8.73 (t, $^3J_{HH}$ = 8.2, 1H, py), 8.52 (d, $^3J_{HH}$ = 8.0, 2H, py), 7.88 – 7.67 (m, 24H, Ar{axle}), 7.60 (d, $^3J_{HH}$ = 8.2, 4H, Ar{macro}), 7.25 (d, $^3J_{HH}$ = 8.3, 4H, Ar{macro}), 5.91 (app t, J_{HH} = 9.3, 2H, ox), 5.69 (dd, J_{HH} = 13.9, J_{HH} = 9.8, 2H, ox), 5.09 (dd, J_{HH} = 14.4, J_{HH} = 9.1, 2H, ox).

6.4.2. Synthesis of rhodium and iridium 2,2'-biphenyl complexes

6.4.2.1. Generation of macrocyclic 2,2'-biphenyl complexes

[Ir(**^{M}pybox**)(biph)Cl] (**34**)

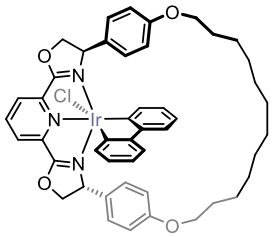

A solution of **^{M}pybox** (11.4 mg, 20 μmol) and $[Ir(COD)(biph)Cl]_2$ (9.7 mg, 10 μmol) in CH_2Cl_2 (5 mL) was stirred at rt for 18 h, quantitative conversion was observed by ^{1}H NMR spectroscopy. The volatiles were removed *in vacuo* and the brown-yellow residue washed with hexane (3 × 10 mL, with sonication) to afford the title compound. Characterised *in situ*.

^{1}H NMR (400 MHz, CD_2Cl_2): δ 8.02 – 7.85 (m, 3H, 3×py), 7.29 (d, $^3J_{HH}$ = 7.2, 1H, biph), 6.99 (d, $^3J_{HH}$ = 7.5, 1H, biph), 6.81 (d, $^3J_{HH}$ = 7.5, 1H, biph), 6.77 (d, $^3J_{HH}$ = 8.1, 2H, Ph), 6.69 (t, $^3J_{HH}$ = 7.3, 1H, biph), 6.51 – 6.30 (m, 5H, 2×Ph, 3×biph), 6.13 (d, $^3J_{HH}$ = 8.2, 2H, Ph), 6.06 (d, $^3J_{HH}$ = 8.2, 2H, Ph), 5.52 (d, $^3J_{HH}$ = 7.3, 1H, biph), 5.18 (app t, J_{HH} = 9.7, 1H, ox), 5.01 (app t, J_{HH} = 9.5, 1H, ox), 4.93 (app t, J_{HH} = 11.4, 1H, ox), 4.54 (dd, J_{HH} = 13.7, 9.1, 1H, ox), 4.46 (dd, J_{HH} =

12.5, 9.1, 1H, ox), 4.19 (dd, J_{HH} = 13.7, 9.9, 1H, ox), 4.09 – 4.00 (m, 1H, CH_2), 3.99 – 3.88 (m, 2H, CH_2), 3.88 – 3.77 (m, 1H, CH_2), 1.90 – 1.67 (m, 6H, CH_2), 1.48 (br, 12H, CH_2), 1.29 (br, 2H, CH_2).

HR ESI-MS (CH_3CN, 180 °C, 3 kV) positive ion: 912.3354 ($[M-Cl]^+$, calcd 912.3350) *m*/*z*.

[Ir(**^{M}pybox**)(biph)][BAr^F_4] (**35**)

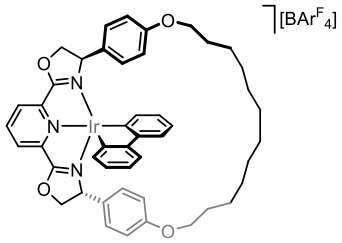

A solution of **34** (20 μmol, generated *in situ*) and Na[BAr^F_4] (17.7 mg, 20 μmol) in CD_2Cl_2 (0.5 mL) was stirred at rt for 18 h, quantitative conversion was observed by ^{1}H NMR spectroscopy. The resulting dark red suspension was filtered and the filtrate concentrated to dryness *in vacuo* to afford the title compound as a dark yellow solid. Characterised *in situ*.

^{1}H NMR (400 MHz, CD_2Cl_2): δ 8.23 (t, $^3J_{HH}$ = 8.0, 1H, py), 8.11 (d, $^3J_{HH}$ = 8.1, 2H, py), 7.73 (br, 8H, Ar^F), 7.56 (s, 4H, Ar^F), 7.06 (br, 4H), 6.50 (br, 8H), 6.08 (vbr, fwhm = 60, 4H), 5.12 (vbr, fwhm = 90, 1H, ox), 4.67 (vbr, fwhm = 90, 3H, ox), 3.97 (br, 6H), 3.84 (br, 4H), 1.90 – 1.72 (m, 6H, CH_2), 1.67 – 1.35 (m, 14H, CH_2). The ^{1}H NMR spectrum was unassigned as a consequence of the significant line broadening.

[Ir(**^{M}pybox**)(H_x)][BAr^F_4] (**36**)

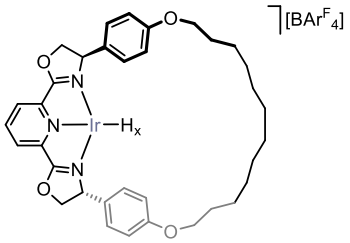

A solution of **35** (20 μmol, generated *in situ*) in CD_2Cl_2 (0.5 mL) was freeze-pump-thaw degassed, placed under an atmosphere of H_2, and then stirred at rt for 36 h generated the title compound in *ca*. 80% purity. Characterised *in situ*.

^{1}H NMR (400 MHz, CD_2Cl_2/H_2, selected data): δ 8.07 – 7.98 (m, 1H, py), 7.93 (d, $^3J_{HH}$ = 7.9, 2H, py), 7.73 (br, 8H, Ar^F), 7.56 (s, 4H, Ar^F), 7.17 (d, $^3J_{HH}$ = 8.1, 4H, Ph), 6.94 (d, $^3J_{HH}$ = 8.2, 4H, Ph), 5.40 (app t, J_{HH} = 9.6, 2H, ox), 5.00 (app t, J_{HH} = 10.9, 2H, ox), 4.85 (dd, J_{HH} = 13.1, J_{HH} = 9.3, 2H, ox), 4.19 – 3.95 (m, 4H, CH_2), 1.87 – 1.09 (br m, 20 H, CH_2), −23.12 (vbr, fwhm = 105, 2H, IrH).

6.4.2.2. Generation of rotaxane 2,2'-biphenyl complexes

[Rh(**ᴿpybox**)(biph)Cl] (**37**)

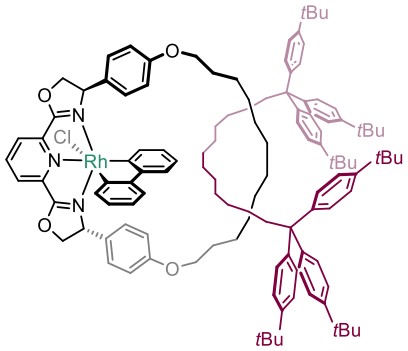

A solution of **ᴿpybox** (23.2 mg, 15 μmol) and [Rh(dtbpm)(biph)Cl] (8.9 mg, 15 μmol) in CD_3CN (0.5 mL) was stirred at 85 °C for 14 d. The volatiles were removed *in vacuo*. The yellow residue was extracted with pentane (5 mL), precipitated from toluene/TMS, filtered and then washed with HMDSO (3 × 5 mL) to afford the title compound as a brown-red solid in *ca*. 83% purity. Characterised *in situ*.

^{1}H NMR (400 MHz, CD_2Cl_2): δ 8.27 (d, $^3J_{HH}$ = 7.8, 1H, Ar), 8.18 (d, $^3J_{HH}$ = 8.4, 1H, Ar), 8.04 (d, $^3J_{HH}$ = 7.8, 1H, Ar), 7.84 (t, $^3J_{HH}$ = 7.7, 1H, Ar), 7.61 (d, $^3J_{HH}$ = 7.8, 1H, Ar), 7.45 (t, $^3J_{HH}$ = 7.5, 1H, Ar), 7.35 – 7.14 (m, 24H, Ar), 7.05 (d, $^3J_{HH}$ = 8.2, 6H, Ar{axle}), 6.94 (d, $^3J_{HH}$ = 8.3, 2H, Ar), 6.70 (d, $^3J_{HH}$ = 8.2, 2H, Ar), 6.63 (d, $^3J_{HH}$ = 8.4, 2H, Ar), 5.45 (q, J_{HH} = 7.5, 1H, biph), 5.25 (app t, J_{HH}= 8.9, 1H, ox), 4.71 (app t, J_{HH} = 9.3, 1H, ox), 4.28 (app t, J_{HH} = 8.1, 1H, ox), 4.08 – 3.69 (m, 7H, 3×ox, 4×CH_2), 2.54 – 2.40 (m, 4H, {Ar_3C}CH_2), 1.76 – 1.42 (m, 4H, CH_2), 1.44 – 1.08 (m, 78H, 24×CH_2, 54×*t*Bu), 1.06 – 0.50 (m, 12H, CH_2).

[Rh(**ᴿpybox**)(biph)][BAr^F_4] (**38**)

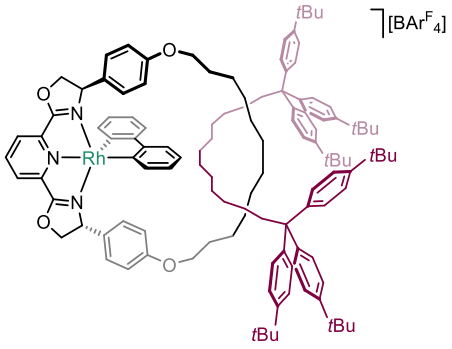

A solution of **37** (15 μmol, generated *in situ*) and Na[BAr^F_4] (13.3 mg, 15 μmol) in CD_2Cl_2 (0.5 mL) was stirred at rt for 18 h. The suspension was filtered followed by removal of the volatiles *in vacuo*, and washed with cold pentane (3 × 5 mL, −78 °C) to afford the title compound as a dark orange solid in *ca*. 90% purity. Characterised *in situ*.

^{1}H NMR (400 MHz, CD_2Cl_2): δ 8.05 – 7.87 (m, 2H, py), 7.73 (br, 8H, Ar^F), 7.56 (s, 4H, Ar^F), 7.41 – 7.05 (m, 35H, Ar), 6.97 (d, $^3J_{HH}$ = 8.1, 2H, Ar), 6.71 (d, $^3J_{HH}$ = 8.7, 2H, Ar), 6.66 (d, $^3J_{HH}$ = 7.9, 2H, Ar), 5.23 – 5.13 (m, 1H, ox), 4.91 (app t, J_{HH} = 9.6, 1H, ox), 4.75 – 4.60 (m, 1H, ox), 4.57 (br, 1H, ox), 4.03 – 3.63 (m, 6H, 2×ox, 4×CH_2), 2.59 – 2.20 (m, 4H, {Ar_3C}CH_2), 1.85 – 0.40 (m, 94H, 40×CH_2, 54×*t*Bu).

HR ESI-MS (CH_3CN, 180 °C, 3 kV) positive ion: 1814.0844 ([M]$^+$, calcd 1814.0832) *m*/*z*.

[Ir(**^{R}pybox**)(biph)Cl] (**39**)

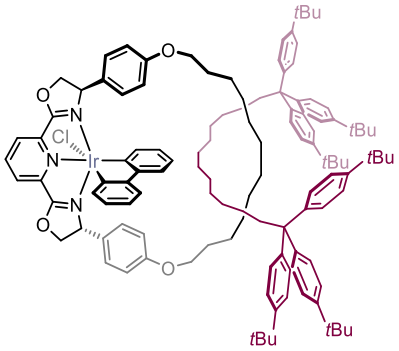

A solution of **^{R}pybox** (15.6 mg, 10 μmol) and [Ir(COD)(biph)Cl]$_2$ (4.9 mg, 5 μmol) in CD_2Cl_2 (0.5 mL) was stirred at rt for 18 h. The volatiles were removed *in vacuo* and the brown-yellow residue washed with cold pentane (3 × 5 mL, −78 °C) to afford the title compound as a brown solid in *ca*. 75% purity. Characterised *in situ*.

^{1}H NMR (400 MHz, CD_2Cl_2): δ 8.07 – 7.88 (m, 2H, py), 7.75 – 7.58 (m, 1H, py), 7.42 – 7.07 (m, 26H, Ar), 6.89 (d, $^3J_{HH}$ = 8.1, 1H, Ar), 6.69 (d, $^3J_{HH}$ = 7.2, 4H, Ar), 6.63 (d, $^3J_{HH}$ = 8.2, 2H, Ar), 6.54 – 6.41 (m, 2H, Ar), 6.31 – 6.20 (m, 2H, Ar), 5.66 – 5.58 (m, 1H, biph), 5.11 (d, $^3J_{HH}$ = 7.8, 1H, biph), 5.04 (app t, J_{HH} = 9.7, 1H, ox), 4.95 (app t, J_{HH} = 9.7, 1H, ox), 4.68 (app t, J_{HH} = 9.2, 1H, ox), 4.59 (app t, J_{HH} = 9.3, 1H, ox), 4.44 – 4.39 (br m, 1H, biph), 4.36 (obsc t, 1H, ox), 4.26 (app t, J_{HH} = 9.9, 1H, ox), 4.04 – 3.86 (br m, 4H, CH_2), 2.63 – 2.40 (m, 4H, {Ar_3C}CH_2), 1.87 – 1.56 (m, 4H, CH_2), 1.50 – 0.58 (br m, 90H, 36×CH_2, 54×*t*Bu).

LR ESI-MS (CH_3CN, 180 °C, 3 kV) positive ion: 1904.0 ([M−Cl]$^+$, calcd 1904.1) *m*/*z*.

[Ir(**[R]pybox**)(biph)][BAr^F_4] (**40**)

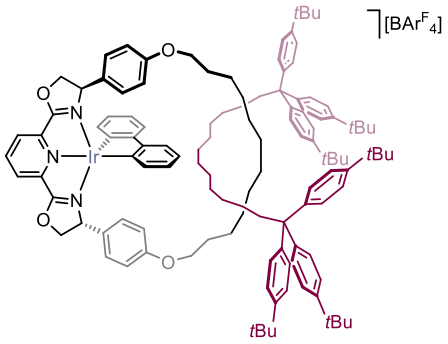

A solution of **39** (10 μmol, generated *in situ*) and Na[BAr^F_4] (8.9 mg, 10 μmol) in CD_2Cl_2 (0.5 mL) was stirred at rt for 18 h. The dark brown suspension was filtered to afford the title compound as a brown solid in *ca*. 80% purity. Characterised *in situ*.

^{1}H NMR (300 MHz, CD_2Cl_2, selected data): δ 8.22 – 8.04 (m, 2H, py), 7.73 (br, 8H, Ar^F), 7.56 (s, 4H, Ar^F), 7.37 – 7.10 (br m, 34H, Ar), 6.91 – 6.59 (br m, 4H, Ar), 6.59 – 6.30 (br m, 3H, Ar), 5.10 (br, 2H, ox), 4.40 (br, 2H, ox), 4.11 – 3.55 (br m, 6H, 2×ox, 4×CH_2), 2.68 – 2.34 (br m, 4H, {Ar_3C}CH_2), 1.73 (s, 4H, CH_2), 1.54 – 0.76 (m, 90H, 36×CH_2, 54×*t*Bu).

6.4.3. Synthesis of ruthenium complexes

6.4.3.1. Preparation of macrocyclic ruthenium complexes

[Ru(**[M]pybox**)Cl_2(THF)] (**THF-41**)

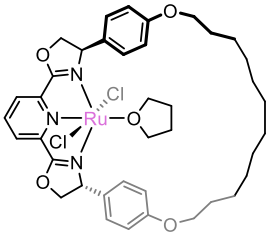

A solution of **[M]pybox** (5.7 mg, 10 μmol) and [Ru(*p*-cymene)Cl_2]$_2$ (3.1 mg, 5 μmol) in THF (0.5 mL) was stirred at rt for 1 h after which the volatiles were removed *in vacuo*. The resulting residue was washed with hexane (3 × 1 mL) to yield the title compound as a as a dark purple solid. Yield: 6.3 mg (78%).

^{1}H NMR (500 MHz, THF, selected data): δ 7.99 (d, $^3J_{HH}$ = 7.8, 2H, py), 7.89 (d, $^3J_{HH}$ = 6.4, 4H, Ph), 7.75 – 7.70 (m, 1H, py), 7.17 (d, $^3J_{HH}$ = 6.5, 4H, Ph), 5.65 (app t, J_{HH} = 8.8, 2H, ox{CH_2}), 5.62 – 5.55 (m, 2H, ox{CH}), 4.69 (dd, $^3J_{HH}$ = 12.7, 8.2, 2H, ox{CH_2}).

Characterised in CD_2Cl_2 as approximately a 1:1 mixture of **THF-41** to **DCM-41**.

^{1}H NMR (600 MHz, CD_2Cl_2): δ 7.67 (d, $^3J_{HH}$ = 7.8, 2H, py), 7.45 (t, $^3J_{HH}$ = 8.0, 2H, py), 7.40 (d, $^3J_{HH}$ = 8.4, 4H, Ph), 6.89 (d, $^3J_{HH}$ = 8.6, 4H, Ph), 5.36 – 5.23 (m, 4H, 2×ox{CH_2}, 2×ox{CH}),

4.61 (dd, $^{2}J_{HH}$ = 13.0, $^{3}J_{HH}$ = 8.4, 2H, ox{CH_2}), 4.13 – 4.04 (m, 2H, CH_2), 4.01 – 3.94 (m, 2H, CH_2), 3.77 (q, $^{3}J_{HH}$ = 7.4, 2H, THF), 3.28 (q, $^{3}J_{HH}$ = 6.6, 5.9, 2H, THF), 1.78 – 1.64 (m, 8H, 4×THF, 4×CH_2), 1.47 – 1.36 (m, 4H, CH_2), 1.34 – 1.13 (m, 12H, CH_2).

$^{13}C\{^{1}H\}$ NMR (151 MHz, CD_2Cl_2): δ 169.5 (ox{OCN}), 160.0 (Ph), 153.9 (py), 131.1 (Ph), 128.9 (Ph), 125.1 (py), 124.1 (py), 115.5 (Ph), 78.9 (ox{CH_2}), 73.1 (THF), 69.8 (ox{CH}), 67.8 (CH_2), 30.3 (CH_2), 29.8 (CH_2), 29.2 (CH_2), 28.9 (CH_2), 26.1 (CH_2), 25.5 (THF).

HR ESI-MS (CH_3OH, 180 °C, 3 kV) positive ion: 773.2154 ([M–Cl–THF+NaOEt]$^{+}$, calcd 773.2147) *m*/*z*.

Generation of [Ru(**^{M}pybox**)Cl_2(CD_2Cl_2)] (**DCM-41**)

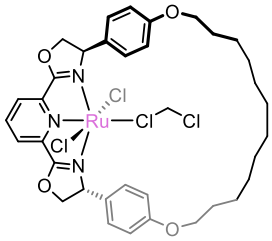

Generated from **THF-41** (*vide supra*).

^{1}H NMR (600 MHz, CD_2Cl_2): δ 7.76 (d, $^{3}J_{HH}$ = 7.9, 2H, py), 7.58 (t, $^{3}J_{HH}$ = 7.9, 1H, py), 7.48 (d, $^{3}J_{HH}$ = 8.5, 4H, Ph), 6.86 (d, $^{3}J_{HH}$ = 8.5, 4H, Ph), 5.36 – 5.23 (m, 4H, 2×ox{CH_2}, 2×ox{CH}), 4.52 – 4.42 (m, 2H, ox{CH_2}), 4.13 – 4.04 (m, 2H, CH_2), 4.01 – 3.94 (m, 2H, CH_2), 1.78 – 1.64 (m, 4H, CH_2), 1.47 – 1.36 (m, 4H, CH_2), 1.34 – 1.13 (m, 12H, CH_2).

$^{13}C\{^{1}H\}$ NMR (151 MHz, CD_2Cl_2): δ 168.1 (ox{OCN}), 159.4 (Ph), 153.9 (py), 130.6 (Ph), 129.7 (Ph), 128.7 (py), 124.0 (py), 115.1 (Ph), 78.7 (ox{CH_2}), 70.0 (ox{CH}), 67.8 (CH_2), 30.2 (CH_2), 29.9 (CH_2), 29.4 (CH_2), 29.0 (CH_2), 26.2 (CH_2).

Generation of [Ru(**^{M}pybox**)Cl_2(CO)] (**42**)

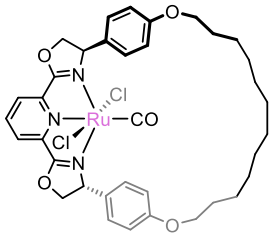

A solution of **^{M}pybox** (5.7 mg, 10 µmol) and [Ru(*p*-cymene)Cl_2]$_2$ (3.1 mg, 5 µmol) in THF (0.5 mL) was stirred at rt for 1 h. The purple solution was freeze-pump-thaw degassed, placed under an atmosphere of CO, and then stirred at rt for 18 h. The suspension was filtered and the volatiles were removed *in vacuo*. The residue was then washed with hexane (3 × 1 mL) to yield the title compound as a as a dark green solid. Yield: 7.1 mg

(92%). Dark green crystals suitable for X-ray crystallography were obtained from diffusion of *n*-hexane into a CH_2Cl_2 solution at rt.

^{1}H NMR (500 MHz, CD_2Cl_2): δ 8.18 (t, $^3J_{HH}$ = 8.0, 1H, py), 7.98 (d, $^3J_{HH}$ = 8.0, 2H, py), 7.29 (d, $^3J_{HH}$ = 8.5, 4H, Ph), 6.89 (d, $^3J_{HH}$ = 8.6, 4H, Ph), 5.25 (app t, J_{HH} = 9.3, 2H, ox{CH_2}), 5.08 (dd, $^3J_{HH}$ = 13.7, $^3J_{HH}$ = 9.8, 2H, ox{CH}), 4.54 (dd, $^3J_{HH}$ = 13.8, $^2J_{HH}$ = 8.8, 2H, ox{CH_2}), 4.11 – 3.95 (m, 4H, CH_2), 1.80 – 1.67 (m, 4H, CH_2), 1.50 – 1.38 (m, 4H, CH_2), 1.38 – 1.19 (m, 12H, CH_2).

^{13}C{^{1}H} NMR (126 MHz, CD_2Cl_2): δ 203.6 (RuCO), 165.5 (ox{OCN}), 160.1 (Ph), 148.1 (py), 139.9 (py), 131.0 (Ph), 127.7 (Ph), 124.3 (py), 115.5 (Ph), 78.9 (ox{CH_2}), 70.7 (ox{CH}), 68.2 (CH_2), 29.7 (CH_2) 29.4 (CH_2), 28.9 (CH_2), 28.7 (CH_2), 25.9 (CH_2).

HR ESI-MS (CH_3OH, 180 °C, 3 kV) positive ion: 764.2037 ([M–Cl+CH_3OH]$^+$, calcd 764.2041) *m*/*z*.

FT-IR (CH_2Cl_2): ν(CO) 1980 cm^{-1}.

6.4.3.2. Preparation of rotaxane ruthenium complexes

[Ru(**^{R}pybox**)Cl_2] (**43**)

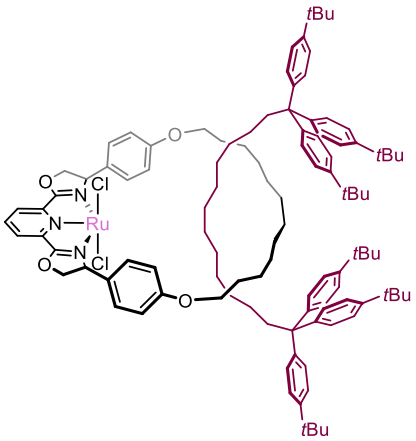

A solution of **^{R}pybox** (21.1 mg, 13.5 μmol) and [Ru(*p*-cymene)Cl_2]$_2$ (4.1 mg, 6.75 μmol) in THF (0.5 mL) was stirred at rt for 7 d. The volatiles were removed *in vacuo*. The residue was extracted into hexane (3 × 1 mL), concentrated to dryness and washed with TMS (3 × 10 mL, with sonication) to yield the title compound as a as a dark pink solid in *ca*. 85% purity. Characterised *in situ* by NMR spectroscopy as a mixture a major sharp species and a minor broad species (85:15).

Major species:

^{1}H NMR (400 MHz, THF, selected data): δ 8.06 (d, $^3J_{HH}$ = 7.7, 2H, py), 7.81 (d, $^3J_{HH}$ = 8.2, 4H, Ar{macro}), 7.68 – 7.44 (m, 25H, 1×py, 24×Ar{macro}), 7.07 (d, $^3J_{HH}$ = 8.2, 4H, Ar{macro}), 5.62 (br, 4H, ox).

^{1}H NMR (500 MHz, CD_2Cl_2, 298 K, selected data): δ 7.73 (d, $^{3}J_{HH}$ = 7.8, 2H, py), 7.48 – 7.34 (m, 5H, 1×py, 4×Ar{macro}), 7.30 (d, $^{3}J_{HH}$ = 8.3, 12H, Ar{axle}), 7.26 – 6.98 (m, 8H, 12×Ar{axle}), 6.72 (d, $^{3}J_{HH}$ = 8.4, 4H, Ar{macro}), 5.31 – 5.21 (m, 4H, 2×ox{CH_2}, 2×ox{CH}), 4.58 – 4.45 (m, 2H, ox{CH_2}), 3.91 – 3.74 (m, 4H, CH_2), 2.58 – 2.38 (m, 4H, {Ar_3C}CH_2), 1.71 (br, 4H, CH_2), 1.50 – 0.87 (m, 90H, 36×CH_2, 54×*t*Bu).

^{1}H NMR (600 MHz, CD_2Cl_2, 200 K, selected data): δ 7.74 (d, $^{3}J_{HH}$ = 7.8, 2H, py), 7.47 (t, $^{3}J_{HH}$ = 8.0, 1H, py), 7.35 (d, $^{3}J_{HH}$ = 7.9, 4H, Ar{macro}), 7.31 – 6.94 (m, 24H, Ar{axle}), 6.62 (d, $^{3}J_{HH}$ = 8.1, 4H, Ar{macro}), 5.32 (obsc, 2H, ox), 5.19 (app t, J_{HH} = 12.8, 2H, ox), 4.50 (dd, J_{HH} = 14.3, J_{HH} = 8.3, 2H, ox), 3.72 (br, 2H, CH_2), 3.62 (br, 2H, CH_2), 2.43 (br, 3H, {Ar_3C}CH_2), 2.36 (br, 1H, {Ar_3C}CH_2), 1.76 – 0.63 (m, 94H, 40×CH_2, 54×*t*Bu), −1.84 (br, 0.22H), −11.03 (br, 0.05H).

^{13}C{^{1}H} NMR (126 MHz, CD_2Cl_2, 298 K, selected data): δ 169.0 (ox{OCN}), 160.1 (Ar{macro}), 153.4 (py), 148.7 (Ar{axle}), 145.6 (Ar{axle}), 130.8 (Ar{macro}), 129.3 (Ar{axle}), 128.3 (Ar{macro}), 125.5 (py), 125.1 (Ar{axle}), 123.8 (py), 115.1 (Ar{macro}), 78.3 (ox{CH_2}) , 69.4 (ox{CH}), 67.8 (CH_2), 55.9 (Ar_3C), 40.7 ({Ar_3C}CH_2), 34.7 (*t*Bu{C}), 31.7 (*t*Bu{CH_3}), 30.9 – 30.4 (m, CH_2), 30.3 – 29.9 (m, CH_2), 29.4 (CH_2), 29.3 (CH_2), 26.6 (CH_2), 25.8 (CH_2).

Minor species:

^{1}H NMR (500 MHz, CD_2Cl_2, 298 K, selected data): δ 8.13 (br, 2H, py), 5.93 (br, 4H, Ar{macro}), 5.11 (br, 1H, ox), 4.41 (br, 2H, ox), 2.64 (br, 4H, {Ar_3C}CH_2), −0.20 (br, 1H), −0.69 (br d, J = 62.8, 1H), −1.78 (br, 1H).

HR ESI-MS (CH_3OH, 180 °C, 3 kV) positive ion: 1763.0283 ([M−Cl+CH_3OH+2H_2O]$^{+}$, calcd 1763.0284) m/z.

[Ru(**R**-**pybox**)Cl_2(CO)] (**44**)

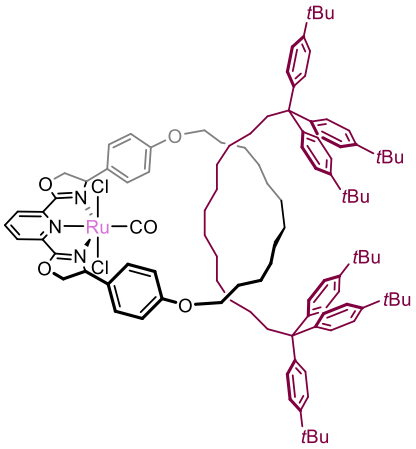

A solution of **43** (13.5 µmol, generated *in situ*) in CD_2Cl_2 (0.5 mL) was freeze-pump-thaw degassed, placed under an atmosphere of CO (1 atm), and then stirred at rt for 72 h. The volatiles were removed *in vacuo* and the crude compound was purified on a short plug of silica (99:1 CH_2Cl_2:CH_3OH, *Rf* = 0.66) to yield the title compound as a as a brown-red glassy solid. Yield: 6.6 mg (28%).

^{1}H NMR (500 MHz, CD_2Cl_2): δ 8.15 (t, $^3J_{HH}$ = 8.0, 1H, py), 7.96 (d, $^3J_{HH}$ = 7.9, 2H, py), 7.29 (d, $^3J_{HH}$ = 8.5, 12H, Ar{axle}), 7.25 – 7.12 (m, 16H, 12×Ar{axle}, 4×Ar{macro}), 6.73 (d, $^3J_{HH}$ = 8.7, 4H, Ar{macro}), 5.18 (app t, J_{HH} = 8.8, 2H, ox{CH_2}), 5.11 (dd, $^3J_{HH}$ = 14.2, $^3J_{HH}$ = 9.4, 2H, ox{CH}), 4.48 (dd, $^3J_{HH}$ = 14.2, $^2J_{HH}$ = 8.2, 2H, ox{CH_2}), 3.82 (t, $^3J_{HH}$ = 7.1, 4H, CH_2), 2.50 (t, $^3J_{HH}$ = 8.1, 4H, {Ar_3C}CH_2), 1.73 (p, $^3J_{HH}$ = 7.1, 4H, CH_2), 1.45 – 1.06 (m, 74H, 20×CH_2, 54×*t*Bu), 1.04 – 0.88 (m, 16H, CH_2).

^{13}C{^{1}H} NMR (126 MHz, CD_2Cl_2): δ 203.5 (RuCO), 166.0 (ox{OCN}), 160.5 (Ar{macro}), 148.7 (Ar{axle}), 148.3 (py), 145.8 (Ar{axle}), 139.6 (py), 131.1 (Ar{macro}), 129.4 (Ar{axle}), 129.3 (Ar{macro}), 125.1 (Ar{axle}), 124.1 (py), 115.3 (Ar{macro}), 78.7 (ox{CH_2}), 71.2 (ox{CH}), 68.0 (CH_2), 56.0 (Ar_3C), 40.8 ({Ar_3C}CH_2), 34.7 (*t*Bu{C}), 31.7 (*t*Bu{CH_3}), 31.3 (CH_2), 30.7 (CH_2), 30.6 (CH_2), 30.3 (CH_2), 30.2 (CH_2), 30.0 (CH_2), 29.4 (CH_2), 29.1 (CH_2), 26.7 (CH_2), 25.5 (CH_2).

HR ESI-MS (CH_3OH, 180 °C, 3 kV) positive ion: 1694.9850 ([M–CO–Cl]$^+$, calcd 1694.9832) *m*/*z*.

FT-IR (CH_2Cl_2): ν(CO) 1993 cm^{-1}.

6.5. Crystallographic data

Structure determinations were carried out by Dr A. B. Chaplin. Relevant crystallographic data are given in Table 6.1. Data were collected on an Oxford Diffraction Gemini Ruby CCD or Rigaku Oxford Diffraction SuperNova AtlasS2 CCD diffractometer using graphite monochromated Mo Kα (λ = 0.71073 Å) or CuKα (λ = 1.54178 Å) radiation and a low-temperature device. Data were collected and reduced using CrysAlisPro and refined using SHELXL,[371] through the Olex2 interface.[372]

Table 6.1. Crystallographic data.

	4	11	13a	13b	20b
CCDC / ID	0281abc17s	0324abc17s	1922374 / 0256abc16s	1922377 / 0485abc19smo	1922380 / 0499abc19s
Figure	Figure 2.7	Figure 2.9	Figure 3.5	Figure 3.6	Figure 3.9
Formula	$C_{47}H_{40}B_2Cl_2F_8N_6NiO_4$	$C_{74}H_{86}B_2F_8N_6NiO_8$	$C_{23}H_{19}ClN_3O_2Rh$	$C_{24}H_{23}Cl_3N_3O_3Rh$	$C_{56}H_{31}BCl_2F_{24}N_3O_3Rh$
M	1056.08	1419.81	507.77	610.71	1434.46
Crystal system	Orthorhombic	Tetragonal	Orthorhombic	Orthorhombic	Monoclinic
Space group	$C222_1$	$P4_1$	$P2_12_12$	$P2_12_12_1$	$P2_1$
Radiation	MoKα	CuKα	CuKα	MoKα	CuKα
***T* / K**	150(2)	150(2)	150(2)	150(2)	150(2)
***a* / Å**	13.5613(3)	15.3396(4)	5.86532(6)	12.0797(2)	13.42480(18)
***b* / Å**	15.3955(3)	15.3396(4)	13.34317(16)	12.7002(2)	15.7823(2)
***c* / Å**	22.4158(4)	30.1856(10)	12.82701(13)	15.6655(3)	13.68940(16)
***α* / °**	90	90	90	90	90
***β* / °**	90	90	90	90	97.9903(12)
***γ* / °**	90	90	90	90	90
***V* / Å^3**	4680.04(15)	7102.8(4)	1003.866(19)	2403.32(7)	2872.27(6)
***Z* (*Z'*)**	4 (1)	4 (1)	2 (1)	4 (1)	2 (1)
Density / gcm^{-3}	1.499	1.328	1.680	1.688	1.659
***μ* / mm^{-1}**	0.612	1.070	8.317	1.077	4.405
***θ* range / °**	$3.210 \leq \theta \leq 27.103$	$6.452 \leq \theta \leq 58.925$	$6.636 \leq \theta \leq 70.036$	$3.056 \leq \theta \leq 29.571$	$6.491 \leq \theta \leq 70.048$
Reflections collected	33744	46220	22100	20182	30162
R_{int}	0.0228	0.0609	0.0488	0.0268	0.0528
Completeness / %	99.7	99.8	99.8	99.9	99.8
No. of data/restr/param	5152/0/319	10054/1751/820	1913/0/138	6721/259/304	10736/884/986
R_1 / $I > 2\sigma(I)$]	0.0318	0.1591	0.0200	0.0246	0.0831
wR_2 / all data	0.0841	0.2827	0.0532	0.0578	0.2220
GoF	1.039	1.048	1.151	1.043	1.076
Largest diff. pk and hole / eÅ^{-3}	0.520/-0.357	0.648/-0.457	0.357/-0.250	1.184/-0.430	3.531/-2.091
Flack (*x*)	-0.006(3)	0.03(4)	-0.011(6)	-0.044(11)	-0.018(15)

	Tol-22	THF-25	26	42
CCDC / ID	0508abc19s	0571abc19s	0573abc19s	0594abc20s
Figure	Figure 3.13	Figure 3.16	Figure 3.18	Figure 4.22
Formula	$C_{74}H_{47}BF_{24}N_3O_2Rh$	$C_{27}H_{27}Cl_2N_3O_3Ru$	$C_{24}H_{19}Cl_2N_3O_3Ru$	$C_{36}H_{41}Cl_2N_3O_5Ru$
M	1579.86	613.48	569.39	767.69
Crystal system	Monoclinic	Monoclinic	Monoclinic	Monoclinic
Space group	$P2_1$	$P2_1$	$I2$	$P2_1/c$
Radiation	CuKα	CuKα	MoKα	CuKα
***T* / K**	150.00(10)	150(2)	150(2)	150(2)
***a* / Å**	13.05734(18)	17.9619(2)	8.02909(9)	23.1797(3)
***b* / Å**	17.51477(18)	8.25430(10)	17.17263(19)	13.60294(12)
***c* / Å**	30.7906(4)	36.0420(3)	16.6288(2)	11.55041(14)
***α* / °**	90	90	90	90
***β* / °**	93.0761(12)	102.4640(10)	92.8803(11)	103.1623(13)
***γ* / °**	90	90	90	90
***V* / Å^3**	7031.56(16)	5217.75(10)	2289.90(5)	3546.30(7)
***Z* (*Z*')**	4 (2)	8 (4)	4 (2×0.5)	4 (1)
Density / gcm^{-3}	1.492	1.562	1.652	1.438
***μ* / mm^{-1}**	2.964	7.031	0.950	5.333
***θ* range / °**	$6.526 \leq \theta \leq 66.599$	$6.557 \leq \theta \leq 66.594$	$3.413 \leq \theta \leq 29.574$	$6.508 \leq \theta \leq 66.587$
Reflections collected	79998	51089	42262	65818
R_{int}	0.0872	0.0471	0.0280	0.0593
Completeness / %	99.8	99.7	99.8	99.8
No. of data/restr/param	22725/2683/1902	17489/61/1307	6410/1/303	6248/968/548
R_1 / $I > 2\sigma(I)$]	0.1159	0.0406	0.0191	0.0420
wR_2 / all data	0.3236	0.1047	0.0499	0.1150
GoF	1.354	1.056	1.045	1.092
Largest diff. pk and hole / eÅ^{-3}	4.135/-2.149	0.552/-0.582	0.354/-0.383	2.003/-0.832
Flack (*x*)	0.025(14)	-0.033(9)	-0.035(13)	-

References

1 E. Peris and R. H. Crabtree, *Chem. Soc. Rev.*, 2018, **47**, 1959–1968.
2 J. Choi, A. H. R. MacArthur, M. Brookhart and A. S. Goldman, *Chem. Rev.*, 2011, **111**, 1761–1779.
3 E. Suárez, P. Plou, D. G. Gusev, M. Martín and E. Sola, *Inorg. Chem.*, 2017, **56**, 7190–7199.
4 M. Hernández-Juárez, M. Vaquero, E. Álvarez, V. Salazar and A. Suárez, *Dalton Trans.*, 2013, **42**, 351–354.
5 M. A. W. Lawrence, K. A. Green, P. N. Nelson and S. C. Lorraine, *Polyhedron*, 2018, **143**, 11–27.
6 Z. Cao, H. Qiao and F. Zeng, *Organometallics*, 2019, **38**, 797–804.
7 M. Albrecht and G. Van Koten, *Angew. Chem. Int. Ed.*, 2001, **40**, 3750–3781.
8 G. Van Kotex, K. Timmer, J. G. Noltes and A. L. Spek, *J. Am. Chem. Soc., Chem. Commun.*, 1978, 250–252.
9 C. J. Moulton and B. L. Shaw, *J. Am. Chem. Soc., Dalt. Trans.*, 1976, 1020–1024.
10 G. van Koten, *Pure Appl. Chem.*, 1989, 61, 1681–1694.
11 M. E. Van Der Boom and D. Milstein, *Chem. Rev.*, 2003, **103**, 1759–1792.
12 C. Gunanathan and D. Milstein, *Chem. Rev.*, 2014, **114**, 12024–12087.
13 Y. Q. Zou, S. Chakraborty, A. Nerush, D. Oren, Y. Diskin-Posner, Y. Ben-David and D. Milstein, *ACS Catal.*, 2018, **8**, 8014–8019.
14 A. Bugarin and B. T. Connell, *Chem. Commun.*, 2011, **47**, 7218–7220.
15 D. R. Pahls, K. E. Allen, K. I. Goldberg and T. R. Cundari, *Organometallics*, 2014, **33**, 6413–6419.
16 K. Wang, M. E. Goldman, T. J. Emge and A. S. Goldman, *J. Organomet. Chem.*, 1996, **518**, 55–68.
17 M. Gupta, C. Hagen, R. J. Flesher, W. C. Kaska and C. M. Jensen, *Chem. Commun.*, 1996, 2083–2084.
18 C. M. Jensen, *Chem. Commun.*, 1999, 2443–2449.
19 R. H. Crabtree, J. M. Mihelcic and J. M. Quirk, *J. Am. Chem. Soc.*, 1979, **101**, 7738–7740.
20 M. Gupta, C. Hagen, W. C. Kaska, R. E. Cramer and C. M. Jensen, *J. Am. Chem. Soc.*, 1997, **119**, 840–841.
21 T. R. Cundari, *J. Am. Chem. Soc.*, 1994, **116**, 340–347.
22 F. Liu and A. S. Goldman, *Chem. Commun.*, 1999, 655–656.
23 W. W. Xu, G. P. Rosini, M. Gupta, C. M. Jensen, W. C. Kaska, K. Krogh-Jespersen and A. S. Goldman, *Chem. Commun.*, 1997, 2273–2274.
24 J. Zhao, A. S. Goldman and J. F. Hartwig, *Science*, 2005, **307**, 1080–1082.
25 M. Kanzelberger, X. Zhang, T. J. Emge, A. S. Goldman, J. Zhao, C. Incarvito and J. F. Hartwig, *J. Am. Chem. Soc.*, 2003, **125**, 13644–13645.
26 J. I. Van Der Vlugt and J. N. H. Reek, *Angew. Chem. Int. Ed.*, 2009, **48**, 8832–8846.
27 A. S. Goldman, A. H. Roy, Z. Huang, R. Ahuja, W. Schinski and M. Brookhart, *Science*, 2006, **312**, 257–261.
28 J. Zhang, G. Leitus, Y. Ben-David and D. Milstein, *Angew. Chem. Int. Ed.*, 2006, **45**, 1113–1115.
29 C. Gunanathan and D. Milstein, *Acc. Chem. Res.*, 2011, **44**, 588–602.
30 C. Gunanathan, Y. Ben-David and D. Milstein, *Science*, 2007, **317**, 790–792.

31 S. W. Kohl, L. Weiner, L. Schwartsburd, L. Konstantinovski, L. J. W. Shimon, Y. Ben David, M. A. Iron and D. Milstein, *Science*, 2009, **324**, 74–77.
32 L. Alig, M. Fritz and S. Schneider, *Chem. Rev.*, 2019, **119**, 2681–2751.
33 R. Tanaka, M. Yamashita and K. Nozaki, *J. Am. Chem. Soc.*, 2009, **131**, 14168–14169.
34 R. B. Bedford, S. M. Draper, P. N. Scully and S. L. Welch, *New J. Chem.*, 2000, **24**, 745–747.
35 E. Peris, J. A. Loch, J. Mata and R. H. Crabtree, *Chem. Commun.*, 2001, 201–202.
36 S. Medici, M. Gagliardo, S. B. Williams, P. A. Chase, S. Gladiali, M. Lutz, A. L. Spek, G. P. M. Van Klink and G. Van Koten, *Helv. Chim. Acta*, 2005, **88**, 694–705.
37 J. I. Ito, S. Ujiie and H. Nishiyama, *Chem. Commun.*, 2008, 1923–1925.
38 C. A. Huff, J. W. Kampf and M. S. Sanford, *Organometallics*, 2012, **31**, 4643–4645.
39 D. A. Smith, D. E. Herbert, J. R. Walensky and O. V. Ozerov, *Organometallics*, 2013, **32**, 2050–2058.
40 D. M. Grove, G. van Koten, P. Mul, R. Zoet, J. G. M. van der Linden, J. Legters, J. E. J. Schmitz, N. W. Murrall and A. J. Welch, *Inorg. Chem.*, 1988, **27**, 2466–2473.
41 E. Kounalis, M. Lutz and D. L. J. Broere, *Organometallics*, 2020, **39**, 585–592.
42 R. L. Melen and L. H. Gade, in *The Privileged Pincer-Metal Platform: Coordination Chemistry & Applications*, eds. G. van Koten and R. A. Gossage, Springer, Cham, 2015, pp. 179–208.
43 Q. H. Deng, R. L. Melen and L. H. Gade, *Acc. Chem. Res.*, 2014, **47**, 3162–3173.
44 S. Z. Tasker, E. A. Standley and T. F. Jamison, *Nature*, 2014, **509**, 299–309.
45 E. L. Dias, M. Brookhart and P. S. White, *Chem. Commun.*, 2001, 423–424.
46 M. E. O'Reilly and A. S. Veige, *Chem. Soc. Rev.*, 2014, **43**, 6325–6369.
47 J. S. Freundlich, R. R. Schrock and W. M. Davis, *J. Am. Chem. Soc.*, 1996, **118**, 3643–3655.
48 J. S. Freundlich, R. R. Schrock and W. M. Davis, *Organometallics*, 1996, **15**, 2777–2783.
49 W. W. Weare, X. Dai, M. J. Byrnes, J. M. Chin, R. R. Schrock and P. Müller, *Proc. Natl. Acad. Sci. U. S. A.*, 2006, **103**, 17099–17106.
50 P. Kumar and R. Gupta, *Dalton Trans.*, 2016, **45**, 18769–18783.
51 C. M. Killian, D. J. Tempel, L. K. Johnson and M. Brookhart, *J. Am. Chem. Soc.*, 1996, **118**, 11664–11665.
52 L. K. Johnson, C. M. Killian and M. Brookhart, *J. Am. Chem. Soc.*, 1995, **117**, 6414–6415.
53 B. L. Small, M. Brookhart and A. M. A. Bennett, *J. Am. Chem. Soc.*, 1998, **120**, 4049–4050.
54 V. C. Gibson, C. Redshaw and G. A. Solan, *Chem. Rev.*, 2007, **107**, 1745–1776.
55 E. L. Dias, M. Brookhart and P. S. White, *Organometallics*, 2000, **19**, 4995–5004.
56 H. F. Haarman, J. M. Ernsting, M. Kranenburg, H. Kooijman, N. Veldman, A. L. Spek, P. W. N. M. Van Leeuwen and K. Vrieze, *Organometallics*, 1997, **16**, 887–900.
57 K. J. Bradd, B. T. Heaton, C. Jacob, J. T. Sampanthar and A. Steiner, *J. Am. Chem. Soc., Dalt. Trans.*, 1999, 1109–1112.
58 H. Nishiyama, M. Horihata, T. Hirai, S. Wakamatsu and K. Itoh, *Organometallics*, 1991, **10**, 2706–2708.
59 G. M. Adams, F. M. Chadwick, S. D. Pike and A. S. Weller, *Dalton Trans.*, 2015, **44**, 6340–6342.
60 S. C. Bart, E. Lobkovsky and P. J. Chirik, *J. Am. Chem. Soc.*, 2004, **126**, 13794–13807.

61 S. C. Bart, E. Lobkovsky, E. Bill and P. J. Chirik, *J. Am. Chem. Soc.*, 2006, **128**, 5302–5303.
62 A. M. Archer, M. W. Bouwkamp, M. P. Cortez, E. Lobkovsky and P. J. Chirik, *Organometallics*, 2006, **25**, 4269–4278.
63 M. W. Bouwkamp, A. C. Bowman, E. Lobkovsky and P. J. Chirik, *J. Am. Chem. Soc.*, 2006, **128**, 13340–13341.
64 M. Gallagher, N. L. Wieder, V. K. Dioumaev, P. J. Carroll and D. H. Berry, *Organometallics*, 2010, **29**, 591–603.
65 G. T. Morgan and F. H. Burstall, *J. Am. Chem. Soc.*, 1932, 20–30.
66 C. Wei, Y. He, X. Shi and Z. Song, *Coord. Chem. Rev.*, 2019, **385**, 1–19.
67 A. Winter and U. S. Schubert, *ChemCatChem*, 2020, **12**, 2890–2941.
68 Y. H. Budnikova, D. A. Vicic and A. Klein, *Inorganics*, 2018, **6**, 18.
69 A. M. W. Cargill Thompson, *Coord. Chem. Rev.*, 1997, **160**, 1–52.
70 M. Heller and U. S. Schubert, *Eur. J. Org. Chem.*, 2003, **2003**, 947–961.
71 A. Boddien, B. Loges, F. Gärtner, C. Torborg, K. Fumino, H. Junge, R. Ludwig and M. Beller, *J. Am. Chem. Soc.*, 2010, **132**, 8924–8934.
72 F. H. Case and T. J. Kasper, *J. Am. Chem. Soc.*, 1956, **78**, 5842–5844.
73 R. A. Fallahpour, M. Neuburger and M. Zehnder, *New J. Chem.*, 1999, **23**, 53–61.
74 J. Wang and G. S. Hanan, *Synlett*, 2005, **2005**, 1251–1254.
75 T. Mutai, J. D. Cheon, S. Arita and K. Araki, *J. Chem. Soc., Perkin Trans. 2*, 2001, 1045–1050.
76 Y. M. Zhang, S. H. Wu, C. J. Yao, H. J. Nie and Y. W. Zhong, *Inorg. Chem.*, 2012, **51**, 11387–11395.
77 S. Y. Wang, J. H. Fu, Y. P. Liang, Y. J. He, Y. S. Chen and Y. T. Chan, *J. Am. Chem. Soc.*, 2016, **138**, 3651–3654.
78 M. Heller and U. S. Schubert, *J. Org. Chem.*, 2002, **67**, 8269–8272.
79 S. Das, C. D. Incarvito, R. H. Crabtree and G. W. Brudvig, *Science*, 2006, **312**, 1941–1943.
80 E. C. Constable, in *Advances in Inorganic Chemistry*, ed. H. J. Emeléus, Academic Press, 1986, vol. 30, pp. 69–121.
81 R. Zhou, G. F. Manbeck, D. G. Wimer and K. J. Brewer, *Chem. Commun.*, 2015, **51**, 12966–12969.
82 K. Kamata, A. Suzuki, Y. Nakai and H. Nakazawa, *Organometallics*, 2012, **31**, 3825–3828.
83 G. D. Jones, C. McFarland, T. J. Anderson and D. A. Vicic, *Chem. Commun.*, 2005, 4211–4213.
84 T. J. Anderson, G. D. Jones and D. A. Vicic, *J. Am. Chem. Soc.*, 2004, **126**, 8100–8101.
85 J. T. Ciszewski, D. Y. Mikhaylov, K. V. Holin, M. K. Kadirov, Y. H. Budnikova, O. Sinyashin and D. A. Vicic, *Inorg. Chem.*, 2011, **50**, 8630–8635.
86 G. D. Jones, J. L. Martin, C. McFarland, O. R. Allen, R. E. Hall, A. D. Haley, R. J. Brandon, T. Konovalova, P. J. Desrochers, P. Pulay and D. A. Vicic, *J. Am. Chem. Soc.*, 2006, **128**, 13175–13183.
87 H. Nagao, T. Mizukawa and K. Tanaka, *Inorg. Chem.*, 1994, **33**, 3415–3420.
88 M. R. Prinsell, D. A. Everson and D. J. Weix, *Chem. Commun.*, 2010, **46**, 5743–5745.
89 A. Nemati Kharat, A. Bakhoda and B. Tamaddoni Jahromi, *Polyhedron*, 2011, **30**, 2768–2775.
90 Q. Han, X. X. Guo, X. T. Zhou and H. B. Ji, *Inorg. Chem. Commun.*, 2020, **112**, 107544.

91 F. Shi, M. K. Tse and M. Beller, *Chem. Asian J.*, 2007, **2**, 411–415.
92 D. Gnanamgari, C. H. Leung, N. D. Schley, S. T. Hilton and R. H. Crabtree, *Org. Biomol. Chem.*, 2008, **6**, 4442–4445.
93 D. Inoki, T. Matsumoto, H. Hayashi, K. Takashita, H. Nakai and S. Ogo, *Dalton Trans.*, 2012, **41**, 4328–4334.
94 D. Inoki, T. Matsumoto, H. Nakai and S. Ogo, *Organometallics*, 2012, **31**, 2996–3001.
95 H. L. Kwong, W. L. Wong, W. S. Lee, L. S. Cheng and W. T. Wong, *Tetrahedron Asymmetry*, 2001, **12**, 2683–2694.
96 C. T. Yeung, W. S. Lee, C. S. Tsang, S. M. Yiu, W. T. Wong, W. Y. Wong and H. L. Kwong, *Polyhedron*, 2010, **29**, 1497–1507.
97 G. Chelucci, A. Saba, D. Vignola and C. Solinas, *Tetrahedron*, 2001, **57**, 1099–1104.
98 G. Chelucci, A. Saba, F. Soccolini and D. Vignola, *J. Mol. Catal. A Chem.*, 2002, **178**, 27–33.
99 M. E. O'Reilly, D. R. Pahls, J. R. Webb, N. C. Boaz, S. Majumdar, C. D. Hoff, J. T. Groves, T. R. Cundari and T. B. Gunnoe, *Dalton Trans.*, 2014, **43**, 8273–8281.
100 M. E. O'Reilly, D. R. Pahls, T. R. Cundari and T. B. Gunnoe, *Organometallics*, 2014, **33**, 6504–6510.
101 H. Nishiyama, H. Sakaguchi, T. Nakamura, M. Horihata, M. Kondo and K. Itoh, *Organometallics*, 1989, **8**, 846–848.
102 G. Desimoni, G. Faita and P. Quadrelli, *Chem. Rev.*, 2003, **103**, 3119–3154.
103 G. Chelucci, S. Deriu, G. A. Pinna, A. Saba and R. Valenti, *Tetrahedron Asymmetry*, 1999, **10**, 3803–3809.
104 J. S. Poh, S. Makai, T. von Keutz, D. N. Tran, C. Battilocchio, P. Pasau and S. V. Ley, *Angew. Chem. Int. Ed.*, 2017, **56**, 1864–1868.
105 H. Nishiyama, S. Yamaguchi, M. Hondo and K. Itoh, *J. Org. Chem.*, 1992, **57**, 4306–4309.
106 S. B. Park, K. Murata, H. Matsumoto and H. Nishiyama, *Tetrahedron Asymmetry*, 1995, **6**, 2487–2494.
107 D. A. Evans, M. C. Kozlowski, J. A. Murry, C. S. Burgey, K. R. Campos, B. T. Connell and R. J. Staples, *J. Am. Chem. Soc.*, 1999, **121**, 669–685.
108 T. Ollevier, *Catal. Sci. Technol.*, 2016, **6**, 41–48.
109 S. A. Babu, K. K. Krishnan, S. M. Ujwaldev and G. Anilkumar, *Asian J. Org. Chem.*, 2018, **7**, 1033–1053.
110 D. A. Evans, K. R. Fandrick, H. J. Song, K. A. Scheidt and R. Xu, *J. Am. Chem. Soc.*, 2007, **129**, 10029–10041.
111 A. M. Tondreau, J. M. Darmon, B. M. Wile, S. K. Floyd, E. Lobkovsky and P. J. Chirik, *Organometallics*, 2009, **28**, 3928–3940.
112 M. K. Tse, S. Bhor, M. Klawonn, G. Anilkumar, H. Jiao, A. Spannenberg, C. Döbler, W. Magerlein, H. Hugl and M. Beller, *Chem. Eur. J.*, 2006, **12**, 1875–1888.
113 M. Panera, J. Díez, I. Merino, E. Rubio and M. P. Gamasa, *Inorg. Chem.*, 2009, **48**, 11147–11160.
114 H. Nishiyama, M. Kondo, T. Nakamura and K. Itoh, *Organometallics*, 1991, **10**, 500–508.
115 D. Cuervo, M. P. Gamasa and J. Gimeno, *J. Mol. Catal. A Chem.*, 2006, **249**, 60–64.
116 D. Cuervo, J. Díez, M. P. Gamasa and J. Gimeno, *Organometallics*, 2005, **24**, 2224–2232.
117 D. Cuervo, J. Díez, M. P. Gamasa, S. García-Granda and J. Gimeno, *Inorg. Chem.*, 2002,

41, 4999–5001.
118 H. Nishiyama, Y. Itoh, H. Matsumoto, S. B. Park and K. Itoh, *J. Am. Chem. Soc.*, 1994, **116**, 2223–2224.
119 H. Nishiyama, Y. Itoh, Y. Sugawara, H. Matsumoto, K. Aoki and K. Itoh, *Bull. Chem. Soc. Jpn.*, 1995, **68**, 1247–1262.
120 K. Nomura, S. Warit and Y. Imanishi, *Macromolecules*, 1999, **32**, 4732–4734.
121 D. G. Musaev and S. B. Blakey, *Organometallics*, 2012, **31**, 4950–4961.
122 E. Milczek, N. Boudet and S. Blakey, *Angew. Chem. Int. Ed.*, 2008, **47**, 6825–6828.
123 V. Cadierno, M. P. Gamasa, J. Gimeno, L. Iglesias and S. García-Granda, *Inorg. Chem.*, 1999, **38**, 2874–2879.
124 D. Cuervo, M. P. Gamasa and J. Gimeno, *Chem. Eur. J.*, 2004, **10**, 425–432.
125 C. X. Zhao, M. O. Duffey, S. J. Taylor and J. P. Morken, *Org. Lett.*, 2001, **3**, 1829–1831.
126 H. Miyabe, A. Matsumura, K. Moriyama and Y. Takemoto, *Org. Lett.*, 2004, **6**, 4631–4634.
127 J. Díez, M. P. Gamasa, J. Gimeno and P. Paredes, *Organometallics*, 2005, **24**, 1799–1802.
128 D. Cuervo, J. Díez, M. P. Gamasa, J. Gimeno and P. Paredes, *Eur. J. Inorg. Chem.*, 2006, **2006**, 599–608.
129 P. Paredes, J. Díez and M. P. Gamasa, *J. Organomet. Chem.*, 2008, **693**, 3681–3687.
130 P. Paredes, J. Díez and M. P. Gamasa, *Organometallics*, 2008, **27**, 2597–2607.
131 E. De Julián, J. Díez, E. Lastra and M. P. Gamasa, *J. Mol. Catal. A Chem.*, 2014, **394**, 295–302.
132 E. Geist, A. Kirschning and T. Schmidt, *Nat. Prod. Rep.*, 2014, **31**, 441–448.
133 F. O. Arp and G. C. Fu, *J. Am. Chem. Soc.*, 2005, **127**, 10482–10483.
134 C. Fischer and G. C. Fu, *J. Am. Chem. Soc.*, 2005, **127**, 4594–4595.
135 J. Zhou and G. C. Fu, *J. Am. Chem. Soc.*, 2003, **125**, 14726–14727.
136 S. W. Smith and G. C. Fu, *J. Am. Chem. Soc.*, 2008, **130**, 12645–12647.
137 X. Yu, T. Yang, S. Wang, H. Xu and H. Gong, *Org. Lett.*, 2011, **13**, 2138–2141.
138 X. Hu, *Chem. Sci.*, 2011, **2**, 1867–1886.
139 N. D. Schley and G. C. Fu, *J. Am. Chem. Soc.*, 2014, **136**, 16588–16593.
140 M. Rezaeivala and H. Keypour, *Coord. Chem. Rev.*, 2014, **280**, 203–253.
141 G. Tseberlidis, D. Intrieri and A. Caselli, *Eur. J. Inorg. Chem.*, 2017, **2017**, 3589–3603.
142 S. O. Kang, T. S. Johnson, V. W. Day and K. Bowman-James, *Supramol. Chem.*, 2018, **30**, 305–314.
143 E. C. Constable and J. Lewis, *Polyhedron*, 1982, **1**, 303–306.
144 T. Suzuki, Y. Tateishi, T. Sugimoto, S. Shinkai and K. Sada, *Sci. Technol. Adv. Mater.*, 2006, **7**, 605–608.
145 E. Wasserman, *J. Am. Chem. Soc.*, 1960, **82**, 4433–4434.
146 C. O. Dietrich-Buchecker, J. P. Sauvage and J. M. Kern, *J. Am. Chem. Soc.*, 1984, **106**, 3043–3045.
147 C. O. Dietrich-Buchecker, J. P. Sauvage and J. P. Kintzinger, *Tetrahedron Lett.*, 1983, **24**, 5095–5098.
148 J. P. Sauvage, *Angew. Chem. Int. Ed.*, 2017, **56**, 11080–11093.
149 I. T. Harrison and S. Harrison, *J. Am. Chem. Soc.*, 1967, **89**, 5723–5724.
150 G. Schill and H. Zollenkopf, *Justus Liebigs Ann. Chem.*, 1969, **721**, 53–74.
151 G. Schill, C. Zürcher and W. Vetter, *Chem. Ber.*, 1973, **106**, 228–235.
152 *Nachr. Chem. Tech.*, 1967, **15**, 149–150.

153 R. Brückner, *Eur. J. Org. Chem.*, 2019, **2019**, 3289–3319.
154 M. Franz, J. A. Januszewski, D. Wendinger, C. Neiss, L. D. Movsisyan, F. Hampel, H. L. Anderson, A. Görling and R. R. Tykwinski, *Angew. Chem. Int. Ed.*, 2015, **54**, 6645–6649.
155 L. D. Movsisyan, M. Franz, F. Hampel, A. L. Thompson, R. R. Tykwinski and H. L. Anderson, *J. Am. Chem. Soc.*, 2016, **138**, 1366–1376.
156 V. Aucagne, K. D. Hänni, D. A. Leigh, P. J. Lusby and D. B. Walker, *J. Am. Chem. Soc.*, 2006, **128**, 2186–2187.
157 J. D. Crowley, S. M. Goldup, N. D. Gowans, D. A. Leigh, V. E. Ronaldson and A. M. Z. Slawin, *J. Am. Chem. Soc.*, 2010, **132**, 6243–6248.
158 J. E. M. Lewis, J. Winn, L. Cera and S. M. Goldup, *J. Am. Chem. Soc.*, 2016, **138**, 16329–16336.
159 M. Denis and S. M. Goldup, *Nat. Rev. Chem.*, 2017, **1**, 61.
160 S. M. Goldup, D. A. Leigh, R. T. McBurney, P. R. McGonigal and A. Plant, *Chem. Sci.*, 2010, **1**, 383–386.
161 J. Echavarren, M. A. Y. Gall, A. Haertsch, D. A. Leigh, V. Marcos and D. J. Tetlow, *Chem. Sci.*, 2019, **10**, 7269–7273.
162 H. M. Cheng, D. A. Leigh, F. Maffei, P. R. McGonigal, A. M. Z. Slawin and J. Wu, *J. Am. Chem. Soc.*, 2011, **133**, 12298–12303.
163 J. J. Danon, D. A. Leigh, P. R. McGonigal, J. W. Ward and J. Wu, *J. Am. Chem. Soc.*, 2016, **138**, 12643–12647.
164 M. R. Netherton and G. C. Fu, *Adv. Synth. Catal.*, 2004, **346**, 1525–1532.
165 T. T. Tsou and J. K. Kochi, *J. Am. Chem. Soc.*, 1979, **101**, 6319–6332.
166 T. T. Tsou and J. K. Kochi, *J. Am. Chem. Soc.*, 1979, **101**, 7547–7560.
167 D. A. Everson, R. Shrestha and D. J. Weix, *J. Am. Chem. Soc.*, 2010, **132**, 920–921.
168 Y. Peng, L. Luo, C. S. Yan, J. J. Zhang and Y. W. Wang, *J. Org. Chem.*, 2013, **78**, 10960–10967.
169 G. Gil-Ramírez, D. A. Leigh and A. J. Stephens, *Angew. Chem. Int. Ed.*, 2015, **54**, 6110–6150.
170 P. R. Ashton, T. T. Goodnow, A. E. Kaifer, M. V. Reddington, A. M. Z. Slawin, N. Spencer, J. F. Stoddart, C. Vicent and D. J. Williams, *Angew. Chem. Int. Ed.*, 1989, **28**, 1396–1399.
171 M. Juríček, J. C. Barnes, N. L. Strutt, N. A. Vermeulen, K. C. Ghooray, E. J. Dale, P. R. McGonigal, A. K. Blackburn, A. J. Avestro and J. F. Stoddart, *Chem. Sci.*, 2014, **5**, 2724–2731.
172 D. A. Ben-Efraim, C. Batich and E. Wasserman, *J. Am. Chem. Soc.*, 1970, **92**, 2133–2135.
173 G. Schill and A. Lüttringhaus, *Angew. Chem. Int. Ed.*, 1964, **3**, 546–547.
174 G. Schill and C. Zürcher, *Angew. Chem. Int. Ed.*, 1969, **8**, 988–988.
175 G. Schill, *Chem. Ber.*, 1967, **100**, 2021–2037.
176 G. Schill, E. Logemann and W. Vetter, *Angew. Chem. Int. Ed.*, 1972, **11**, 1089–1090.
177 E. Logemann and G. Schill, *Chem. Ber.*, 1978, **111**, 2615–2629.
178 G. Schill, N. Schweickert, H. Fritz and W. Vetter, *Chem. Ber.*, 1988, **121**, 961–970.
179 J. F. Nierengarten, C. O. Dietrich-Buchecker and J. P. Sauvage, *J. Am. Chem. Soc.*, 1994, **116**, 375–376.
180 C. Dietrich-Buchecker, J. P. Sauvage and J. M. Kern, *J. Am. Chem. Soc.*, 1989, **111**, 7791–7800.

181 B. Mohr, M. Weck, J. P. Sauvage and R. H. Grubbs, *Angew. Chem. Int. Ed.*, 1997, **36**, 1308–1310.
182 M. Weck, B. Mohr, J. P. Sauvage and R. H. Grubbs, *J. Org. Chem.*, 1999, **64**, 5463–5471.
183 C. O. Dietrich-Buchecker, A. Khemiss and J. P. Sauvage, *J. Am. Chem. Soc., Chem. Commun.*, 1986, 1376–1378.
184 F. Bitsch, C. O. Dietrich-Buchecker, A. K. Khémiss, J. P. Sauvage and A. Van Dorsselaer, *J. Am. Chem. Soc.*, 1991, **113**, 4023–4025.
185 C. O. Dietrich-Buchecker, C. Hemmert, A. K. Khémiss and J. P. Sauvage, *J. Am. Chem. Soc.*, 1990, **112**, 8002–8008.
186 N. H. Evans and P. D. Beer, *Chem. Soc. Rev.*, 2014, **43**, 4658–4683.
187 J. P. Sauvage and M. Ward, *Inorg. Chem.*, 1991, **30**, 3869–3874.
188 C. Piguet, G. Hopfgartner, B. Bocquet, A. F. Williams and O. Schaad, *J. Am. Chem. Soc.*, 1994, **116**, 9092–9102.
189 C. Piguet, G. Bernardinelli, A. F. Williams and B. Bocquet, *Angew. Chem. Int. Ed.*, 1995, **34**, 582–584.
190 D. A. Leigh, P. J. Lusby, S. J. Teat, A. J. Wilson and J. K. Y. Wong, *Angew. Chem. Int. Ed.*, 2001, **40**, 1538–1543.
191 D. A. Leigh, P. J. Lusby, R. T. McBurney, A. Morelli, A. M. Z. Slawin, A. R. Thomson and D. B. Walker, *J. Am. Chem. Soc.*, 2009, **131**, 3762–3771.
192 J. C. Loren, P. Gantzel, A. Linden and J. S. Siegel, *Org. Biomol. Chem.*, 2005, **3**, 3105–3116.
193 N. Belfrekh, C. Dietrich-Buchecker and J. P. Sauvage, *Inorg. Chem.*, 2000, **39**, 5169–5172.
194 J. F. Ayme, J. Lux, J. P. Sauvage and A. Sour, *Chem. Eur. J.*, 2012, **18**, 5565–5573.
195 L. Hogg, D. A. Leigh, P. J. Lusby, A. Morelli, S. Parsons and J. K. Y. Wong, *Angew. Chem. Int. Ed.*, 2004, **43**, 1218–1221.
196 J. D. Crowley, S. M. Goldup, A. L. Lee, D. A. Leigh and R. T. Mc Burney, *Chem. Soc. Rev.*, 2009, **38**, 1530–1541.
197 S. M. Goldup, D. A. Leigh, T. Long, P. R. McGonigal, M. D. Symes and J. Wu, *J. Am. Chem. Soc.*, 2009, **131**, 15924–15929.
198 W. R. Dichtel, O. Š. Miljanić, W. Zhang, J. M. Spruell, K. Patel, I. Aprahamian, J. R. Heath and J. F. Stoddart, *Acc. Chem. Res.*, 2008, **41**, 1750–1761.
199 Y. Sato, R. Yamasaki and S. Saito, *Angew. Chem. Int. Ed.*, 2009, **48**, 504–507.
200 S. J. Loeb, *Chem. Soc. Rev.*, 2007, **36**, 226–235.
201 J. E. M. Lewis, P. D. Beer, S. J. Loeb and S. M. Goldup, *Chem. Soc. Rev.*, 2017, **46**, 2577–2591.
202 J. Emerson-King, R. C. Knighton, M. R. Gyton and A. B. Chaplin, *Dalton Trans.*, 2017, **46**, 11645–11655.
203 J. Ferrando-Soria, A. Fernandez, I. J. Vitorica-Yrezabal, D. Asthana, C. A. Muryn, F. Tuna, G. A. Timco and R. E. P. Winpenny, *Chem. Commun.*, 2019, **55**, 2960–2963.
204 C. J. Bruns and J. F. Stoddart, *Molecular Switches and Machines with Mechanical Bonds. In The Nature of the Mechanical Bond*, John Wiley & Sons, Inc., 2016.
205 A. Goswami and M. Schmittel, *Coord. Chem. Rev.*, 2018, **376**, 478–505.
206 A. Joosten, Y. Trolez, J. P. Collin, V. Heitz and J. P. Sauvage, *J. Am. Chem. Soc.*, 2012, **134**, 1802–1809.
207 M. C. Jiménez, C. Dietrich-Buchecker and J. P. Sauvage, *Angew. Chem. Int. Ed.*, 2000,

39, 3284–3287.
208 A. Livoreil, C. O. Dietrich-Buchecker and J. P. Sauvage, *J. Am. Chem. Soc.*, 1994, **116**, 9399–9400.
209 L. Raehm, J. M. Kern and J. P. Sauvage, *Chem. Eur. J.*, 1999, **5**, 3310–3317.
210 N. Armaroli, V. Balzani, J. P. Collin, P. Gaviña, J. P. Sauvage and B. Ventura, *J. Am. Chem. Soc.*, 1999, **121**, 4397–4408.
211 A. M. Albrecht-Gary, Z. Saad, C. O. Dietrich-Buchecker and J. P. Sauvage, *J. Am. Chem. Soc.*, 1985, **107**, 3205–3209.
212 C. O. Dietrich-Buchecker, J. M. Kern and J. P. Sauvage, *J. Am. Chem. Soc., Chem. Commun.*, 1985, 760–762.
213 N. Armaroli, L. De Cola, V. Balzani, J. P. Sauvage, C. O. Dietrich-Buchecker, J. M. Kern and A. Bailal, *J. Am. Chem. Soc., Dalt. Trans.*, 1993, 3241–3247.
214 M. Cesario, J. Guilhem, C. Pascard, C. O. Dietrich, A. Edel, J. P. Sauvage and J. P. Kintzinger, *J. Am. Chem. Soc.*, 1986, **108**, 6250–6254.
215 H. V. Schröder and C. A. Schalley, *Chem. Sci.*, 2019, **10**, 9626–9639.
216 K. M. Bąk, K. Porfyrakis, J. J. Davis and P. D. Beer, *Mater. Chem. Front.*, 2020, **4**, 1052–1073.
217 M. Cirulli, A. Kaur, J. E. M. Lewis, Z. Zhang, J. A. Kitchen, S. M. Goldup and M. M. Roessler, *J. Am. Chem. Soc.*, 2019, **141**, 879–889.
218 J. E. M. Lewis, R. J. Bordoli, M. Denis, C. J. Fletcher, M. Galli, E. A. Neal, E. M. Rochette and S. M. Goldup, *Chem. Sci.*, 2016, **7**, 3154–3161.
219 Z. Zhang, G. J. Tizzard, J. A. G. Williams and S. M. Goldup, *Chem. Sci.*, 2020, **11**, 1839–1847.
220 F. C. Hsueh, C. Y. Tsai, C. C. Lai, Y. H. Liu, S. M. Peng and S. H. Chiu, *Angew. Chem. Int. Ed.*, 2020, **59**, 11278–11282.
221 Y. Trolez, A. D. Finke, F. Silvestri, F. Monti, B. Ventura, C. Boudon, J. P. Gisselbrecht, W. B. Schweizer, J. P. Sauvage, N. Armaroli and F. Diederich, *Chem. Eur. J.*, 2018, **24**, 10422–10433.
222 A. W. Heard and S. M. Goldup, *Chem*, 2020, **6**, 994–1006.
223 B. Leforestier, M. R. Gyton and A. B. Chaplin, *Angew. Chem. Int. Ed.*, , DOI:10.1002/anie.202009546.
224 T. M. Hood and A. B. Chaplin, *Dalton Trans.*, 2020, **49**, 16649–16652.
225 C. M. Storey, M. R. Gyton, R. E. Andrew and A. B. Chaplin, *Angew. Chem. Int. Ed.*, 2018, **57**, 12003–12006.
226 C. M. Storey, M. R. Gyton, R. E. Andrew and A. B. Chaplin, *Chem. Eur. J.*, 2020, **26**, 14715–14723.
227 L. Steemers, M. J. Wanner, A. W. Ehlers, H. Hiemstra and J. H. Van Maarseveen, *Org. Lett.*, 2017, **19**, 2342–2345.
228 M. D. Cornelissen, S. Pilon, L. Steemers, M. J. Wanner, S. Frölke, E. Zuidinga, S. I. Jørgensen, J. I. Van Der Vlugt and J. H. Van Maarseveen, *J. Org. Chem.*, 2020, **85**, 3146–3159.
229 A. W. Heard and S. M. Goldup, *ACS Cent. Sci.*, 2020, **6**, 117–128.
230 D. A. Leigh, V. Marcos and M. R. Wilson, *ACS Catal.*, 2014, **4**, 4490–4497.
231 R. Barat, T. Legigan, I. Tranoy-Opalinski, B. Renoux, E. Péraudeau, J. Clarhaut, P. Poinot, A. E. Fernandes, V. Aucagne, D. A. Leigh and S. Papot, *Chem. Sci.*, 2015, **6**, 2608–2613.
232 J. A. Labinger and J. E. Bercaw, *Nature*, 2002, **417**, 507–514.

233 C. Hall and R. N. Perutz, *Chem. Rev.*, 1996, **96**, 3125–3146.
234 T. Gensch, M. N. Hopkinson, F. Glorius and J. Wencel-Delord, *Chem. Soc. Rev.*, 2016, **45**, 2900–2936.
235 S. J. Blanksby and G. B. Ellison, *Acc. Chem. Res.*, 2003, **36**, 255–263.
236 P. Gandeepan, T. Müller, D. Zell, G. Cera, S. Warratz and L. Ackermann, *Chem. Rev.*, 2019, **119**, 2192–2452.
237 F. Roudesly, J. Oble and G. Poli, *J. Mol. Catal. A Chem.*, 2017, **426**, 275–296.
238 X. Chen, K. M. Engle, D. H. Wang and Y. Jin-Quan, *Angew. Chem. Int. Ed.*, 2009, **48**, 5094–5115.
239 J. Chatt and J. M. Davidson, *J. Am. Chem. Soc.*, 1965, 843–855.
240 M. L. H. Green and D. O'Hare, *Pure Appl. Chem.*, 1985, **57**, 1897–1910.
241 M. A. Bennett and D. L. Milner, *Chem. Commun.*, 1967, 581–582.
242 E. K. Barefield, G. W. Parshall and F. N. Tebbe, *J. Am. Chem. Soc.*, 1970, **92**, 5234–5235.
243 A. H. Janowicz and R. G. Bergman, *J. Am. Chem. Soc.*, 1982, **104**, 352–354.
244 J. K. Hoyano and W. A. G. Graham, *J. Am. Chem. Soc.*, 1982, **104**, 3723–3725.
245 R. H. Crabtree, *Chem. Rev.*, 1985, **85**, 245–269.
246 A. E. Shilov and A. A. Shteinman, *Coord. Chem. Rev.*, 1977, **24**, 97–143.
247 M. Brookhart and M. L. H. Green, *J. Organomet. Chem.*, 1983, **250**, 395–408.
248 M. Brookhart, M. L. H. Green and G. Parkin, *Proc. Natl. Acad. Sci. U. S. A.*, 2007, **104**, 6908–6914.
249 Z. Dawoodi, M. L. H. Green, V. S. B. Mtetwa, K. Prout, A. J. Schultz, J. M. Williams and T. F. Koetzle, *J. Am. Chem. Soc., Dalt. Trans.*, 1986, 1629–1637.
250 H. Urtel, C. Meier, F. Eisenträger, F. Rominger, J. P. Joschek and P. Hofmann, *Angew. Chem. Int. Ed.*, 2001, **40**, 781–784.
251 S. K. Brayshaw, J. C. Green, G. Kociok-Köhn, E. L. Sceats and A. S. Weller, *Angew. Chem. Int. Ed.*, 2006, **45**, 452–456.
252 M. R. Gyton, B. Leforestier and A. B. Chaplin, *Organometallics*, 2018, **37**, 3963–3971.
253 R. H. Crabtree, *Chem. Rev.*, 1995, **95**, 987–1007.
254 R. J. Hodges, D. E. Webster and P. B. Wells, *J. Am. Chem. Soc. A*, 1971, 3230–3238.
255 R. N. Perutz and J. J. Turner, *J. Am. Chem. Soc.*, 1975, **97**, 4791–4800.
256 J. J. Turner, J. K. Burdett, R. N. Perutz and M. Poliakoff, *Pure Appl. Chem.*, 1977, 49, 271–285.
257 J. M. Kelly, H. Hermann and E. K. Von Gustorf, *J. Am. Chem. Soc., Chem. Commun.*, 1973, 105–106.
258 R. Bonneau and J. M. Kelly, *J. Am. Chem. Soc.*, 1980, **102**, 1220–1221.
259 H. Hermann, F. W. Grevels, A. Henne and K. Schaffner, *J. Phys. Chem.*, 1982, **86**, 5151–5154.
260 G. R. Dobson, P. M. Hodges, M. A. Healy, M. Poliakoff, J. J. Turner, S. Firth and K. J. Asali, *J. Am. Chem. Soc.*, 1987, **109**, 4218–4224.
261 J. M. Morse, G. H. Parker and T. J. Burkey, *Organometallics*, 1989, **8**, 2471–2474.
262 C. E. Brown, Y. Ishikawa, P. A. Hackett and D. M. Rayner, *J. Am. Chem. Soc.*, 1990, **112**, 2530–2536.
263 S. E. Bromberg, H. Yang, M. C. Asplund, T. Lian, B. K. McNamara, K. T. Kotz, J. S. Yeston, M. Wilkens, H. Frei, R. G. Bergman and C. B. Harris, *Science*, 1997, **278**, 260–263.
264 J. M. Buchanan, J. M. Stryker and R. G. Bergman, *J. Am. Chem. Soc.*, 1986, **108**, 1537–

1550.
265 R. M. Bullock, C. E. L. Headford, K. M. Hennessy, S. E. Kegley and J. R. Norton, *J. Am. Chem. Soc.*, 1989, **111**, 3897–3908.
266 A. A. Bengali, R. H. Schultz, B. C. Moore and R. G. Bergman, *J. Am. Chem. Soc.*, 1994, **116**, 9585–9589.
267 S. Geftakis and G. E. Ball, *J. Am. Chem. Soc.*, 1998, **120**, 9953–9954.
268 G. E. Ball, 2010, pp. 262–287.
269 S. A. Bartlett, N. A. Besley, A. J. Dent, S. Diaz-Moreno, J. Evans, M. L. Hamilton, M. W. D. Hanson-Heine, R. Horvath, V. Manici, X. Z. Sun, M. Towrie, L. Wu, X. Zhang and M. W. George, *J. Am. Chem. Soc.*, 2019, **141**, 11471–11480.
270 O. Torres, J. A. Calladine, S. B. Duckett, M. W. George and R. N. Perutz, *Chem. Sci.*, 2015, **6**, 418–424.
271 W. H. Bernskoetter, C. K. Schauer, K. I. Goldberg and M. Brookhart, *Science*, 2009, **326**, 553–556.
272 M. Findlater, K. M. Schultz, W. H. Bernskoetter, A. Cartwright-Sykes, D. M. Heinekey and M. Brookhart, *Inorg. Chem.*, 2012, **51**, 4672–4678.
273 M. D. Walter, P. S. White, C. K. Schauer and M. Brookhart, *J. Am. Chem. Soc.*, 2013, **135**, 15933–15947.
274 W. H. Bernskoetter, S. K. Hanson, S. K. Buzak, Z. Davis, P. S. White, R. Swartz, K. I. Goldberg and M. Brookhart, *J. Am. Chem. Soc.*, 2009, **131**, 8603–8613.
275 M. D. Walter, P. S. White, C. K. Schauer and M. Brookhart, *New J. Chem.*, 2011, **35**, 2884–2893.
276 D. R. Evans, T. Drovetskaya, R. Bau, C. A. Reed and P. D. W. Boyd, *J. Am. Chem. Soc.*, 1997, **119**, 3633–3634.
277 I. Castro-Rodriguez, H. Nakai, P. Gantzel, L. N. Zakharov, A. L. Rheingold and K. Meyer, *J. Am. Chem. Soc.*, 2003, **125**, 15734–15735.
278 E. D. Bloch, W. L. Queen, R. Krishna, J. M. Zadrozny, C. M. Brown and J. R. Long, *Science*, 2012, **335**, 1606–1610.
279 N. R. Andreychuk and D. J. H. Emslie, *Angew. Chem.*, 2013, **125**, 1740–1743.
280 S. D. Pike, A. L. Thompson, A. G. Algarra, D. C. Apperley, S. A. Macgregor and A. S. Weller, *Science*, 2012, **337**, 1648–1651.
281 F. M. Chadwick, T. Krämer, T. Gutmann, N. H. Rees, A. L. Thompson, A. J. Edwards, G. Buntkowsky, S. A. Macgregor and A. S. Weller, *J. Am. Chem. Soc.*, 2016, **138**, 13369–13378.
282 A. I. McKay, T. Krämer, N. H. Rees, A. L. Thompson, K. E. Christensen, S. A. Macgregor and A. S. Weller, *Organometallics*, 2017, **36**, 22–25.
283 S. D. Pike, F. M. Chadwick, N. H. Rees, M. P. Scott, A. S. Weller, T. Krämer and S. A. Macgregor, *J. Am. Chem. Soc.*, 2015, **137**, 820–833.
284 F. M. Chadwick, N. H. Rees, A. S. Weller, T. Krämer, M. Iannuzzi and S. A. Macgregor, *Angew. Chem. Int. Ed.*, 2016, **55**, 3677–3681.
285 T. M. Boyd, B. E. Tegner, G. J. Tizzard, A. J. Martínez-Martínez, S. E. Neale, M. A. Hayward, S. J. Coles, S. A. Macgregor and A. S. Weller, *Angew. Chem. Int. Ed.*, 2020, **59**, 6177–6181.
286 A. J. Martínez-Martínez, B. E. Tegner, A. I. McKay, A. J. Bukvic, N. H. Rees, G. J. Tizzard, S. J. Coles, M. R. Warren, S. A. Macgregor and A. S. Weller, *J. Am. Chem. Soc.*, 2018, **140**, 14958–14970.
287 A. S. Weller, F. M. Chadwick and A. I. McKay, in *Advances in Organometallic*

Chemistry, ed. P. J. B. T.-A. in O. C. Pérez, Academic Press, 2016, vol. 66, pp. 223–276.
288 E. M. Fry, *J. Org. Chem.*, 1950, **15**, 802–806.
289 G. R. Newkome, D. C. Hager and G. E. Kiefer, *J. Org. Chem.*, 1986, **51**, 850–853.
290 S. Takahashi and H. Togo, *Synthesis*, 2009, **2009**, 2329–2332.
291 H. W. Gibson, S. H. Lee, P. T. Engen, P. Lecavalier, J. Sze, Y. X. Shen and M. Bheda, *J. Org. Chem.*, 1993, **58**, 3748–3756.
292 H. J. Reich, *Chem. Rev.*, 2013, **113**, 7130–7178.
293 H. J. Reich and W. H. Sikorski, *J. Org. Chem.*, 1999, **64**, 14–15.
294 J. Clayden and S. A. Yasin, *New J. Chem.*, 2002, **26**, 191–192.
295 M. Denis, J. Pancholi, K. Jobe, M. Watkinson and S. M. Goldup, *Angew. Chem. Int. Ed.*, 2018, **57**, 5310–5314.
296 W. Clegg, C. Gimenez-Saiz, D. A. Leigh, A. Murphy, A. M. Z. Slawin and S. J. Teat, *J. Am. Chem. Soc.*, 1999, **121**, 4124–4129.
297 C. A. Scarff, J. R. Snelling, M. M. Knust, C. L. Wilkins and J. H. Scrivens, *J. Am. Chem. Soc.*, 2012, **134**, 9193–9198.
298 J. J. Danon, D. A. Leigh, S. Pisano, A. Valero and I. J. Vitorica-Yrezabal, *Angew. Chem. Int. Ed.*, 2018, **57**, 13833–13837.
299 D. F. Evans, *J. Am. Chem. Soc.*, 1959, 2003–2005.
300 G. A. Bain and J. F. Berry, *J. Chem. Educ.*, 2008, **85**, 532–536.
301 C. Piguet, *J. Chem. Educ.*, 1997, **74**, 815–816.
302 W. G. Jia, D. D. Li, L. Q. Yan, E. H. Sheng and Y. C. Dai, *J. Coord. Chem.*, 2014, **67**, 363–371.
303 C. Provent, G. Bernardinelli, A. F. Williams and N. Vulliermet, *Eur. J. Inorg. Chem.*, 2001, **2001**, 1963–1967.
304 K. E. Burrows, S. E. McGrath, R. Kulmaczewski, O. Cespedes, S. A. Barrett and M. A. Halcrow, *Chem. Eur. J.*, 2017, **23**, 9067–9075.
305 J. Guo, B. Wang, J. Bi, C. Zhang, H. Zhang, C. Bai, Y. Hu and X. Zhang, *Polymer*, 2015, **59**, 124–132.
306 P. Roquette, A. Maronna, M. Reinmuth, E. Kaifer, M. Enders and H. J. Himmel, *Inorg. Chem.*, 2011, **50**, 1942–1955.
307 J. E. M. Lewis, M. Galli and S. M. Goldup, *Chem. Commun.*, 2017, **53**, 298–312.
308 D. B. Amabilino and J. F. Stoddart, *Chem. Rev.*, 1995, **95**, 2725–2828.
309 C. A. Schalley, P. Ghosh and M. Engeser, *Int. J. Mass Spectrom.*, 2004, **232**, 249–258.
310 G. L. Parker, S. Lau, B. Leforestier and A. B. Chaplin, *Eur. J. Inorg. Chem.*, 2019, **2019**, 3791–3798.
311 C. N. Iverson and W. D. Jones, *Organometallics*, 2001, **20**, 5745–5750.
312 Z. Lu, C. H. Jun, S. R. de Gala, R. H. Crabtree, M. P. Sigalas and O. Eisenstein, *Organometallics*, 1995, **14**, 1168–1175.
313 R. C. Knighton, J. Emerson-King, J. P. Rourke, C. A. Ohlin and A. B. Chaplin, *Chem. Eur. J.*, 2018, **24**, 4927–4938.
314 T. M. Hood, B. Leforestier, M. R. Gyton and A. B. Chaplin, *Inorg. Chem.*, 2019, **58**, 7593–7601.
315 T. M. Hood, M. R. Gyton and A. B. Chaplin, *Dalton Trans.*, 2020, **49**, 2077–2086.
316 M. R. Gyton, A. E. Kynman, B. Leforestier, A. Gallo, J. R. Lewandowski and A. B. Chaplin, *Dalton Trans.*, 2020, **49**, 5791–5793.
317 E. De Julián, E. Menéndez-Pedregal, M. Claros, M. Vaquero, J. Díez, E. Lastra, P. Gamasa and A. Pizzano, *Org. Chem. Front.*, 2018, **5**, 841–849.

318 D. G. Gusev, M. Madott, F. M. Dolgushin, K. A. Lyssenko and M. Y. Antipin, *Organometallics*, 2000, **19**, 1734–1739.
319 J. Zhang, K. A. Barakat, T. R. Cundari, T. B. Gunnoe, P. D. Boyle, J. L. Petersen and C. S. Day, *Inorg. Chem.*, 2005, **44**, 8379–8390.
320 A. Ramaraj, K. H. K. Reddy, H. Keil, R. Herbst-Irmer, D. Stalke, E. D. Jemmis and B. R. Jagirdar, *Organometallics*, 2017, **36**, 2736–2745.
321 S. D. Pike, M. R. Crimmin and A. B. Chaplin, *Chem. Commun.*, 2017, **53**, 3615–3633.
322 O. Eisenstein, J. Milani and R. N. Perutz, *Chem. Rev.*, 2017, **117**, 8710–8753.
323 S. A. Hauser, J. Emerson-King, S. Habershon and A. B. Chaplin, *Chem. Commun.*, 2017, **53**, 3634–3636.
324 A. B. Chaplin and A. S. Weller, *Organometallics*, 2011, **30**, 4466–4469.
325 S. K. Brayshaw, E. L. Sceats, J. C. Green and A. S. Weller, *Proc. Natl. Acad. Sci. U. S. A.*, 2007, **104**, 6921–6926.
326 M. Etienne and A. S. Weller, *Chem. Soc. Rev.*, 2014, **43**, 242–259.
327 S. T. H. Willems, J. C. Russcher, P. H. M. Budzelaar, B. De Bruin, R. De Gelder, J. M. M. Smits and A. W. Gal, *Chem. Commun.*, 2002, **2**, 148–149.
328 A. K. W. Chan, D. Wu, K. M. C. Wong and V. W. W. Yam, *Inorg. Chem.*, 2016, **55**, 3685–3691.
329 A. K. W. Chan, M. Ng, K. H. Low and V. W. W. Yam, *J. Am. Chem. Soc.*, 2018, **140**, 8321–8329.
330 G. Bistoni, S. Rampino, N. Scafuri, G. Ciancaleoni, D. Zuccaccia, L. Belpassi and F. Tarantelli, *Chem. Sci.*, 2016, **7**, 1174–1184.
331 S. H. Strauss, *Chemtracts*, 1997, 10, 77–103.
332 N. S. Hush and M. L. Williams, *J. Mol. Spectrosc.*, 1974, **50**, 349–368.
333 C. A. Tolman, *J. Am. Chem. Soc.*, 1970, **92**, 2953–2956.
334 C. A. Tolman, *Chem. Rev.*, 1977, **77**, 313–348.
335 A. R. Chianese, X. Li, M. C. Janzen, J. W. Faller and R. H. Crabtree, *Organometallics*, 2003, **22**, 1663–1667.
336 R. A. Kelly, H. Clavier, S. Giudice, N. M. Scott, E. D. Stevens, J. Bordner, I. Samardjiev, C. D. Hoff, L. Cavallo and S. P. Nolan, *Organometallics*, 2008, **27**, 202–210.
337 S. Leuthäußer, D. Schwarz and H. Plenio, *Chem. Eur. J.*, 2007, **13**, 7195–7203.
338 S. Wolf and H. Plenio, *J. Organomet. Chem.*, 2009, **694**, 1487–1492.
339 T. Dröge and F. Glorius, *Angew. Chem. Int. Ed.*, 2010, **49**, 6940–6952.
340 L. Maser, C. Schneider, L. Vondung, L. Alig and R. Langer, *J. Am. Chem. Soc.*, 2019, **141**, 7596–7604.
341 J. J. Davidson, J. C. Demott, C. Douvris, C. M. Fafard, N. Bhuvanesh, C. H. Chen, D. E. Herbert, C. I. Lee, B. J. McCulloch, B. M. Foxman and O. V. Ozerov, *Inorg. Chem.*, 2015, **54**, 2916–2935.
342 H. V. Huynh, Y. Han, R. Jothibasu and J. A. Yang, *Organometallics*, 2009, **28**, 5395–5404.
343 A. Reinholdt and J. Bendix, *Inorg. Chem.*, 2017, **56**, 12492–12497.
344 R. E. Andrew and A. B. Chaplin, *Inorg. Chem.*, 2015, **54**, 312–322.
345 D. G. Gusev, *Organometallics*, 2009, **28**, 763–770.
346 O. Kühl, *Coord. Chem. Rev.*, 2005, **249**, 693–704.
347 W. D. Jones and L. Dong, *J. Am. Chem. Soc.*, 1989, **111**, 8722–8723.
348 J. P. Collin, I. M. Dixon, J. P. Sauvage, J. A. G. Williams, F. Barigelletti and L. Flamigni, *J. Am. Chem. Soc.*, 1999, **121**, 5009–5016.

349 B. C. De Pater, H. W. Frühauf, K. Vrieze, R. De Gelder, E. J. Baerends, D. McCormack, M. Lutz, A. L. Spek and F. Hartl, *Eur. J. Inorg. Chem.*, 2004, **2004**, 1675–1686.
350 S. Y. Brauchli, E. C. Constable, K. Harris, D. Häussinger, C. E. Housecroft, P. J. Rösel and J. A. Zampese, *Dalton Trans.*, 2010, **39**, 10739–10748.
351 H. Yoo, P. J. Carroll and D. H. Berry, *J. Am. Chem. Soc.*, 2006, **128**, 6038–6039.
352 P. Braunstein and F. Naud, *Organometallics*, 2000, **19**, 2676–2683.
353 E. W. Abel, K. G. Orrell, A. G. Osborne, H. M. Pain and V. Šik, *J. Am. Chem. Soc., Dalt. Trans.*, 1994, 111–116.
354 C. J. Bruns and J. F. Stoddart, in *The Nature of the Mechanical Bond*, John Wiley & Sons, Inc., Hoboken, NJ, USA, 2016, pp. 1–54.
355 R. M. P. Veenboer, A. Collado, S. Dupuy, T. Lebl, L. Falivene, L. Cavallo, D. B. Cordes, A. M. Z. Slawin, C. S. J. Cazin and S. P. Nolan, *Organometallics*, 2017, **36**, 2861–2869.
356 E. L. Zins, B. Silvi and M. E. Alikhani, *Phys. Chem. Chem. Phys.*, 2015, **17**, 9258–9281.
357 R. Díaz-Torres and S. Alvarez, *Dalton Trans.*, 2011, **40**, 10742–10750.
358 R. J. Bushby and G. J. Ferber, *J. Chem. Soc., Perkin Trans. 2*, 1976, 1688–1695.
359 J. M. Wilson, G. J. Sunley, H. Adams and A. Haynes, *J. Organomet. Chem.*, 2005, **690**, 6089–6095.
360 R. E. Andrew, D. W. Ferdani, C. A. Ohlin and A. B. Chaplin, *Organometallics*, 2015, **34**, 913–917.
361 R. Mitra, H. Zhu, S. Grimme and J. Niemeyer, *Angew. Chem. Int. Ed.*, 2017, **56**, 11456–11459.
362 S. Hoekman, M. O. Kitching, D. A. Leigh, M. Papmeyer and D. Roke, *J. Am. Chem. Soc.*, 2015, **137**, 7656–7659.
363 R. Ziessel, V. Grosshenny, M. Hissler and C. Stroh, *Inorg. Chem.*, 2004, **43**, 4262–4271.
364 J. L. Bon and S. B. Blakey, *Heterocycles*, 2012, **84**, 1313–1323.
365 J. Yu and C. Zhang, *Synthesis*, 2009, **2009**, 2324–2328.
366 W. E. Buschman, J. S. Miller, K. Bowman-James, C. N. Miller, in *Inorg. Synth.*, John Wiley & Sons, Ltd, 2002, pp. 75–121.
367 J. G. Park, I. R. Jeon and T. D. Harris, *Inorg. Chem.*, 2015, **54**, 359–369.
368 A. Van Der Ent, A. L. Onderdelinden and R. A. Schunn, *Inorg. Synth.*, 2007, 90–92.
369 M. V. Jiménez, M. I. Bartolomé, J. J. Pérez-Torrente, F. J. Lahoz and L. A. Oro, *ChemCatChem*, 2012, **4**, 1298–1310.
370 M. A. Bennett and A. K. Smith, *J. Am. Chem. Soc., Dalt. Trans.*, 1974, 233–241.
371 G. M. Sheldrick, *Acta Cryst. A*, 2008, **64**, 112–122.
372 O. V. Dolomanov, L. J. Bourhis, R. J. Gildea, J. A. K. Howard and H. Puschmann, *J. Appl. Crystallogr.*, 2009, **42**, 339–341.